# REPORT DOCUMENTATION PAGE

Public reporting burden for this collection of information is estimated to average 1 hour per response, including the time for reviewing instructions, searching existing data sources, gathering and maintaining the data needed, and completing and reviewing the collection of information. Send comments regarding this burden estimate or any other aspect of this collection of information, including suggestions for reducing this burden, to Washington Headquarters Services, Directorate for Information Operations and Reports, 1215 Jefferson Davis Highway, Suite 1204, Arlington, VA 22202-4302, and to the Office of Management and Budget, Paperwork Reduction Project (0704-0188), Washington, DC 20503.

| 1. AGENCY USE ONLY (Leave blank) | 2. REPORT DATE 12/1/94 | 3. REPORT TYPE AND DATES COVERED Final: 11/1/90 - 4/30/94 |
|---|---|---|

**4. TITLE AND SUBTITLE**
Modal Interactions in Weakly Nonlinear Multi-Degree-of-Freedom Systems

**5. FUNDING NUMBERS**
DAAL03-90-G-0220

**6. AUTHOR(S)**
A.K. Bajaj , P. Davies

**7. PERFORMING ORGANIZATION NAME(S) AND ADDRESS(ES)**
Purdue Research Foundation
Hovde Hall, 3rd. Floor
West Lafayette, iN 47907

**PERFORMING ORGANIZATION REPORT NUMBER**

**9. SPONSORING / MONITORING AGENCY NAME(S) AND ADDRESS(ES)**
U.S. Army Research Office
P. O. Box 12211
Research Triangle Park, NC 27709-2211

**10. SPONSORING / MONITORING AGENCY REPORT NUMBER**
ARO 27300.10-EG

**11. SUPPLEMENTARY NOTES**
The view, opinions and/or findings contained in this report are those of the author(s) and should not be construed as an official Department of the Army position, policy, or decision, unless so designated by other documentation.

**12a. DISTRIBUTION / AVAILABILITY STATEMENT**
Approved for public release; distribution unlimited.

**12b. DISTRIBUTION CODE**

**13. ABSTRACT (Maximum 200 words)**

The analysis of forced nonlinear response of mechanical and structural systems, subjected to harmonic excitations, is considered in this report. It is shown that the presence of internal resonances in the various linear modes of vibration of the structure can result in quite complex dynamical motions and the motion may not settle down to either a periodic or a sub/super-harmonic response. Internal resonances, which allow for the exchange of energy between the participating modes give rise to beat-like fluctuations in the amplitudes of vibration. The nonlinear amplitude variation is very slow and can be either periodic or chaotic, depending on the level of forcing, damping and the nonlinearity coefficients. The analytical and numerical results are derived for the nonlinear vibrations of a thin rectangular plate, the response of the pendulum vibration absorber, and a double pendulum. Some experimental results of the measured response for a harmonically forced rectangular plate are also presented and compared to analytical predictions.

**14. SUBJECT TERMS**
Nonlinear vibrations, bifurcations, chaotic dynamics, internal resonance, amplitude modulations, averaging.

**15. NUMBER OF PAGES**
191

**16. PRICE CODE**

| 17. SECURITY CLASSIFICATION OF REPORT | 18. SECURITY CLASSIFICATION OF THIS PAGE | 19. SECURITY CLASSIFICATION OF ABSTRACT | 20. LIMITATION OF ABSTRACT |
|---|---|---|---|
| UNCLASSIFIED | UNCLASSIFIED | UNCLASSIFIED | UL |

DTIC SELECTED MAR 10 1995 B

19950308 237

# Modal Interactions and Complex Responses in Weakly Nonlinear Multi-Degree-of-Freedom Mechanical Systems

## Final Report
## on Contract DAAL03-90-G-0220

Submitted to:

Dr. Gary L. Anderson
Chief, Structural Dynamics Branch
U. S. Army Research Office
Engineering Sciences Division
P. O. Box 12211
Research Triangle Park, NC 27709-2211

By:

A. K. Bajaj
P. Davies

Ray W. Herrick Laboratories
School of Mechanical Engineering
Purdue University
West Lafayette, IN 47907

# TABLE OF CONTENTS

**Executive Summary of " Modal Interactions and Complex Responses in Weakly Nonlinear Multi-Degree-of-Freedom Mechanical Systems"**

This final report documents the work performed at Purdue University during the period of November 1990 to April 1994. The original ARO Contract (#DAAL-90-G-0220) was written for three years and an no cost extension was granted subsequently. The objective of the proposed research was to understand and characterize complex dynamical responses in harmonically and parametrically excited nonlinear mechanical and structural systems. The primary focus was on the responses of multi degree-of-freedom systems that arise due to the modal interactions in the presence of internal resonances. The work was motivated by the recognition that in order to improve the design and performance, and to devise efficient control schemes, it is first necessary to understand the conditions and design parameters that can lead to large amplitude and complex responses. More specifically, it was proposed to study the weakly nonlinear response of structures near resonant conditions by using the asymptotic techniques of averaging and integral manifolds. The limits of applicability of the asymptotic techniques, and hence the range of their usefulness, was to be also investigated by using direct numerical integration of the equations of motion of the systems under consideration, and by comparing these results with those predicted by the asymptotic analyses. The results were proposed to be applied to study responses of various physical systems including the autoparametric pendulum vibration absorber, and the multi-mode response of rectangular plates.

**Status:**

The work associated with the essential objectives of the project is almost complete and is included in this final report. A first and then a second-order asymptotic averaging analysis of the response of the autoparametric pendulum vibration absorber, under conditions of external as well as 2:1 internal resonance, has been accomplished and the results are presented in a journal paper, #12 below, and in Appendix 1. Some conclusions are derived with respect to the range of applicability of the averaging technique depending on the smallness of the asymptotic parameter which is also related to the amplitude of the forcing. The analysis of multi-mode response of rectangular plates to harmonic forcing, under 1:1 internal resonance between two distinct plate modes is reported in a journal paper, #4 below, and in Appendix 2. The complete work reported in the thesis of S. I. Chang includes the cases of weak resonant forcing as well as the response to sub- and super-hamonic excitations. An experimental rig was

constructed to confirm and observe some of the nonlinear and complex response predictions for the plate. These results are given in Appendix 3. In order to consider inertial nonlinearities, as opposed to the geometric nonlinearities that are included in the thin plate models, the dynamics of an orthogonal double pendulum with base excitations is studied. The bifurcation structure, including the number of stable periodic solutions and bifurcations there from, is found to be extremely rich, and the results are reported in a journal paper, #5 below.

In a more general study of two-degree-of-freedom systems with quadratic nonlinearities and 2:1 internal resonances it is shown that, in the absence of damping, essentially any level of resonant harmonic excitation will lead to the presence of Smale horseshoes, and hence, complex chaotic dynamics. These results are given in the paper attached in Appendix 4. Note that the autoparametric pendulum vibration absorber is a typical example of this class of systems.

While working on the various aspects of the project, and specially the experimental study of the response of the plate, it was realized that the control parameters are really not constants. Rather, they are varied sufficiently slowly in order to generate the complete frequency response diagrams. In some cases, there can be significant differences between the response predicted by assuming that the parameters are varied quasi-statically, and those actually observed in the experiments. Thus, analysis was undertaken to understand the phenomena of slow passage through bifurcation and turning points. Results of an extensive study on this subject are reported in Appendix 5.

**Publications:**

Several journal and conference papers have been developed from the research undertaken in this project. Three journal papers ( #4, 5, 12) have already been published, two manuscripts ( #16, 17) have recently been submitted, and one ( #13) has been accepted for publication. In addition, two book chapters ( #14, 15) as invited contributions were prepared and they will appear shortly. Many conference proceeding papers and presentations were also made. All these are listed below:

1. Bajaj, A. K., Johnson, J. M. and Chang, S. I., Amplitude dynamics of an two-degree-of-freedom autoparametric system, Proceedings of the 13th Biennial ASME Conference on Mechanical Vibration and Noise, September 22-25, 1991, Miami, Florida.

2. Samaranayake, S. and Bajaj, A. K., Bifurcations in the dynamics of an orthogonal double pendulum, 4th Conference on Nonlinear Vibrations, Stability, and Dynamics of Structures and Systems, VPISU, Blacksburg, VA, June 7-11, 1992.

3. McCabe, S. A., Davies, P., Chang, S. I. and Bajaj, A. K., Experiments on the nonlinear resonant response of thin elastic plates, 4th Conference on Nonlinear Vibrations, Stability, and Dynamics of Structures and Systems, VPISU, Blacksburg, VA, June 7-11, 1992.

4. Chang, S. I., Bajaj, A. K. and Krousgrill, C. M., Non-linear vibrations and chaos in harmonically excited rectangular plates with internal resonances, <u>Nonlinear Dynamics</u>, 4, 1993, 433-460.

5. Samaranayake, S. and Bajaj, A. K., Bifurcations in the dynamics of an orthogonal double pendulum, <u>Nonlinear Dynamics</u>, 4, 1993, 605-633.

6. Chang, S. I., Bajaj, A. K. and Davies, P., Local and global nonlinear dynamics of harmonically excited rectangular plates, Proceedings of the 7th US Army Symposium on Gun Dynamics, Newport, RI, May 11-13, 1993.

7. Banerjee, B., Bajaj, A. K. and Davies, P., Second order averaging study of an autoparametric system, Proceedings of the 14th ASME Biennial Conference on Mechanical Vibration and Noise, Sept. 19-22, 1993, Albuquerque, NM.

8. Raman, A., Davies, P. and Bajaj, A. K., Analytical prediction of nonlinear system response to nonstationary excitation, Proceedings of the 14th ASME Biennial Conference on Mechanical Vibration and Noise, Sept. 19-22, 1993, Albuquerque, NM.

9. McCabe, S. A., Chang, S. I., Davies, P. and Bajaj, A. K., Nonlinear response of a clamped plate to nonstationary excitation: experiments and theory, Proceedings of the 14th ASME Biennial Conference on Mechanical Vibration and Noise, Sept. 19-22, 1993, Albuquerque, NM.

10. Chang, S. I., Bajaj, A. K. and Davies, P., Multimode nonlinear dynamics of harmonically excited rectangular plates, 2nd US National Congress on Computational Mechanics, Aug. 16-18, 1993, Washington, DC.

11. Bajaj, A. K., On internal resonances in mechanical systems, International Symposium on Nonlinear Dynamics and Stochastic Mechanics, The Fields Institute, Aug. 29- Sept. 1, 1993, Waterloo, Canada.

12. Bajaj, A. K., Chang, S. I. and Johnson, J. M., Amplitude modulated dynamics of a resonantly excited autoparametric two degree-of-freedom system, <u>Nonlinear Dynamics</u>, 5, 1994, 433-457.

13. Banerjee, B. and Bajaj, A. K., Chaotic responses in two degree-of-freedom systems with 1:2 internal resonances, <u>Fields Institute Communications</u>, American Mathematical Society (accepted for publication).

14. Bajaj, A. K., Davies, P. and Chang, S. I., On internal resonancs in mechanical systems, in <u>Stochastic Modelling and Nonlinear Dynamics: Applications to Mechanical Systems</u> ( eds: W. Kliemann and N. Sri Namachchivaya) CRC Press, 1994.

15. Chang, S. I., Bajaj, A. K. and Davies, P., Bifurcations and chaotic motions in resonantly excited structures, in <u>Bifurcations and Chaos: Theory and Applications</u> ( ed: J. Awrejcewicz) Springer Verlag, 1995.

16. Raman, A., Bajaj, A. K. and Davies, P., On the slow transition across bifurcations in some classical nonlinear systems, <u>Journal of Sound and Vibration</u> ( submitted).

17. Banerjee, B., Bajaj, A. K. and Davies, P., Resonant dynamics of an autoparametric system: a study using higher order averaging, <u>International Journal of Non-Linear Mechanics</u> ( submitted).

**Personnel**

Two faculty members and four graduate students were partially funded by this contract.

FACULTY: Professor Anil K. Bajaj, Professor P. Davies.

GRADUATE STUDENTS: Mr. B. Banerjee ( Doctoral student), Mr. S. I. Chang ( Doctoral student), Ms. S. McCabe ( Doctoral student).

Mr. A. Raman ( Masters student).

Mr. S. I. Chang completed his **doctoral thesis** " *Studies on nonlinear multi-mode dynamics of resonantly excited rectangular plates*" in September 1993 and was awarded the degree in December 1993. Mr. A. Raman completed his **masters thesis** " *A study of the response of nonlinear systems to nonstationary excitations*" in July 1993, and was awarded the degree in August 1993.

# 1. INTRODUCTION

## 1.1 Problem Statement

The central aim of the present project has been to:

(i) Understand and characterize complex dynamical responses in harmonically and parametrically excited mechanical and structural systems that arise due to modal interactions in the presence of internal and external resonances, and to do so through the use of asymptotic techniques of the method of averaging and integral manifolds.

(ii) Investigate the limits of applicability of the asmptotic techniques through the comparison of results derived by the use of asymptotic techniques with those obtained by direct numerical simulation of the equations of motion.

(iii) Study the responses of structural and mechanical systems including the autoparametric pendulum vibration absorber and thin rectangular plates.

## 1.2 Background and Overview

The prediction of nonlinear dynamic response of mechanical and structural systems has been an area of very active research for quite some time. Traditionally, externally excited systems have been analyzed for their periodic or harmonic response around positions of stable equilibrium. For systems with parametric excitations, the interest has focused on dynamic instabilities of the equilibrium positions and the resulting nonlinear responses. In either case, the motions have been considered *small*, and perturbation and asymptotic techniques have been the main tools of analysis. See Nayfeh and Mook [1] for an excellent coverage of the classic developments.

In the early 1960's Sethna [2] studied and classified weakly nonlinear and externally excited two degree-of-freedom systems based on the various resonances. He showed that the steady-state motions are expected to be most interesting and unusual when the system possesses *external* as well as *internal* resonances. An external resonance provides a mechanism of feeding energy into the system under appropriate phase relationship. An internal resonance allows for an exchange of energy between the interacting modes. Thus, internal resonance is one of the primary mechanisms by which various modes of a structure can interact and influence each other. Miles [3] and Sethna [4], subsequently, studied the spherical pendulum and a system with quadratic nonlinearities. For some specific cases of internal and external resonance, they observed that over a range of excitation frequencies the averaged equations do not possess any stable constant solution. Numerical integration of these amplitude equations resulted in

bounded limit cycle motions. Sufficiently large damping was able to suppress these motions. Similar observations were later reported in studies with many externally excited as well as parametrically excited systems. There also existed some experimental studies on the response of structural systems where complicated responses not explained by assuming only a single mode analysis were observed.

The existence of limit cycle motions for the amplitude equations, and hence the periodically-modulated harmonic motions for the forced dynamical systems was explained by Sethna and Bajaj [5]. For systems with quadratic nonlinearities, they showed that these motions resulted due to a Hopf bifurcation in the averaged equations. This was later extended [6, 7] to other examples of two degree-of-freedom systems with cubic nonlinearities, where direct numerical integration of the averaged equations of motion in the parameter regions of Hopf bifurcation resulted in period-doubling cascades to chaotic motions. Since then, studies with forced response of many more physical systems have uncovered these motions. One of the most comprehensive studies of this type, where a direct comparison of the dynamic behavior and amplitude-modulated chaotic motions, as predicted by the averaged equations, is made with the numerically generated response of the original dynamical system, is the work of Bajaj and Johnson [8]. This study investigated the nonlinear resonant motions of a stretched string which is excited in a plane, but is allowed to undergo nonplanar motions. The equations of motion for displacements in the two transverse directions are identical and hence all the natural modes of free vibration occur in pairs, that is, vibrational motions in the two planes have identical natural frequencies and mode shapes. It turns out that these motions are nonlinearly coupled due to the presence of stretching nonlinearity and this gives rise to one-to-one internal resonance. Due to this coupling, over certain range in the frequency and amplitude of external excitation, there result periodic motions that are not confined to the plane of excitation. These whirling motions of the string undergo bifurcations to amplitude-modulated motions, which can be either periodic or more complex depending on the other system parameters.

As indicated in the **problem statement** given above, one of the primary focus of the research undertaken in this project was to understand modal interactions in weakly nonlinear multi degree-of-freedom mechanical and structural systems. To accomplish this goal, the project followed five distinct modeling and analysis routes. On the analytical side, three distinct models of physical systems were considered and studied for resonant motions under harmonic forcing: **1.** Resonant motions and mode coupling in thin rectangular panels, **2.** An autoparametric two degree-of-freedom pendulum vibration absorber, and **3.** A double pendulum with the two pendulums oscillating in

two orthogonal planes. The rectangular plate system exemplifies systems with cubic, geometric nonlinearities with additional reflection symmetry. The latter two systems possess, respectively, quadratic, and cubic inertial nonlinearities, in addition to the gravitational restoring forces which are also odd functions. Additionally, having recognized that in all experimental involving resonant motions, the frequency response is more likely to be obtained by a slow sweep of the frequency through the resonant region, a study was initiated into the nonstationary response of single degree-of-freedom systems. Here the nonstationarity of the response arises due to the deterministic but time varying nature of the external excitation. Typical examples considered are the Duffing's equation with forcing and the Mathieu-Duffing equation; in each case the frequency of excitation are slowly varied in a linear fashion through the resonant region.

On the experimental side, an experimental rig was constructed for conducting experiments with rectangular plates with various aspect ratios under different harmonic excitations. The test rig allowed for the plate to be provided with different amounts of tension in the two orthogonal directions, although during the study funded by this project, only uniform in-plane loading case was considered. In the discussions of the four components of the study, we only present a summary of our findings. More detailed accounts are available in the Appendices of this report and the relevant publications.

## 2. NONLINEAR RESONANT RESPONSE OF RECTANGULAR PLATES
( publications: #4,6,10,15)

In this study, the weakly nonlinear response of isotropic rectangular plates to transverse harmonic loading has been investigated. The plate is modeled as a thin rectangular panel with uniform in-plane membrane loading, which is undergoing transverse vibrations. The model accounts for the effects of transverse bending. The plate is assumed to be sufficiently thin so as to neglect the effects of shear deformation and rotary inertia. It is assumed that the only nonlinearities that contribute to the response are those due to the in-plane stretching and they arise as a result of large transverse motions. This is the usual von Karman model for nonlinear motions and is known to be sufficiently accurate for the type of motions investigated. The plate is assumed to be simply supported at all the four sides. The equations for nonlinear plate motion, consisting of an equation for transverse motions, and an equation governing the in-plane stress function (Airy stress function), are coupled only nonlinearly, and depend on the aspect ratio of the plate. These equations are studied in this project, using the

standard Galerkin approximation, where by, the solution is assumed to be separable in terms of products of spatial and temporal functions. The spatial functions are the so called admissible functions that satisfy the appropriate boundary conditions. The solution for the coupled partial differential equations of motion for the plate are thus assumed to consist of a linear combination of N spatial functions whose amplitudes are unknown functions of time. Following the standard procedure, they are then reduced to a system of N second-order, nonlinear, ordinary differential equations for the temporal amplitude coefficients of the admissible functions.

In general, the spatial functions are often taken as the modal functions for the linear plate vibration problem satisfying the appropriate boundary conditions. Then, the N nonlinear ordinary differential equations are the equations governing the modal amplitudes. In their linear approximations, these equations are uncoupled, each one representing an oscillator with the corresponding plate frequency as the natural frequency. These natural frequencies are determined by the aspect ratio, the bending stiffness, and the in-plane tension or membrane forces in the plate.

The focus in this research is on modal coupling between the motions with different natural modes of vibration, and these are expected to arise when the natural frequencies are commensurable. The analysis of linear frequencies shows that, given an aspect ratio of the plate, there exist mode number combinations for which two or more modes are in 1:1 internal resonance. For example, when the aspect ratio is 1.633, the (3,1) mode and the (1,2) mode have the same natural frequency. Clearly, for a square plate, with aspect ratio one, all (m,n) modes are in 1:1 internal resonance with the corresponding (n,m) modes for n≠m. We have excluded the case of aspect ratio one from our study as it was considered earlier by Sethna and Yang [9]. Additionally, the square plate satisfies certain symmetry conditions, called the symmetry of the square, or the $D_4$ symmetry. We focus our attention on cases where only the reflection symmetry conditions are satisfied.

Now, given that two free vibration modes have close natural frequencies, nonlinear analysis needs to be performed to see if there arise the appropriate kind of nonlinear terms that lead to coupling in the motions of these two modes. This coupling can give rise to complex steady-state motions under resonant excitations. The resonant excitation can be either in primary resonance, or in secondary (sub- or super-harmonic) resonance, with the natural frequencies. Both the possibilities are investigated for the multi-mode Galerkin approximation of the rectangular plate, and results of these studies are summarized in the following subsections.

## 2.1 Primary Resonance

In this investigation, it is first shown that when two spatial modes are in 1:1 internal resonance, and these are the only modes that are directly excited by a harmonic transverse loading, the N-mode model for the plate response can be reduced further to only a two-mode model with only the modes in resonance being retained in the model. These conclusions are derived in the asymptotic limit of small nonlinear motions, using the method of averaging. This two-mode model is sufficient for predicting first-order approximations to the response of the plate. Thus, the subsequent analysis is restricted to the study of response, under resonant forcing, of two weakly coupled oscillators with nearly equal linear frequencies. The analysis is completely general in that it is valid for any two modes which satisfy the required resonance conditions.

Let the two modes in 1:1 internal resonance be two distinct, say, the (m,n) and the (r,s), modes of the plate. Furthermore, let the external transverse loading be harmonic in time with frequency near the natural frequency of the modes in resonance, and in the form of either the (m,n) or the (r,s) spatial mode. Then, using the method of averaging, the two second-order nonautonomous equations are reduced to four first-order equations governing the evolution of the amplitudes and phases of these spatial modes. These amplitude or averaged equations are nonlinearly coupled with cubic nonlinear terms, and contain nonhomogeneous terms pertaining to the external resonant excitation. They depend on the modal dampings, the amplitude and frequency of excitation, and the mode combinations assumed in internal resonance. A careful analysis of the steady-state constant solutions, and the various local bifurcations as a function of the system parameters, is undertaken and the results are interpreted in physical terms in relation to the motions of the plate. Initially, general results valid for any mode combination are derived. Numerical results are then presented for some typical cases. The principal findings can be summarized as follows:

1. Suppose that only one mode is directly excited. For small amplitude of excitation ( which is a function of the modal dampings), only the directly excited mode has a nonzero amplitude and it is essentially like the resonant response of the Duffing's equation. The response is of the hardening type with the slope depending on the aspect ratio and the mode number being considered. Thus, over a frequency interval, there are three possible periodic motions, the smallest and the largest ones being stable.

   As the amplitude of excitation is increased, there arise two pitchfork bifurcation points. As the frequency of excitation is slowly increased to come near exact external resonance, the single mode response in the upper branch becomes unstable and some of the energy is transferred to the mode that is not directly excited. This is essentially due to autoparametric instability of the single-

mode response. This nonzero response of the coupled-mode type exists over a frequency interval and connects to the other pitchfork bifurcation point. Analysis results show that the two pitchfork bifurcation points can either be in the upper branch , or one is in the upper branch and the other is in the middle branch. The nature of solutions (their number and stability) in this frequency interval is different in the two cases, and the two cases are distinguished by the ratios of the nonlinear coefficients. Thus, it is possible to classify the system based on the nonlinear coefficients and, hence, on the aspect ratio and the mode combination in resonance. While vibrating in a coupled-mode, the plate motion can be interpreted as consisting of a rotary wave which is in the form of a rotating nodal pattern. The actual shape of the nodal pattern is determined by the relative amplitudes of the two modes.

Further increase in the level of excitation results in the coupled-mode solutions branch undergoing a Hopf bifurcation over a frequency interval, thus giving rise to harmonically modulated periodic response of the plate. This corresponds to a modulated rotary wave traveling around the plate. As the amplitude of forcing is increased again, there arise period-doubling bifurcations in the averaged equations which ultimately result in chaotic amplitude modulations of the rotary wave motion in the plate. The phenomenon called crisis' is then seen to occur and the plate response settles down to periodic motion after long chaotic transients.

2. In order to understand the effects of various system parameters of damping, and forcing amplitude and frequency, bifurcation sets are constructed in the parameter space which clearly show the various type of solutions that exist in the different parameter regions.

3. When both modes are directly excited with force levels which differ by an order of magnitude, perturbed bifurcation theory provides an effective tool for understanding the resulting complicated response diagrams. Pitchfork bifurcations to coupled-mode solutions are modified to result in isolated solution branches.

4. It is also possible to study the dynamics of the averaged equations to predict analytically the existence of chaotic behavior for the harmonically excited plate. Preliminary results towards this end are derived in #6 to show that the unforced and undamped averaged system is integrable with homoclinic orbits biasymptotic to a saddle point. In the presence of small forcing, these orbits break to intersect transversely, leading to Smale horseshoes in the dynamics. Numerical evidence is given of this and it is shown that the parameter space can be divided into regions of differing dynamic response.

## 2.2 Secondary Resonances

One of the important characteristics of the response of nonlinear systems is the existence of subharmonic resonances [1]. When some appropriate conditions are satisfied, it is possible, even in the presence of damping, for a periodically excited nonlinear system to possess a response which is a combination of a contribution at the excitation frequency and a component at the system natural frequency. The system

natural frequency being a submultiple of the excitation frequency implies that the resulting response is a subharmonic oscillation. In general, there also coexists, for the system, a response at the excitation frequency, and the initial conditions determine which of the steady-state responses is achieved in an experiment or a numerical simulation. In single degree-of-freedom systems with harmonic excitation, depending on the type of nonlinearity, e.g., cubic or quadratic, the frequency of subharmonic response is respectively, one-third or one-half of that of the excitation frequency.

Although subharmonic resonance is one of the principal characteristics of a nonlinear system, the subharmonic responses of structures in the presence of internal resonances have been studied very rarely. In Mook et al. [10] were the first investigators to consider subharmonic response of structural elements with internal resonances. Their attention was focused on the case $\Omega \approx 2\omega_2$, both in the absence and in the presence of internal resonance of the form $\omega_2 \approx 2\omega_1$, where $\Omega$ is the forcing frequency , and $\omega_1$ and $\omega_2$ are the two natural frequencies. In the presence of 2-to-1 internal resonance, it was noted that the energy may be transferred between the two modes, and this can lead to a saturation phenomenon in the subharmonic response.

In the present study, following the approach taken in the primary resonance case, a two-mode model of the rectangular plate, retaining the two distinct modes in 1-to-1 internal resonance, is considered. The method of averaging is used to obtain a first-order approximation to the response to harmonic excitation transverse to the plate surface. The averaged equations represent the evolution of amplitudes and phases of the interacting spatial modes, and they depend on the amplitudes and frequency of the components of excitation in the two spatial modes. They, in addition, depend on the nonlinear coefficients of the system determined by the plate aspect ratio and the modes in resonance. As in the case of primary resonance, the cases of direct excitation of only one of the modes, and of both the modes simultaneously, are considered separately. The results of the study can be summarized as follows:

1. Two different approaches are utilized to perform the 'so-called' averaging. One approach is based on the formal theory of averaging [11], where a small parameter, a measure of smallness, is explicitly introduced in the analysis. In the other approach, harmonic balance is utilized to obtain the amplitude equations. The analysis clearly shows the range of system parameters where the results of the two approaches are essentially the same, and where substantial differences arise.
2. There are different types of steady-state constant solutions. The zero solution corresponds to the harmonic solution and a stability analysis shows that it is always stable. When only one plate mode is directly excited, the subharmonic

response can be either unimodal or may be coupled-mode. This is found to depend on the excitation parameters as well as on the nonlinear coefficients. For example, it is found that when the (1,2) mode is directly excited, only harmonic and unimodal subharmonic responses exist. The response of the plate when (3,1) mode is directly excited, is however qualitatively quite different. For some excitation levels, it is possible to find a frequency interval in which, a single-mode subharmonic, a coupled-mode subharmonic, and a single-mode harmonic response are all stable and coexist. Chaotic motions also arise in this case for the averaged equations, implying amplitude modulated subharmonic response of the plate. Bifurcation sets, clearly showing the parameter combinations leading to the various types of response diagrams are also constructed.

3. The results of averaging analysis are also verified using direct numerical integration of the modal equations. The results show a good correspondence between the solutions of the averaged system and those of the original system.

## 3. DYNAMICS OF THE PENDULUM VIBRATION ABSORBER
## (publications: #1,7,12,13,17)

The autoparametric system considered in this study consists of a primary spring-mass-dashpot system coupled to a damped simple pendulum. Its equations of motion, to the first order nonlinear approximation, have coupled quadratic nonlinearities. Many investigations have been performed in the literature to determine the dynamics of the system for small nonlinear motions, both, in the absence and presence of external excitations. The most interesting dynamics, and coupling between the translational and rotational motions is found to occur when the linear natural frequency of the translational mode of vibration is approximately twice the natural frequency of the rotational mode of vibration. When the external forcing is in resonance with the translational mode, the amplitude of the translational mode builds up as the frequency of excitation is slowly increased through the resonance region. At some frequency before the exact resonance is reached, the pendulum motion gets excited through its quadratic nonlinear coupling with the translational mode, and the amplitude of the primary mass (translational mode) saturates to a constant value.

In a series of works [12,13], Hatwal et al. used the harmonic balance technique to construct approximate periodic solutions and discuss the dynamic behavior of the pendulum vibration absorber. They also undertook direct numerical simulation of the equations of motion and conducted experiments with a system fabricated to confirm to the model. They observed some amplitude modulated response of the system in the coupled mode over a frequency interval near the resonance frequency, and found chaotic motions in their experimental system.

### 3.1 First-Order Averaging Analysis

In one study (publications #1,12) undertaken as part of this project, we have used the first-order averaging technique to investigate the saturation behavior of the system and have constructed parameter regions where the pendulum is effective in terms of limiting the motion of the translational mode. The following conclusions are drawn based on this investigation:

1. The amplitude of harmonic response of the primary mass, when excited by a harmonic force with frequency near the natural frequency, gets limited by saturation in a small frequency interval around resonance. This frequency interval is a function of the modal dampings, and the difference in frequency of the translational mode and twice the frequency of the rotational mode. It is interesting to note that there is a frequency interval over which both the saturated coupled mode periodic response and the single mode translational response coexist, and both of them are stable. In addition, the saturated periodic response of the primary mass over this frequency interval is larger than the response in only the translational mode in which the pendulum is essentially stationary. This has interesting implications for the usefulness of the device as a vibration absorber.

2. If the modal dampings are small compared to the amplitude of external excitation, the saturated periodic response can be unstable over a small frequency interval and result in amplitude-modulated motion. The amplitude modulations exhibit quite a complex dynamics including chaotic behavior and transient chaos.

## 3.2 Second-Order Averaging Analysis

In the next part of the study of the response of the absorber system, a second-order averaging analysis is undertaken (publication #17). It is motivated by the desire to explore the dependence of the dynamics on the forcing amplitude, and the expectation that the saturation phenomenon must be mathematically unstable in the sense that the amplitude of periodic response in this mode is really not constant, but changes slowly with the frequency. This analysis, performed in part using symbolic computations and AUTO (a package for numerical bifurcation analysis), clearly shows that the saturation phenomenon does not persist and is an artifact of the first-order approximation. The bigger surprise is the occurrence of many additional branches in the periodic solutions possible. Some of these solutions turn out to be spurious and should not be taken seriously as they are outside of the range of parameter values for which the averaging analysis is expected to be valid. This analysis also shows that as the amplitude of forcing is increased the frequency interval over which complex amplitude-modulated motions occur shrinks. One of the mechanisms responsible for the emergence of chaotic behavior is identified to be that of the Silnikov type. It is associated with the existence of a homoclinic orbit bi-asymptotic to the single-mode solution which is a saddle-focus.

Thus, the periodic coupled-mode motions, which are almost saturated, exist over most of the frequency interval of the existence of the coupled-mode response.

## 3.3 Chaotic Dynamics of Two Degree-of-Freedom Systems with 1:2 Internal Resonance

As already explained, the pendulum vibration absorber is effective when it is in internal resonance with the primary mass, and the frequency of the primary system is nearly twice that of the pendulum. In general, many two degree-of-freedom systems with quadratic nonlinearities exhibit similar dynamics. In fact, it can be shown that in the first approximation, the dynamics of all these systems is governed, upto a change in scale, by the same set of averaged equations. Thus, the existence of amplitude-modulated dynamics is also assured in this class of systems. A natural question to then consider is: are there situations or parameter combinations for which one can analytically show the existence of chaotic behavior? This is answered in an affirmative in this part of the study. The study results are significant in that there are very few dynamical systems of two degrees-of-freedom for which it has been possible to show the existence of chaos in an analytical manner.

In this study, general dynamical systems with two degrees-of-freedom, with quadratic nonlinearities and harmonic external excitation are investigated. The 1:2 subharmonic internal resonance case is analyzed. Under resonant forcing conditions, the method of averaging is used to obtain a set of four first-order amplitude equations that govern the first-order approximation to the response. An analytical technique, based on Melnikov's method is used to predict the parameter range for which the chaotic dynamics exists in the undamped averaged system. It is shown that there exist heteroclinic orbits in the unforced and undamped averaged system which is completely integrable. Analysis results then show that any amount of external forcing will result in transversal intersections of the perturbed stable and unstable manifolds leading to Smale horseshoes in the dynamics of the system. It is essential for this that the internal mistuning be nonzero. This is significant since the same condition was needed to be satisfied in order for a Hopf bifurcation, and the resulting amplitude-modulated dynamics, to arise in the averaged equations. Although, the analytical results are not available when damping is included in the system model, numerical studies show that the chaotic responses are quite common in these systems and they occur even in the presence of damping.

## 4. DYNAMICS OF THE ORTHOGONAL DOUBLE PENDULUM
## (publications: #2,5)

In this study, we consider the nonlinear dynamical motions of an orthogonal double pendulum under base excitation. The system consists of two pendulums , one attached to a suspension point and the other attached at the free end of the first one. The axes of the two pivots or suspensions are orthogonal to each other, and thus the motions of the two pendulums are confined to two orthogonal planes. The equations of motion for the two pendulums are coupled only due to inertial terms, and these are cubic in generalized coordinates and velocities. Thus, the two pendulums essentially execute independent linear motions in two orthogonal planes, and the natural frequencies for linear motions can be changed by adjusting their lengths. One set of internal resonance conditions arises when the two modes have near identical frequencies, and this is the case pursued in this investigation. The reason for interest in this system is the inertial nature of nonlinearities as opposed to geometric nonlinearities in the case of the rectangular plate system.

The response of the system to harmonic base motions is considered. The base excitation can be in either the plane of one of the pendulums, or can excite both the pendulums. For the case when the excitation frequency is near the linear natural frequencies (external resonance), method of averaging is used to obtain the averaged or amplitude equations. These equations depend on seven parameters including the frequency of external excitation, the two linear natural frequencies, the amplitude of excitation, the modal dampings, and the mass of each pendulum. These averaged equations are perturbations of a class of systems called the systems with $Z_2 \oplus Z_2$ symmetry, and have arisen in previous studies with many physical systems; namely, the motions of a nearly square plate, and the dynamics of surface waves in nearly square containers. Solutions of these amplitude equations are investigated using the local bifurcation theory. The following results are derived from the study:

1. When the motion of the point of suspension is restricted to the plane of either of the two pendulums, sufficiently large amplitude of base motion results in nonplanar motions of the system. Many stable branches of nonplanar periodic responses, called the mixed-mode motions, are possible. These solutions exist for excitation frequencies above as well as below the resonant frequency. Thus, in some frequency interval near resonance, upto two stable mixed-mode solutions can coexist with a stable single-mode solution. Depending on other system parameters, the mixed-mode solutions can be of much larger amplitude compared to the response in single mode.

2. For certain regions in the parameter space, the periodic nonplanar motions become unstable and bifurcate to stable quasiperiodic amplitude-modulated

motions with a slow and a fast frequency. For higher excitation levels, the quasiperiodic motions may also loose stability and result in stable chaotic amplitude-modulated motions.

3. Although, the linear dynamics of the system is independent of the mass ratio of the two particles, there is a critical value of the mass ratio which distinguishes two distinct types of response curves for the nonlinear system.

# 5. RESPONSE OF NONLINEAR SYSTEMS TO NONSTATIONARY EXCITATIONS (publications: #8,16)

Nonlinear dynamical systems are often characterized by control parameters that are not stationary but vary slowly in time. The response of the nonlinear system, in such a case, is qualitatively different from the response when the parameters are stationary, especially in the neighborhood of the bifurcation points. In general, an effective bifurcation occurs, away from the point at which the static bifurcation occurs and the resulting motion exhibits interesting phenomena such as sudden jumps and oscillations around the static equilibrium solutions. A variety of engineering and physical systems can exhibit these phenomena. The passage through resonance in rotating machinery and gyroscopic systems, vibrations in some aerospace structures, and flow-induced vibrations due to deceleration during re-entry, are some relevant examples.

Analytical studies into the vibrations of weakly nonlinear systems have been traditionally carried out by the method of averaging, and multiple time scale analysis, etc. These methods can be extended to study the response when certain parameters are non-stationary, if the parameters are assumed to be varying slowly in time. An overview of asymptotic methods used in the study of these non-stationary systems can be found in Mitropolskii [14]. The application of these techniques to nonlinear systems with slowly varying parameters results in an averaged system of equations which is time-dependent. Consider a specific example; the transition through primary resonance in the Duffing's oscillator, with the excitation frequency as the slowly varying system parameter. In dimensionless form, the Duffing's equation is given by:

$$\frac{d^2x}{dt^2} + 2\delta\frac{dx}{dt} + x + x^3 = E_1 \sin\theta,$$

where, $\chi$ is the displacement of the oscillator and is of $O(\varepsilon^{1/2})$, with $\varepsilon \ll 1$. The damping $\delta$ is of $O(\varepsilon)$, and the amplitude of forcing $E_1$ is of $O(\varepsilon^{3/2})$. The instantaneous frequency of excitation is $\lambda = \lambda(\varepsilon t) = \frac{d\theta}{dt}$, so that the frequency changes slowly with time. If the solution is assumed to be of the form $\chi = a(t)\cos(\theta + \psi)$, where a and $\psi$ are the slowly varying amplitude and phase, respectively, the amplitude and the phase satisfy the following equations:

$$\frac{da}{dt} = -\delta a - \frac{E_1}{1+\lambda(T)}\cos\psi,$$

$$\frac{d\psi}{dt} = 1 - \lambda(T) + \frac{3a^2}{8} + \frac{E_1}{a(1+\lambda(T))}\sin\psi,$$

where T=εt is the slow time. This is a non-autonomous system and most investigations into such systems have relied on direct numerical integration of these equations.

As is well known, in the case when the frequency λ is a constant, the response curves for the above system have two turning points where the solution jumps down or up to another stable solution branch. An unstable solution branch connects the two turning points. When the parameter λ changes with time, however, numerical simulations show that the jump is delayed in both the forward and backward sweep. The length of time delay depends on the sweep rate as well as on the initial conditions. Furthermore, the solution oscillates around the stable equilibrium branch towards which it has jumped before settling down. These results are derived in this investigation, using ideas from the center manifold theory, and the developments in dynamic bifurcation theory [15]. The reader is referred to the publications cited above for details of the analysis technique and results.

## 6. EXPERIMENTAL INVESTIGATIONS INTO THE FORCED RESPONSE OF A RECTANGULAR PLATE (publications: #3,9):

In this component of the research, it was proposed to construct an experimental rig which would then be used to investigate the forced response of rectangular plates to harmonic excitation. One important objective of the research was to compare the analytically predicted motions in coupled-mode responses in the plate with specific aspect ratio (item 2. above) with those actually observed in an experiment. As explained above, the theoretical analysis was performed for thin isotropic metallic plates undergoing nonlinear motions when there are two distinct spatial modes with nearly identical linear natural frequencies. There arises nonlinear coupling in the two modes under appropriate excitation conditions and the response can be quite complex. It was shown that, over a frequency interval near the natural frequency, coupled-mode harmonic motions can co-exist with single-mode harmonic motions and amplitude-modulated coupled-mode motions.

In order to duplicate analytical results in the experimental investigation, it is critical that the conditions assumed for the analysis be clearly understood and a careful attempt be made to reproduce these conditions in the experiment. With this in mind, a thin rectangular plate of mild steel (thickness = 0.265 mm) with aspect ratio κ=1.633

(length = 65.41 cm, width = 40.16 cm) was chosen as the desired plate. The plate needs to have simply supported boundary conditions, and should have a uniform and large in-plane tension. For this aspect ratio and boundary conditions, the linear plate analysis predicts that the (3,1) and (1,2) plates modes are in 1:1 internal resonance. There were two major difficulties in reproducing the linear analytical results. First was the problem of creating a simply supported edge. Since the plate is very thin, a clamped edge should be a good approximation to a simply supported edge. There are, however, irregularities in the clamp and plate surfaces and nonuniformities in the clamping force. The second major obstacle was that of producing a uniform tension force in the plate. In order to achieve this, the clamping fixture was mounted on 14 bolts around the perimeter of the plate. Each of these bolts could be individually tightened with a measured torque. The relation between this torque and the tension force in the bolt was presumed to be the same for each bolt, which is certainly not the case. These nonuniformities in the tension and boundary conditions resulted in differences between the natural frequencies and mode shapes of the experimental plate and those predicted by the theory.

A variety of techniques for exciting the plate were attempted. Yasuda and Asano [16], whose work was the original motivation for this study, used electromagnetic exciters. In our set-up, they were found to be inadequate for exciting nonlinear behavior of the plate. An electromechanical shaker was also not satisfactory as it's force input could not be maintained constant. It was therefore decided to use an array of 6 loudspeakers to acoustically excite the plate. This had the added advantage that the mode shape of the forcing could be controlled relatively easily.

To determine the linear natural frequencies of the plate, it was excited by a loudspeaker with low-amplitude random noise. The input to the loudspeaker and the response of the plate were recorded with the same B&K 2032 signal analyzer which generated the random noise signal. The linear transfer function was then calculated by taking 100 averages in the estimation process. The resulting transfer function has a frequency resolution of 0.5 Hz. It was found in the experiment that the (1,2) mode occurred at nearly twice the natural frequency of the (1,1) mode, had a small damping factor and was well isolated from other modes. The (2,2) mode in theory occurs at twice the natural frequency of the (1,1) mode. Although the theory predicts that the (3,1) and (1,2) modes have coincident natural frequencies, in the experimental set-up these modes were well separated. However, the (3,2) and (4,1) modes of the experimental plate were nearly coincident and therefore, the responses of these modes were used to demonstrate the complex dynamics possible due to coupled-mode behavior.

Details of the experimental set-up, the excitation mechanisms, the measurement instrumentation, and the experimental results obtained, can be found in the conference publication given in Appendix 3. Because of the differences in theoretical linear frequencies and the experimentally measured plate frequencies, and the modes that were near coincident in the two cases, only qualitative comparisons between the expected and experimental nonlinear responses for the isolated and coincident modes were meaningful. These were found to be reasonable though there is much room for improvement, both in the experimental rig in approximating the idealized conditions of the theoretical analysis, and in the instrumentation used for data acquisition and analysis. These are the objects of our on going research.

## 7. CONCLUSIONS

The research supported through this grant has allowed us to more clearly understand the role played by modal interactions in giving rise to complex responses even under conditions of seemingly simple external excitations. It is found that both 1:1 and 1:2 internal resonances result in amplitude-modulated dynamic response of the system when the system is excited by a resonant harmonic forcing. Under some conditions, for sufficiently small damping, even a small forcing can result in chaotic dynamics for the equations that determine the evolution of the amplitudes and phases of the harmonic response of coupled two degrees-of-freedom system. It is clearly shown that the results obtained by asymptotic techniques are valid for the original physical systems even when the responses are not periodic. Preliminary results of some experiments on a harmonically excited thin rectangular steel plate agree, qualitatively, with the results of theoretical analyses.

## 8. REFERENCES

1. Nayfeh, A. H. and Mook, D. T., Nonlinear oscillations, Wiley-Interscience, New York, 1979.

2. Sethna, P. R., Coupling in certain classes of weakly nonlinear vibrating systems, In Nonlinear Differential Equations and Nonlinear Mechanics, J. P. LaSalle and S. Lefschetz, eds., Academic Press, New York, 1963, 58-70.

3. Miles, J. W., Stability of forced oscillations of a spherical pendulum, Q. Appl. Math., 20, 1962, 21-32.

4. Sethna, P. R., Vibrations of dynamical systems with quadratic nonlinearities, J. Appl. Mech., 32, 1965, 576-582.

5. Sethna, P. R. and Bajaj, A. K., Bifurcations in dynamical systems with internal resonance, J. Appl. Mech., 45, 1978, 895-902.

6. Miles, J. W., Resonant motion of a spherical pendulum, Physica D, 11, 1984, 309-323.

7. Tousi, S. and Bajaj, A. K., Period-doubling bifurcations and modulated motions in forced mechanical systems, J. Appl. Mech., 52, 1985, 446-452.

8. Bajaj, A. K. and Johnson, J. M., On the amplitude dynamics and crisis in resonant motions of stretched strings, Phil. Trans. Roy. Soc. Lond. A, 338, 1992, 1-41.

9. Yang, X. L. and Sethna, P. R., Nonlinear phenomena in forced vibrations of a nearly square plate - antisymmetric case, J. Sound and Vibration, 155, 1992, 413-441.

10. Mook, D. T., Plaut, R. H. and HaQuang, N., The influence of an internal resonance on non-linear structural vibrations under subharmonic resonance conditions, J. Sound and Vibration, 102, 1985, 473-492.

11. Hale, J. K., Ordinary differential equations, Wiley-Interscience, New York, 1969.

12. Hatwal, H, Mallik, A. K. and Ghosh, A., Forced nonlinear oscillations of an autoparametric system-part 1: periodic responses, J. Appl. Mech., 50, 1983, 657-662.

13. Hatwal, H, Mallik, A. K. and Ghosh, A., Forced nonlinear oscillations of an autoparametric system-part 2: chaotic responses, J. Appl. Mech., 50, 1983, 663-668.

14. Mitropolskii, V. A., Problems of the asymptotic theory of nonstationary vibrations, Israel Program of Scientific Translation, 1965.

15. Haberman, R., Slowly varying jump and transition phenomena associated with algebraic bifurcation problems, SIAM J. Appl. Math., 37(1), 1979, 69-106.

16. Yasuda, K. and Asano, T., Nonlinear forced oscillations of a rectangular membrane with degenerate modes, Bull. of JSME, 29, 1986, 3090-3095.

# APPENDIX 1

## Resonant dynamics of an autoparametric system. a study using higher order averaging

B. Banerjee, A. K. Bajaj, P. Davies

submitted to

# Resonant Dynamics of an Autoparametric System.
## A Study Using Higher order Averaging

Bappaditya Banerjee
Anil K. Bajaj
Patricia Davies

School of Mechanical Engineering
Purdue University
West Lafayette, IN 47907-1288

July 1994

## Abstract

The autoparametric system considered here consists of a primary spring-mass-dashpot system coupled with a damped simple pendulum. It serves as an useful example of two degree-of-freedom nonlinear systems that exhibit complex dynamic behavior. The system exhibits 1:2 internal resonance and amplitude-modulated chaos under harmonic forcing conditions. First-order averaging studies of this system using AUTO and DSTOOLS have yielded useful information about the amplitude dynamics of this system. Response curves of the system indicate saturation. The Pitchfork bifurcation sets and the Hopf bifurcation sets are found to be symmetric. The period-doubling route to chaotic solutions is observed. However, questions about the range of the small parameter $\epsilon$ (a function of the forcing amplitude) for which the solutions are valid cannot be answered by a first-order study. Also, some unstable dynamical behavior, like saturation, may not persist when higher-order nonlinear effects are taken into account. Second-order averaging of the system is undertaken to address these issues. Loss of saturation is observed in the steady-state amplitude responses. The breaking of symmetry in the various bifurcation sets becomes apparent as a consequence of $\epsilon$ appearing in the averaged equations. The dynamics of the system is found to be very sensitive to damping, with extremely complicated behavior arising for low values of damping. For larger $\epsilon$, second-order averaging predicts additional Pitchfork and Hopf bifurcation points in the single-mode response. For the response between the two Hopf bifurcation points from the coupled-mode solution branch, the period-doubling as well as the Silnikov mechanism for chaos are observed. The predictions of the averaged equations are verified qualitatively for the original equations.

# 1   Introduction

The Autoparametric Vibration Absorber (the autoparametric system) of Haxton and Barr (1972) is an useful example to illustrate the weakly non-linear, resonant response of a multi degree-of-freedom system. The device consists of a main spring-mass-damper system, with a damped pendulum attached to it (Figure 1). Both subsystems are basically linear elements, with quadratic inertial nonlinearities arising at the lowest order due to the large

amplitudes of motion. Internal resonances give rise to coupling between the two linear response modes.

Haxton and Barr (1979) introduced the autoparametric system with limitations on the amplitude of excitation so as to maintain a harmonic response. Hatwal et al. (1983a, 1983b), used the method of Harmonic Balance and direct numerical integration to demonstrate amplitude-modulated and chaotic motions in the system. A study of general two degrees-of-freedom systems with quadratic nonlinearities was carried out by Sethna (1965). Sethna and Bajaj (1978) and Tousi and Bajaj (1985) used averaging to show that for certain superharmonic resonances, the averaged system can undergo Hopf bifurcations, leading to amplitude and phase-modulated motions. Miles (1984) showed that these amplitude-modulated motions can themselves bifurcate to chaotic amplitude modulations. Bajaj et al. (1994) carried out a detailed stability and bifurcation analysis of the averaged equations for the autoparametric system. Their first-order averaging analysis reveals that the locked-pendulum response of the system bifurcates to a coupled-mode response for some ranges of excitation frequencies. The locked-mode motion corresponds to the motion of the primary mass when the pendulum remains vertical. The coupled-mode response can itself undergo Hopf bifurcation to limit cycle motions, and these limit cycles can undergo a period-doubling transition to chaos. They also demonstrate the existence of phenomenon like saturation, in the amplitude of response.

In accordance with the theory of averaging, (Murdock, 1991, 1988), constant solutions of the averaged equations correspond to periodic solutions of the original system. Periodic solutions of the averaged equations imply almost periodic (amplitude and phase-modulated) motions of the autoparametric system. All these results hold for sufficiently small values of the expansion parameter $\epsilon$. However, in a first-order averaging analysis, $\epsilon$ gets absorbed into the slow time scale. Therefore, to understand the effects of $\epsilon$ upon the predictions of the averaging analysis, it is essential to go from first-order to a higher-order averaging. In the second-order averaged equations of the autoparametric system, $\epsilon$ appears explicitly and its effects upon the motion can be studied by varying $\epsilon$ as a parameter. Further, the results from the second-order analysis are expected to hold for a larger time scale of $O(\frac{1}{\epsilon^2})$ as discussed in Holmes and Holmes (1981) and Robinson (1983).

The purpose of this study is to investigate the modifications of the results predicted by the first-order averaging study. The effects of $\epsilon$ as a parameter

3

upon the amplitude dynamics of the autoparametric system is studied. It is found that unstable phenomena like saturation, described by the first-order-averaging, do not persist (Lee and Perkins, 1992). It is easy to see the change in the nature of the amplitude response of the averaged system as $\epsilon$ is varied. However, with the aid of numerical methods, it is found that for large $\epsilon$, the second-order analysis itself gives rise to predictions which do not correspond to the behavior observed in the physical system. It is now possible to qualitatively gauge the $\epsilon$ for which the second order analysis no longer holds. The predictions which are consistent with both the first-order and second-order analysis must therefore be indicative of the true response of the autoparametric system.

# 2    System description and equations of motion

The equations of motion for the autoparametric system (Hatwal et al., 1983a,b) are

$$
\begin{aligned}
(M + m)\ddot{x} + c_1\dot{x} + k_1 x - ml(\ddot{\theta}\sin\theta + \dot{\theta}^2\cos\theta) &= P_0\cos\omega t, \\
ml^2\ddot{\theta} + c_2\dot{\theta} + (mgl - ml\ddot{x})\sin\theta &= 0,
\end{aligned}
\tag{1}
$$

where

M is the mass of the block; $c_1$ and $c_2$ are the coefficients of viscous damping; $k_1$ is the spring constant; m is the mass of the pendulum bob; $l$ is the length of the pendulum; $x$ is the vertical displacement of the block; $\theta$ is the angular displacement of the pendulum; $P_0$ is the amplitude of external forcing; and $\omega$ is the frequency of the forcing.

In nondimensional form, these equations can be written as (Bajaj et al., 1994),

$$
\begin{aligned}
\eta'' &+ \frac{2\xi_1}{p(1+R)}\eta' + \frac{1}{p^2(1+R)}\eta - \frac{R}{1+R}(\theta''\sin\theta + \theta'^2\cos\theta) = \frac{F}{(1+R)p^2}\cos\tau, \\
\theta'' &+ \frac{2\xi_2 q}{p\sqrt{1+R}}\theta' + \left[\frac{q^2}{p^2(1+R)} - \eta''\right]\sin\theta = 0,
\end{aligned}
\tag{2}
$$

where the following transformations have been used:

4

$\tau = \omega t$, dimensionless time ; $\eta = x/l$ ; $r = m/M$, mass ratio ; $F = P_0/(k_1 l)$ ; $p = \omega/\Omega_1$, excitation frequency ratio ; $\Omega_1 = \sqrt{(k_1/M)}$, natural frequency of the block ; $q = \omega_2/\omega_1$, frequency ratio of the combined system ; $\omega_1 = \sqrt{k_1/(M+m)}$, frequency of the locked pendulum ; $\omega_2 = \sqrt{g/l}$, natural frequency of the pendulum ; $\xi_1 = c_1/(2M\Omega_1)$, damping ratio of the block and $\xi_2 = c_2/(2ml^2\omega_2)$, damping ratio of the pendulum .

# 3   Formulation and the averaged equations

To study small motions near resonant excitations, we introduce the small expansion parameter $\epsilon$ as

$\eta = \epsilon\hat{\eta}, \theta = \epsilon\hat{\theta}, \xi_1 = \epsilon\hat{\xi}_1, \xi_2 = \epsilon\hat{\xi}_2, F = \epsilon^2\hat{F}$, where $0 < \epsilon \ll 1$,

into equations (2) and expand in a Taylor's series about $\epsilon = 0$ up to $O(\epsilon^3)$ to obtain

$$
\begin{aligned}
\hat{\eta}'' + \Omega_{n1}^2\hat{\eta} &= \epsilon(\hat{F}\Omega_{n1}^2\cos\tau - 2\bar{\xi}_1\Omega_{n1}^2\hat{\eta}' + 8\bar{\theta}'^2 - 8\Omega_{n2}^2\bar{\theta}^2) \\
&- 8\bar{\theta}\epsilon^2(4\bar{\xi}_2\Omega_{n2}\bar{\theta}' + \Omega_{n1}^2\bar{\theta}\hat{\eta}) \\
&+ O(\epsilon^3), \\
\bar{\theta}'' + \Omega_{n2}^2\bar{\theta} &= \epsilon(-4\bar{\xi}_2\Omega_{n2}\bar{\theta}' - \Omega_{n1}^2\bar{\theta}\hat{\eta}) \\
&+ \epsilon^2\bar{\theta}[\Omega_{n1}^2(\hat{F}\cos\tau - 2\bar{\xi}_1\hat{\eta}') + 8\bar{\theta}'^2 \\
&+ \bar{\theta}^3\Omega_{n2}^2(4(1+R)/(3R) - 8)] \\
&+ O(\epsilon^3),
\end{aligned} \tag{3}
$$

where the following scale transformations have also been used
$\bar{\theta} = \hat{\theta}\sqrt{R/(8(1+R))}$, $\bar{\xi}_1 = p\hat{\xi}_1$, $\bar{\xi}_2 = \hat{\xi}_2/2$, $\Omega_{n1} = 1/(p\sqrt{1+R})$, and $\Omega_{n2} = q/(p\sqrt{1+R})$.

By defining the state vector as

$$
\underline{z} = [\hat{\eta}_1, \hat{\eta}_2, \bar{\theta}_1, \bar{\theta}_2]^T = [\hat{\eta}, \hat{\eta}', \bar{\theta}, \bar{\theta}']^T, \tag{4}
$$

we obtain the equations (3) in the vector form

$$
\underline{z}' = \underline{A}\,\underline{z} + \epsilon\underline{h}_1(\underline{z}, \tau) + \epsilon^2\underline{h}_2(\underline{z}, \tau) + O(\epsilon^3), \tag{5}
$$

5

where

$$A = \begin{bmatrix} 0 & 1 & 0 & 0 \\ -\Omega_{n1}^2 & 0 & 0 & 0 \\ 0 & 0 & 0 & 1 \\ 0 & 0 & -\Omega_{n2}^2 & 0 \end{bmatrix}, \tag{6}$$

$$\underline{h}_1 = \left\{ \begin{array}{c} 0 \\ \hat{F}\Omega_{n1}^2 \cos\tau - 2\bar{\xi}_1\Omega_{n1}^2\hat{\eta}_2 + 8\bar{\theta}_2^{\,2} - 8\Omega_{n2}^2\bar{\theta}_1^{\,2} \\ 0 \\ -4\bar{\xi}_2\Omega_{n2}\bar{\theta}_2 - \Omega_{n1}^2\bar{\theta}_1\hat{\eta}_1 \end{array} \right\}, \tag{7}$$

and

$$\underline{h}_2 = \left\{ \begin{array}{c} 0 \\ -8\bar{\theta}_1(4\bar{\xi}_2\Omega_{n2}\bar{\theta}_2 + \Omega_{n1}^2\bar{\theta}_1\hat{\eta}_1) \\ 0 \\ \bar{\theta}_1\left[\Omega_{n1}^2(\hat{F}\cos\tau - 2\bar{\xi}_1\hat{\eta}_2) + 8\bar{\theta}_2^{\,2}\right] + \bar{\theta}_1^{\,3}\Omega_{n2}^2\left(\frac{4(1+R)}{3R} - 8\right) \end{array} \right\}. \tag{8}$$

Let $\underline{\phi}$ be a fundamental matrix solution of the system (5), with $\epsilon = 0$, that is,

$$\underline{\phi} = \begin{bmatrix} \cos(\Omega_{n1}\tau) & \sin(\Omega_{n1}\tau) & 0 & 0 \\ -\Omega_{n1}\sin(\Omega_{n1}\tau) & \Omega_{n1}\cos(\Omega_1\tau) & 0 & 0 \\ 0 & 0 & \cos(\Omega_{n2}\tau) & \sin(\Omega_{n2}\tau) \\ 0 & 0 & -\Omega_{n2}\sin(\Omega_{n2}\tau) & \Omega_{n2}\cos(\Omega_{n2}\tau) \end{bmatrix}. \tag{9}$$

Then, choosing $\underline{\phi}$ as a variation of parameter transformation, that is $\underline{z} = \underline{\phi}\underline{u}$, where $\underline{u} = [u_1, u_2, u_3, u_4]^T$, equation (5) reduces to the standard form for averaging

$$\underline{u}' = \epsilon\underline{X}_1(\underline{u}, \tau) + \epsilon^2\underline{X}_2(\underline{u}, \tau) + O(\epsilon^3). \tag{10}$$

Now, let $\underline{X}_i = M_n[\underline{X}_i] + O_s[\underline{X}_i]$, where the two terms on the right hand side are the mean part of $\underline{X}_i$, $M_n[\underline{X}_i] = \lim_{T\to\infty}\frac{1}{T}\int_0^T \underline{X}_i(\underline{u}, \tau)d\tau$, and the oscillatory part of $\underline{X}_i$, $O_s[\underline{X}_i] = \underline{X}_i - M_n[\underline{X}_i]$.

The essential idea of the method of averaging is to seek a near identity transformation

$$\underline{u} = \underline{x} + \epsilon \underline{w}_1(\underline{x},\tau) + \epsilon^2 \underline{w}_2(\underline{x},\tau) + O(\epsilon^3), \tag{11}$$

which transforms equation (10) into a much simpler and an autonomous system for the variable $\underline{x}$, atleast for sufficiently small $\epsilon$. For this, we substitute equation (11) into equation (10). Note here that $\underline{x} = [x_1, y_1, x_2, y_2]^T$. Now expand the functions $\underline{X}_i$ in powers of $\epsilon$. This results in an equation for $\underline{x}$ which involves time derivatives and Jacobians of the $\underline{w}_i$. Now we seek $\underline{w}_i$ such that the first-order and second-order oscillatory terms in the equations for $\underline{x}$ are eliminated. Dropping terms of $O(\epsilon^3)$ and higher, we obtain the second-order averaged equations (Murdock, 1988, 1991; Wiggins, 1990):

$$\underline{x}' = M_n[\underline{X}_1] + \epsilon M_n[\underline{f}_2]. \tag{12}$$

The prime here denotes the derivative with respect to the slow time $\bar{\tau} = \epsilon\tau$ and

$$
\begin{aligned}
\underline{f}_2 &= M_n[\underline{X}_1]_{,\underline{x}}\,\underline{w}_1 + O_s[\underline{X}_1]_{,\underline{x}}\,\underline{w}_1 + M_n[\underline{X}_2] + O_s[\underline{X}_2] - \underline{w}_{1,\underline{x}}\,M_n[\underline{X}_1], \\
M_n[\underline{f}_2] &= M_n[\underline{X}_2] + M_n[O_s[\underline{X}_1]_{,\underline{x}}\,\underline{w}_1], \\
O_s[\underline{f}_2] &= M_n[\underline{X}_1]_{,\underline{x}}\,\underline{w}_1 + O_s[O_s[\underline{X}_1]_{,\underline{x}}\,\underline{w}_1] + O_s[\underline{X}_2] - \underline{w}_{1,\underline{x}}\,M_n[\underline{X}_1], \\
O_s[\underline{X}_1] &= \underline{X}_1 - M_n[\underline{X}_1], \\
\underline{w}_1 &= \int O_s[\underline{X}_1]d\tau, \\
\underline{w}_2 &= \int O_s[\underline{X}_2]d\tau, 
\end{aligned}
\tag{13}
$$

where $[\underline{X}_i]_{,\underline{x}}$ is the Frechet derivative of $\underline{X}_i$ with respect to $\underline{x}$.

To study the 1:2 subharmonic internal resonance case, we choose $\Omega_{n1}^2 = 1 + 2\epsilon\sigma_1$ and $\Omega_{n2}^2 = \frac{1}{4} + \epsilon\sigma_2$, where $\sigma_1$ and $\sigma_2$ are the mistuning parameters. They characterize the differences between the excitation and the two natural frequencies $\Omega_{n1}$ and $\Omega_{n2}$ respectively. Thus, the second-order averaged equations for the autoparametric vibration absorber, become

$$
\begin{aligned}
x_1' &= -\bar{\xi}_1 x_1 + \sigma_1 y_1 + 2x_2 y_2 \\
&\quad + \epsilon[(\hat{F}\bar{\xi}_1)/4 - 2\sigma_1\bar{\xi}_1 x_1 + x_2 y_2(4\sigma_2 - \sigma_1) - y_1(\sigma_1^2 + \bar{\xi}_1^2)/2
\end{aligned}
$$

7

$$
\begin{aligned}
&- \ x_2^2(\bar\xi_1/2 + 2\bar\xi_2) + 3y_1(x_2^2 + y_2^2)/2 + y_2^2(\bar\xi_1/2 + 2\bar\xi_2)], \\
y_1' \ = \ & \hat F/2 - \sigma_1 x_1 - \bar\xi_1 y_1 + y_2^2 - x_2^2 \\
&+ \ \epsilon[3\hat F\sigma_1/4 - 2\sigma_1\bar\xi_1 y_1 - x_2 y_2(\bar\xi_1 + 4\bar\xi_2) + x_1(\sigma_1^2 + \bar\xi_1^{\,2})/2 \\
&+ \ x_2^2(\sigma_1/2 - 2\sigma_2) - 3x_1(x_2^2 + y_2^2)/2 + y_2^2(2\sigma_2 - \sigma_1/2)], \\
x_2' \ = \ & -\bar\xi_2 x_2 + (x_2 y_1 - x_1 y_2)/2 + \sigma_2 y_2 \\
&+ \ \epsilon[3\hat F y_2/8 - 2\sigma_2\bar\xi_2 x_2 - x_1 x_2(3\bar\xi_1/4 + \bar\xi_2) + x_2 y_1(3\sigma_1/4 - \sigma_2) \\
&+ \ x_1 y_2(\sigma_2 - 3\sigma_1/4) - y_1 y_2(3\bar\xi_1/4 + \bar\xi_2) \\
&- \ y_2(\sigma_2^2 - \bar\xi_2^{\,2}) - y_2(x_1^2 + y_1^2)/8 + (y_2 x_2^2 + y_2^3)(1/2 - 1/(4R))], \\
y_2' \ = \ & -\sigma_2 x_2 - (x_1 x_2 + y_1 y_2)/2 - \bar\xi_2 y_2 \\
&+ \ \epsilon[3\hat F x_2/8 + x_1 x_2(\sigma_2 - 3\sigma_1/4) - x_2 y_1(\bar\xi_2 + 3\bar\xi_1) - 2\sigma_2\bar\xi_2 y_2 \\
&+ \ x_1 y_2(3\bar\xi_1/4 + \bar\xi_2) + y_1 y_2(\sigma_2 - 3\sigma_1) \\
&+ \ x_2(\sigma_2^2 + \bar\xi_2^{\,2}) + x_2(x_1^2 + y_1^2)/8 - (x_2^3 - x_2 y_2^2)(1/2 - 1/(4R))]. \quad (14)
\end{aligned}
$$

Observe that if we set $\epsilon = 0$ in the second-order averaged equations, equations (14), we obtain the first-order averaged equations in Bajaj et al. (1994). We should also note that much of the tedious algebra associated with the second-order averaging as well as many of the analytical calculations in the subsequent sections were performed using the symbolic computation package Mathematica (Wolfram, 1991; Maeder, 1991).

The divergence of the flow defined by equations (14) is

$$
\frac{\partial x_1'}{\partial x_1} + \frac{\partial y_1'}{\partial y_1} + \frac{\partial x_2'}{\partial x_2} + \frac{\partial y_2'}{\partial y_2} = -2(\bar\xi_1 + \bar\xi_2) - 4\epsilon(\sigma_1\bar\xi_1 + \sigma_2\bar\xi_2), \qquad (15)
$$

which is a function of the small parameter $\epsilon$. If $\epsilon > 0$ and $\bar\xi_1 = \bar\xi_2 > 0$, then the divergence will be negative definite if,

$$
1 + \epsilon(\sigma_1 + \sigma_2) > 0. \qquad (16)
$$

When this condition holds, every solution of the system in four dimensional state space is ultimately confined to a subspace of dimension smaller than four and the system remains a dissipative system. While this requirement is unconditionally satisfied for the first-order averaged equations, for each fixed $\epsilon$, there exist values of mistunings $\sigma_1$ and $\sigma_2$ for which the divergence does not remain negative.

8

# 4 Steady-state constant solutions of the averaged equations

A more physical interpretation of the results of the analysis of the steady-state motions is possible when the averaged equations (14) are transformed into polar coordinates by the following change of variables

$$x_1 = a_1 \cos \beta_1 \ , y_1 = -a_1 \sin \beta_1 \ , x_2 = a_2 \cos \beta_2 \ , y_2 = -a_2 \sin \beta_2. \tag{17}$$

The resulting equations in polar form are

$$
\begin{aligned}
a_1' \ &= \ -a_1 \bar{\xi}_1 - \hat{F} \sin \beta_1/2 - a_2^2 \sin(\beta_1 - \beta_2) \\
&+ \ \epsilon[-2a_1\sigma_1\bar{\xi}_1 + \hat{F}(\bar{\xi}_1 \cos \beta_1 - 3\sigma_1 \sin \beta_1)/4 \\
&- \ a_2^2((\bar{\xi}_1/2 + 2\bar{\xi}_2)\cos(\beta_1 - 2\beta_2) - (2\sigma_2 - \sigma_1/2)\sin(\beta_1 - 2\beta_2))], \\
a_1\beta_1' \ &= \ a_1\sigma_1 - \hat{F} \cos \beta_1/2 + a_2^2 \cos(\beta_1 - \beta_2) \\
&+ \ \epsilon[a_1(3a_2^2 - \sigma_1^2 - \bar{\xi}_1^{\,2})/2 - \hat{F}(3\sigma_1 \cos \beta_1 + \bar{\xi}_1 \sin \beta_1) \\
&+ \ a_2^2((2\sigma_2 - \sigma_1/2)\cos(\beta_1 - 2\beta_2) + (\bar{\xi}_1/2 + 2\bar{\xi}_2)\sin(\beta_1 - 2\beta_2))], \\
a_2' \ &= \ -a_2\bar{\xi}_2 - a_1a_2 \sin(\beta_1 - 2\beta_2)/2 \\
&+ \ \epsilon[-a_2(2\sigma_2\bar{\xi}_2 + 3\hat{F} \sin(2\beta_2)/8) \\
&+ \ a_1a_2(-(3\bar{\xi}_1/4 + \bar{\xi}_2)\cos(\beta_1 - 2\beta_2) + (\sigma_2 - 3\sigma_1/4)\sin(\beta_1 - 2\beta_2))], \\
a_2\beta_2' \ &= \ a_2\sigma_2 + a_1a_2 \cos(\beta_1 - 2\beta_2)/2 \\
&+ \ \epsilon[-a_2(a_1^2/8 - \sigma_2^2 + \bar{\xi}_2^{\,2} + 3\hat{F} \cos(2\beta_2)/8) + a_2^3(1/2 - 1/(4R)) \\
&+ \ a_1a_2((3\sigma_1/4 - \sigma_2)\cos(\beta_1 - 2\beta_2) - (3\bar{\xi}_1/4 + \bar{\xi}_2)\sin(\beta_1 - 2\beta_2))].
\end{aligned}
\tag{18}
$$

Again it is interesting to note that on setting $\epsilon = 0$ we recover the first-order averaged equations (Bajaj et al., 1994) from equations (18).

The locked-mode (or locked-pendulum mode) motions of the system (the solutions for which the pendulum is stationary and remains vertical), are governed by equations (18) with $a_2 = 0$ and $\beta_2 = 0$. Explicitly, these equations are

$$a_1' \ = \ -a_1\bar{\xi}_1 - \hat{F} \sin \beta_1/2$$

9

$$+ \quad \epsilon \left[ -2a_1 \sigma_1 \bar{\xi}_1 + \hat{F}(\bar{\xi}_1 \cos \beta_1 - 3\sigma_1 \sin \beta_1)/4 \right],$$

$$a_1 \beta_1' = a_1 \sigma_1 - \hat{F} \cos \beta_1 / 2$$

$$+ \quad \epsilon \left[ a_1(-\sigma_1^2 - \bar{\xi}_1^2)/2 - \hat{F}(3\sigma_1 \cos \beta_1 + \bar{\xi}_1 \sin \beta_1) \right]. \qquad (19)$$

Note that equations (19) for $a_1$ and $\beta_1$ are linear in the amplitude $a_1$. Similarly, equations (14) with $x_2 = y_2 = 0$ are a linear system in $x_1$ and $y_1$. Thus, the steady-state solution as a function of the system parameters is unique.

On setting $a_1' = 0$, $\beta_1' = 0$ in equations (19), we obtain the steady-state, locked-mode solutions as

$$a_1 = \pm \frac{\hat{F}}{2} \sqrt{\frac{4 + 12\epsilon\sigma_1 + \epsilon^2(9\sigma_1^2 + \bar{\xi}_1^2)}{(4(\sigma_1^2 + \bar{\xi}_1^2) + 4\epsilon\sigma_1(3\bar{\xi}_1^2 - \sigma_1^2) + \epsilon^2(\sigma_1^4 + 18\sigma_1^2\bar{\xi}_1^2 + \bar{\xi}_1^4))}},$$

$$\tan \beta_1 = -\frac{\bar{\xi}_1(4 + 12\epsilon\sigma_1 + \epsilon^2(13\sigma_1^2 + \bar{\xi}_1^2)}{\sigma_1(4 + 4\epsilon\sigma_1 + \epsilon^2(\bar{\xi}_1^2 - 3\sigma_1^2))}. \qquad (20)$$

The stability of the locked-pendulum solution is studied in the next section in conjunction with the response of the whole system.

# 5 Response, stability and bifurcation analysis of the averaged system

The numerical investigation of the averaged system described by equations (15) (or equivalently, by equations (18) ) is carried out using the softwares AUTO (Doedel, 1986), CHAOS (Aronson, 1991) and DSTOOL (Guckenheimer et al., 1992). The response of the system is characterized by the steady-state solutions of these averaged equations as a function of the system parameters. Where algebraically feasible, analytical investigations are also performed to obtain the stability conditions on system parameters. We should note here that $a_1$ and $a_2$ are not really the amplitudes of the physical motion of the block element and the pendulum element. They are only first-order approximations to the harmonic terms in the Fourier series which describes the motion. For the purposes of this study, they can be interpreted as the *approximate* amplitudes in the vertical and the angular directions of motion.

Since $\epsilon$ is explicitly present in the averaged equations, its effect on the response $a_1$ and $a_2$ (plotted versus the mistuning $\sigma_1$) can be seen by fixing the other system parameters. Here we choose $\hat{F} = 1$, R = 0.5, $\sigma_2 = 0.66$, $\bar{\xi} = \bar{\xi}_1 = \bar{\xi}_2 = 0.10$ and vary $\epsilon$ from 0.0 to 0.1. A low value of damping allows for a rich variety of behavior to be observed in the dynamics of the system. Results of these numerical studies are shown in Figures 2(a)-2(d). All subsequent results are shown for these constant values of the parameters, $\hat{F}$, R, $\bar{\xi}$ and $\sigma_2$.

It is found that the response curves for various $\epsilon$ can be classified and studied in two qualitatively distinct sets. The nature of the response curves, $a_1$ and $a_2$ versus the mistuning $\sigma_1$, undergoes a qualitative change at $\epsilon \approx$ 0.08931. One type of response diagram exists for $\epsilon < 0.08931$, and another type for $\epsilon > 0.08931$.

Consider the response curves for $\epsilon = 0$, as shown in Figure 2(a). For $\epsilon = 0$, the second-order averaged equations reduce to the first-order averaged equations. The single-mode or locked-mode solution, in which the pendulum is stationary, is stable for all mistunings $\sigma_1 < -0.3609$ and $\sigma_1 > 0.3609$. At $\sigma_1 = -0.3609$, a stable coupled-mode solution arises as a result of a Pitchfork bifurcation (open squares) from the single-mode solution. This coupled-mode solution co-exists with another, although unstable, coupled-mode solution over the interval $0.3609 < \sigma_1 < 1.84$. The unstable coupled-mode solution bifurcates subcritically from the single-mode solution and thus, over the frequencies $0.3609 < \sigma_1 < 1.84$, a stable coupled-mode response coexists with the stable single-mode response. Thereafter, the single-mode response is the only response and is stable. The larger coupled-mode solution is unstable in the frequency interval $-0.3440 < \sigma_1 < -0.0236$ due to a Hopf bifurcation, indicated by solid squares on the response diagrams. Note that the coupled-mode solutions appear in symmetric pairs which are phase shifted by $\pi$. Also, in the coupled-mode motion, the primary mass oscillates with a constant amplitude regardless of the frequency $\sigma_1$. This phenomenon has been termed saturation in the literature (Nayfeh and Mook, 1979; Bajaj et al. , 1994) and is the essential process by which the autoparametric vibration absorber functions in limiting the response of the primary system. Details of the stability analysis for single-mode and coupled-mode solutions in its most general form, in the context of first-order averaging, can be found in Bajaj et al. (1994) and are not repeated here. We just point out that along the mistuning $\sigma_1$ axis, there are only five different bifurcation points (already

11

described in this paragraph). Thus, for $\sigma_1 < -0.3609$ and $\sigma_1 > 1.84$, only the single-mode solution exists. It is unique and stable. For $\epsilon > 0$, this is not the case as discussed below.

As $\epsilon$ increases from 0.00 to 0.10, the response is characterized by ten types of special or bifurcation points that appear in the interval $\sigma_1 \in (-10.00, 40.00)$ . Along the $\sigma_1$ axis, there is one Hopf bifurcation point on the single-mode solution at $A_1$. There are four Pitchfork bifurcation points on the single-mode solution at $B_1 < B_2 < B_3 < B_4$, there are four Hopf bifurcation points on the coupled-mode solution at $C_1 < C_2 < C_3 < C_4$ and one turning point at $D_1$. In order of increasing $\sigma_1$, these points appear as :
$-10.00 < A_1 < B_1 < C_1 < C_2 < 0.00 < B_2 < D_1 < B_3 < C_3 < B_4 < C_4 < -40.00$.

For $\epsilon = 0.00$, $B_1 = -0.3609, C_1 = -0.3440, C_2 = -0.0236, B_2 = 0.3609, D_1 = 1.8400$. The point $A_1$ is at $-\infty$ and the points $B_3, C_3, B_4, C_4$ are at $\infty$, beyond the interval of observation.

For $\epsilon = 0.075$, all the ten bifurcation points are at finite values of $\sigma_1$, with $B_1 = -0.3335, C_1 = -0.3170, C_2 = -0.0717, B_2 = 0.3707, D_1 = 2.6025$. The points $B_3, C_3, B_4, C_4$ are still beyond the interval of observation, whereas $A_1 = -6.6666$, moves inside the interval of observation. Thus, for every $\epsilon > 0$, there arise additional Pitchfork bifurcations to coupled-mode solutions, as well as Hopf bifurcations to limit cycle motions, all from the single-mode branch.

For $\epsilon = 0.08931$, $A_1 = -5.5984, B_1 = -0.3288, C_1 = -0.3122, C_2 = -0.0799, B_2 = 0.3728, D_1 = 4.2500, B_3 = 17.2364, C_3 = 21.6977, B_4 = 30.0944, C_4 = 31.6126$. All the special points are now in the interval of observation. The coupled-mode response (the 'primary response', that is, the response branch that exists for $\epsilon = 0$) in the interval of observation collides at $D_1$, with the coupled-mode branch coming in from $\infty$, as $\epsilon$ increases.

For $\epsilon = 0.10$, $A_1 = -4.9999, B_1 = -0.3253, C_1 = -0.3087, C_2 = -0.0859, B_2 = 0.3744, B_3 = 14.9262, C_3 = 19.3249, B_4 = 28.1226, C_4 = 29.1222$. The point $D_1$ no longer exists, the two coupled-mode branches finally join together to form a continuous branch with no turning points in the interval of observation. A careful explanation of this observation will be given later in the paper.

The range of mistuning parameter $\sigma_1$ over which the primary coupled-mode response exists increases with $\epsilon$. For example, in Figure 2(b) ($\epsilon = 0.075$), the coupled-mode solutions exist up to $\sigma_1 = 2.6025$, whereas they

12

exist only up to $\sigma_1 = 1.8400$ for $\epsilon = 0.00$.

We observe that the frequency interval (or the distance) between the Hopf bifurcation points of the type $C_1$ and $C_2$ decreases with increasing $\epsilon$. This trend is seen even more clearly on studying the Hopf bifurcation sets (Figure 3) for the coupled-mode solutions. It is seen that the area enclosed by the sets decreases as $\epsilon$ increases. The set for $\epsilon = 0.00$ encloses all the other sets for $\epsilon > 0$, that is, the region of instability shrinks as $\epsilon$ is increased. This effect is similar to the effect of increasing damping (Bajaj et al., 1994). It is interesting to note that from $\sigma_1 = -0.4$ to $\sigma_1 = -0.2$, all the sets are nearly coincident, with $\sigma_2 \approx 0.25$ changing very little. This means that if a Hopf bifurcation arises in the coupled-mode solution branch for $\sigma_1$ varying over this range, it will exist for other values of $\epsilon$ as well and the position of the special point $C_1$ changes very little with changing $\epsilon$. This Hopf point is independent of the parameter $\epsilon$ which is related to the forcing amplitude through the scaling. As $\epsilon$ increases, the damping in the system also increases. Therefore the range of $\sigma_1$ for which periodic or amplitude-modulated motions can exist, also decreases.

Now observe the change in the special points of the type $B_1$ and $B_2$. For $\epsilon = 0.00$, the two points are symmetric about $\sigma_1 = 0.00$. On increasing $\epsilon$, this symmetry breaks and the frequency interval between the two points decreases. Finally, additional Pitchfork bifurcation points of the type $B_3$ and $B_4$ start to appear in the $\sigma_1$ window of observation. The Pitchfork bifurcation sets for single-mode solutions in the $(\sigma_1 - \sigma_2)$ plane (Figure 4), are found to shrink, that is, the region of instability decreases on increasing $\epsilon$. It is also noticed that the sets are no longer symmetric about a $\sigma_1$ or a $\sigma_2$ axis. They tend to meet for a negative $\sigma_1$. On increasing the value of $\epsilon$ from $\epsilon = 0.00$ to $\epsilon = 0.20$, it is seen that addition Pitchfork bifurcation sets start appearing for larger $\sigma_2$. Now, the Pitchfork bifurcation set is determined by the roots of the Hurwitz condition on the coefficients of the characteristic equation for the Jacobian of the averaged equations (14). For equation (14) and its single-mode solutions (equations (20) ), the Jacobian is a $4 \times 4$ matrix and has the structure

$$Jac = \begin{bmatrix} \underline{A} & 0 \\ 0 & \underline{B} \end{bmatrix}, \tag{21}$$

where $\underline{A}$ and $\underline{B}$ are $2 \times 2$ matrices. The trace of $\underline{A}$ (denoted by $S_{11}$), the

13

determinant of $\underline{A}$ (denoted by $P_{11}$), the trace of $\underline{B}$ (denoted by $S_{22}$), and the determinant of $\underline{B}$ (denoted by $P_{22}$), are given by

$$
\begin{aligned}
S_{11} &= -2\bar{\xi}_1(1 + 2\epsilon\sigma_1), \\
P_{11} &= \sigma_1^2 + \bar{\xi}_1^{\,2} + (3\bar{\xi}_1^{\,2} - \sigma_1^2)\sigma_1\epsilon + (\sigma_1^4/4 + 9\sigma_1^2\bar{\xi}_1^{\,2}/2 + \bar{\xi}_1^{\,4}/4)\epsilon^2, \\
S_{22} &= -2\bar{\xi}_2(1 + 2\epsilon\sigma_2), \\
P_{22} &= P_{22}(\hat{F}, R, \sigma_1, \sigma_2, \bar{\xi}_1, \bar{\xi}_2, \epsilon),
\end{aligned}
\tag{22}
$$

where $P_{22}$ is a complicated function of the parameters indicated. The characteristic equation of the Jacobian for the single-mode solution can be written as

$$
(\lambda^2 - S_{11}\lambda + P_{11})(\lambda^2 - S_{22}\lambda + P_{22}) = 0,
\tag{23}
$$

where the two factors correspond respectively, to the disturbances in the plane and out of the plane of the single-mode response. The Hurwitz condition for Pitchfork bifurcation from the single-mode solution is given by $P_{22} = 0$, which is found to be a fourth order polynomial in $\sigma_2$ that is multiplied in the highest degree terms by $\epsilon$. For small $\epsilon$, two of its zeros approach $\infty$ asymptotically. For larger $\epsilon$, they move closer to observable $\sigma_2$ values. Therefore, two semiclosed curves (with four branches, corresponding to the four zeros in $\sigma_2$ ) are observed for larger $\epsilon$. On increasing $\epsilon$, two additional Pitchfork points $B_3$ and $B_4$, corresponding to the additional Pitchfork bifurcation set are seen. The introduction of additional Pitchfork bifurcation points in second-order analysis was also noted by Lee and Perkins (1992).

From equation (23), it can be seen that for the special point $A_1$ to appear, the conditions for a Hopf bifurcation in the single-mode solution branch, ($S_{11} = 0$ and $P_{11} > 0$) should be satisfied. From equations (22), for a fixed $\epsilon$, if $\sigma_1 = \frac{-1}{2\epsilon}$, then $S_{11} = 0$ and $P_{11} = \frac{(5+4\bar{\xi}_1^{\,2}\epsilon^2)^2}{64\epsilon^2} > 0$. Therefore at this point, a Hopf bifurcation can take place from the single-mode solution branch. It is interesting to note from the definition of the mistuning $\sigma_1$ that at precisely this value of $\sigma_1$, $\Omega_{n1} = 0$ as well. For the original equations (3) (and hence, equations (2) ), this implies that the zero equilibrium position undergoes a Pitchfork bifurcation to a nonzero equilibrium position in the absence of external excitation. These observations are also made from the numerical investigation using AUTO and through direct simulation of the

original equations (discussed later in the paper). It is seen that as $\epsilon \to 0$, this Hopf bifurcation point goes to $-\infty$.

The response curves, as noted earlier, can be classified into two distinct structures, depending on whether $\epsilon < 0.08931$ or $\epsilon > 0.08931$. This distinction is based on the nature of the special point $D_1$. As $\epsilon$ increases from $\epsilon = 0.00$ to $\epsilon = 0.075$, (Figures 2(a) and 2(b) ) the turning point moves along the $\sigma_1$ axis, from $\sigma_1 = 1.8400$ to $\sigma_1 = 2.6025$, that is, in the direction of increasing $\sigma_1$. At $\epsilon = 0.08931$, the primary coupled-mode solution collides at the turning point $D_1$ with another branch coming in towards $\sigma_1 = 4.25$ from $\sigma_1 \to \infty$ (that is, from the right (see Figure 2(c) ). The branch coming in from the right arises due to Pitchfork bifurcations from the single-mode branch (at $B_3$ and $B_4$) and two additional Hopf bifurcation points appear on it. It interacts with the coupled-mode response, in a manner so as to form a closed unstable loop (coupled-mode $a_2$ response) and a continuation of the stable coupled-mode response. The stable and unstable coupled-mode branches separate on increasing $\epsilon$, to establish their distinct identities. For example, for $\epsilon = 0.10$, Figure 2(d), the two branches of the coupled-mode response do not intersect at all. This interesting behaviour can be explained using the information in Figure 5, the limit point (or turning point) set generated for the coupled-mode solution branch. It is seen that as $\epsilon$ increases, the limit point sets start becoming concave upwards, that is, start developing a local minimum. The line $\sigma_2 = 0.66$, the value of $\sigma_2$ used for this analysis, intersects only two limit point sets, the ones for $\epsilon = 0.00$ and for $\epsilon = 0.075$, at $\sigma_1 = 1.84$ and $\sigma_1 = 2.60$, respectively. And thus, the special point $D_1$ moves to the right. On further increasing $\epsilon$ to $\epsilon = 0.08931$, the line $\sigma_2 = 0.66$ is tangent to the corresponding limit point set at $\sigma_1 = 4.25$, which corresponds to the point of collision of the two coupled-mode branches. For still higher $\epsilon$, for example $\epsilon = 0.10$, the local minimum in the corresponding limit point set lies entirely above the line $\sigma_2 = 0.66$, and hence no limit points are seen on the response curves. It is interesting to note that on increasing $\sigma_2$ from $\sigma_2 = 0.66$, the limit point sets could intersect *twice*, for $\epsilon > 0.08931$, leading to multiple limit points on the response curves. On increasing $\sigma_2$ to $\sigma_2 = 1.05$, the limit point sets for *all* the $\epsilon$ seem to intersect with this line of constant $\sigma_2$ at about $\sigma_1 = 1.50$. This leads us to conclude that at least one limit point of the response curve would not move along the $\sigma_1$ axis on changing $\epsilon$, that is, would be independent of $\epsilon$. Therefore in this region of the parameter space, a first-order analysis would be sufficient to predict the

position of the point $D_1$.

Consider now the response curves for $\epsilon = 0.075$ (Figure 2(b)). There are certain essential features resulting from the explicit appearance of $\epsilon$ in the second-order averaged equations and the discussion here is limited only to those features. The response curves show loss of saturation (compare Figure 2(a) to Figure 2(b)). The response of the primary mass now slowly decreases with increase in the mistuning $\sigma_1$. This can be explained by the observation that saturation is an unstable phenomenon in the sense of structural stability and is predicted only by a first-order averaging analysis. The second-order analysis allows for the saturated solution to be perturbed by terms dependent on $\epsilon$, and saturation no longer persists. In other words, saturation is a degeneracy of the first-order analysis. The second-order analysis simply splits the degenerate stable and unstable periodic solutions predicted by the first-order analysis (Lee and Perkins, 1992).

For $\epsilon = 0.08931$, from Figure 2(c), a secondary (unstable) peak is observed in the single-mode branch. The two peaks in the single-mode response (that is, at $\sigma_1 = 0.00$ and at $\sigma_1 = 22.3939$) can be established from the expression for the locked single-mode response $a_1$ (equation (20) ). For the given values of the parameters $\bar{\xi}$, $\hat{F}$ and $\epsilon$, these peaks correspond to the maxima of $a_1$ with respect to the mistuning $\sigma_1$. Similarly, for $\epsilon = 0.10$, in Figure 2(d), the maxima of $a_1$ are at $\sigma_1 = 0.00$ and $\sigma_1 = 20.004$, which correspond to the position of the two peaks in the response curve. We also note that on setting $\epsilon = 0.00$ (which yields the amplitude of the locked-mode response for the first-order averaged equations), $a_1$ has only one maximum at $\sigma_1 = 0.00$, which corresponds to the single peak observed in the response curve in Figure 2(a). Therefore, as $\epsilon \to 0$, the value of $\sigma_1$ at which the secondary maximum occurs goes to $\infty$. As $\epsilon$ increases, the secondary maximum arises at lower $\sigma_1$ values. However, it is quite likely that this unstable secondary maximum is only an artifact of the second-order averaging and is not valid as far as the original system is concerned. For example, the second peak in the single-mode branch, for $\epsilon = 0.08931$, is at $\sigma_1 = 22.3939$. Hence, the product $\epsilon\sigma_1 = 2.23939$, is of $O(1)$ in $\epsilon$, and not an $O(\epsilon)$ quantity as assumed for averaging of the system. Similarly, for other large $\epsilon$, the $\sigma_1$ at which the second peak is observed, lie beyond the range of applicability of the averaging analysis.

The effect of damping on the response (for $\epsilon = 0.075$) is seen in Figures 6. On comparing these response curves with the response curves at lower

16

damping (Figures 2(b) ), it is observed that as damping is increased from $\bar{\xi} = 0.10$ to $\bar{\xi} = 0.21$, the amplitudes of the single-mode response and the coupled-mode response decrease significantly (Banerjee et al., 1993). The Hopf bifurcation points which exist for $\bar{\xi} = 0.10$ cease to exist for higher damping, that is, much of the possible complex dynamics of the system can be eliminated by simply increasing the damping. On further increasing the damping to $\bar{\xi} = 0.30$, the loss of saturation effects also can no longer be observed for $\epsilon = 0.075$ (Banerjee et al., 1993). Since $\epsilon$ is related, through scaling, to the amplitude of external forcing, much higher values of $\epsilon$ need to be considered at higher damping, to be able to observe any of the characteristics of the response that were seen at lower damping values. Or simply, higher forcing is required to overcome the effects of higher damping.

# 6 Periodic and chaotic solutions of the averaged system

Extremely interesting behaviour of the system is seen between the Hopf bifurcation points of the type $C_1$ and $C_2$. On continuing the bifurcating limit cycles or periodic solutions, using AUTO, it is seen that both points $C_1$ and $C_2$ are supercritical Hopf bifurcation points. These continued solutions are seen in Figure 7(a). Figure 7(b) shows a magnified view of the region near $C_1$ and Figure 7(c) shows a magnified view of the region near $C_2$. Filled circles denote stable periodic solutions and open circles denote unstable periodic solutions. We observe that the period-one ($P_1$) solution from $C_1$ period-doubles almost immediately to a period-two ($P_2$) solution. On following this branch, we obtain a cascade of period-doublings, which eventually lead to chaos. This period-doubling route to chaos is seen in Figures 8(a), 8(b), 8(c) and 8(d). The polar form of the averaged equations have been simulated in DSTOOLS to obtain these responses.

From AUTO, on continuing the $P_1$ solution from $C_1$, we can obtain the time-period (T) of the Hopf bifurcating periodic orbit as a function of the mistuning $\sigma_1$, as shown in Figure 9. We observe that the period T increases rapidly and tends to $\infty$. A very large T indicates that the corresponding orbit is close to a homoclinic orbit (since a homoclinic orbit has infinite T). From Figure 9, on choosing the $\sigma_1 = -0.3069$, corresponding to the maximum T

17

and integrating the averaged equations, we obtain an approximate homoclinic orbit as shown in Figure 10(a). Note that in the parameter interval where Hopf bifurcations arise in the coupled-mode branch, the single-mode solution is of saddle-type. It is found that the orbit initiated by the one-dimensional unstable manifold of the single-mode constant solution, corresponding to $\sigma_1$ for Figure 10(a) approximates the homoclinic orbit. Calculating the eigenvalues from equation (23) for this $\sigma_1$, we obtain $\lambda_1 = -0.3963$, $\lambda_2 = 0.1765$, $\lambda_{3,4} = -0.0953 \pm 0.3105i$, that is, $\lambda_1 < 0$, $\lambda_2 > 0$ and $\lambda_{3,4}$ are complex. Thus, for the saddle-type single-mode equilibrium point, one eigenvalue is positive and real, one eigenvalue is negative and real and the two other eigenvalues are complex conjugates with negative real parts. Calculating $\delta = \frac{Re(\lambda_{3,4})}{\lambda_2} = 0.5399$, we see that $\delta < 1$, thus the conditions of the Silnikov theorem for the existance of Smale horseshoes (Wiggins, 1988) in the dynamics of the averaged system are satisfied and indeed, for $\sigma_1 = -0.3068$, we find that the homoclinic orbit breaks to form a chaotic attractor (Figure 10(b) ). The variation of the period of a periodic orbit as a function of the system parameter, as shown in Figure 9, is also a characteristic of the Silnikov phenomenon.

On increasing the mistuning $\sigma_1$ still further, we encounter yet another sequence of period-doublings which again leads to chaos (Figure 11(a), 11(b), 11(c), 11(d) and 11(e) ). We find that the chaotic attractor persists beyond $C_2$, the second Hopf bifurcation point, beyond which the coupled-mode constant solution is stable. Although $C_2$ is also a supercritical Hopf bifurcation point, the stable $P_1$ branch quickly turns around and becomes an unstable $P_1$ solution. The chaotic attractor, which is a continuation of the attractor shown in Figure 11(e), eventually touches the unstable saddle-type $P_1$ solution and is destroyed. This behaviour is called 'crisis' or transient chaos (Grebogi et al., 1983). Thus, any initial condition eventually leads to the stable coupled-mode constant solution. Since the system is still in the vicinity where an attractor existed previously, the transients trace out the attractor before dying out. This behaviour is seen in Figure 12. This was also shown by Bajaj et al. (1994) for the first-order averaged case.

As described in the last section, the single-mode or the locked-pendulum mode constant solution branch also exhibits a Hopf bifurcation at $A_1$, for $\epsilon > 0$. Continuation of periodic solutions from this Hopf point, using AUTO, indicates that the bifurcation is essentially vertical. Thus, the periodic solution has a very large amplitude and it is essentially impossible to continue

the solution branch as a function of $\sigma_1$.

# 7   Comparison with the original system

A good description of the relationship between the solutions of the original system and those of its averaged form can be found in Bajaj and Johnson (1992). From a more recent viewpoint, averaging yields an approximate Poincare map of the original system (Wiggins, 1990). Therefore, hyperbolic fixed points of the averaged system correspond to periodic orbits in the original system. A hyperbolic limit cycle (or a $P_1$ solution) in the averaged system corresponds to an amplitude-modulated motion ($T_2$ or two-torus solution) in the original system. It is expected that chaotic solutions of the averaged equations will correspond to amplitude-modulated chaotic responses for the original system.

On making the scale changes and the coordinate transformations described in section 2, in the original system (equations (2)), we obtain

$$
\begin{aligned}
\hat{\eta}'' - 8\sin(\epsilon\alpha\bar{\theta})\bar{\theta}''\hat{\eta} &= \epsilon[\hat{F}\cos\tau - 2\bar{\xi}_1\hat{\eta}' - 2\sigma_1\hat{\eta} + 8\cos(\epsilon\alpha\bar{\theta})\bar{\theta}'^2] \\
&+ \epsilon^2[2\sigma_1\hat{F}\cos\tau - 4\sigma_1\bar{\xi}_1\hat{\eta}'], \\
\hat{\eta}''\sin(\epsilon\alpha\bar{\theta})/\alpha - \bar{\theta}'' &= (1/4 + \epsilon\sigma_2)\sin(\epsilon\alpha\bar{\theta})/(\epsilon\alpha) \\
&+ 2\epsilon\bar{\xi}_2\bar{\theta}'\sqrt{1 + 4\epsilon\sigma_2},
\end{aligned}
\tag{24}
$$

where $\alpha = \sqrt{\frac{8(1+R)}{R}}$. These are the exact form of equations (3) before the Taylor series approximation is carried out. Using equation (4) to write this as a vector system we get

$$
\begin{aligned}
\hat{\eta}_1' &= \hat{\eta}_2, \\
\hat{\eta}_2' &= (f_1 + 8\beta f_2)/(1 - 8\beta^2), \\
\bar{\theta}_1' &= \bar{\theta}_2, \\
\bar{\theta}_2' &= (f_2 + \beta f_1)/(1 - 8\beta^2),
\end{aligned}
\tag{25}
$$

where $\beta = \frac{\sin(\epsilon\alpha\bar{\theta}_1)}{\alpha}$ and

19

$$\begin{aligned}
f_1 &= -\hat{\eta}_1 + \epsilon[\hat{F}\cos\tau - 2\bar{\xi}_1\hat{\eta}_2 - 2\sigma_1\hat{\eta}_1 + 8\cos(\epsilon\alpha\bar{\theta}_1)\bar{\theta}_2^2] \\
&+ \epsilon^2[2\sigma_1\hat{F}\cos\tau - 4\sigma_1\bar{\xi}_1\hat{\eta}_2], \\
f_2 &= -(1/4 + \epsilon\sigma_2)\sin(\epsilon\alpha\bar{\theta}_1)/(\epsilon\alpha), \\
&- 2\epsilon\bar{\xi}_2\bar{\theta}_2\sqrt{1 + 4\epsilon\sigma_2}.
\end{aligned} \tag{26}$$

This form of the equations is useful for a direct comparison of its solutions with those of the averaged equations.

The equations (25) are simulated in DSTOOLS for $\epsilon = 0.075$. For $\sigma_1 = -0.32$, a $4\pi$-periodic solution is obtained, whose projection in the $(\hat{\eta}_1 - \hat{\eta}_2)$ plane and in the $(\hat{\eta}_1 - \bar{\theta}_1)$ plane are shown in Figure 13(a) and Figure 13(b), respectively. The motion of the block $(\hat{\eta}_1)$, and the corresponding response of the pendulum $(\bar{\theta}_1)$, are shown in Figures 13(c) and 13(d) respectively. The two motions are essentially harmonic, with the motion of the block at twice the frequency of the pendulum. This verifies the predictions of the second-order averaging analysis.

On increasing $\sigma_1$ to $\sigma_1 = -0.30$, the $4\pi$-periodic solution becomes unstable and the response becomes amplitude-modulated. The phase-plane projections of the motion onto the $(\hat{\eta}_1 - \hat{\eta}_2)$ and $(\hat{\eta}_1 - \bar{\theta}_1)$ planes are given in Figures 14(a) and 14(b), respectively. The various projections of the Poincare-section of time-response are shown in Figures 14(c) and 14(d). The actual time-responses for the block $(\hat{\eta}_1)$ and the pendulum $(\bar{\theta}_1)$ are shown in Figures 14(e) and 14(f). Note that in the later time-response plots, only the *envelope* of the response will be shown (for the sake of clarity in the figure). The envelope of the response is obtained by simply plotting the response $(\hat{\eta}_1)$ and $(\bar{\theta}_1)$, corresponding to their respective Poincare-sections, versus *time* $(\tau)$. Clearly, the Poincare sections of the motion are dense closed curves, implying an invariant circle for the associated Poincare mapping, and a motion with two distinct frequencies for the system. The torus winding frequency is much smaller compared to the excitation frequency, and hence the motion is interpreted as amplitude-modulated.

On increasing $\sigma_1$, a torus-doubling is observed at $\sigma_1 = -0.24$. The projection onto the $(\hat{\eta}_1 - \hat{\eta}_2)$ phase-plane is seen in Figure 15(a) and that onto the $(\hat{\eta}_1 - \bar{\theta}_1)$ phase-plane is seen in Figure 15(b). That the solution has indeed torus-doubled becomes obvious by studying the Poincare-section of this $T_2$ solution in the $(\hat{\eta}_1 - \hat{\eta}_2)$ plane, shown in Figure 15(c) and the Poincare-section

in the $(\hat{\eta}_1 - \bar{\theta}_1)$ plane shown in Figure 15(d). The envelope of the $\hat{\eta}_1$ time-response is shown in Figure 15(e) and the envelope of the $\bar{\theta}_1$ time-response is shown in Figure 15(f). The $\bar{\theta}_1$ time-response shows different envelopes, each of which corresponds to a section at a different phase.

This solution doubles yet again to a $T_4$ solution for $\sigma_1 = -0.16$. The Poincare-section of this solution in the $(\hat{\eta}_1 - \hat{\eta}_2)$ plane is shown in Figure 16(a) and the Poincare-section in the $(\hat{\eta}_1 - \bar{\theta}_1)$ plane is shown in Figure 16(b). The envelope of the $\hat{\eta}_1$ time-response is shown in Figure 16(c) and the envelope of the $\bar{\theta}_1$ time-response is shown in Figure 16(d). The minimum amplitude of the $\hat{\eta}_1$ response is nearly constant, but the maximum amplitude of the response shows considerable variation.

This cascade of torus-doublings (described above) finally yields a chaotic solution at $\sigma_1 = -0.08$. The projections in various phase-planes of the Poincare-section of this solution are shown in Figure 17(a) and in Figure 17(b). The projection in the $(\hat{\eta}_1 - \bar{\theta}_1)$ plane has a distinct *butterfly* shape which persists for increasing $\sigma_1$ in the neighbourhood of $\sigma_1 = -0.08$. The envelope of the $\hat{\eta}_1$ time-response is shown in Figure 17(c) and that of the $\bar{\theta}_1$ time-response is shown in Figure 17(d).

On increasing $\sigma_1$ still further to $\sigma_1 = -0.01$, the chaotic attractor is destroyed via a boundary 'crisis' and goes to a fixed point. The transients still trace out the ghost of the attractor for some time. The Poincare-section of this solution in the $(\hat{\eta}_1 - \bar{\theta}_1)$ plane is shown in Figure 18(a). The *butterfly* structure of this attractor is no longer distinct and it is easy to see that the solution is going to a fixed point. The envelope of the $\hat{\eta}_1$ time-response is shown in Figure 18(b) and the envelope of the $\bar{\theta}_1$ time-response is shown in Figure 18(c).

For $\sigma_1 = 0.00$, it becomes even more clear that the solutions go to a fixed point in the Poincare section, that is, they go to a $P_1$ or a periodic solution in the phase-plane. The Poincare-section in the $(\hat{\eta}_1 - \bar{\theta}_1)$ plane is shown in Figure 19(a). The envelope of the $\hat{\eta}_1$ time-response is shown in Figure 19(b). It is seen from the time history of the solutions that the transient response is amplitude-modulated, with the modulations decreasing. On further observation, it is seen that the amplitude of response decreases to a constant value.

21

# 8 Discussion and conclusions

A second-order averaging analysis of the autoparametric system has been carried out under resonant excitation conditions with 2:1 internal resonances. This analysis has allowed us to investigate the effects of the small parameter, $\epsilon$, on the dynamics of the system.

Second-order averaging analysis shows the loss of saturation in the amplitude of the primary mass as predicted by the averaged equations. Since, simply by going to a higher-order analysis, this structurally unstable behavior is eliminated, it can be concluded that it was only an artifact of the first-order averaging and hence is not to be observed in the real physical system. One can, however, say that for sufficiently small $\epsilon$, the response of the primary system is 'nearly constant'.

The second-order averaging predicts that as $\epsilon$ is increased, the symmetry in the bifurcation sets is destroyed. Additional Pitchfork bifurcation points appear in the single-mode (locked-mode steady-state) solution branch. The intervals of mistuning $\sigma_1$ over which coupled-mode solutions coexist with the single-mode motion either increase or decrease depending on the mistuning $\sigma_2$. For small $\sigma_2$, the coupled-mode motions exist over a larger frequency interval in $\sigma_1$. The Hopf instability interval for the coupled-mode motions shrinks, thereby indicating that some of the amplitude-modulated motions predicted by first-order averaging may be stabilized to harmonic motions.

For larger values of the parameter $\epsilon$, some additional features of the solution are introduced by the second-order equations. These include a Hopf bifurcation and a secondary peak in the locked-pendulum mode of response. However, the secondary peak is merely an artifact of the second-order averaging and does not correspond to any physically realizable motion.

The averaged equations are compared with the original equations and their behavior is found to be in qualitative agreement. Interesting structures like *butterfly* like attractors are also observed in the original equations.

# 9 Acknowledgement

# 10 References

Aronson, J.W., 1991 "Chaos, A Sun Based Program for Analyzing Systems. A User's Guide", National Institute of Standard and Technology, Gaithersburg, MD.

Bajaj, A.K., Chang, S.I. and Johnson, J., 1994, "Amplitude Modulated Dynamics of a Resonantly Excited Autoparametric Two Degree of Freedom System", Nonlinear Dynamics, Vol. 5, pp. 433-457.

Banerjee, B., Bajaj, A.K. and Davies, P., 1993, "Second-order averaging study of an autoparametric system", Proceedings of the Fourteenth Biennial ASME Conference on Mechanical Vibration and Noise, Albuquerque, NM.

Doedel, E., 1986, "AUTO: Software for Continuation and Bifurcation Problems in Ordinary Differential Equations", Report, Department of Applied Mathematics, California Institute of Technology, Pasadena, CA.

Grebogi, C., Ott, E. and Yorke, J. A., 1983, "Crises, Sudden Changes in Chaotic Attractors and Chaotic Transients", Physica D, Vol. 7, pp. 181.

Guckenheimer, J. and Holmes, P., 1990, "Nonlinear Oscillations, Dynamical Systems and Bifurcation of Vector Fields" Springer-Verlag, NY.

Guckenheimer, J., Kim, S., Myers, M. R., Wicklin, F. J., Worfolk, P. A., 1992, "dstool : A Dynamical System Toolkit with an Interactive Graphical Interface", Users Manual, Centre for Applied Mathematics, Cornell University, Ithaca, NY.

Hatwal, H., Mallik, A.K. and Ghosh, A., 1983a, "Forced Nonlinear Oscillations of an Autoparametric System - Part 1: Periodic Responses", ASME Journal of Applied Mechanics, Vol. 50, pp. 657-662.

Hatwal, H., Mallik, A.K. and Ghosh, A., 1983b, "Forced Nonlinear Oscillations of an Autoparametric System - Part 2: Chaotic Responses", ASME Journal of Applied Mechanics, Vol. 50, pp. 663-668.

Haxton, R.S. and Barr, A.D.S., 1972, "The Autoparametric Vibration Absorber", ASME Journal for Engineering for Industry, Vol. 94, pp. 119-125.

Holmes, C and Holmes, P., 1981, "Second-order Averaging and Bifurcations to Subharmonics in Duffing's Equation", Journal of Sound and Vibra-

tion, Vol. 78(2), pp. 161-174.

Maeder, R., 1991, "Programming in Mathematica", Addition-Wesley Publishing Company, CA.

Miles, J.W., 1984, "Resonantly Fo ed Motion of Two Quadratically Coupled Oscillators", Physica D, Vol. 13, pp. 247-260.

Lee, C.L. and Perkins, N.C., 1992, "Nonlinear Oscillations of Suspended Cables Containing a Two-to-One Internal Resonance", Nonlinear Dynamics, Vol. 3, pp. 465-490.

Murdock, J.A., 1991, "Perturbations: Theory and Methods", John Wiley and Sons, NY.

Murdock, J.A., 1988, "Qualitative Theory of Nonlinear Resonance by Averaging and Dynamical Systems Methods", Dynamics Reported, Vol. 1, pp. 91-172.

Nayfeh, A.H. and Mook, D.T., 1979, "Nonlinear Oscillations" , Wiley-Interscience, NY.

Robinson, C., 1983, "Second-order Averaging of Forced and Coupled Nonlinear Oscillators", IEEE Transactions on Circuits and Systems , Vol. CAS-30, pp. 591-598.

Sethna, P.R. and Bajaj, A.K., 1978, "Bifurcations in Dynamical Systems with Internal Resonances", ASME Journal of Applied Mechanics, Vol. 45, pp. 895-902.

Sethna, P.R., 1965, "Vibrations of Dynamical Systems with Quadratic Nonlinearities", ASME Journal of Applied Mechanics, Vol. 32, pp. 576-582.

Tousi, S. and Bajaj, A.K., 1985, "Period Doubling Bifurcation and Modulated Motions in Forced Mechanical Systems", ASME Journal of Applied Mechanics, Vol. 52, pp. 446-452.

Wiggins, S., 1990, "Introduction to Applied Nonlinear Dynamical Systems and Chaos", Springer-Verlag, NY.

Wiggins, S., 1988, "Global Bifurcations and Chaos", Springer-Verlag, NY.

Wolfram, S., 1991, "Mathematica: A System for Mathematics by Computer", Addition Wesley Publishing Company, CA.
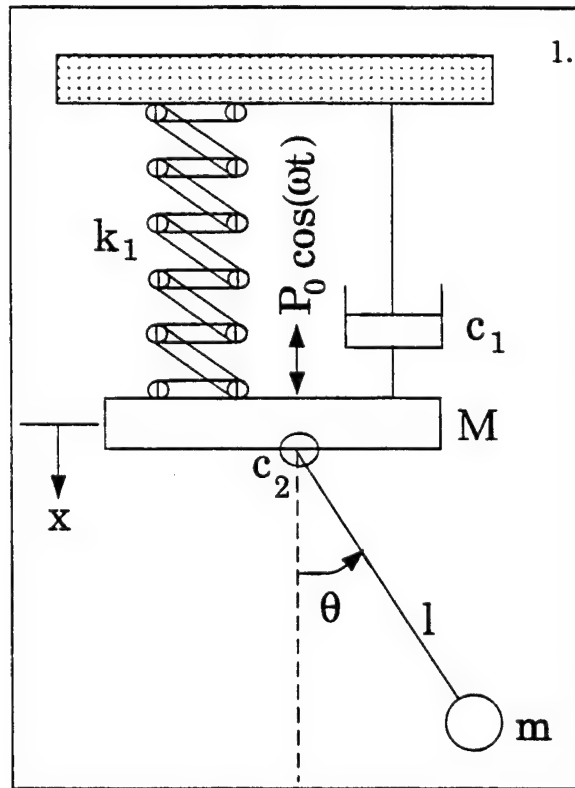
# 1   List of Figures

Figure 1. The autoparametric vibration absorber.

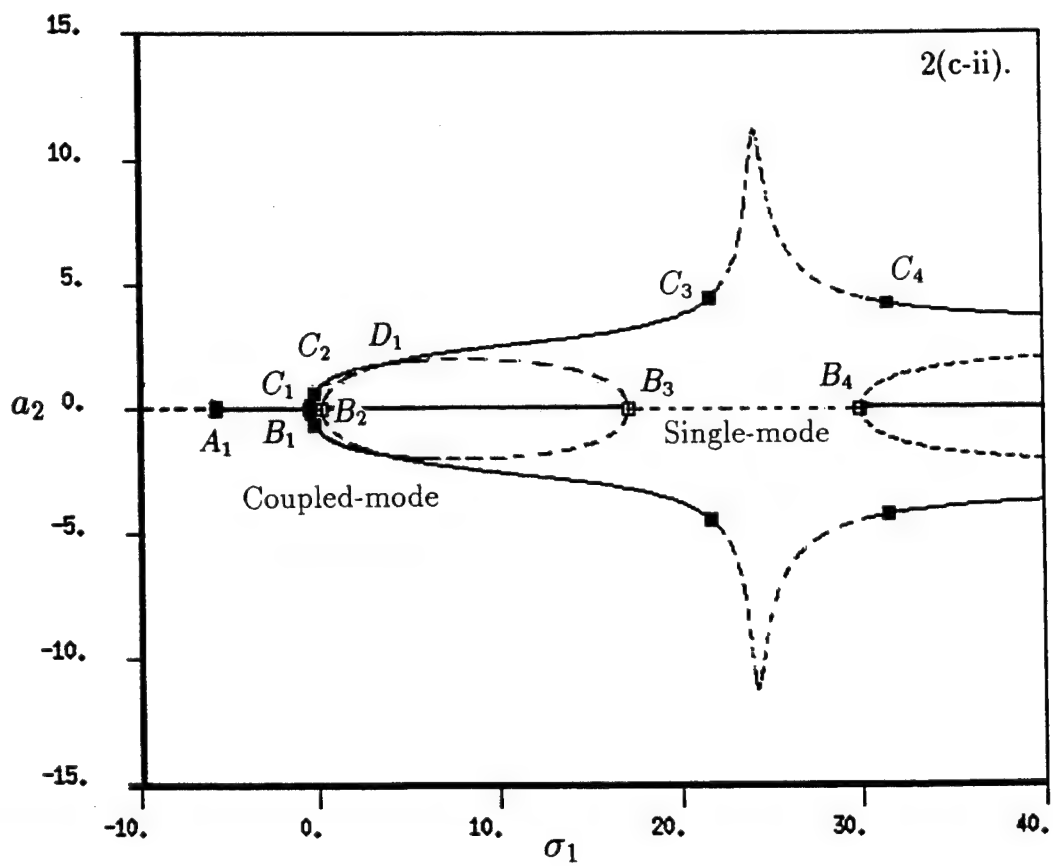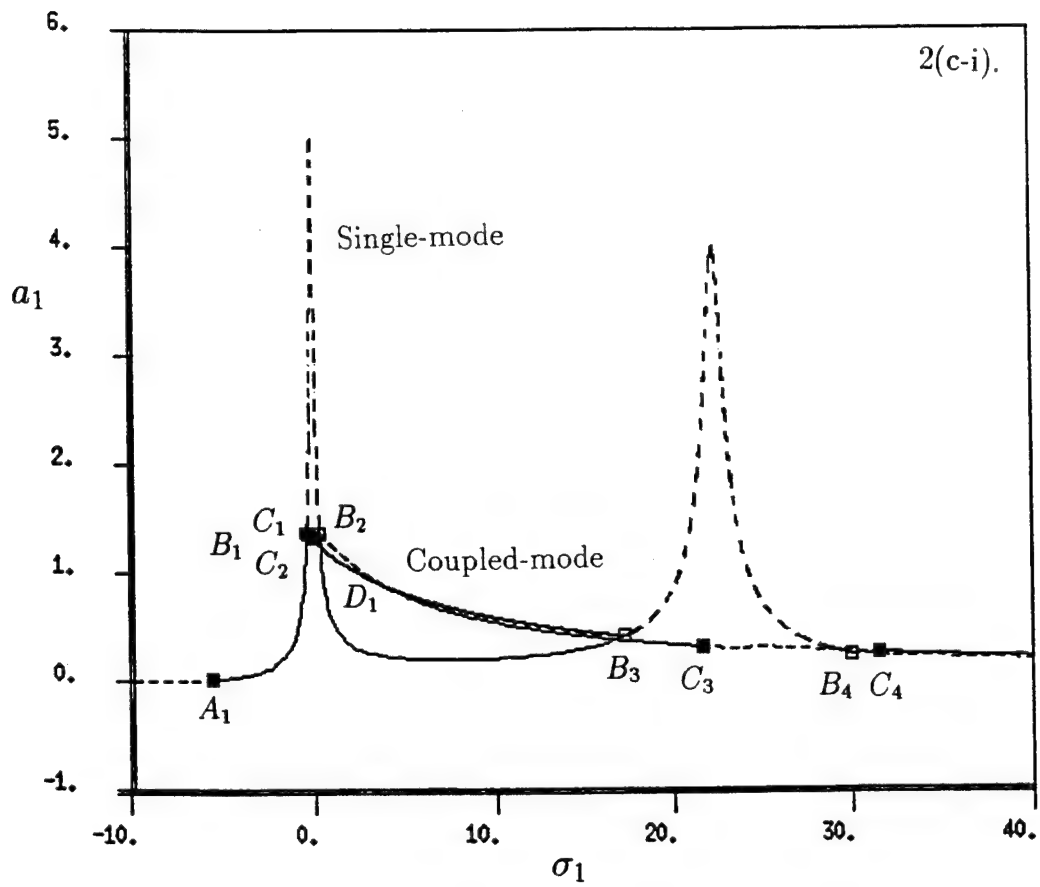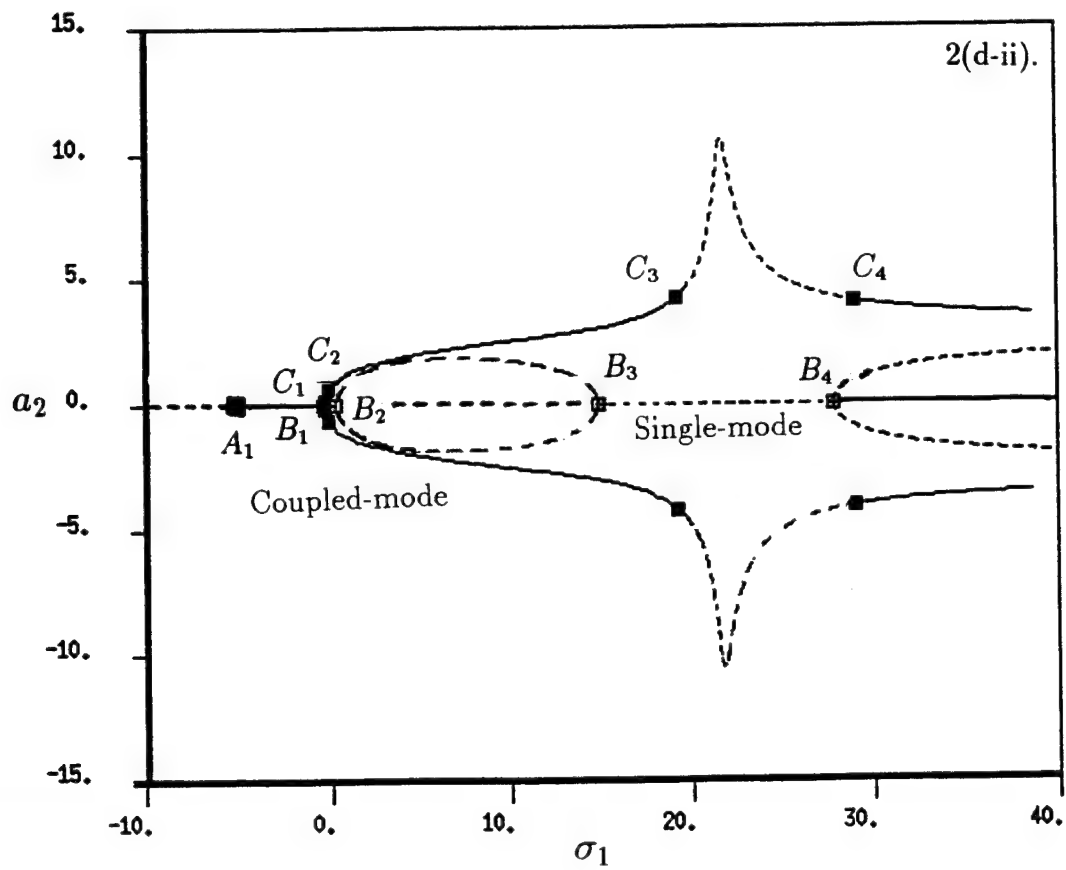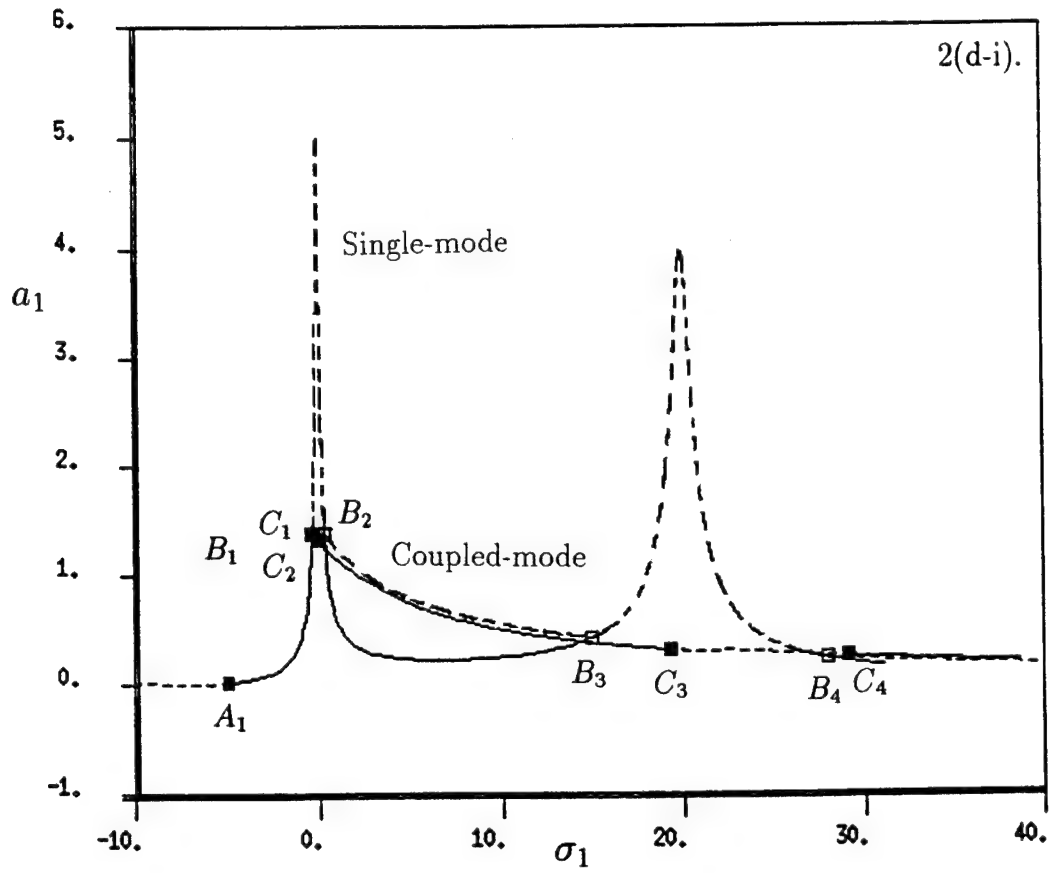Figure 2. Response curves for $\hat{F} = 1.0, \sigma_2 = 0.66, \bar{\xi} = 0.10$ ; (a) $\epsilon = 0.0$, (b) $\epsilon = 0.075$, (c) $\epsilon = 0.08931$ , (d) $\epsilon = 0.1$.
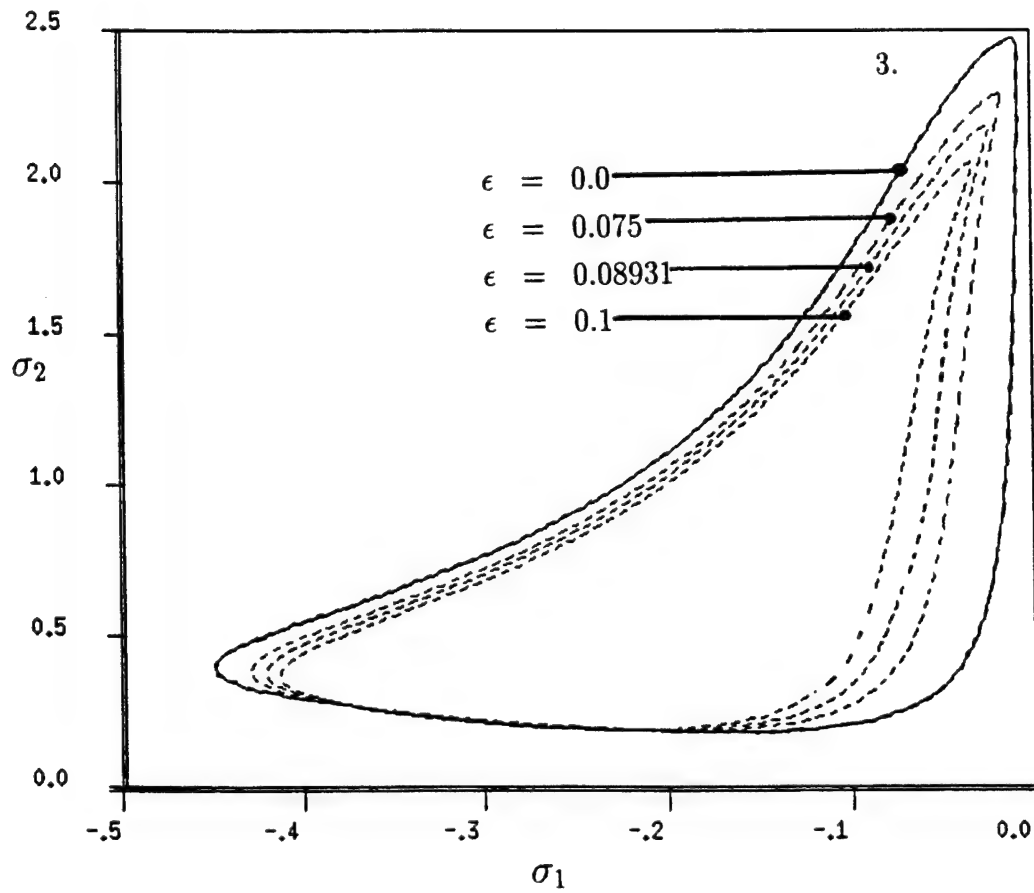
Figure 3. Hopf bifurcation sets in $(\sigma_1, \sigma_2)$ plane for the coupled-mode solution branch $(\hat{F} = 1.0, \bar{\xi} = 0.10)$ ; $\epsilon = 0.00, 0.075, 0.08931, 0.10$ .

Figure 4. Pitchfork bifurcation sets in $(\sigma_1, \sigma_2)$ plane for single-mode solution $(\hat{F} = 1.0, \bar{\xi} = 0.10)$ ; $\epsilon = 0.00, 0.20$

Figure 5. Limit point sets in $(\sigma_1, \sigma_2)$ plane for the coupled-mode solution branch $(\hat{F} = 1.0, \bar{\xi} = 0.10)$ ; $\epsilon = 0.00, 0.075, 0.08931, 0.10$.
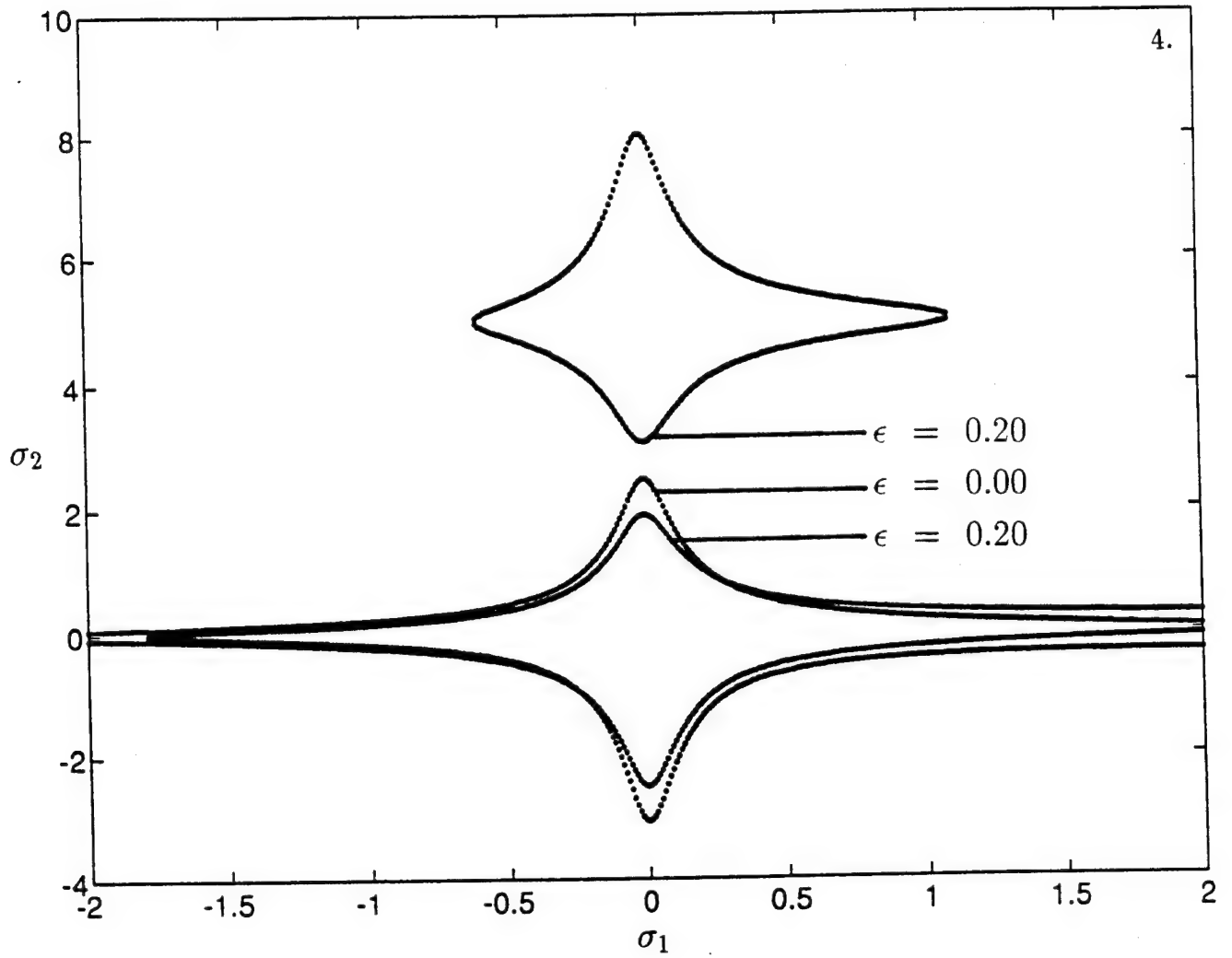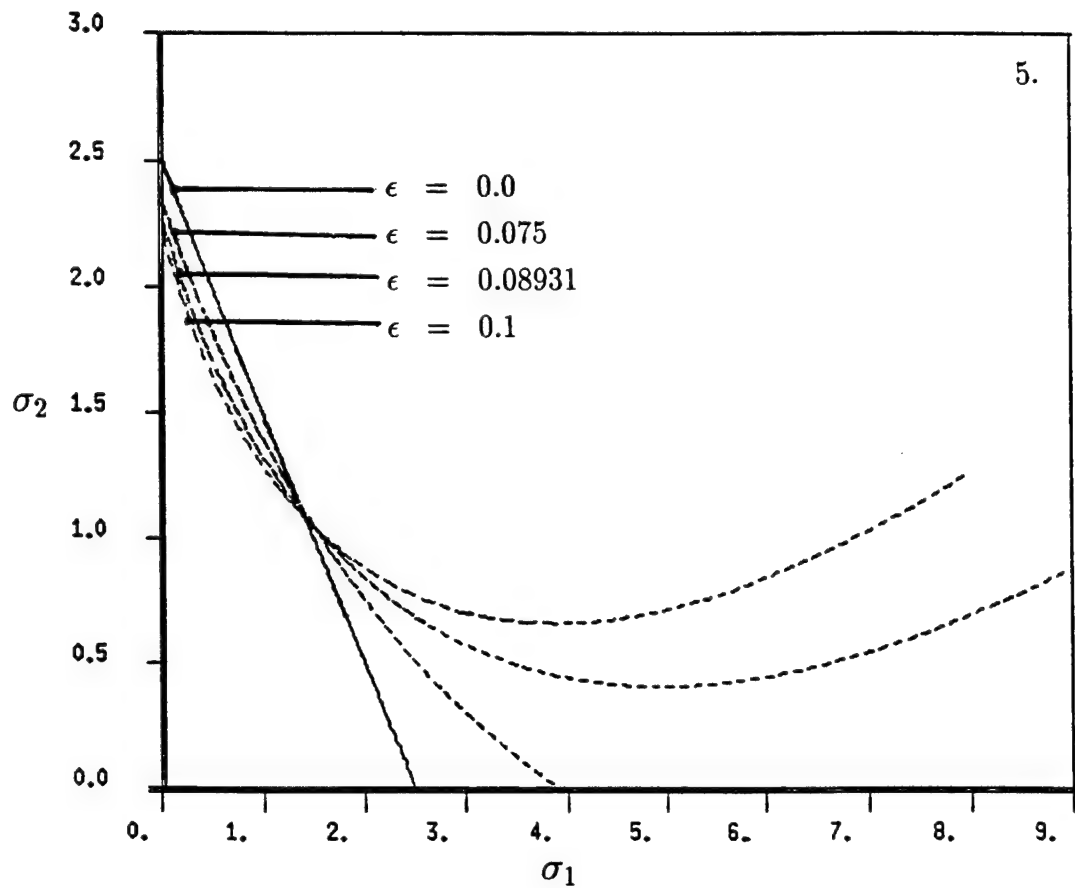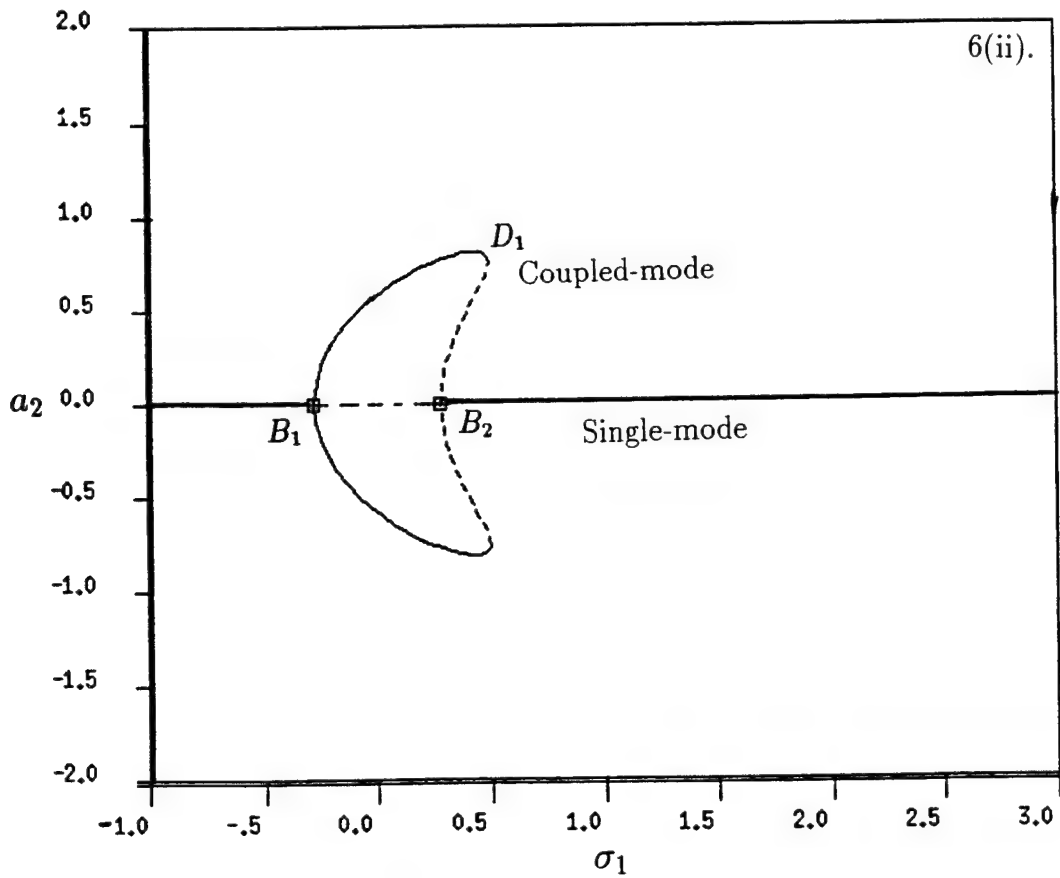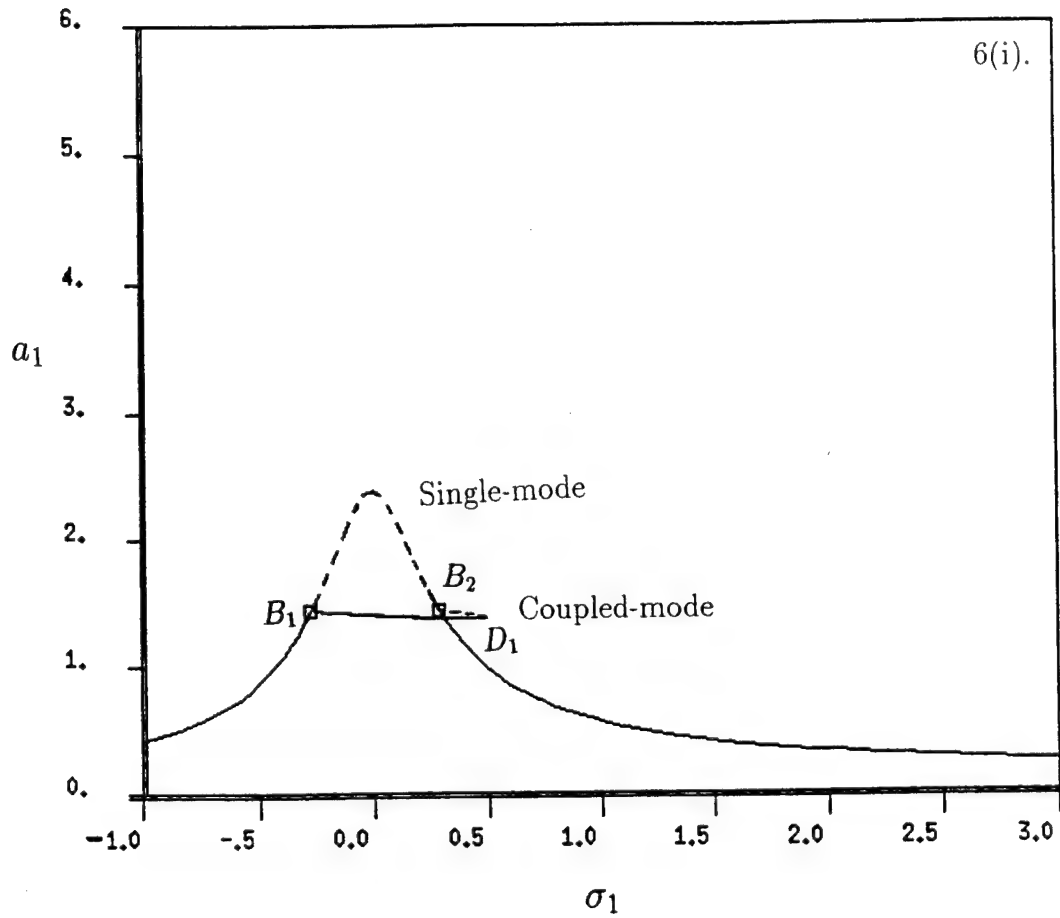
Figure 6. The effect of damping ; Response curves for $\hat{F} = 1.0, \sigma_2 = 0.66, \epsilon = 0.075, \bar{\xi} = 0.21$.

Figure 7. Continuation of periodic solutions on the coupled-mode branch from $C_1$ and $C_2$ ; $\hat{F} = 1.0, \sigma_2 = 0.66, \bar{\xi} = 0.10, \epsilon = 0.075$. (a) Continuation of periodic solutions , (b) Magnified region near the Hopf bifurcation point $C_1$ , (c) Magnified region near the Hopf bifurcation point $C_2$ .

Figure 8. The sequence of period-doublings from $C_1$ ; $\hat{F} = 1.0, \sigma_2 = 0.66, \bar{\xi} = 0.10, \epsilon = 0.075$. (a) $P_1$ solution $(\sigma_1 = -0.316)$ , (b) $P_2$ solution $(\sigma_1 = -0.3105)$ , (c) $P_4$ solution $(\sigma_1 = -0.3093)$ , (d) Chaos $(\sigma_1 = -0.309)$ .

Figure 9. The time-period of the $P_1$ orbit from $C_1$ ; $\hat{F} = 1.0, \sigma_2 = 0.66, \bar{\xi} = 0.10, \epsilon = 0.075$.

Figure 10. Breaking of a homoclinic orbit ; $\hat{F} = 1.0, \sigma_2 = 0.66, \bar{\xi} = 0.10, \epsilon = 0.075$. (a) Approximate homoclinic orbit $(\sigma_1 = -0.3069)$ , (b) Chaotic attractor $(\sigma_1 = -0.3068)$ .

1
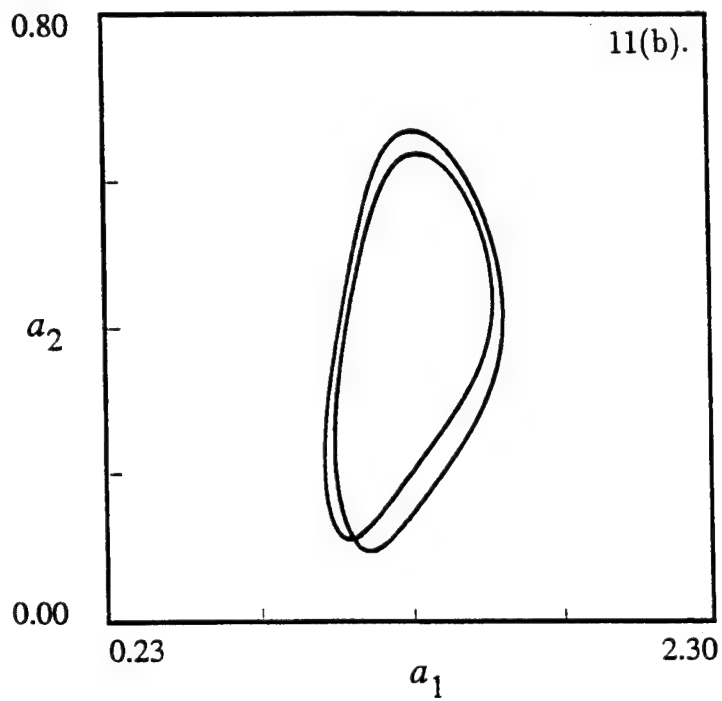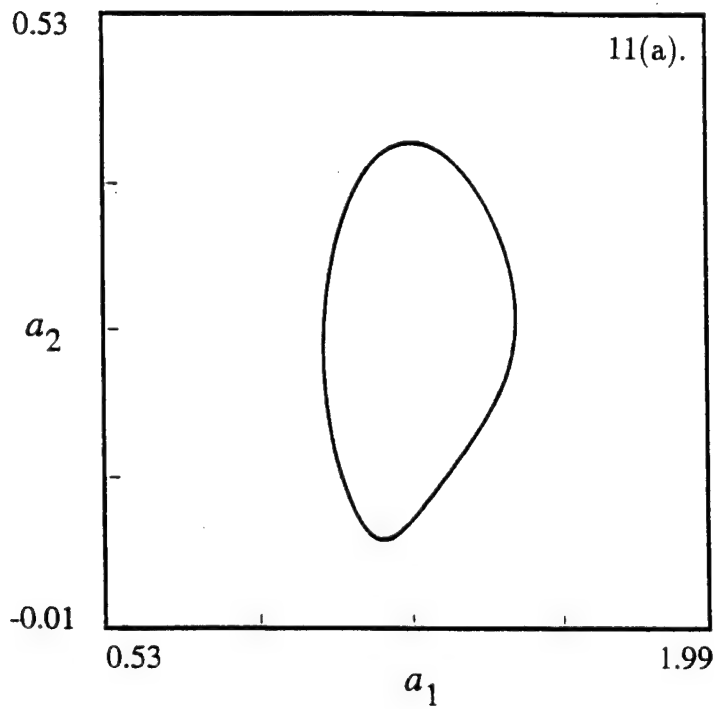
Figure 11. Another cascade of period-doublings ; $\hat{F} = 1.0$, $\sigma_2 = 0.66$, $\bar{\xi} = 0.10$, $\epsilon = 0.075$. (a) $P_1$ solution ($\sigma_1 = -0.304$) , (b) $P_2$ solution ($\sigma_1 = -0.25$) , (c) $P_4$ solution ($\sigma_1 = -0.185$) , (d) $P_8$ solution ($\sigma_1 = -0.175$) , (e) Chaotic attractor ($\sigma_1 = -0.15$) .

Figure 12. 'Crisis' and destruction of the chaotic attractor beyond $C_2$; $\hat{F} = 1.0$, $\sigma_2 = 0.66$, $\bar{\xi} = 0.10$, $\epsilon = 0.075$. ($\sigma_1 = -0.05$)

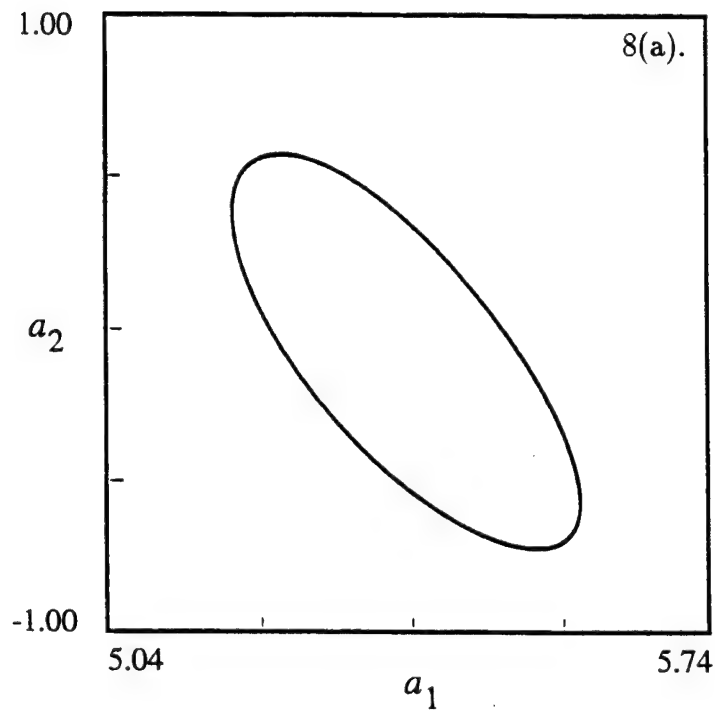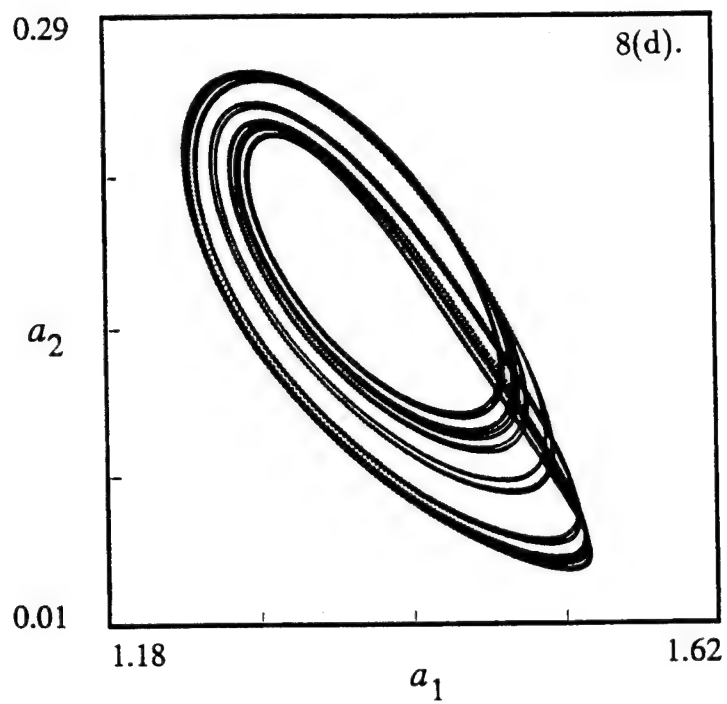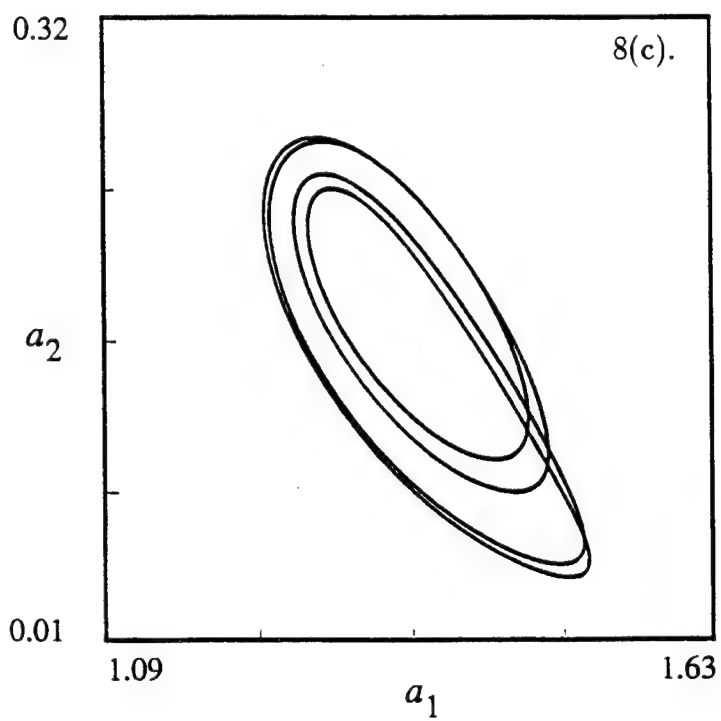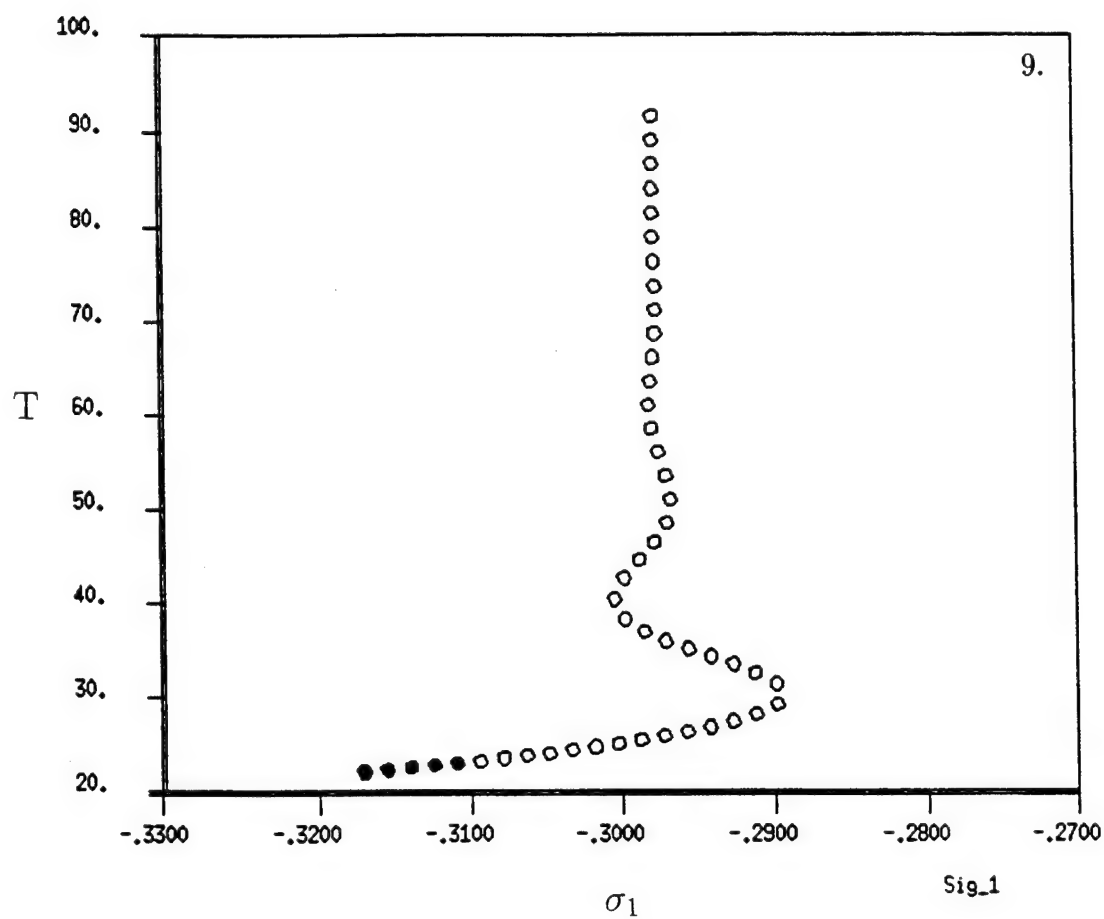Figure 13. Simulation of the original system. Phase portraits and time histories ; $\hat{F} = 1.0$, $\sigma_2 = 0.66$, $\bar{\xi} = 0.10$, $\epsilon = 0.075$. $\sigma_1 = -0.32$. (a) $P_1$ solution in the ($\hat{\eta}_1 - \hat{\eta}_2$) phase-plane, (b) $P_1$ solution in the ($\hat{\eta}_1 - \bar{\theta}_1$) phase-plane, (c) The $\hat{\eta}_1$ time response, (d) The $\bar{\theta}_1$ time response.
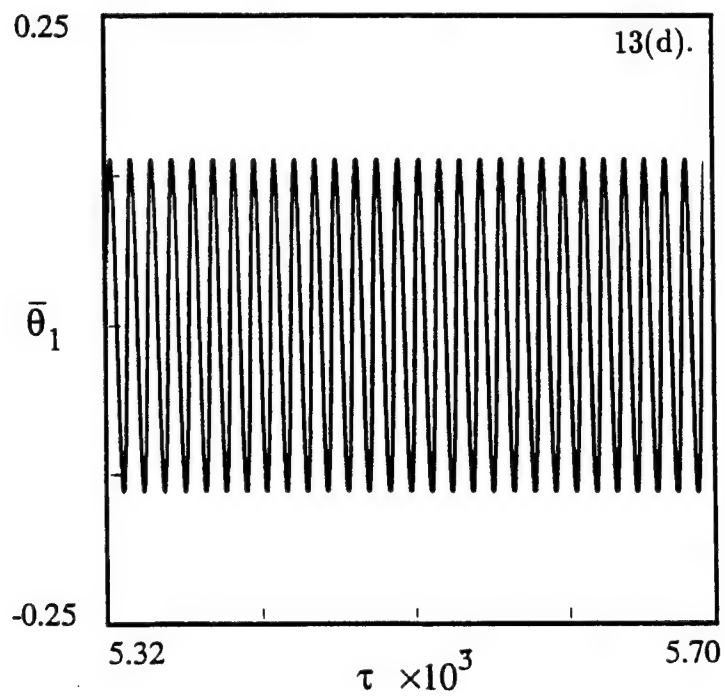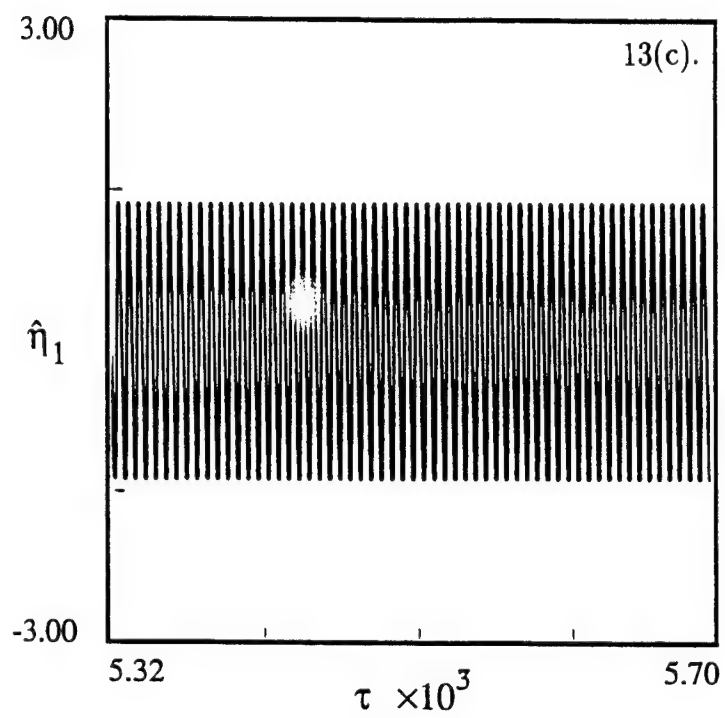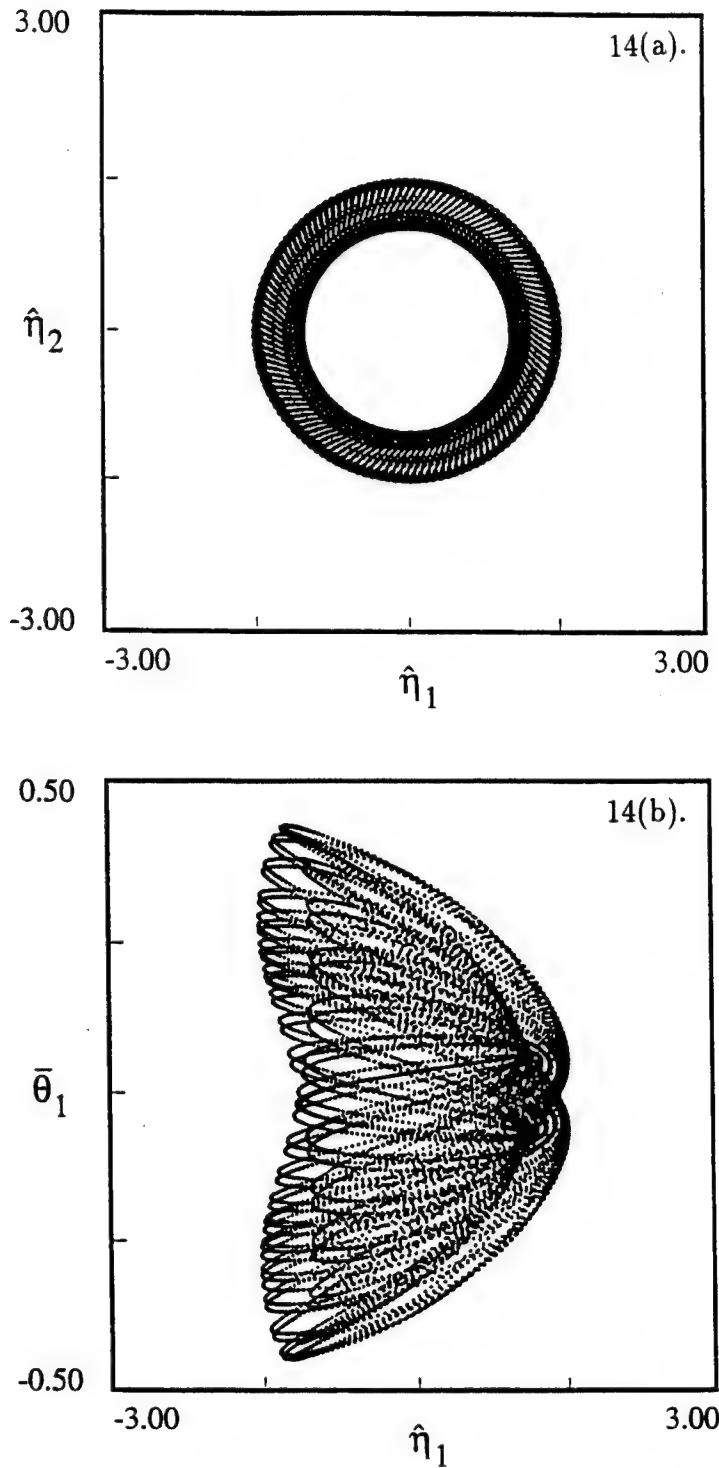
Figure 14. Simulation of the original system. Phase portraits, Poincare-sections and time histories. A $T_1$ solution ; $\hat{F} = 1.0$, $\sigma_2 = 0.66$, $\bar{\xi} = 0.10$, $\epsilon = 0.075$. $\sigma_1 = -0.30$. (a) $T_1$ solution in the ($\hat{\eta}_1 - \hat{\eta}_2$) phase-plane, (b) $T_1$ solution in the ($\hat{\eta}_1 - \bar{\theta}_1$) phase-plane, (c) Poincare-section of the $T_1$ solution in the ($\hat{\eta}_1 - \hat{\eta}_2$) plane, (d) Poincare-section of the $T_1$ solution in the ($\hat{\eta}_1 - \bar{\theta}_1$) plane, (e) $\hat{\eta}_1$ time response, (f) $\bar{\theta}_1$ time response.

Figure 15. Simulation of the original system. Phase portraits, Poincare-sections and time histories. Torus-doubling to a $T_2$ solution ; $\hat{F} = 1.0$, $\sigma_2 = 0.66$, $\bar{\xi} = 0.10$, $\epsilon = 0.075$. $\sigma_1 = -0.24$. (a) $T_2$ solution in the ($\hat{\eta}_1 - \hat{\eta}_2$) phase-plane, (b) $T_2$ solution in the ($\hat{\eta}_1 - \bar{\theta}_1$) phase-plane, (c) Poincare-section of the $T_2$ solution in the ($\hat{\eta}_1 - \hat{\eta}_2$) plane, (d) Poincare-section of the $T_2$ solution in the ($\hat{\eta}_1 - \bar{\theta}_1$) plane, (e) *Envelope* of the $\hat{\eta}_1$ time response, (f) *Envelope* of the $\bar{\theta}_1$ time response.

Figure 16. Simulation of the original system. Poincare-sections and time histories. Another torus-doubling to a $T_4$ solution ; $\hat{F} = 1.0$, $\sigma_2 = 0.66$, $\bar{\xi} = 0.10$, $\epsilon = 0.075$. $\sigma_1 = -0.16$. (a) Poincare-section of the $T_2$ solution in the $(\hat{\eta}_1 - \hat{\eta}_2)$ plane, (b) Poincare-section of the $T_2$ solution in the $(\hat{\eta}_1 - \bar{\theta}_1)$ plane, (c) *Envelope* of the $\hat{\eta}_1$ time response, (d) *Envelope* of the $\bar{\theta}_1$ time response.
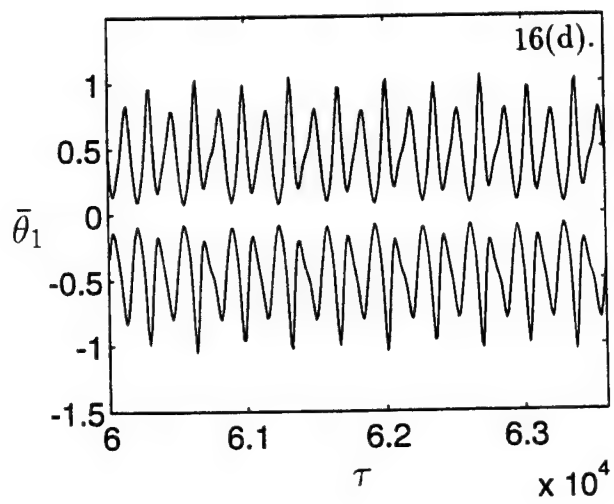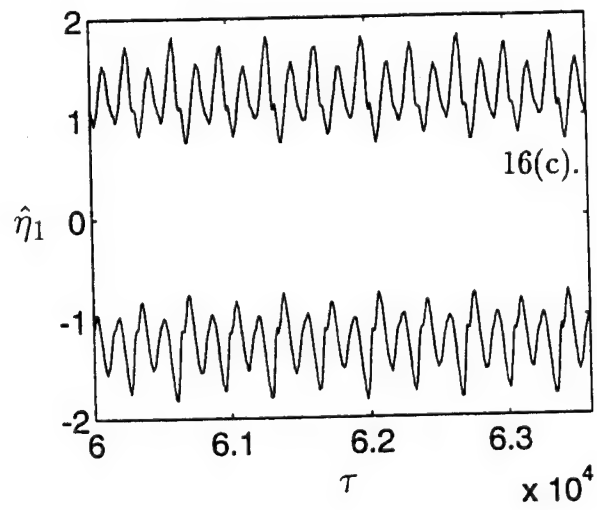
Figure 17. Simulation of the original system. Poincare-sections and time histories ; $\hat{F} = 1.0$, $\sigma_2 = 0.66$, $\bar{\xi} = 0.10$, $\epsilon = 0.075$. $\sigma_1 = -0.08$. (a) Poincare-section of the chaotic solution in the $(\hat{\eta}_1 - \hat{\eta}_2)$ plane, (b) Poincare-section of the chaotic solution in the $(\hat{\eta}_1 - \bar{\theta}_1)$ plane. The *butterfly* attractor, (c) *Envelope* of the $\hat{\eta}_1$ time response, (d) *Envelope* of the $\bar{\theta}_1$ time response.
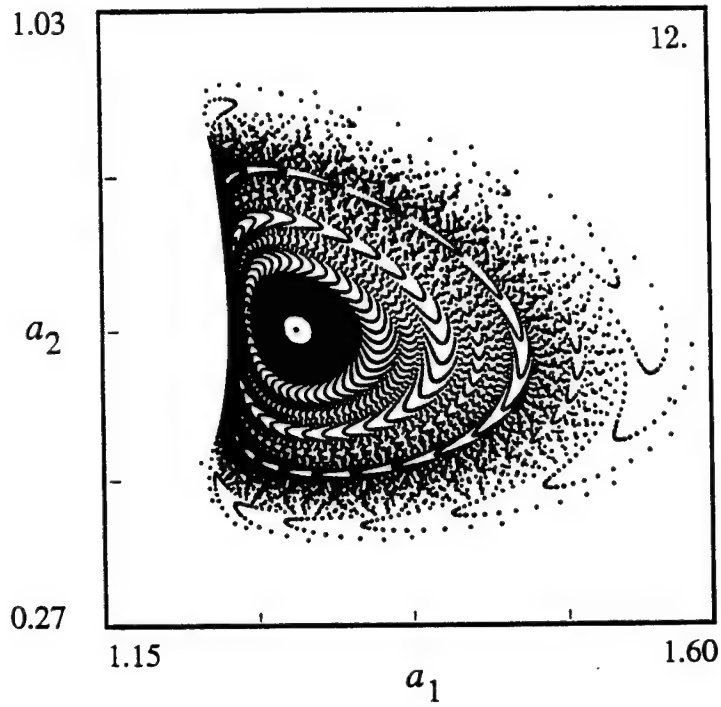
Figure 18. Simulation of the original system. Poincare-sections and time histories. Destruction of the chaotic attractor ; $\hat{F} = 1.0$, $\sigma_2 = 0.66$, $\bar{\xi} = 0.10$, $\epsilon = 0.075$. $\sigma_1 = -0.01$. (a) Poincare-section of the chaotic solution in the $(\hat{\eta}_1 - \bar{\theta}_1)$ plane, (b) *Envelope* of the $\hat{\eta}_1$ time response, (c) *Envelope* of the $\bar{\theta}_1$ time response.

Figure 19. Simulation of the original system. Poincare-sections and time histories. $P_1$ solutions arise again ; $\hat{F} = 1.0$, $\sigma_2 = 0.66$, $\bar{\xi} = 0.10$, $\epsilon = 0.075$. $\sigma_1 = 0.00$. (a) Poincare-section of the chaotic solution in the $(\hat{\eta}_1 - \bar{\theta}_1)$ plane , (b) *Envelope* of the $\hat{\eta}_1$ time response.

3

Figure 1. The autoparametric vibration absorber.

Figure 2. Response curves for $\hat{F} = 1.0$, $\sigma_2 = 0.66$, $\bar{\xi} = 0.10$ ;
(a) $\epsilon = 0.0$, (b) $\epsilon = 0.075$, (c) $\epsilon = 0.08931$ , (d) $\epsilon = 0.1$.

2(b-i).

2(b-ii).

2(c-i).



2(c-ii).

2(d-i).

2(d-ii).

Figure 3. Hopf bifurcation sets in $(\sigma_1, \sigma_2)$ plane for the coupled-mode solution branch $(\hat{F} = 1.0, \bar{\xi} = 0.10)$ ; $\epsilon = 0.00, 0.075, 0.08931, 0.10$ .

Figure 4. Pitchfork bifurcation sets in $(\sigma_1, \sigma_2)$ plane for single-mode solution ($\hat{F} = 1.0, \bar{\xi} = 0.10$) ; $\epsilon = 0.00, 0.20$

Figure 5. Limit point sets in $(\sigma_1, \sigma_2)$ plane for the coupled-mode solution branch $(\hat{F} = 1.0, \bar{\xi} = 0.10)$; $\epsilon = 0.00, 0.075, 0.08931, 0.10$.

Figure 6. The effect of damping ; Response curves for $\hat{F}$ = 1.0, $\sigma_2$ = 0.66, $\epsilon$ = 0.075, $\bar{\xi}$ = 0.21.

Figure 7. Continuation of periodic solutions on the coupled-mode branch from $C_1$ and $C_2$ ; $\hat{F} = 1.0$, $\sigma_2 = 0.66$, $\bar{\xi} = 0.10$, $\epsilon = 0.075$. (a) Continuation of periodic solutions , (b) Magnified region near the Hopf bifurcation point $C_1$ , (c) Magnified region near the Hopf bifurcation point $C_2$ .

7(b).

7(c).

Figure 8. The sequence of period-doublings from $C_1$ ; $\hat{F} = 1.0$, $\sigma_2 = 0.66$, $\bar{\xi} = 0.10$, $\epsilon = 0.075$. (a) $P_1$ solution ($\sigma_1 = -0.316$) , (b) $P_2$ solution ($\sigma_1 = -0.3105$) , (c) $P_4$ solution ($\sigma_1 = -0.3093$) , (d) Chaos ($\sigma_1 = -0.309$) .

8(c).



8(d).

Figure 9. The time-period of the $P_1$ orbit from $C_1$ ; $\hat{F} = 1.0, \sigma_2 = 0.66$, $\bar{\xi} = 0.10, \epsilon = 0.075$.

Figure 10. Breaking of a homoclinic orbit ; $\hat{F} = 1.0$, $\sigma_2 = 0.66$, $\bar{\xi} = 0.10$, $\epsilon = 0.075$. (a) Approximate homoclinic orbit ($\sigma_1 = -0.3069$) , (b) Chaotic attractor ($\sigma_1 = -0.3068$) .

Figure 11. Another cascade of period-doublings ; $\hat{F} = 1.0$, $\sigma_2 = 0.66$, $\bar{\xi} = 0.10$, $\epsilon = 0.075$. (a) $P_1$ solution ($\sigma_1 = -0.304$) , (b) $P_2$ solution ($\sigma_1 = -0.25$) , (c) $P_4$ solution ($\sigma_1 = -0.185$) , (d) $P_8$ solution ($\sigma_1 = -0.175$) , (e) Chaotic attractor ($\sigma_1 = -0.15$) .

11(c).



11(d).

11(e).

Figure 12. 'Crisis' and destruction of the chaotic attractor beyond $C_2$; $\hat{F} = 1.0$, $\sigma_2 = 0.66$, $\bar{\xi} = 0.10$, $\epsilon = 0.075$. ($\sigma_1 = -0.05$)

Figure 13. Simulation of the original system. Phase portraits and time histories ; $\hat{F} = 1.0$, $\sigma_2 = 0.66$, $\bar{\xi} = 0.10$, $\epsilon = 0.075$. $\sigma_1 = -0.32$. (a) $P_1$ solution in the $(\hat{\eta}_1 - \hat{\eta}_2)$ phase-plane, (b) $P_1$ solution in the $(\hat{\eta}_1 - \bar{\theta}_1)$ phase-plane, (c) The $\hat{\eta}_1$ time response, (d) The $\bar{\theta}_1$ time response.
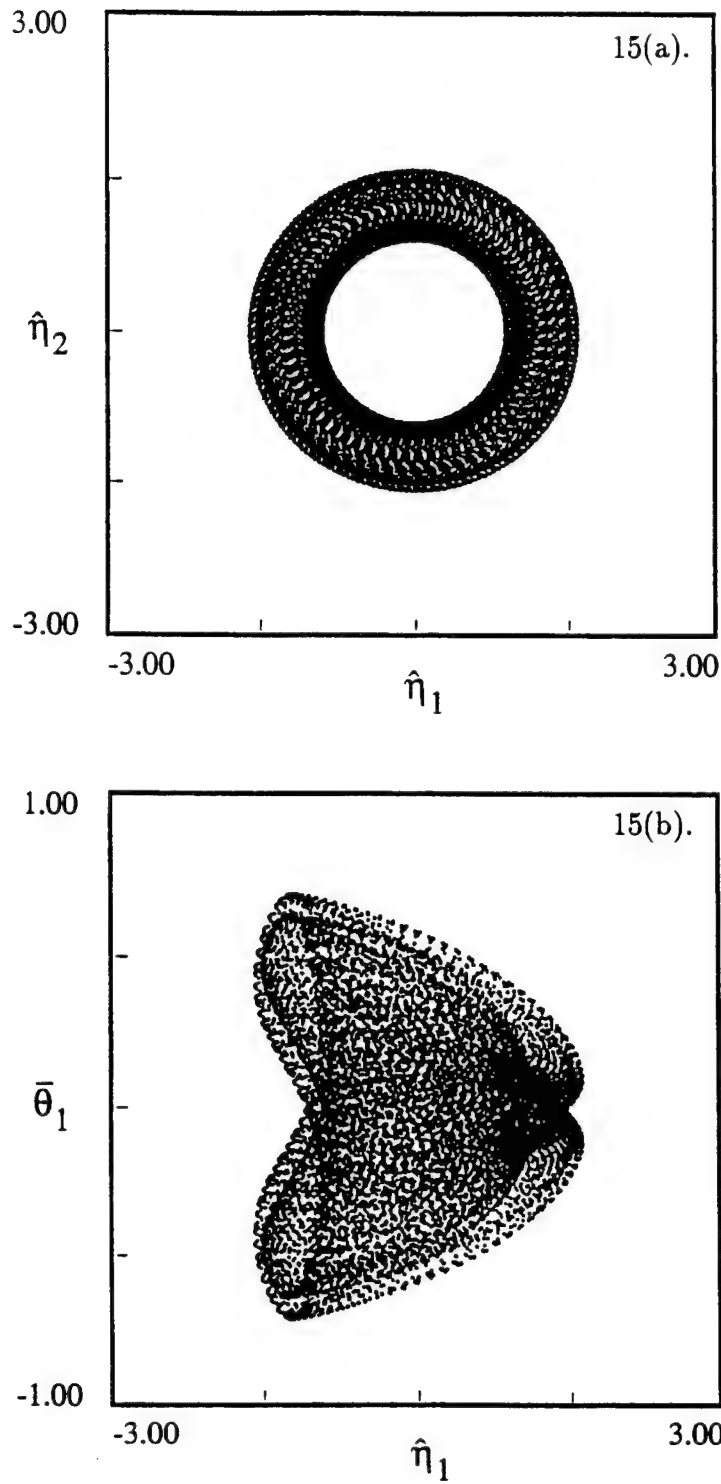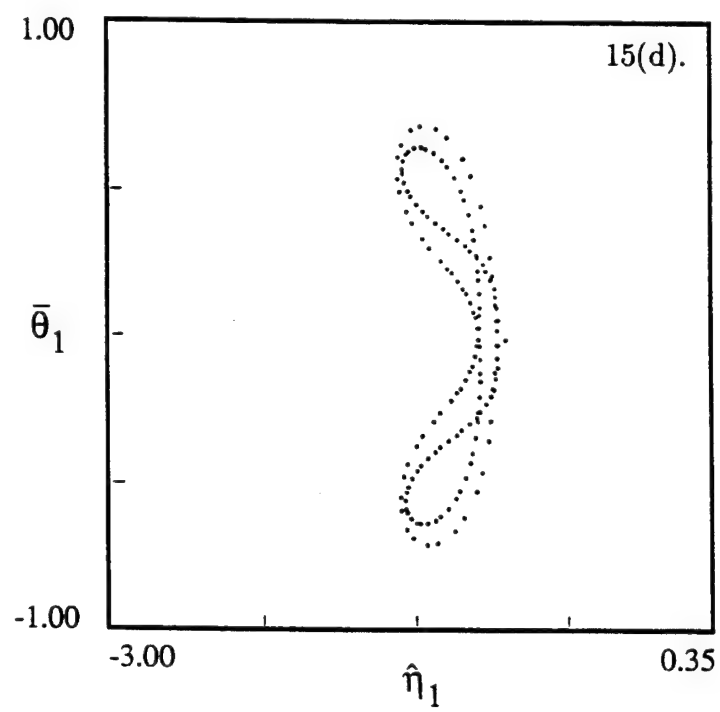
13(c).

13(d).
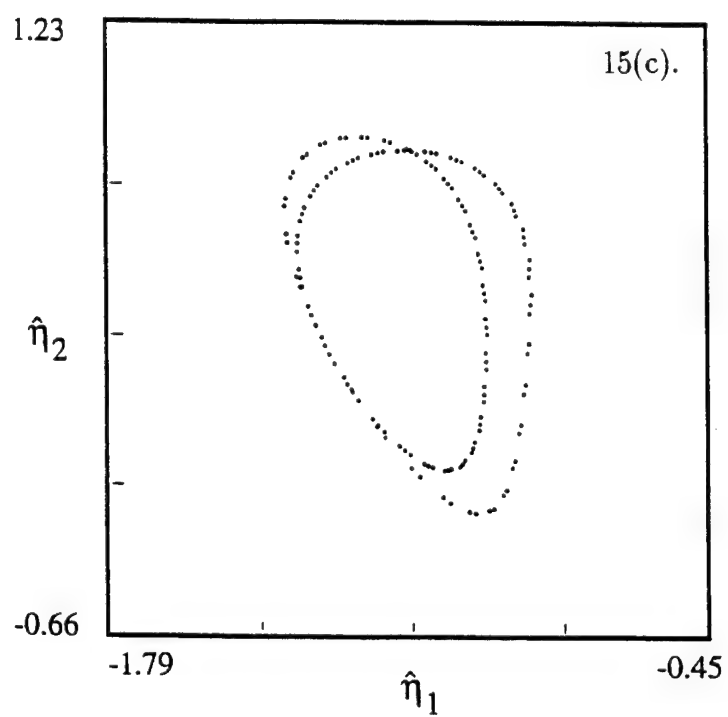
Figure 14. Simulation of the original system. Phase portraits, Poincare-sections and time histories. A $T_1$ solution ; $\hat{F} = 1.0$, $\sigma_2 = 0.66$, $\bar{\xi} = 0.10$, $\epsilon = 0.075$. $\sigma_1 = -0.30$. (a) $T_1$ solution in the $(\hat{\eta}_1 - \hat{\eta}_2)$ phase-plane, (b) $T_1$ solution in the $(\hat{\eta}_1 - \bar{\theta}_1)$ phase-plane, (c) Poincare-section of the $T_1$ solution in the $(\hat{\eta}_1 - \hat{\eta}_2)$ plane, (d) Poincare-section of the $T_1$ solution in the $(\hat{\eta}_1 - \bar{\theta}_1)$ plane, (e) $\hat{\eta}_1$ time response, (f) $\bar{\theta}_1$ time response.
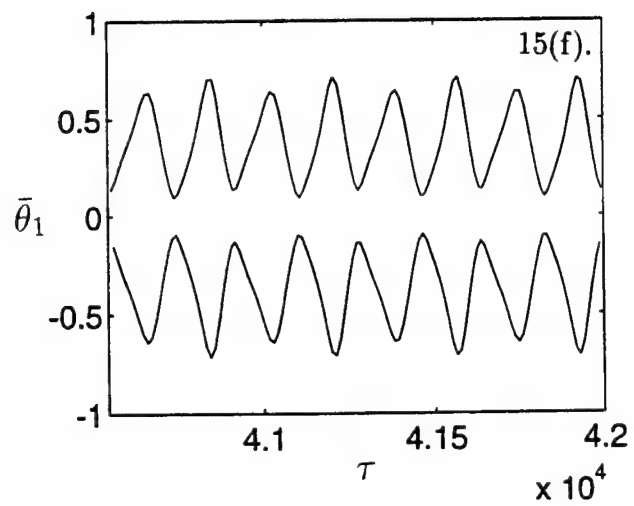
14(c).



14(d).

14(e).

$\hat{\eta}_1$
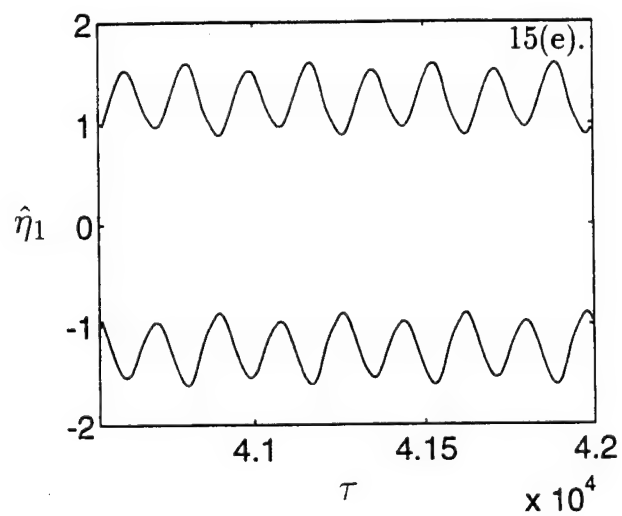


14(f).

$\bar{\theta}_1$

Figure 15. Simulation of the original system. Phase portraits, Poincare-sections and time histories. Torus-doubling to a $T_2$ solution ; $\hat{F} = 1.0$, $\sigma_2 = 0.66$, $\bar{\xi} = 0.10$, $\epsilon = 0.075$. $\sigma_1 = -0.24$. (a) $T_2$ solution in the $(\hat{\eta}_1 - \hat{\eta}_2)$ phase-plane, (b) $T_2$ solution in the $(\hat{\eta}_1 - \bar{\theta}_1)$ phase-plane, (c) Poincare-section of the $T_2$ solution in the $(\hat{\eta}_1 - \hat{\eta}_2)$ plane, (d) Poincare-section of the $T_2$ solution in the $(\hat{\eta}_1 - \bar{\theta}_1)$ plane, (e) *Envelope* of the $\hat{\eta}_1$ time response, (f) *Envelope* of the $\bar{\theta}_1$ time response.
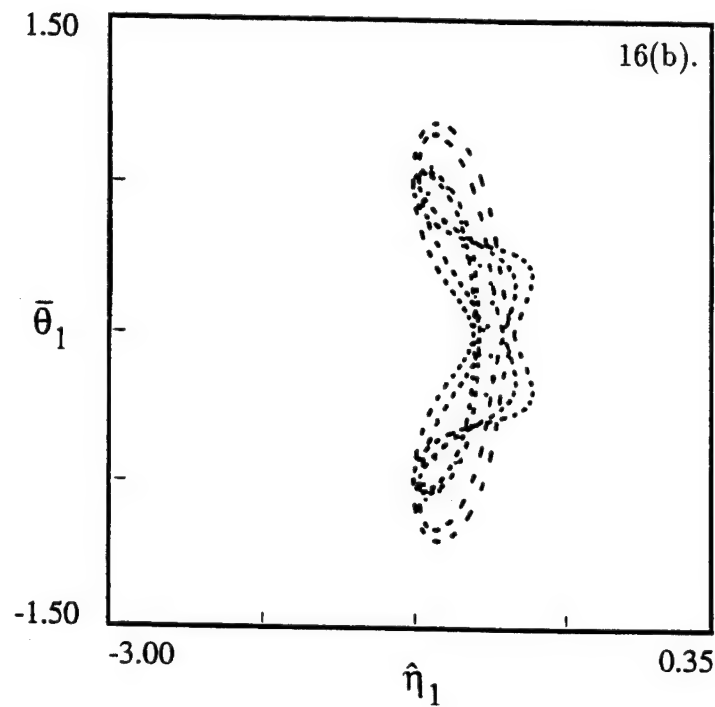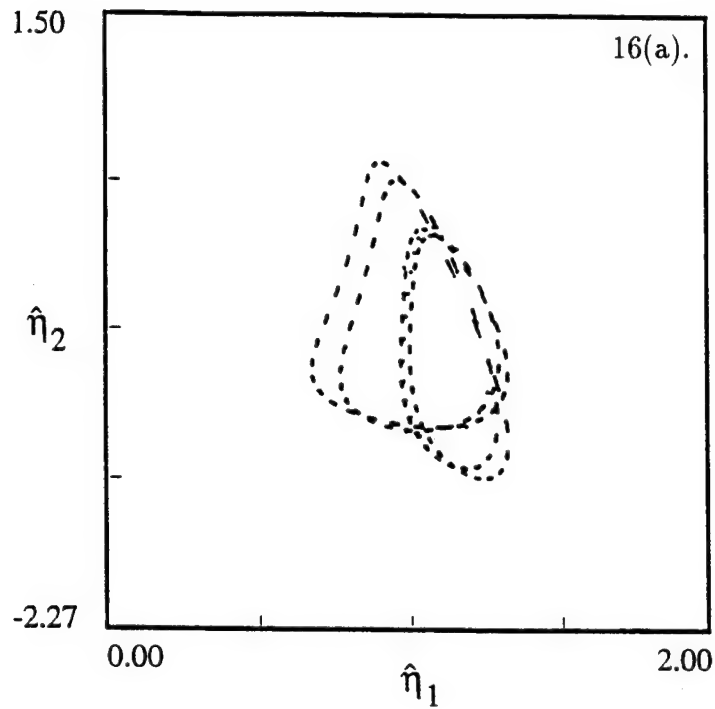
15(c).



15(d).

15(e).



15(f).

Figure 16. Simulation of the original system. Poincare-sections and time histories. Another torus-doubling to a $T_4$ solution ; $\hat{F} = 1.0$, $\sigma_2 = 0.66$, $\bar{\xi} = 0.10$, $\epsilon = 0.075$. $\sigma_1 = -0.16$. (a) Poincare-section of the $T_2$ solution in the $(\hat{\eta}_1 - \hat{\eta}_2)$ plane, (b) Poincare-section of the $T_2$ solution in the $(\hat{\eta}_1 - \bar{\theta}_1)$ plane, (c) *Envelope* of the $\hat{\eta}_1$ time response, (d) *Envelope* of the $\bar{\theta}_1$ time response.
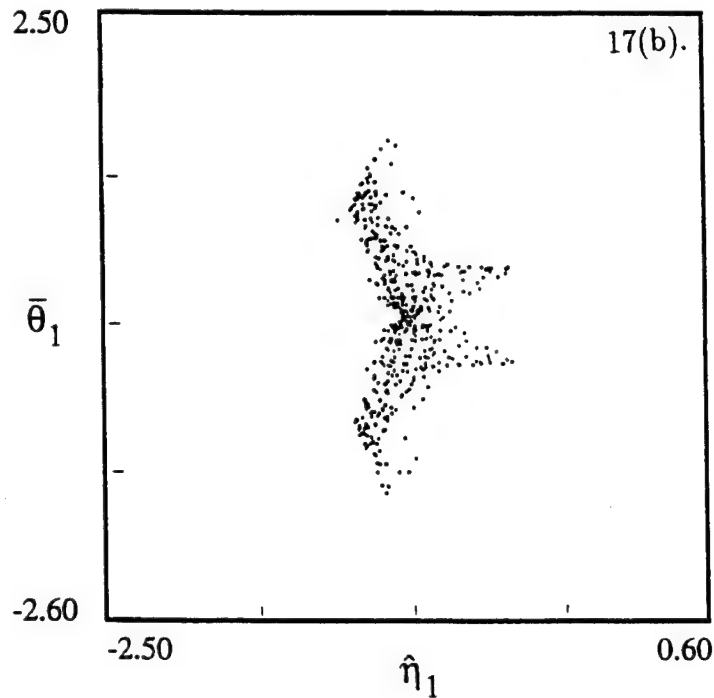
16(c).

16(d).

Figure 17. Simulation of the original system. Poincare-sections and time histories ; $\hat{F} = 1.0$, $\sigma_2 = 0.66$, $\bar{\xi} = 0.10$, $\epsilon = 0.075$. $\sigma_1 = -0.08$. (a) Poincare-section of the chaotic solution in the $(\hat{\eta}_1 - \hat{\eta}_2)$ plane, (b) Poincare-section of the chaotic solution in the $(\hat{\eta}_1 - \bar{\theta}_1)$ plane. The *butterfly* attractor, (c) *Envelope* of the $\hat{\eta}_1$ time response, (d) *Envelope* of the $\bar{\theta}_1$ time response.

17(c).



17(d).

Figure 18. Simulation of the original system. Poincare-sections and time histories. Destruction of the chaotic attractor ; $\hat{F}$ = 1.0, $\sigma_2$ = 0.66, $\bar{\xi}$ = 0.10, $\epsilon$ = 0.075. $\sigma_1 = -0.01$. (a) Poincare-section of the chaotic solution in the $(\hat{\eta}_1 - \bar{\theta}_1)$ plane, (b) *Envelope* of the $\hat{\eta}_1$ time response, (c) *Envelope* of the $\bar{\theta}_1$ time response.
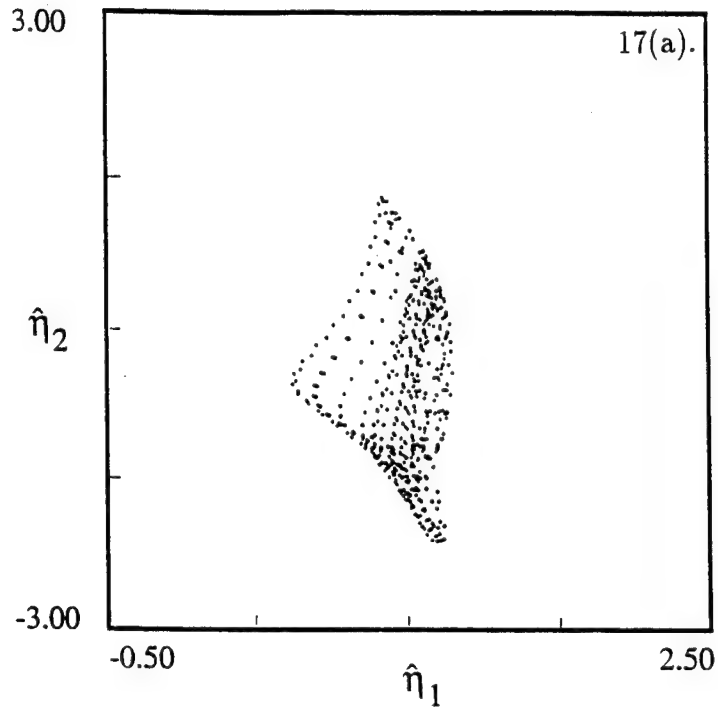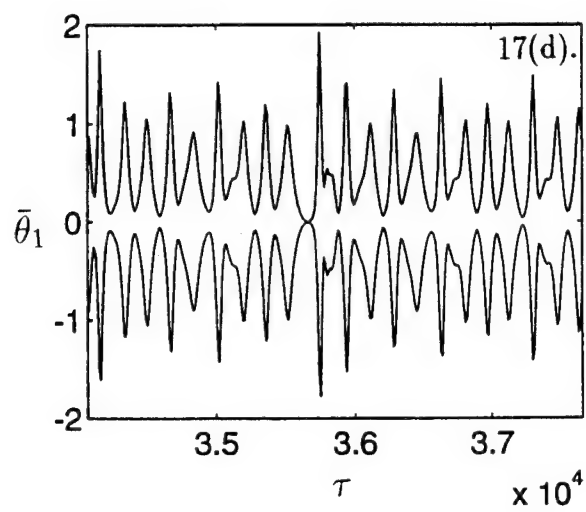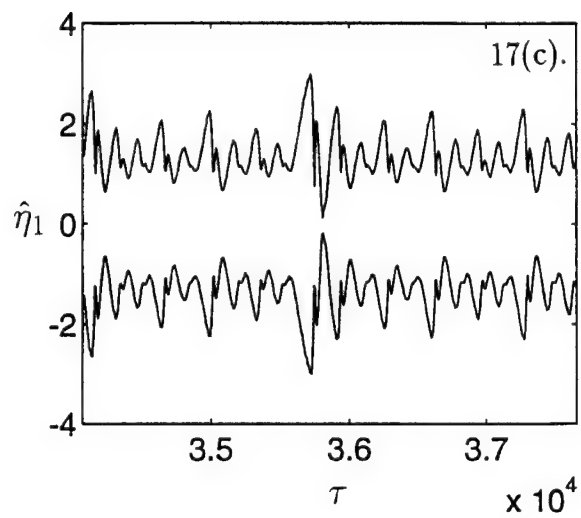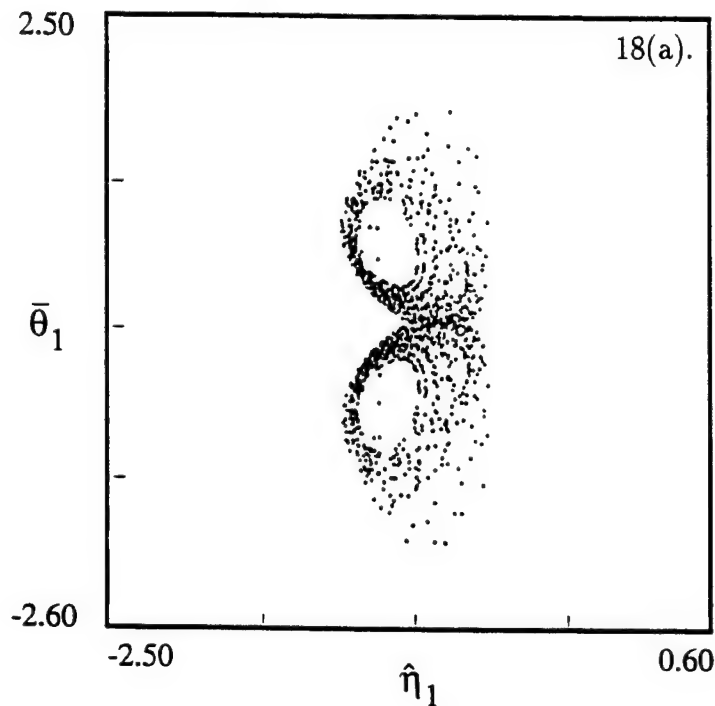
18(b).



18(c).

Figure 19. Simulation of the original system. Poincare-sections and time histories. $P_1$ solutions arise again ; $\hat{F}$ = 1.0, $\sigma_2$ = 0.66, $\bar{\xi}$ = 0.10, $\epsilon$ = 0.075. $\sigma_1 = 0.00$. (a) Poincare-section of the chaotic solution in the $(\hat{\eta}_1 - \bar{\theta}_1)$ plane , (b) *Envelope* of the $\hat{\eta}_1$ time response.

# APPENDIX 2

## Bifurcations and chaotic motions in resonantly excited structures

S. I. Chang, A. K. Bajaj, P. Davies

to appear in

Bifurcations and Chaos: Theory and Applications
( ed: J. Awrejcewicz) Springer Verlag, 1995.

# BIFURCATIONS AND CHAOTIC MOTIONS
# IN RESONANTLY EXCITED STRUCTURES

S. I. Chang, A. K. Bajaj, P. Davies

School of Mechanical Engineering
Purdue University
West Lafayette, IN  47907-1288, U.S.A.

## ABSTRACT

The focus of this chapter is a discussion of the behavior of multi-degree-of-freedom models of structures with nonlinearities. While an overview of the research conducted in this area is given, the latter part of the chapter is devoted to a study of the response of weakly nonlinear multi-degree-of-freedom models under harmonic excitation. These models were derived from the von Karman equations that describe the behavior of a thin rectangular plate under initial tension. Of particular interest is the types of behavior that result from internal resonances, whereby one mode is driven directly but other modes are excited through the nonlinear coupling between the modes. Energy sharing between the directly driven mode and the other modes leads to an amplitude-modulated coupled-mode response that can become chaotic. The approach is to develop, through averaging, models of the slowly varying amplitude and phase of the nonlinear response of the interacting modes. These equations are studied by using local bifurcation theory for their steady-state solutions. Various bifurcation points are identified in order to understand which types of solutions are possible for a given set of excitation conditions and model parameter values. It is shown that the response of the plate is qualitatively distinct and depends on the mode which is directly excited by the external loading.

# 1. INTRODUCTION

The nonlinear behavior of structures, including that of strings, beams, arches, and plates and shells, has been studied, both statically and dynamically, for a long time[1,2]. The source of the nonlinearity may be geometric, inertial, due to material properties, or may arise because of damping mechanisms or boundary conditions. The geometric nonlinearity may be induced by the nonlinear stretching or by curvature effects that are significant when deformations are large. The membrane forces, induced by stretching, accompany transverse motion of the structure, if the boundary is constrained against movement in the longitudinal direction. This longitudinal stretching leads to a nonlinear relationship between the strain and the displacement. Therefore, when large amplitude vibrations of a structure are studied, this nonlinear geometric effect needs to be considered. Nonlinear inertial effects, caused by the presence of concentrated or distributed masses, also couple the transverse and in-plane motion. Material nonlinearity in structures arises when the relationship between the stress and the strain is nonlinear.

By including these various sources of nonlinearities in the models of the dynamical response of structures, many phenomena, not predicted by a linear theory, can be explained. For example, multiple solutions, jumps, subharmonic and superharmonic resonances, and amplitude modulated motions including period-doublings and chaos. These phenomena can occur whenever a structure is in external resonance, that is, the frequency of excitation is close to either a natural frequency of a specific mode of the structure, or to some multiple or submultiple of a natural frequency. Under these conditions, the structure can be modeled as a single degree-of-freedom system if the interactions with other modes are negligible or unimportant. Similar behavior can also arise when the structure undergoes dynamic instabilities as a result of parametric excitations or loadings.

When the structure, however, has commensurable or nearly commensurable natural frequencies with small integer ratios, the interaction among the modes through *internal resonances* can be of significance depending on the type of nonlinearity present in the system. The nonlinear system behavior can be classified into several cases[1,3] depending on the presence or the absence of the internal and/or the external resonances. Systems which possess internal, as well as external, resonances are found to exhibit interesting responses, arising because of the exchange of energy between the modes in internal resonance. Through the external resonance, energy can be fed to one or many modes in internal resonance. Even when only one mode is directly excited, the system can exhibit the so called "coupled-mode response" (contrasted to the "single-mode response") due to the exchange of energy between the various modes. This modal coupling in the structure is caused by the nonlinearities present. A classical example of this behavior is the stretched nonlinear string, which exhibits non-planar whirling motions even when the resonant

harmonic excitation is restricted to one plane[4-6]. Higher levels of excitation are usually necessary to destabilize the single-mode response into a coupled-mode response. Some studies[7-9] have shown that this coupled-mode response can be in the form of traveling waves, and that the steady-state traveling waves become amplitude-modulated, period-double and finally become chaotic as a system parameter is varied.

The kind of internal resonance which a specific structure can exhibit is determined by the type of nonlinearity inherent in the structure. The modes which can be coupled through internal resonance are determined by the geometric conditions of the structure. For example, an Euler-Bernoulli beam, with rectangular cross section and cross-sectional aspect ratio near unity, exhibits a coupling of the identical spatial modes in the two orthogonal planes, whereas, with an aspect ratio near 6.27, it exhibits a coupling of the first spatial mode in one plane to the second spatial mode in the orthogonal plane[10]. In both cases, the beam possesses one-to-one internal resonance.

The literature on nonlinear structural vibrations is quite extensive with both single and multiple degree-of-freedom models having been investigated. Studies with single degree-of-freedom models include weakly nonlinear[1] as well as global or strongly nonlinear responses[11], whereas, the studies with multiple degree-of-freedom models are mostly restricted to the weakly nonlinear behavior involving modal interactions. The methods used for analyzing the weakly nonlinear responses, usually consisting of perturbation and asymptotic techniques[1], are quite distinct from the geometric-perturbation methods[12-14] used in predicting the strongly nonlinear behavior including the existence of chaotic dynamics. Applications of the geometric-perturbation methods to the study of the global behavior of structural systems include the works of Holmes and Marsden[11] and Yagasaki[15] for one-mode responses, and the works of Yang and Sethna[7,16] for coupled-mode dynamics. The work described in this chapter is limited mostly to coupled-mode response and only a brief remark will be made with respect to the application of global analysis techniques to prove the existence of chaos in these averaged systems.

The coupled-mode behavior of resonantly excited structures has received considerable attention in recent years, although, there do exist classical studies[17-19] that were conducted two to three decades ago. The authors of more recent studies were able to utilize developments in local bifurcation theory. In the following section, recent studies on nonlinear behavior of basic structural elements are first reviewed and then briefly discussed. The discussion here is restricted to works which use local bifurcation theory. In subsequent sections, the nonlinear flexural motions of rectangular plates are considered and some new results on the coupled-mode dynamics under resonant harmonic excitation are presented.

## 2. NONLINEAR STRUCTURAL MEMBERS

In this section the recent literature on the nonlinear response of structural elements will be reviewed. The systems discussed include strings, beams, shells and rings, and plates. They are subjected to either external or parametric harmonic excitations. The governing partial differential equations for the continuous systems are, in most studies, transformed to a nonlinear temporal set of ordinary differential equations by a Galerkin procedure. The finite set of second-order ordinary differential equations are then analyzed by using the asymptotic methods of multiple time scales or averaging, to obtain a first-order approximate solution for the case of weakly nonlinear systems. The form of the amplitude equations, obtained by the asymptotic methods, depends on the types of "internal" and "combination" resonances and on the nature of the nonlinearities in the structure. The responses of specific structures are discussed below.

### 2.1 Strings

The prediction of the nonlinear response of stretched strings to harmonic excitations is a classic problem. There have been studies, numerous both the analytical and experimental; the results of which are summarized in Nayfeh and Mook[1]. This system, and in particular the non-planar response, has received considerable attention in recent years beginning with the work of Miles[20] who revisited the problem of stretched string vibration by using local bifurcation theory. Here, the spatial modes in two orthogonal directions are always in a 1:1 internal resonance. Miles showed that, when excited in a plane in a particular frequency interval, the steady-state planar response bifurcates to the steady-state non-planar response. When this occurs, many stable periodic planar and non-planar responses coexist. He also showed that some steady-state non-planar solutions of the amplitude or averaged equations lose stability via a Hopf bifurcation as damping is lowered.

Following Miles' work, Bajaj and Johnson[4,21,22], took up the problem of the non-planar response of a string and showed that periodically and chaotically modulated responses are possible for some parameter values. The results of their study are a detailed picture of possible bifurcations in the motion of a string. They showed that for the amplitude equations there are two limit cycle branches, one arising due to the Hopf bifurcation and the other due to a global saddle-node bifurcation. With variation in detuning (excitation frequency), the isolated branch exhibits period-doubling bifurcation, chaotic attractors and merging of attractors, giving rise to Rössler as well as Lorenz-type attractors.

They also directly integrated the truncated string equations. There are non-planar periodic responses that bifurcate into amplitude-modulated motions on a two-torus. (Motion on a two-torus is a geometric way to describe motion with two frequencies.) Changes in the

parameter values of damping and excitation frequency result in torus-doubling, coexisting torus branches, and merging as well as destruction of the torus, leading to chaotic amplitude modulation. Results from the investigations of the averaged system were interpreted for the truncated system by using the averaging theory and the theory of integral manifolds. The bifurcation values of parameters were found to exhibit a scaling behavior and the results of the averaged equations were found to be in good qualitative agreement with the actual response. Numerical investigations with the single-mode truncation of the non-autonomous string system showed that there is a good correspondence, even between chaotic solutions of the averaged system and those of the original system.

Tufillaro[5] adopted a very simple single-mode model for string vibrations. Bajaj and Johnson had, on the other hand, started with the first order continuum model which accounts for axial motions but considers the longitudinal wave speed to be much higher than the transverse wave speed, an assumption valid for metallic strings. Tufillaro's model is capable of showing nonlinear phenomena including hysteresis, periodic, quasiperiodic, and chaotic motions. Chaotic vibrations were predicted for an experimentally accessible regime. Molteno and Tufillaro[23] reported experimental results that show good qualitative agreement with the theoretical and numerical results described by Johnson and Bajaj[4] for a torus doubling transition to chaos. They observed the following bifurcation sequence as the frequency was varied: periodic → quasi-periodic → chaotic → quasi-periodic → periodic and, at lower forcing amplitude, periodic → quasi-periodic → periodic. They also observed torus mergings for excitation frequencies near the second harmonic with the bifurcation sequence: period one → period two → two separate tori → torus merging → torus doubling.

O'Reilly and Holmes[6] also reported both experimental and theoretical results for the nonlinear motions of a stretched string. They observed multiple periodic motions, planar and non-planar, as well as quasi-periodic whirling and irregularly precessing oscillations. They found that two kinds of irregularly precessing oscillations coexist with stable planar and whirling motions. A two degree-of-freedom model was derived, and it was shown that these motions can be partially understood in terms of the completely integrable Hamiltonian system obtained when damping and forcing tend to zero in that model. In a more recent work, O'Reilly[24] showed how Silnikov's analysis can be used to predict the existence of chaotic behavior in the averaged equations when the string produces non-planar or whirling motions. This analysis requires the existence of a homoclinic orbit which was observed in the numerical work of both Bajaj and Johnson[22] and O'Reilly and Holmes[6].

## 2.2 Beams

Studies of the nonlinear resonant response of inextensible as well as extensible elastic beams have been widely reported in the literature. The most studied cases correspond to

coupled-mode responses with 1:1 and 1:3 internal resonances among the participating modes. The 1:1 resonances naturally arise in the study of non-planar responses when, in the beams with symmetric sections, the two identical spatial modes in two orthogonal planes are coupled through weak nonlinearities. In beams with motion restricted to only one plane, hinged-clamped boundary conditions and boundary conditions with restraining springs can result in 1:3 internal resonance among the in-plane flexural modes[1].

Crespo da Silva and Glynn[25,26] investigated the nonlinear, non-planar oscillations of inextensional elastic beams. They derived a set of equations of motion for inextensional elastic beams which model the flexure about two principal axes, account for torsion and retain the order-three nonlinear inertia and curvature terms[25]. They studied the non-planar resonant forced vibration of inextensional elastic beams with fixed-free boundary conditions, and 1:1 resonance in the in-plane and out-of-plane flexural modes. They showed that the nonlinear curvature term is of significance for the response in the first spatial mode. Crespo da Silva[27] reported that, for some range of excitation frequency and for particular values of parameters, no stable steady-state response, either planar or non-planar, exists, and the tip of the cantilever wanders in space without reaching a steady-state.

Maewal[28] studied the problem of resonant motions of simply-supported elastic beams whose cross-sections are invariant with respect to planar rotation of ninety degrees. The equations for describing the dynamics of the amplitudes and phases of a harmonically excited beam were numerically integrated. He showed that, for certain values of the frequency of excitation, the response of the beam may be chaotically modulated and that one of the Lyapunov exponents is positive for the cases of chaotic responses. Additionally, the response exhibits a broadening of the power spectra. For the chaotic responses, he also numerically constructed the Poincare' sections of the attractors which clearly show a fractal structure.

Nayfeh and Pai[29] investigated the planar and the non-planar responses of a fixed-free beam, with a 1:1 internal resonance between in-plane and out-of-plane flexural modes, to a principal parametric excitation. They showed that the nonlinear inertia terms play a significant role in the planar response of higher frequency modes. On the other hand, the nonlinear geometric terms dominate the planar response of low frequency modes and the non-planar response for all the modes. For some range of parameters, Hopf bifurcations exist and the response consists of amplitude-and phase-modulated, or chaotic motions. Similar results were found for the cantilever beam with lateral base excitation[10].

Restuccio, Krousgrill and Bajaj[30] investigated the nonlinear response of a clamped-clamped/sliding inextensional elastic beam subjected to a harmonic axial load. The amplitude equations for the two-mode approximation were analyzed for steady-state and

periodic solutions arising from Hopf bifurcations. Depending on the amplitude of excitation, the damping and the ratio of principal flexural rigidities, various qualitatively different frequency response diagrams are uncovered and limit cycles and chaotic motions were found. The authors also compared the above determined response, derived by using the method of multiple scales, with the one obtained by directly integrating the coupled second-order equations, and found good qualitative agreement between the two responses. The mistuning between the two orthogonal modes was found to play a critical role in determining the dynamics.

## 2.3 Cylindrical Shells and Rings

Some of the earliest studies on the coupled-mode responses of rings and shells are the works of Evensen[18] and Chen and Babcock[19] who reported, respectively, experimental observations of coupling and modal interaction between in-plane and out-of-plane modes in a thin elastic ring, and between two flexural modes in a finite circular cylinder. Both the studies involved 1:1 internal resonance between the appropriate modes. In more recent years Maewal[31,32] investigated the two related problems in order to study the influence of gyroscopic forces on nonlinear harmonic oscillations of rotationally symmetric shell structures. The amplitude-frequency equation for circumferentially traveling waves in a rotating ring were derived via the Lyapunov-Schmidt method. The results show that, for the range of rotational speeds considered, the backward traveling waves exhibit a hardening type of response, whereas, for the forwarding traveling waves there is a transition from a hardening to a softening type of behavior as the rotational speed increases. The second part of his work is an analysis of the interactions between the two traveling waves. The results show the existence of a secondary bifurcation, and the response on the secondary branch is found to be close to standing waves which do not appear in linear free vibration model of the system.

Maewal[32] showed that the evolution equations of Miles[20,33,34] for the amplitudes of the two modes in 1:1 internal resonance also appear in studies of the nonlinear dynamics of axisymmetric elastic shells. Results of numerical integration of the evolution equations for a ring and a cylindrical shell indicate that both of these elastic structures can exhibit chaotically modulated behavior for some values of damping and frequency of excitation. He pointed out that the equations are very similar to those for a spherical pendulum, a stretched elastic string, an elastic beam, and surface waves in a cylindrical container. In fact, they form a two-parameter family of equations valid for any system with O(2) symmetry (Bajaj and Johnson[22]).

Maganty and Bickford[35] derived a set of geometrically nonlinear equations of motion that describe the behavior of a thin circular ring. The resulting equations for free oscillations

are analyzed with a single bending mode approximation for both the in-plane and the out-of-plane motions. The results for the resonant case indicate the presence of unsteady oscillations with an exchange of energy between the in-plane and the out-of-plane modes. The equations of free oscillations are then extended to include the effect of the in-plane and the out-of-plane excitations[36] . Qualitative and quantitative information about the primary response, subject to either a distributed harmonic in-plane or a distributed harmonic out-of-plane load, is obtained in the presence of an internal resonance. The response due to the in-plane excitation exhibits unsteady motions with an exchange of energy between the in-plane and the out-of-plane modes.

Nayfeh and Raouf[37] investigated the nonlinear forced response of infinitely long circular cylindrical shells, in the presence of 2:1 (autoparametric) internal resonances between a flexural mode and a breathing mode. A saturation phenomenon was found to exist when the excitation frequency is close to the natural frequency of the breathing mode. Results of numerical investigations showed that Hopf bifurcations occur, yielding amplitude-and phase-modulated motion. The amplitudes and phases experience a cascade of period-doubling bifurcations ending up with a chaotic response. Raouf and Nayfeh[38] also studied the case of 1:1 (autoparametric) internal resonance between a flexural mode and its companion mode. They found results similar to those of the case of 2:1 internal resonance. Numerical integration of the amplitude equations in the frequency range between the two Hopf bifurcation points showed two branches of attractors which exhibited types of behavior similar to those found in a string (Johnson and Bajaj[4] ). Nayfeh, Raouf and Nayfeh[39] studied the response of infinitely long, circular, cylindrical shells to subharmonic radial excitation, of order one-half, in the presence of a 2:1 internal resonance. Amplitude-and phase-modulated solutions were found to exist. Some limit cycle solutions, corresponding to the modulated solutions, underwent symmetry-breaking bifurcations, whereas some others underwent cyclic-fold bifurcations. Some cyclic-folds were also found to result in a transition to chaos.

## 2.4 Plates

The nonlinear response of thin, as well as thick, plates has been the subject of extensive studies and many recent reviews exist on the subject[40]. Sridhar, Mook and Nayfeh[8,9] used the dynamic analogue of von Karman equations to study the forced response of the plate. They analyzed symmetric as well as asymmetric vibrations, and traveling waves in a clamped circular plate subjected to harmonic excitations, when the frequency of excitation is near one of the natural frequencies. For the symmetric responses in the presence of an internal resonance among the first three modes, when more than one mode is directly excited, the lower modes can dominate the response even when the frequency of the excitation is near

that of the highest mode. When the response is asymmetric, they found that in the absence of internal resonance, or when the frequency of excitation is near one of the lower frequencies involved in internal resonance, the steady-state response can only have the form of a standing wave. However, when the frequency of excitation is near the highest frequency involved in the internal resonance it is possible for a traveling wave component of the highest mode to appear in the steady-state response. Hadian and Nayfeh[41] showed that in the case of a symmetric response, a multi-mode motion loses its stability through a Hopf bifurcation, resulting in periodically- or chaotically-modulated motions of the plate.

Yang and Sethna[16] studied nonlinear flexural vibrations of nearly square plates subjected to parametric in-plane excitations. The spatial symmetry of the plate resulted in 1:1 resonance in the various m:n modes. For dynamically unstable motions in the region of principal parametric instability, the asymptotic method of averaging was used to obtain a set of four amplitude equations governing the evolution of interacting modes. Local bifurcation analysis of the amplitude equations showed that the system is capable of extremely complex standing as well as traveling wave motions including periodic, almost-periodic and chaotic oscillations. These motions were physically interpreted in terms of rotations of the nodal patterns. A global bifurcation analysis, based on a Melnikov type theory for two degree-of-freedom Hamiltonian systems, was also undertaken. It showed the existence of heteroclinic loops which, when they break, lead to Smale horseshoes and chaotic behavior on an extremely long time scale. Yang and Sethna[7] did a similar analysis of plate motions with harmonic excitations normal to the midplane of the plates.

Earlier, Yasuda and Torii[42] had also studied the response of square membranes to transverse harmonic excitations which can lead to a coupled-mode response arising from 1:1 internal resonance. Following the analytical and experimental work of Yasuda and Asano[43], in which they analytically predicted, as well as experimentally observed amplitude-modulated motions, Chang et al.[44] investigated nonlinear flexural vibrations of rectangular plates with uniform stretching subject to excitations normal to the midplane. They showed that, depending on the spatial distribution of the external forces, the plate can undergo harmonic motions either in one of the two individual modes or in a combination of the two modes. For low damping levels, the presence of a Hopf bifurcation in the multi-mode response leads to complicated amplitude-modulated dynamics including period-doubling bifurcations, chaos, coexistence of multiple chaotic motions, and crisis, whereby the chaotic attractor suddenly disappears and the plate resumes small amplitude harmonic motions in a single-mode.

# 3. RESONANT MOTIONS OF RECTANGULAR PLATES WITH INTERNAL AND EXTERNAL RESONANCES

In this section, results of an investigation into the dynamic response of a rectangular plate to harmonic excitations are presented. The von Karman plate equations, accounting for membrane forces, are first reduced via the Galerkin procedure, to a set of second-order nonlinear modal equations. The method of averaging is then utilized to transform the modal equations to a set of first-order ordinary differential equations representing the slow-time evolution of amplitudes of harmonic motion of the interacting modes. These amplitude or averaged equations are a generalization of those that describe the motion of square plates[7] and a membrane[43], and when the additional restriction of circular symmetry is imposed, they have arisen in the study of resonant motion of a spherical pendulum[34], a stretched string[4], and forced response of axisymmetric shells[32] and beams[28]. The amplitude equations for the rectangular plate depend on three nonlinear coefficients, in contrast to the two independent nonlinear coefficients found in the above mentioned studies.

The conditions for various external and internal resonances are identified and among them, the case for primary external resonance with 1:1 internal resonance is studied extensively. The amplitude equations are analyzed for steady-state constant solutions and their various local bifurcations as a function of the excitation frequency, amplitude and the modal damping. Dynamic solutions created by local and global bifurcations are studied numerically by using AUTO[45], a bifurcation analysis and two-parameter continuation computer software package, and by direct time integration of the amplitude equations.

## 3.1 Equations of Motion

Consider a rectangular plate of thickness h, and edge lengths a and b. Let Oxyz be a Cartesian coordinate system with Oxy in the midplane of the plate and the origin at a corner. The plate is subjected to a uniform stretching force $N_0$ (in x-and y-directions). Under these conditions, the von Karman-type equations of motion for the plate, in nondimensional form, are as follows:

$$w_{,tt} - \frac{1}{\pi^2}(w_{,xx} + \kappa^2 w_{,yy}) + D(w_{,xxxx} + 2\kappa^2 w_{,xxyy} + \kappa^4 w_{,yyyy}) \tag{1}$$

$$= \varepsilon(F_{,yy} w_{,xx} - 2F_{,xy} w_{,xy} + F_{,xx} w_{,yy}) - cw_{,t} + q ,$$

$$F_{,xxxx} + 2\kappa^2 F_{,xxyy} + \kappa^4 F_{,yyyy} = w_{,xy}^2 - w_{,xx} w_{,yy} , \tag{2}$$

where $w(x,y,t)$, $F(x,y,t)$ and $q(x,y,t)$ are the nondimensional transverse deflection, the stress function, and the external force normal to the plate, respectively. The dimensionless parameters $\varepsilon$, $\kappa$, D and c represent the thickness parameter, the aspect ratio, the ratio of

bending stiffness to uniform stretching force and the damping coefficient, respectively. Furthermore, the subscript x, y or t denotes a partial differentiation with respect to that nondimensional variable. In equations (1) and (2) the following transformations for the variables and parameters have been used:

$$x = \frac{\bar{x}}{a} \ , \ y = \frac{\bar{y}}{b} \ , \ \kappa = \frac{a}{b} \ , \ t = \frac{\pi}{a}\sqrt{\frac{N_0}{\rho h}}\,\bar{t}, \ w = \frac{\bar{w}}{h} \ ,$$

$$c = \frac{a}{\pi}\sqrt{\frac{1}{\rho h N_0}}\,\bar{c}, \ q = \frac{a^2}{\pi^2 h N_0}\,\bar{q} \ , \ F = \frac{\bar{F}}{Eh^3\kappa^2} \ , \ \varepsilon = \frac{Eh^3\kappa^2}{N_0\pi^2 b^2} \ , \ D = \frac{\bar{D}}{\pi^2 N_0 a^2} \ . \quad (3)$$

Here the variables and parameters with an overbar represent the physical quantities.

The boundary conditions considered here are that all the edges are simply supported and immovable. The transverse displacement w then satisfies

$$w = w_{,xx} = 0 \quad \text{at} \quad x = 0,1 \ , \quad \text{and} \quad w = w_{,yy} = 0 \quad \text{at} \quad y = 0,1 . \quad (4)$$

The in-plane boundary conditions of u = v = 0 along the four sides of the plate, where u and v are the in-plane displacements in the x and y direction, respectively, can be satisfied only on the average[43]. These conditions, put in terms of the stress function F, and expressed in nondimensional form, are as follows:

$$\int_0^1 \int_0^1 (\kappa^4 F_{,yy} - \nu\kappa^2 F_{,xx} - \frac{1}{2} w_{,x}^2) \, dxdy = 0 \ ,$$

$$\int_0^1 \int_0^1 (F_{,xx} - \nu\kappa^2 F_{,yy} - \frac{1}{2} w_{,y}^2) \, dxdy = 0 \ , \quad (5)$$

$$\int_0^1 \int_0^1 (2(1 + \nu)\kappa^2 F_{,xy} + w_{,x} w_{,y}) \, dxdy = 0 \ ,$$

where $\nu$ is the Poisson's ratio.

To investigate the nonlinear dynamical response of the plate, we use the Galerkin technique. Thus, the transverse deflection w can, in general, be chosen as

$$w(x,y,t) = \sum_{m}^{\infty} \sum_{n}^{\infty} W_{mn}(t) \, \phi_m(x)\psi_n(y) \ , \quad (6)$$

where $\phi_m(x)$, $\psi_n(y)$ are groups of comparison functions satisfying the appropriate boundary conditions. For simply supported boundary conditions on the four sides, we can choose

$$\phi_m(x) = \sin m\pi x \ , \quad \psi_n(y) = \sin n\pi y \ , \quad (7)$$

which together define the shape of an (m,n) mode of the plate.

Thus, the motion consists of a linear combination of an infinite number of spatial modes. The modal amplitudes $W_{mn}$ are a function of time, and the nonlinear terms in the system determine their time evolution. Substituting equations (6) and (7) into equation (2), the solution for the resulting linear partial differential equation in the stress function F can be written as

$$F(x,y,t) = F^h(x,y,t) + F^p(x,y,t) ,\qquad(8)$$

where $F^h$ is the homogeneous solution that includes the effect of in-plane stretching forces independent of the transverse deflection, and $F^p$ is the particular solution that includes the effect of out-of-plane boundary conditions. The particular solution $F^p$ can be shown to be

$$F^p(x,y,t) = \sum_{m,n,r,s}^{\infty} [a_{mnrs} \cos(m-r)\pi x \cos(n-s)\pi y + b_{mnrs} \cos(m-r)\pi x \cos(n+s)\pi y$$

$$+ c_{mnrs} \cos(m+r)\pi x \cos(n-s)\pi y + d_{mnrs} \cos(m+r)\pi x \cos(n+s)\pi y] W_{mn} W_{rs} ,\qquad(9)$$

where $a_{mnrs}$, $b_{mnrs}$, $c_{mnrs}$ and $d_{mnrs}$ are functions of mode numbers $(m,n)$, $(r,s)$ and the aspect ratio $\kappa$. Their expressions are given in the Appendix. For $F^h$ to satisfy the boundary conditions, equations (5), the homogeneous solution $F^h$ can be assumed to be

$$F^h(x,y,t) = \frac{1}{2} N_{x0} y^2 + \frac{1}{2} N_{y0} x^2 + N_{xy0} xy .\qquad(10)$$

Substituting $F = F^p + F^h$ into the in-plane boundary conditions, equations (5), and carrying through the algebra, the time dependent functions $N_{x0}$, $N_{y0}$, and $N_{xy0}$ turn out to be

$$N_{x0} = \sum_{m,n}^{\infty} S_{x0mn} W_{mn}^2 , \quad N_{y0} = \sum_{m,n}^{\infty} S_{y0mn} W_{mn}^2 , \quad N_{xy0} = \sum_{m,n,r,s}^{\infty} S_{xy0mnrs} W_{mn} W_{rs} ,\qquad(11)$$

where $S_{x0mn}$, $S_{y0mn}$ and $S_{xy0mnrs}$ are functions of the mode numbers $(m,n)$, $(r,s)$, the Poisson ratio, $\nu$, and the aspect ratio, $\kappa$. Their expressions are also given in the Appendix.

Substituting the solution for F obtained above, and equations (6) and (7), into equation (1), multiplying by $\sin k\pi x \sin l\pi y$, and integrating over the domain of the plate, we get the following discretized equations of motion:

$$\ddot{W}_{kl} + \Omega_{kl}^2 W_{kl} + c\dot{W}_{kl} + \sum_{m,n,r,s,i,j}^{\infty} L_{mnrsijkl} W_{mn} W_{rs} W_{ij} = q_{kl} \quad (k,l = 1,2,\cdots) ,\qquad(12)$$

where $\Omega_{kl}$ is the nondimensional natural frequency of the $(k,l)$ mode, $q_{kl}$ is the contribution of the transverse excitation q to the $(k,l)$ mode, and $L_{mnrsijkl}$ are coefficients for the nonlinear terms of the $(k,l)$ mode. Their expressions are given in the Appendix. For brevity of expressions, and with an N-mode approximation, we write equations (12) as

$$\ddot{X}_m + \Omega_m^2 X_m + c\,\dot{X}_m + \sum_{i,j,k} \bar{L}_{ijkm} X_i X_j X_k = Q_m \cos \omega t \ , \quad m{=}1,2,\cdots,N, \qquad (13)$$

where we have introduced harmonic forces, $q_m = Q_m \cos \omega t$, and $X_i$, $i{=}1,2,....,N$ are the amplitudes of the N modes used in the approximation.

## 3.2 Averaged Equations

When the nonlinear response of equations (13) is small, the method of averaging[1,14,46)] can be used effectively. The plate response depends critically on the modes involved in internal and external resonances, that is, the response depends on the excitation frequency $\omega$, and the natural frequencies $\Omega_{kl}$ or $\Omega_m$. The natural frequencies of the plate, with expressions given in equation (A8), depend on the mode combination, $(k, l)$, the aspect ratio, $\kappa$, and the nondimensional bending stiffness parameter, D. As the aspect ratio and the stiffness parameter are varied, many different mode combinations undergo various internal resonances. A typical plot of natural frequencies as a function of the aspect ratio, for various low order mode shapes, is shown in Figure 1. Now one would like to show that only a small number of modes, which are in internal/combination resonance with the external excitation frequency, contribute to the response in the first approximation. Such an argument was made in Bajaj and Johnson[22)] for the case of a stretched string, and by Holmes[47)] in the case of surface waves in a cylindrical container. Similar results can be expected in the case of a rectangular plate, although the analysis is complicated by the fact that the natural frequencies, and the relationships between them change as a function of the aspect ratio, and hence the N modes that should be considered in the approximation also vary as a function of the aspect ratio. This is clearly evident from Figure 1. Thus, if we restrict the discussion to a four-mode approximation, say at $\kappa \cong 1.633$, the four lowest relevant modes are the $(1,1)$, $(2,1)$, $(1,2)$ and $(3,1)$ modes of the plate. Note that $\Omega_{12}$ and $\Omega_{31}$ are nearly equal for $\kappa \approx 1.633$ so that there is 1:1 internal resonance between the $(1,2)$ and $(3,1)$ modes. An analysis along the line of Bajaj and Johnson[22)] then shows that, for weak excitation with primary resonance $(\omega \approx \Omega_{12} \approx \Omega_{31})$, the response is essentially (to $O(\varepsilon)$) determined by the $(1,2)$ and $(3,1)$ modes.

Keeping the aforementioned results in mind, we analyze a two-mode approximation of the plate system ($N = 2$ in equations (13)) where the two modes of interest are in 1:1 internal resonance. The general discussion and results will be valid for all two-mode pairs in 1:1 resonance, irrespective of the aspect ratio, $\kappa$, of the plate. Specific numerical results will be mostly limited to the $\kappa = 1.633$ case.

As for external resonances, there are various possibilities depending on the strength of the external excitation. These include primary resonance $(\omega \approx \Omega_1, \ \omega \approx \Omega_2)$, subharmonic

resonances ($\omega \approx 3\Omega_1$, $\omega \approx 3\Omega_2$), superharmonic resonances ($3\omega \approx \Omega_1$, $3\omega \approx \Omega_2$) and various combination resonances:

$$\omega \approx \pm 2\Omega_1 \pm \Omega_2 \ , \quad \omega \approx \Omega_1 \pm 2\Omega_2 \ , \quad 2\omega \approx \pm \Omega_1 \pm \Omega_2 \ . \tag{14}$$

The present work concentrates on the case of primary external resonance with 1:1 internal resonance, and the two-mode approximation can then be written as:

$$\ddot{X}_1 + \Omega_1^2 X_1 = \varepsilon(A_1 X_1^2 + A_2 X_2^2) X_1 - c\dot{X}_1 + Q_1 \cos \omega t,$$

$$\ddot{X}_2 + \Omega_2^2 X_2 = \varepsilon(A_2 X_1^2 + A_3 X_2^2) X_2 - c\dot{X}_2 + Q_2 \cos \omega t, \tag{15}$$

where $A_1$, $A_2$ and $A_3$ are the constant non-linear coefficients determined for the specific mode combinations, and $\Omega_1$ and $\Omega_2$ are the corresponding natural frequencies of the two linear modes. Here $X_1$ is the amplitude of some (m,n) mode and $X_2$ is the amplitude of some other (r,s) mode which is in 1:1 internal resonance with the (m,n) mode. The expressions for $A_1$, $A_2$ and $A_3$, in terms of the mode numbers (m,n) and (r,s) and the aspect ratio $\kappa$, are already given in the Appendix, and in Chang et al.[44] Note that these equations possess the reflection symmetry of $Z_2 \times Z_2$ in the absence of external forcing, that is, they are unchanged by the transformations $(X_1, X_2) \rightarrow (-X_1, X_2)$ and $(X_1, X_2) \rightarrow (X_1, -X_2)$. The external excitation breaks this symmetry property partially or completely, depending on the amplitudes $Q_1$ and $Q_2$.

Let

$$X_i = R_i \cos(\omega t - \gamma_i) \ = \ u_i \cos \omega t + v_i \sin \omega t, \quad i = 1, 2. \tag{16}$$

Then, by using a variation of constants procedure and the method of averaging[1,14], and noting that the excitation frequency $\omega$ is near the two close natural frequencies, equations (15) result in the following averaged equations for the amplitudes $R_i$ and the phases $\gamma_i$:

$$\dot{R}_1 = -\frac{c}{2} R_1 + \frac{Q_1}{2\omega} \sin \gamma_1 + \frac{\varepsilon A_2}{8\omega} R_2^2 R_1 \sin 2(\gamma_1 - \gamma_2),$$

$$\dot{\gamma}_1 = \frac{\omega^2 - \Omega_1^2}{2\omega} + \frac{Q_1}{2\omega R_1} \cos \gamma_1 + \frac{3\varepsilon A_1}{8\omega} R_1^2 + \frac{\varepsilon A_2}{8\omega} R_2^2 \{2 + \cos 2(\gamma_1 - \gamma_2)\}, \tag{17}$$

$$\dot{R}_2 = -\frac{c}{2} R_2 + \frac{Q_2}{2\omega} \sin \gamma_2 + \frac{\varepsilon A_2}{8\omega} R_1^2 R_2 \sin 2(\gamma_2 - \gamma_1),$$

$$\dot{\gamma}_2 = \frac{\omega^2 - \Omega_2^2}{2\omega} + \frac{Q_2}{2\omega R_2} \cos \gamma_2 + \frac{3\varepsilon A_3}{8\omega} R_2^2 + \frac{\varepsilon A_2}{8\omega} R_1^2 \{2 + \cos 2(\gamma_2 - \gamma_1)\}.$$

These equations were also derived and studied by Yasuda and Asano in[43] for the case of a rectangular membrane. Given a specific value of the aspect ratio $\kappa$, and the degeneracy of

two specific modes, the plate and the membrane have the same averaged or amplitude equations. The nonlinear coefficients $A_1$, $A_2$ and $A_3$ depend only on the mode combinations, the Poisson's ratio, and the form of the nonlinearity assumed (von Karman-type nonlinearities). The values of the natural frequencies $\Omega_1$ and $\Omega_2$ for the degeneracy of two specific plate modes, are, however, different (equations (A8)) from these for the membrane.

We should note that the procedure used here in deriving the averaged equations is along the lines of[43] although it can be easily formalized by introducing a small parameter and by appropriately scaling the modal amplitudes $X_i$, $i = 1,2$, the damping c, and the external force amplitudes $Q_i$, $i = 1,2$. The resulting amplitude equations will be identical to equations (17), except for the small parameter multiplying the right hand side. Thus, the amplitude equations should be treated in the sense of a slow time scale. Also note that $\Omega_1^2 \approx \Omega_2^2 \approx \omega^2$, and thus, the problem under study is an example of primary resonant motions in systems of coupled oscillators with 1:1 internal resonance and cubic nonlinearities[1].

In a general external loading case, the force amplitudes $Q_1$ and $Q_2$ are not zero. There can be special situations when one (both) of them is (are) zero depending on the spatial distribution of the loading and the mode numbers in internal resonance. Yasuda and Asano[43] presented results for $Q_1 = Q_2 = 10.0$. Here, we are much more interested in the situation when only one mode is externally excited and the second mode is driven due to its nonlinear coupling to the excited mode. Two such specific cases arise, that is, $Q_1 \neq 0$ and $Q_2 = 0$, or $Q_1 = 0$ and $Q_2 \neq 0$. Due to the similar nature of the equations for $(R_1, \gamma_1)$ and for $(R_2, \gamma_2)$, the analytical expressions for various steady-state constant solutions turn out to be identical except for the role of the nonlinear coefficients $A_1$ and $A_3$. In view of the possible bifurcations and stability considerations, however, considerable qualitative as well as quantitative differences in the overall response can arise in the two cases. We describe these in the next section, where a local bifurcation analysis of equations (17) is carried out. In fact, it is shown that the qualitative behavior is strongly dependent on the nonlinear coefficients, and rectangular plates with two interacting modes in 1:1 resonance can be classified based on the nonlinear coefficients.

Finally, it is easy to see that the divergence of the averaged system (17), when expressed in Cartesian form (equations (26)), $\sum\limits_{i=1}^{2} \left[ \dfrac{\partial \dot{u}_i}{\partial u_i} + \dfrac{\partial \dot{v}_i}{\partial v_i} \right]$, is -2c from which it follows that the volume in $(u_1, v_1, u_2, v_2)$ space contracts and that every solution trajectory must ultimately be confined to a limiting subspace of dimension less than four. Furthermore, equations (17) can be combined to show that

$$\frac{dE}{dt} = -\frac{c}{2}E + \frac{Q_1}{2\omega}\left[\frac{R_1 \sin \gamma_1}{E}\right] + \frac{Q_2}{2\omega}\left\{\frac{R_2 \sin \gamma_2}{E}\right\}, \tag{18}$$

where $E^2 = R_1^2 + R_2^2$. This has the implicit solution

$$E(t) = E(0)e^{-(c/2)t} + \int_0^t \left[\frac{Q_1}{2\omega}\left[\frac{R_1 \sin \gamma_1}{E}\right] + \frac{Q_2}{2\omega}\left[\frac{R_2 \sin \gamma_2}{E}\right]\right] e^{-\frac{c}{2}(t-\tau)} d\tau .$$

Noting that $|(R_i \sin \gamma_i/E)| \leq 1$, $i=1,2$, we obtain the inequality

$$|E(t) - E(0)e^{-\frac{c}{2}t}| \leq \frac{1}{c\omega}\left[1 - e^{-\frac{c}{2}t}\right]\left[Q_1 + Q_2\right] . \tag{19}$$

Thus, the steady-state solution is ultimately $(t \to \infty)$ bounded and confined to a hypersphere of radius $(Q_1 + Q_2)/c\omega$.

### 3.3 Steady-State Constant Solutions

As already discussed, we emphasize the cases when only one of the two modes is externally excited. First, consider the case when $Q_2 = 0$ and $Q_1 \neq 0$. Thus, the (m,n) mode is directly excited by an external harmonic force. There are two types of steady-state constant solutions. One set of solutions is characterized by the fact that $R_2 = 0$, that is, the indirectly excited mode is absent. Then the only response is in the (m,n) mode with $R_1 \neq 0$ and this is called the single-mode solution. The other class of solutions corresponds to both $R_1$ and $R_2$ being nonzero and such motions are called the coupled-mode response. A similar situation exists when the (r,s) mode is directly excited and $Q_1 = 0$.

From equations (17), the steady-state constant solutions for single-mode motions $(\bar{R}_2 = 0)$ are determined by

$$\frac{c}{2}\bar{R}_1 - \frac{Q_1}{2\omega}\sin\bar{\gamma}_1 = 0 , \quad \frac{\omega^2 - \Omega_1^2}{2\omega}\bar{R}_1 + \frac{3\varepsilon A_1}{8\omega}\bar{R}_1^3 + \frac{Q_1}{2\omega}\cos\bar{\gamma}_1 = 0 , \tag{20}$$

where an overbar indicates the single-mode steady-state solutions. Combining the equations for $\bar{R}_1$ and $\bar{\gamma}_1$ results in the following polynomial in $\bar{R}_1$:

$$\bar{R}_1^6 + \frac{8(\omega^2 - \Omega_1^2)}{3\varepsilon A_1}\bar{R}_1^4 + \frac{16[\omega^2 c^2 + (\omega^2 - \Omega_1^2)^2]}{9\varepsilon^2 A_1^2}\bar{R}_1^2 - \frac{16 Q_1^2}{9\varepsilon^2 A_1^2} = 0 . \tag{21}$$

Real roots of equation (21), which is identical to those arising in the primary resonant response of the harmonically excited Duffing equation[1], determine the single-mode steady-state constant solutions.

Differentiating equation (21) with respect to $\bar{R}_1$ and setting $\partial\omega/\partial\bar{R}_1 = 0$ gives, the saddle-node bifurcation points[12] or, the points of vertical tangency for single-mode steady-state solutions:

$$\left[\bar{R}_1^2\right]_{SNS} = \frac{4}{9\varepsilon A_1}\left[-2(\omega^2 - \Omega_1^2) \pm \sqrt{(\omega^2 - \Omega_1^2)^2 - 3c^2\omega^2}\right].\tag{22}$$

Here the subscript SNS implies the saddle-node bifurcation for single-mode solutions. We will show later (when the stability of solutions in the single-mode branches is considered) that equation (22) also corresponds to the occurrence of zero eigenvalues.

The problem of finding steady-state constant solutions for the coupled-mode response $(R_1 \neq 0, R_2 \neq 0)$ can also be formulated as that of finding the real roots of a polynomial of the 8th order in $\hat{R}_2^2$, where a hat indicates the coupled-mode steady-state solution. Due to its complexity, the polynomial expression in $\hat{R}_2$ has been determined by using symbolic algebra programs (e.g. SMP, MACSYMA), and is not presented here. The corresponding expression for the coupled-mode steady-state solution $\hat{R}_1$ is given in terms of $\hat{R}_2$ by

$$\hat{R}_1^2 = -2\left[\frac{A_3}{A_2}\hat{R}_2^2 + \frac{4}{3}\frac{(\omega^2 - \Omega_2^2)}{\varepsilon A_2}\right] \pm \sqrt{\left[\frac{A_3}{A_2}\hat{R}_2^2 + \frac{4}{3}\frac{(\omega^2 - \Omega_2^2)}{\varepsilon A_2}\right]^2 - \frac{16}{3}\frac{\omega^2 c^2}{\varepsilon^2 A_2^2}}.\tag{23}$$

When damping is absent, the equation governing the amplitude $\hat{R}_2$ is of the form

$$C_1\hat{R}_2^8 + C_2\hat{R}_2^6 + C_3\hat{R}_2^4 + C_4\hat{R}_2^2 + C_5 = 0,\tag{24}$$

where the coefficients of the polynomial are functions of the parameters $A_1$, $A_2$, $A_3$, $\omega$, $\Omega_1$, $\Omega_2$, $\varepsilon$ and $Q_1$. These expressions for coefficients $C_i$, i=1,2,3,4,5, are given in the work of Chang et al.[44].

Setting $\hat{R}_2 = 0$ in equation (23), we can obtain the critical points for the onset of coupled-mode steady-state harmonic response. The condition for the occurrence of pitchfork bifurcation from the single-mode response is

$$\left[\hat{R}_1^2\right]_{PF} = \frac{4}{3\varepsilon A_2}\left[-2(\omega^2 - \Omega_2^2) \pm \sqrt{(\omega^2 - \Omega_2^2)^2 - 3c^2\omega^2}\right],\tag{25}$$

where PF refers to a pitchfork bifurcation[12]. We will show later that equation (25) also corresponds to the occurrence of a zero eigenvalue.

It is clear from the polynomials (21) and (24) that, given the mode numbers (m,n) and (r,s), and the aspect ratio $\kappa$, the number of real solutions of the single-mode and the coupled-mode type depends on the physical parameters $\Omega_1$, $\Omega_2$, c, $\omega$, and $Q_1$. While the condition of $\kappa = 1.633$ fixes the two natural frequencies $\Omega_1 = \Omega_2$, any small deviations from

the precise value of the aspect ratio lead to small mistuning in the internally resonant modes and thus $(\Omega_1^2 - \Omega_2^2)$ is an important "internal" mistuning parameter. The other frequency parameter is $(\omega^2 - \Omega_1^2)$ or $(\omega^2 - \Omega_2^2)$ which represents the "external" mistuning. Numerical values of the natural frequencies $\Omega_1$ and $\Omega_2$, as indicated earlier, depend also on the bending stiffness D and the Poisson's ratio $\nu$. The nonlinear coefficients $A_1$, $A_2$, and $A_3$, however, depend only on the Poisson's ratio.

In Figure 2 are shown the various single-mode and coupled-mode steady-state constant solutions $R_1$ and $R_2$ as a function of the excitation frequency $\omega$. These response curves are for (1,2) and (3,1) interacting modes with the damping c=0.0, and force amplitudes $Q_1 = 10.0$ and $Q_2 = 0.0$. This situation arises when the loading is symmetric about $x = 0.5$ and is antisymmetric about $y = 0.5$. For all the numerical results presented in this work $\varepsilon = 6 \times 10^{-4}$, $\nu = 0.3$, $\Omega_1^2 = \Omega_2^2 = 35/3$, and $D = 0.0$. The nonlinear coefficients for the (1,2) and (3,1) modes are $A_1 = -326.27$, $A_2 = -274.79$ and $A_3 = -268.32$. The frequency axis is divided into 4 intervals, I, II, III, and IV, according to the nature of solutions. Over the interval I, there exists only one single-mode solution. Over the interval II, we have a stable coupled-mode solution and an unstable single-mode solution. Therefore, in the intervals I and II, the initial conditions are not critical to determining the final steady-state response. In frequency intervals III and IV, there exists a stable single-mode and a stable coupled-mode solution. In frequency interval IV, two stable single-mode solutions and a stable coupled-mode solution exist. Thus, in intervals III and IV, the initial conditions are very important in determining the final steady-state response reached in any experiment or numerical simulation. Note also, that for every mixed-mode solution with some $\gamma_2$, there is another solution with phase angle $\gamma_2 + \pi$ for the same amplitude $R_2$. Thus, the response curves really represent two coupled-mode solutions which are phase shifted by $\pi$ radians.

The points A and C in Figure 2 are associated with equation (25), that is, the pitchfork bifurcation points, and the point B is associated with equation (22), that is, a saddle-node bifurcation point for single-mode solution. The corresponding frequencies at the points A, B, and C coincide with the boundaries of the intervals.

The single-mode and the coupled-mode harmonic motions of the plate can also be interpreted in terms of standing and rotating nodal patterns. Clearly, for the single-mode response, the nodal lines are stationary and the plate vibrates harmonically in the (1,2) mode. When both (1,2) and (3,1) modes are present in the response, the nodal pattern depends on the phases $\gamma_1$ and $\gamma_2$. Only in the case of $\gamma_1 = \gamma_2$ or $\gamma_1 = \gamma_2 \pm \pi$ are the nodal patterns stationary. Otherwise, the nodal pattern changes continuously in a periodic manner, resulting in a traveling wave motion of the plate.

A similar analysis can be performed for the case when $Q_1 = 0$ and $Q_2 \neq 0$. This situation arises when the transverse forcing is symmetric about both $x = 0.5$ and $y = 0.5$. In Figure 3 is shown the response curves for this case with $Q_1 = 0$ and $Q_2 = 10.0$. From the figure, it is seen that over the intervals I, II, and III, we have qualitatively the same results. Over the interval IV, however, there exist two solutions: one stable single-mode and one stable coupled-mode, whereas, there are two stable single-mode solutions and one stable coupled-mode solution for the case with $Q_1 = 10.0$ and $Q_2 = 0$. This qualitative difference arises because here one of the pitchfork bifurcations from the single-mode solutions occurs in the lower branch (point C), while in the earlier case both the pitchfork bifurcations occur only in the upper branch of the single-mode solutions. As is shown in Section 3.4, this is a consequence of the relative magnitude of the nonlinear coefficients $A_i$, i=1,2,3. Further discussion about other qualitative differences between the responses for the two cases will be given following the stability analysis.

## 3.4 Stability Analysis of Constant Solutions

Stability analysis of steady-state constant solutions of the averaged equations is most readily accomplished with equations in Cartesian form. The polar form of the averaged equations (17), when transformed to Cartesian variables $(u_i, v_i)$, i = 1,2, are given by

$$\dot{u}_1 = -\frac{c}{2}u_1 - \frac{\omega^2 - \Omega_1^2}{2\omega}v_1 - \frac{3\varepsilon A_1}{8\omega}v_1(u_1^2 + v_1^2) + \frac{\varepsilon A_2}{8\omega}(-v_1 u_2^2 - 3v_1 v_2^2 - 2u_1 u_2 v_2),$$

$$\dot{v}_1 = -\frac{c}{2}v_1 + \frac{Q_1}{2\omega} + \frac{\omega^2 - \Omega_1^2}{2\omega}u_1 + \frac{3\varepsilon A_1}{8\omega}u_1(u_1^2 + v_1^2) + \frac{\varepsilon A_2}{8\omega}(3u_1 u_2^2 + u_1 v_2^2 + 2v_1 u_2 v_2),$$

$$\dot{u}_2 = -\frac{c}{2}u_2 - \frac{\omega^2 - \Omega_2^2}{2\omega}v_2 - \frac{3\varepsilon A_3}{8\omega}v_2(u_2^2 + v_2^2) + \frac{\varepsilon A_2}{8\omega}(-v_2 u_1^2 - 3v_2 v_1^2 - 2u_2 u_1 v_1), \quad (26)$$

$$\dot{v}_2 = -\frac{c}{2}v_2 + \frac{Q_2}{2\omega} + \frac{\omega^2 - \Omega_2^2}{2\omega}u_2 + \frac{3\varepsilon A_3}{8\omega}u_2(u_2^2 + v_2^2) + \frac{\varepsilon A_2}{8\omega}(3u_2 u_1^2 + u_2 v_1^2 + 2v_2 u_1 v_1).$$

The eigenvalues of the Jacobian matrix of (26), which determine the stability of the single-mode solutions ($u_2 = v_2 = 0$, or $R_2 = 0$) with $Q_2 = 0$, can be shown to satisfy the two quadratics:

$$\lambda^2 + c\lambda + \frac{1}{2}\left[c^2 + \frac{27\varepsilon^2 A_1^2}{16\omega^2}\bar{R}_1^4 + \frac{3\varepsilon A_1(\omega^2 - \Omega_1^2)}{\omega^2}\bar{R}_1^2 + \frac{(\omega^2 - \Omega_1^2)^2}{\omega^2}\right] = 0, \quad (27a)$$

$$\lambda^2 + c\lambda + \frac{1}{2}\left[c^2 + \frac{3\varepsilon^2 A_2^2}{16\omega^2}\bar{R}_1^4 + \frac{\varepsilon A_2(\omega^2 - \Omega_2^2)}{\omega^2}\bar{R}_1^2 + \frac{(\omega^2 - \Omega_2^2)^2}{\omega^2}\right] = 0, \quad (27b)$$

where $\lambda$ represents the eigenvalue. By using equations (27) and the fact that $\bar{R}_1$ is a root of

(21), it can be easily shown that no eigenvalue can be purely imaginary for $c \neq 0$ and, as a result, Hopf bifurcation[12,14] cannot arise from the single-mode steady-state solutions. Therefore, the single-mode steady-state solutions can lose their stability only when an eigenvalue becomes zero. Vanishing of the constant term in equation (27a) is really equivalent to equation (22), the condition for a saddle-node bifurcation or a turning point. Similarly, the vanishing of constant term in equation (27b) is equivalent to equation (25), the condition for a pitchfork bifurcation. It can thus be concluded that the single-mode steady-state constant solutions lose their stability either at the saddle-node bifurcation points or at the pitchfork bifurcation points.

These saddle-node and pitchfork bifurcation sets, for the single-mode solutions, can be obtained in the parameter space by combining equations (21) with the expressions obtained from equations (27). A representative set of these graphs for (1,2) and (3,1) modes are shown in Figure 4 for $c = 0.195$. Note that as the force amplitude $Q_1$ is increased for a fixed damping, the single-mode solution first develops multiplicity and only then pitchfork bifurcations arise. This can be also shown to be the case by a careful examination of the constant terms in equations (27a) and (27b).

The geometry of solutions in the phase space $(u_1, v_1, u_2, v_2)$ is quite interesting. First note that $Q_2 = 0$ implies that the $(u_1, v_1)$ surface, that is, $(u_2, v_2) = (0.0, 0.0)$ is an invariant of the vector field. If initial conditions are chosen in $(u_1, v_1)$ plane, the motion governed by solutions of equations (26) remains confined to it, that is, the dynamics of the plate is a single-mode motion. For single-mode constant solutions, the instability boundary defined by equation (27a) corresponds to disturbances restricted to the $(u_1, v_1)$ plane. The instability condition from equation (27b) arises only when disturbances out of the $(u_1, v_1)$ plane are allowed. Thus, pitchfork bifurcation from single-mode to coupled-mode constant solutions arises only because of coupled-mode disturbances.

A similar stability analysis can be carried out for the coupled-mode steady-state constant solutions. Now both zero and purely imaginary pairs of eigenvalues are possible as a criterion for the loss of stability. A zero eigenvalue can lead to a saddle-node bifurcation and the associated multiple coupled-mode responses, whereas, a purely imaginary eigenvalue leads to Hopf bifurcation and the possibility of limit cycle solutions[12,14] for the amplitude equations. Pitchfork bifurcation points are found to arise only at the points where the coupled-mode solutions meet the single-mode solutions and this set is already identified above. The saddle-node and the Hopf bifurcation sets for the coupled-mode responses were obtained by using AUTO[45] (see Figure 5). Among the points at which the various bifurcation sets intersect, (see both Figures 4 and 5) only the point D has special significance since it corresponds to a double-zero eigenvalue and is therefore a codimension-2 point[12,14]. More complicated bifurcation phenomena are expected for values of parameters near the

codimension - 2 point and results of analytical investigations will be reported in a future work.

The system response depends on four parameters $Q_1$, $\omega$, c and $(\Omega_1^2 - \Omega_2^2)$. The bifurcation sets shown in Figures 4 and 5 correspond to zero internal mistuning $(\Omega_1^2 = \Omega_2^2)$ and a fixed value of damping. The parameters $Q_1$ and c play opposite roles and, in fact, $Q_1$ can be eliminated by an additional scaling. It is therefore expected and seen that the bifurcation sets at other damping values are qualitatively similar to the ones shown here. Though physically more realistic, we have not yet studied in sufficient detail the case of nonzero internal mistuning. One can, however, clearly see from equations (27a) and (27b) that the internal mistuning only effects the pitchfork bifurcation points where coupled-mode solutions arise from single-mode solutions. The locations of these points controls the overall coupled-mode dynamics.

In Figures 4 and 5 it is shown that, beginning with very small values of $Q_1$, as the amplitude of excitation is slowly raised, the plate response undergoes interesting and significant qualitative changes. Figures 6a-6d are a series of bifurcation diagrams depicting these changes with $u_1$ as a function of the excitation frequency $\omega$. For small forcing amplitudes, the response is harmonic and single-valued, that is, for each forcing frequency, the plate undergoes a unique harmonic motion in the (1,2) mode (Figure 6a). At force levels above the cusp point on the SNS curve, the single-mode response undergoes saddle-node bifurcations and now three single-mode responses exist between the frequency boundaries $SNS_1$ and $SNS_2$ (Figure 6b). The upper and the lower solution branches are stable whereas the middle branch is unstable. These saddle-node bifurcations result in the familiar "jump" phenomenon in single-mode response. The next qualitative change occurs when the pitchfork bifurcation set appears. For a very small interval of values of $Q_1$, the pitchfork bifurcations, which occur in the upper single-mode branch, are supercritical and all the coupled-mode motions are stable. Above the codimension-2 point (point D), the pitchfork bifurcation from the right boundary, $PF_2$, becomes subcritical with two possible coupled-mode motions now existing between the curves $PF_2$ and $SNC_1$ (Figure 6c). The subcritical branch is unstable and saddle-type with one real positive eigenvalue. A further increase in the forcing amplitude results in two additional turning points in the coupled-mode branch, $SNC_2$ and $SNC_3$, so that two stable coupled-mode motions are possible. One of the coupled-mode solutions then develops Hopf bifurcation points that asymptotically approach the saddle-node bifurcation points $SNC_2$ and $SNC_1$ as $Q_1$ becomes large. Examples of such response curves are shown in Figure 6d. Over the frequency interval bounded by the two branches of the Hopf bifurcation set, it is expected, from the Hopf bifurcation theorem[12,14], that the amplitude equations will possess limit cycle solutions. These solutions will be explored in some detail in the next section.

A similar stability analysis can be performed for the case of $Q_1 = 0$ and $Q_2 \neq 0$. Analytical expressions for the results are not given here, but the corresponding bifurcation sets are shown in Figures 7 and 8. The set in Figure 7 is for the single-mode branch, now in the plane defined by $(u_2, v_2)$. In Figure 8 is given the bifurcation sets for the coupled-mode motions. There are many qualitatively distinct response diagrams determined by the forcing amplitude $Q_2$. The most significant difference from the case where the (1,2) mode is excited occurs because there is now a codimension-2 point, identified as E in Figures 7 and 8. At this point, the saddle-node, the pitchfork, and the Hopf bifurcation sets meet. In fact the saddle-node and the pitchfork bifurcation sets are tangent without crossing each other. As the forcing amplitude $Q_2$ is increased this allows for one of the pitchfork points to move from the upper to the middle branch in the single-mode solutions. Numerical evidence of this behavior is provided in Chang et al.[44].

In the above discussion, it has been shown for the (1,2) and (3,1) interacting modes that for the second case with $Q_1 = 0$, and $Q_2 \neq 0$ the two pitchfork bifurcation points in the single-mode solutions arise in two different branches. This leads to significant qualitative differences in the response curves for the two cases. These differences can be explained easily, for any interacting modes with 1:1 internal resonance, by a careful consideration of the equations governing single-mode response and its stability under coupled-mode disturbances. The single-mode motions for $c = 0$ are, in general, solutions of a polynomial of the form (equation (21)

$$R^6 + \frac{8\delta}{3\varepsilon A} R^4 + \frac{16\delta^2}{9\varepsilon^2 A^2} R^2 = \left[ \frac{4Q}{3\varepsilon A} \right]^2 ,$$

which can be factored as

$$\left\{ R^2 + \left[ \frac{4\delta}{3\varepsilon A} \right] + \frac{4Q}{3\varepsilon AR} \right\} \left\{ R^2 + \left[ \frac{4\delta}{3\varepsilon A} \right] - \frac{4Q}{3\varepsilon AR} \right\} = 0 ,$$

where $\delta = \omega^2 - \Omega^2$. The first factor represents the upper branch of single-mode solutions, whereas, the second factor represents the middle and the lower branches. The condition for pitchfork bifurcation (from equation (27b)) for the undamped system is of the form

$$\frac{3\varepsilon^2 B^2 R^4}{16} + \varepsilon B\delta R^2 + \delta^2 = 0 ,$$

where B is the nonlinear coupling coefficient. The two pitchfork points are the roots given by

$$\delta_1 = -\frac{3}{4}\,\varepsilon\,B\,R^2 \quad \text{and} \quad \delta_2 = -\frac{1}{4}\,\varepsilon\,B\,R^2\,,$$

with $\delta_1 > \delta_2$ for $B < 0$. By using these roots in the expressions for the upper and the lower branches, and requiring that $R^2 > 0$, it is easy to show that $\delta_2$ occurs in the upper branch if $B/A < 3$. Otherwise, this point occurs in the middle branch. Similarly, the point corresponding to $\delta_1$ occurs in the upper branch if $B/A < 1$, otherwise it arises in the middle branch. These conclusions are made, assuming that both A and B are negative.

The results derived above allow us to classify all the rectangular plate responses with two interacting modes in 1:1 resonance, based on the nonlinear coefficients. Consider, for example, the results of interaction of (1,2) and (3,1) modes presented here. In case of $Q_2 = 0$, $A = A_1 = -326.27$ and $B = A_2 = -274.74$, so that $B/A = 0.84 < 1.0$. Thus, both the points corresponding to $\delta_1$ and $\delta_2$ should appear in the upper branch. In case of $Q_1 = 0$, $A = A_3 = -268.32$ and $B = A_2 = -274.74$, so that $B/A = 1.02$. Thus, the point $\delta_2$ should arise in the upper branch and the point $\delta_1$ should arise in the middle branch. The response curves in Figures 2 and 3 are completely consistent with these predictions.

Response curves have also been determined for mode interactions at many other aspect ratios. In particular, it can be seen from Figure 1 that the (2,2) and (3,1) modes are in 1:1 resonance for $\kappa \approx 1.291$. The corresponding nonlinear coefficients are calculated to be $A_1 = -500.70$, $A_2 = -664.55$, and $A_3 = -630.52$. The above analysis then predicts that the two pitchfork bifurcation points for both the cases of $Q_2 = 0$ and $Q_1 = 0$ arise in different branches, and these results are found to agree with the numerically calculated response curves.

Before closing the discussion of constant solutions we remark on the case when both $Q_1$ and $Q_2$ are nonzero. The two cases of $Q_2 = 0$, on $Q_1 = 0$, are structurally unstable in that, the coupled-mode symmetric solutions arising at pitchfork bifurcation points are destroyed by the smallest of nonzero $Q_2$ or $Q_1$. This is a consequence of the fact that pitchfork bifurcations break under generic parameter perturbations[48]. The saddle-node and Hopf points, however, persist under parameter perturbations. In Figure 9 is shown the response curves at $Q_1 = 10.0$, $Q_2 = 5.0$ for $u_1$ and $u_2$ variables. None of the pitchfork bifurcation points, where coupled-mode responses arise, exist and two kinds of branches of steady-state solutions are seen. We use the term 'primary branch' for the solutions branch which exists over the entire range of excitation frequency $\omega$, and the term 'isolated branch' for the solutions branch isolated from the primary branch. For small $Q_2$, the entire solution set resembles the one corresponding to $Q_2 = 0$, but as $Q_2$ is increased, the isolated branch moves away from the primary branch and the asymmetry of the response curves becomes quite pronounced. The location of the Hopf points in the two sets of solutions also gets altered.

Results presented in this section clearly show that, depending on the amplitude and frequency of the external force, the plate can vibrate in various harmonic motions: single-mode, coupled-mode, etc. There also exists the possibility that the amplitude and phase of the response execute limit cycle motions and this is explored in the next section.

### 3.5 Periodic and Chaotic Solutions of Averaged Equations

A numerical study of periodic solutions of the averaged equations has been performed by using direct time integration as well as using AUTO[45] As was the case in the previous sections, we present the results for the cases of (i) $Q_1 \neq 0$, $Q_2 = 0$, (ii) $Q_1 = 0$, $Q_2 \neq 0$, and (iii) $Q_1 \neq 0$, $Q_2 \neq 0$, separately. Each of the three cases exhibits qualitatively different behavior as described below.

**(i) $Q_1 \neq 0$, $Q_2 = 0$:** For sufficiently low $Q_1$, the response of the averaged equations is limited to equilibrium points in the directly excited (1,2) mode. For higher level of $Q_1$, however, the (3,1) mode also contributes to the response. As the excitation $Q_1$ increases further, some of the coupled-mode steady-state constant solutions lose stability due to Hopf bifurcation and the averaged system develops periodic solutions from the Hopf bifurcation points. These periodic solutions, denoted as $P_1$ solutions, correspond to amplitude- and phase-modulated motions of the rectangular plate and result in a slow oscillation of the nodal pattern. In Figure 10, the solutions of the averaged equations (26) for c = 0.20 are shown. The $P_1$ solutions are stable (denoted by solid circles) over the whole frequency interval connecting the two Hopf points. With a further increase in $Q_1$, these $P_1$ solutions become unstable via period-doubling bifurcations and develop $P_2$ solutions. At some value of $Q_1$, there arises a cascade of period-doublings leading to chaotic solutions.

While numerically investigating the Hopf solution branch, a new periodic solution branch was discovered. This branch of periodic solutions arises due to a saddle-node bifurcation with periodic solutions as the primary solution. That is, a stable and an unstable limit cycle arise due to a saddle-node bifurcation at some low enough damping and the branch exists over a small frequency interval. As the damping c is reduced, the stable periodic solution branch undergoes a sequence of period-doubling bifurcations which ultimately lead to chaotic attractors. For c = 0.19, $Q_1$ = 10.0, the isolated branch arises at $\omega \simeq 4.238$, goes through bifurcations and ultimately terminates at $\omega \simeq 4.291$. In Figure 11 is presented the qualitative relationship between the isolated branch and the branch originating at Hopf points, $\omega \simeq 4.195$ and $\omega \simeq 4.313$. Over the frequency intervals (4.2375, 4.248) and (4.289, 4.2907), stable steady-state solutions are found to exist in both the branches, and phase plots of some representative solutions are shown in Figures 12-13. The chaotic solutions in the isolated branch are found to undergo 'boundary crisis' [22,49], at $\omega \simeq 4.263$

and 4.268 (see Figure 14), whereby the chaotic attractor touches the stable manifold of the saddle-type coupled-mode equilibrium point (denoted by CM) and ceases to exist. Near the above listed frequencies, the averaged equations exhibit transient chaos where the solution, when initiated in the neighborhood of the chaotic solution, traces the ghost of the previous attractor for some time and is then quickly attracted by the single-mode constant solution (SM).

The fact that an isolated solutions branch exists can also be verified using tools of numerical bifurcation analysis. AUTO[45] is one of the powerful packages available for bifurcation analysis and continuation of solutions for ordinary differential equations. It can also compute periodic solution branches, given approximate starting points, and can help construct 'saddle-node' bifurcations sets in two parameter space. Numerical results for the continuation of periodic solutions starting at the two Hopf points are shown, for $c = 0.18755$, in Figure 15. Four turning points are found in each of the curves started from the left and the right Hopf points. These points are identified by numbers 1-4 and 5-8, respectively. As the frequency $\omega$ is varied the turning points 2,4,6 and 8 correspond to locations where the isolated branches are created, whereas, the points 1,3,5 and 7 correspond to frequencies where they merge with other periodic solution branches. Thus, as damping is increased the turning points 1 and 5, and 3 and 7 collide to form isolated branches. This bubble structure is typical of the transition to chaotic behavior observed in various dynamical systems[22,50]. In Figure 16 are shown the saddle-node bifurcation sets for the isolated periodic solution branches corresponding to the points 1-8 in Figure 15. For damping $c > 0.193$, no isolated branch exists and numerical simulations show that there are chaotic solutions in the Hopf branch. The set now confirms that at $c = 0.19$ (corresponding to the qualitative diagram in Figure 11), the isolated branch has not yet merged with the Hopf branch. In fact, the bifurcation sets indicate that on lowering the damping further, another isolated branch is created which merges with the first isolated branch before the merging with the Hopf branch takes place. Thus, the cascade of isolated branch creations and mergers is quite complex.

Before closing this discussion let us point out that, because of the symmetry inherent in the system when $Q_2 = 0$, there is another image branch of coupled-mode solutions in which the solutions undergo an identical evolution as the system parameters are varied. As is shown in the next section, the response exhibited by the averaged equation in the case of $Q_1 = 0$ is quite different from the one presented here.

ii) $Q_1 = 0$, $Q_2 \neq 0$: The bifurcation sets for the single-mode and coupled-mode solutions are, for this case, shown in Figures 7-8. For a fixed damping ($c = 0.195$), the Hopf unstable region in the coupled-mode branch arises only when $Q_2 \geq 4.5$. For values of $Q_2$ slightly above $Q_2 = 4.5$, there are two Hopf points in the solution branch, the bifurcating limit cycles

($P_1$ solutions) are found to be supercritical and the $P_1$ solutions join the two Hopf points. This behavior is very similar to the one observed in case (i) above. Note now that the averaged equations (26) with $Q_1 = 0$ enjoy symmetry under the transformation $(u_1, v_1, u_2, v_2) \to (-u_1, -v_1, u_2, v_2)$ and thus the coupled-mode solutions exist in pairs or are themselves symmetric about the invariant $(u_2, v_2)$ plane. There are two identical Hopf branches.

For higher force ($Q_2$), the $P_1$ solution branch, instead of undergoing a period-doubling bifurcation, as is the behavior in case (i), develops homoclinic orbits and AUTO is unable to continue periodic solutions beyond those points. In Figure 17 are shown the response curves for $Q_2 = 5.5$. In the frequency interval (3.946 - 4.106), no results for periodic solutions are found. A careful direct time integration study in this region shows very interesting behavior, as exemplified by the sequence of phase plots shown in Figure 18. The Hopf bifurcating periodic solution at $\omega = 3.93$ (Figure 18a) deforms ($\omega = 3.94$, Figure 18b) and then merges with its symmetric twin to give the periodic solution shown in Figure 18c ($\omega = 3.95$). In between the frequencies with phase plots shown in Figure 18b and 18c, there is a frequency for which the upper and the lower limit cycles just touch each other at the origin in $(u_1, v_1)$ plane. This is the homoclinic orbit, which is bi-asymptotic to the saddle-type single mode solution. This phenomenon of merging of the two limit cycles via a homoclinic orbit is called a glueing bifurcation[51]. Further increases in $\omega$ result in the phase plots of Figures 18d - 18f, where the single limit cycle again undergoes a glueing bifurcation and this time unglues (detaches) back to the pair of limit cycles (Figure 18f, only one shown).

At much higher excitation amplitudes, each of the two Hopf branches terminating in a homoclinic orbit, already shown in Figure 17, deform to develop turning points and period-doubling instabilities. A representative periodic solution response curve is shown in Figure 19 for $Q_2 = 10.0$. In the frequency intervals over which the $P_1$ solutions are unstable, period-doubling cascades arise leading to chaotic solutions. The accompanying graph shows the variation of the period of the limit cycle solution, and it is clear that the period approaches that of a homoclinic orbit about some excitation frequency.

iii) $Q_1 \neq 0, Q_2 \neq 0$: The response amplitudes of periodic solutions bifurcating from the Hopf points, corresponding to Figure 9, are shown in Figure 20. In the isolated solutions branch, periodic solutions could be continued only from the left Hopf point and the solutions approach a homoclinic orbit via a series of turning points. In the primary solutions branch, however, the Hopf points are joined by the limit cycle solutions. The limit cycles are unstable over a frequency interval through a period-doubling, and lead ultimately to the usual chaotic solutions. Thus, quite interestingly, the isolated branch exhibits a response similar to the case (ii) above, when the (3,1) mode is directly excited. The primary branch exhibits behavior similar to the case (i) above where the (1,2) mode is directly excited.

Before closing the discussion of limit cycles and chaotic solutions exhibited by the averaged equations for a two-mode approximation of the von Karman plate equations, it should be pointed out that the limit cycle solutions of the averaged equations (17) or (26) imply motion on a two-torus for the coupled oscillators (equations (15)) via the intergal manifold theorem (see Bajaj and Johnson[22]). For parameter values close to those for which the averaged equations exhibit chaotic motions, it is expected[22] that, the coupled oscillators also exhibit chaotic behavior. This conclusion should be valid, at least, for sufficiently small excitation amplitudes. Numerical simulation of the two-mode model in equations (15) confirms the expectation and some representative results are shown in Figure 21. These plots show the projection on to the $X_1 - X_2$ plane of the Poincare' sections of the steady-state solutions. The solution for $Q_1 = 10.0$, $Q_2 = 0.0$, $c = 0.18$, and $\omega = 4.232$ is an amplitude-modulated motion, with the modulation being periodic and of a frequency much smaller than the excitation frequency. The solution for $\omega = 4.233$ is an amplitude-modulated motion where the modulation has undergone a period-doubling twice, resulting in a so-called $T_4$ solution. The section in Figure 21c represents the solution for $\omega = 4.234$ where the regular torus has finally cascaded to the chaotic attractor. Again, the chaotic features arise in the modulation of the basic harmonic motion.

## 4. SUMMARY AND CONCLUSIONS

In this work we have reviewed recent literature on the resonant response of weakly nonlinear multi-degree-of-freedom models of structural systems. The focus is placed on conditions under which the structures possess internal resonances, so that more than one modes of vibration participate in the response. The structural members considered include beams, strings, and plates and shells. The latter part of the work is devoted to a study of the N-mode approximation of a resonantly excited thin rectangular plate with uniform in-plane tension. The plate is modeled by the von Karman equations, and it is shown that for the N-mode model, only the resonantly excited mode and the mode in 1:1 internal resonance have a non-zero amplitude in the lowest order approximation.

A careful bifurcation analysis of the averaged equations is carried out as a function of the excitation amplitudes and frequency, and as a function of the damping present in the plate. Various saddle-node, pitchfork, and Hopf bifurcation sets are constructed and it is shown that the response of the plate depends very significantly on the mode which is directly excited. In the parameter regions, where the coupled-mode constant solutions are unstable by a Hopf bifurcation, the steady-state solutions are explored by continuation of periodic solutions and by using direct time integration. The limit cycle, as well as chaotic solutions, of the averaged equations are shown to predict qualitatively similar amplitude-modulated motions

for the original two-mode model for neighboring values of parameter.

## ACKNOWLEDGEMENT

## REFERENCES

1. Nayfeh, A. H. and Mook, D. T., "Nonlinear Oscillations", Wiley-Interscience, New York (1979).

2. Nayfeh, A.H. and Balachandran, B., "Modal Interactions in Dynamical and Structural Systems", App. Mech. Rev., 42, S175-S201 (1989).

3. Sethna, P.R., "Coupling in Certain Classes of Weakly Nonlinear Vibrating Systems", In Nonlinear Differential Equations and Nonlinear Mechanics, edited by J.P. Lasalle and S. Lefschetz, Academic Press, New York, 58-70 (1963).

4. Johnson, J. M. and Bajaj, A. K., "Amplitude Modulated and Chaotic Dynamics in Resonant Motion of Strings", J. Sound and Vib., 128, 87-107 (1989).

5. Tufillaro, N.B., "Nonlinear and Chaotic String Vibrations", Am. J. Phys., 57, 408-414 (1989).

6. O'Reilly, O. and Holmes, P.J., "Non-linear, Non-Planar and Non-Periodic Vibrations of a String", J. Sound and Vib., 153, 413-435 (1992).

7. Yang, X. L. and Sethna, P. R., "Nonlinear Phenomena in Forced Vibrations of a Nearly Square Plate - Antisymmetric Case", J. Sound and Vib., 155, 413-441 (1992).

8. Sridhar, S., Mook, D.T. and Nayfeh, A.H., "Nonlinear Resonances in the Forced Responses of Plates, Part I: Symmetric Responses of Circular Plates", J. Sound and Vib., 41, 359-373 (1975).

9. Sridhar, S., Mook, D.T. and Nayfeh, A.H., "Nonlinear Resonances in the Forced Responses of Plates, Part II: Asymmetric Responses of Circular Plates", J. Sound and Vib., 59, 159-170 (1978).

10. Pai, P.F. and Nayfeh, A.H., "Nonlinear Non-Planar Oscillations of a Cantilever Beam Under Lateral Base Excitations", Int. J. Non-Lin. Mech., 25, 455-474 (1990).

11. Holmes, P.J. and Marsden, J., "A Partial Differential Equation with Infinitely Many Periodic Orbits: Chaotic Oscillations of a Forced Beam", Arch. Rat. Mech. Anal., 76, 135-165 (1981).

12. Guckenheimer, J. and Holmes, P.J., "Nonlinear Oscillations, Dynamical Systems, and Bifurcations of Vector Fields", Springer-Verlag, New York (1983).

13. Wiggins, S., "Global Bifurcations and Chaos - Analytical Methods", Springer-Verlag, New York (1988).

14. Wiggins, S., "Introduction to Applied Nonlinear Dynamical Systems and Chaos", Springer-Verlag, New York (1991).

15. Yagasaki, K., "Chaotic Dynamics of a Quasi-Periodically Forced Beam", ASME J. Appl. Mech., 59, 161-167 (1992).

16. Yang, X.L. and Sethna, P.R., "Local and Global Bifurcations in Parametrically Excited Vibrations of Nearly Square Plates", Int. J. Non-Lin. Mech., 26, 199-220 (1991).

17. Miles, J.W., "Stability of Forced Oscillations of a Vibrating String", J. Acous. Soc. Am., 38, 855-861 (1965).

18. Chen, J.C. and Babcock, C.D., "Nonlinear Vibration of Cylindrical Shells", AIAA J., 13, 868-876 (1975).

19. Evensen, D.A., "Nonlinear Flexural Vibrations of Thin Circular Rings", ASME J. Appl. Mech., 33, 553-560 (1966).

20. Miles, J.W., "Resonant, Nonplanar Motion of a Stretched String", J. Acous. Soc. Am. 75, 1505-1510 (1984).

21. Bajaj, A.K. and Johnson, J.M., "Asymptotic Techniques and Complex Dynamics in Weakly Non-Linear Forced Mechanical Systems", Int. J. Non-Lin. Mech., 25, 211-226 (1990).

22. Bajaj, A.K. and Johnson, J.M., "On the Amplitude Dynamics and 'Crisis' in Resonant Motion of Stretched Strings", Phil. Trans. Soc. Lond., A338, 1-41 (1992).

23. Molteno, T.C.A. and Tufillaro, N.B., "Torus Doubling and Chaotic String Vibrations: Experimental Results", J. Sound and Vib., 137, 327-330 (1990).

24. O'Reilly, O., "Global Bifurcations in the Forced Vibration of a Damped String", Preprint (1991).

25. Crespo da Silva, M.R.M. and Glynn, C.C., "Nonlinear Flexural-Flexural-Torsional Dynamics of Inextensional Beams - I. Equation of Motion", J. Struct. Mech., 6, 437-448 (1978).

26. Crespo da Silva, M.R.M. and Glynn, C.C., "Nonlinear Flexural-Flexural-Torsional Dynamics of Inextensional Beams - II. Forced Motions", J. Struct. Mech., 6, 449-461 (1978).

27. Crespo da Silva, M.R.M., "On the Whirling of a Base-Excited Cantilever Beam", J. Acous. Soc. Am., 67, 704-707 (1980).

28. Maewal, A., "Chaos in a Harmonically Excited Elastic Beam", ASME J. Appl. Mech., 53, 625-632 (1986).

29. Nayfeh, A.H. and Pai, P.F., "Non-Linear Non-Planar Parametric Responses of an Inextensional Beam", Int. J. Non-Lin. Mech., 24, 139-158 (1989).

30. Restuccio, J.M., Krousgrill, C.M. and Bajaj, A.K., "Nonlinear Nonplanar Dynamics of a Parametrically Excited Inextensional Elastic Beam", Nonlinear Dynamics, 2, 263-289 (1991).

31. Maewal, A., "Nonlinear Harmonic Oscillations of Gyroscopic Structural Systems and the Case of a Rotating Ring", ASME J. App. Mech., 48, 627-633 (1981).

32. Maewal, A., "Miles' Evolution Equations for Axisymmetric Shells: Simple Strange Attractor's in Structural Dynamics", Int. J. Non-Lin. Mech., 21, 433-438 (1987).

33. Miles, J.W., "Resonantly Forced Surface Waves in a Circular Cylinder", J. Fluid Mech., 149, 15-31 (1984).

34. Miles, J.W., "Resonant Motions of a Spherical Pendulum", Physica D, 11, 309-323 (1984).

35. Maganty, S.P. and Bickford, W.B., "Large Amplitude Oscillations of Thin Circular Rings", ASME J. Appl. Mech., 54, 315-322 (1987).

36. Maganty, S.P. and Bickford, W.B., "Influence of Internal Resonance on the Non-Linear Oscillations of a Circular Ring Under Primary Resonance Conditions", J. Sound and Vib., 122, 507-521 (1988).

37. Nayfeh, A.H. and Raouf, R.A., "Nonlinear Forced Response of Infinity Long Circular Cylindrical Shells", ASME J. Appl. Mech., 54, 571-577 (1987).

38. Raouf, R.A. and Nayfeh, A.H., "One-to-One Autoparametric Resonances in Infinitely Long Cylindrical Shells", Computers and Structures, 35, 163-173 (1990).

39. Nayfeh, A.H., Raouf, R.A. and Nayfeh, J.F., "Nonlinear Response of Infinitely Long Circular Cylindrical Shells to Subharmonic Radial Loads", ASME J. Appl. Mech., 58, 1033-1041 (1991).

40. Sathyamoorthy, M., "Nonlinear Vibration Analysis of Plates: A Review and Survey of Current Developments", Appl. Mech. Rev., 40, 1553-1561 (1987).

41. Hadian, J. and Nayfeh, A.H., "Modal Interaction in Circular Plates", J. Sound and Vib., 142, 279-292 (1990).

42. Yasuda, K. and Torii, T., "Multi-Mode Response of a Square Membrane", JSME Inter. J., 30, 963-969 (1987).

43. Yasuda, K. and Asano, T., "Nonlinear Forced Oscillations of a Rectangular Membrane with Degenerate Modes", Bull. JSME, 29, 3090-3095 (1986).

44. Chang, S.I., Bajaj, A.K. and Krousgrill, C.M., "Non-Linear Vibrations and Chaos in Harmonically Excited Rectangular Plates with One-to-One Internal Resonance", Nonlinear Dynamics (to appear).

45. Doedel, E., "AUTO: Software for Continuation and Bifurcation Problems in Ordinary Differential Equations", Report, Dept. of Appl. Math., Cal Tech., Pasadena (1986).

46. Nayfeh, A.H., "Introduction of Perturbation Techniques", Wiley-Interscience, New York (1981).

47. Holmes, P.J., "Chaotic Motions in a Weakly Nonlinear Model for Surface Waves", J. Fluid Mech., 162, 365-388 (1986).

48. Matkowsky, B.J. and Reiss, E.L., "Singular Perturbations of Bifurcations", SIAM J. Appl. Math., 33, 230-255 (1977).

49. Grebogi, C., Ott, E. and Yorke, J.E., "Crisis, Sudden Changes in Chaotic Attractors, and Transient Chaos", Physica D, 7, 181-200 (1983).

50. Knobloch, E. and Weiss, N.O., "Bifurcations in a Model of Magneto Convection", Physica D, 9, 379-407 (1983).

51. Glendinning, P., "Global Bifurcations in Flows, "In New Directions in Dynamical Systems, edited by T. Bedford and J. Swift, Cambridge University Press, Cambridge, 120-149 (1988).

# APPENDIX

The expressions for coefficients $a_{mnrs}$, $b_{mnrs}$, $c_{mnrs}$ and $d_{dmnrs}$ in equation (9) are given as follows:

$$a_{mnrs} = \begin{cases} \dfrac{mnrs - m^2 s^2}{4[(m-r)^2 + \kappa^2(n-s)^2]^2} & \text{if } m \neq r \text{ or } n \neq s, \\[2em] 0 & \text{if } m = r \text{ and } n = s, \end{cases} \tag{A1}$$

$$b_{mnrs} = \frac{mnrs + m^2 s^2}{4[(m-r)^2 + \kappa^2(n+s)^2]^2} \quad , \qquad c_{mnrs} = \frac{mnrs + m^2 s^2}{4[(m+r)^2 + \kappa^2(n-s)^2]^2} \quad , \tag{A2-A3}$$

$$d_{mnrs} = \frac{mnrs - m^2 s^2}{4[(m+r)^2 + \kappa^2(n+s)^2]^2} \quad . \tag{A4}$$

The expressions for $S_{x0mn}$, $S_{y0mn}$ and $S_{xy0mnrs}$ in equation (11) are given as follows:

$$S_{x0mn} = \frac{\pi^2}{8(1-\nu^2)\kappa^4}\, (m^2 + \nu\kappa^2 n^2) \quad , \qquad S_{y0mn} = \frac{\pi^2}{8(1-\nu^2)\kappa^4}(\nu m^2 + \kappa^2 n^2) \,, \tag{A5-A6}$$

$$S_{xy0mnrs} = \begin{cases} \dfrac{2}{(1+\nu)\kappa^2}\, \dfrac{mnrs}{(m+n)(m-r)(n+s)(n-s)} \\[1em] \quad -4\,(a_{mnrs} + b_{mnrs} + c_{mnrs} + d_{mnrs})\,, & \text{if } (m \pm r) \text{ and } (n \pm s) \text{ are odd}, \\[1.5em] 0 & \text{if } (m \pm r) \text{ or } (n \pm s) \text{ are even}. \end{cases} \tag{A7}$$

The expressions for $\Omega_{kl}$ and $L_{mnrsijkl}$ in equation (12) are given as follows:

$$\Omega_{kl} = [(k^2 + \kappa^2 l^2) + D\pi^4(k^2 + \kappa^2 l^2)^2]^{\frac{1}{2}} \,, \tag{A8}$$

and

$$L_{mnrsijkl} = 4\pi^2\varepsilon \left[ \frac{1}{4}\, \delta_r^m \delta_s^n \delta_k^i \delta_l^j \,(i^2\, S_{x0mn} + j^2 S_{y0mn}) \right. \tag{A9}$$

$$\left. + 2ij S_{xy0mnrs}\, T_{xy0ijkl} + (i^2 T_{xmnrsijkl} + 2ij T_{xymnrsijkl} + j^2 T_{ymnrsijkl}) \right] \,,$$

where $S_{x0mn}$, $S_{y0mn}$ and $S_{xy0mnrs}$ are given above, and

$$T_{xy0ijkl} = \begin{cases} \dfrac{4}{\pi^2} \dfrac{kl}{(i+k)(i-k)(j+l)(j-l)} & \text{if } (i \pm k) \text{ and } (j \pm l) \text{ are odd}, \\ \\ 0 & \text{if } (i \pm k) \text{ or } (j \pm l) \text{ is even}, \end{cases} \qquad \text{(A10)}$$

$$T_{xmnrijkl} = -\pi^2 [\, (n-s)^2 \, a_{mnrs} \, U_1 U_3 + (n+s)^2 \, b_{mnrs} \, U_1 U_4 \qquad \text{(A11)}$$
$$+ (n-s)^2 \, c_{mnrs} \, U_2 U_3 + (n+s)^2 \, d_{mnrs} \, U_2 U_4 \,],$$

$$T_{ymnrsijkl} = -\pi^2 [\, (m-r)^2 \, a_{mnrs} \, U_1 U_3 + (m-r)^2 \, b_{mnrs} \, U_1 U_4 \qquad \text{(A12)}$$
$$+ (m+r)^2 \, c_{mnrs} \, U_2 U_3 + (m+r)^2 \, d_{mnrs} \, U_2 U_4 \,],$$

$$T_{xymnrsijkl} = \pi^2 [\, (m-r)(n-s) \, a_{mnrs} \, V_1 V_3 + (m-r)(n+s) \, b_{mnrs} \, V_1 V_4 \qquad \text{(A13)}$$
$$+ (m+r)(n-s) \, c_{mnrs} \, V_2 V_3 + (m+r)(n+s) \, d_{mnrs} \, V_2 V_4 \,],$$

with

$$U_1 = \frac{1}{4} \left[ \delta_{k+r}^{i+m} - \delta_{r}^{i+k+m} + \delta_{k+m}^{i+r} - \delta_{m}^{i+k+r} \right] \;,\quad U_2 = \frac{1}{4} \left[ \delta_{k+m+r}^{i} - \delta_{m+r}^{i+k} + \delta_{k}^{i+m+r} \right], \quad \text{(A14)}$$

$$U_3 = \frac{1}{4} \left[ \delta_{l+s}^{j+n} - \delta_{s}^{j+l+n} + \delta_{l+n}^{j+s} - \delta_{n}^{j+l+s} \right] \;,\quad U_4 = \frac{1}{4} \left[ \delta_{l+n+s}^{j} - \delta_{n+s}^{j+l} + \delta_{l}^{j+n+s} \right],$$

$$V_1 = \frac{1}{4} \left[ \delta_{k+r}^{i+m} - \delta_{r}^{i+k+m} - \delta_{k+m}^{i+r} + \delta_{m}^{i+k+r} \right] \;,\quad V_2 = \frac{1}{4} \left[ -\delta_{k+m+r}^{i} + \delta_{m+r}^{i+k} + \delta_{k}^{i+m+r} \right], \quad \text{(A15)}$$

$$V_3 = \frac{1}{4} \left[ \delta_{l+s}^{j+n} - \delta_{s}^{j+l+n} - \delta_{l+n}^{j+s} + \delta_{n}^{j+l+s} \right] \;,\quad V_4 = \frac{1}{4} \left[ -\delta_{l+n+s}^{j} + \delta_{n+s}^{j+l} + \delta_{l}^{j+n+s} \right],$$

where the Kronecker's delta is defined as $\delta_b^a = \begin{cases} 1 & \text{if } a = b, \\ 0 & \text{if } a \neq b. \end{cases}$

## APPENDIX II

Here we select a rectangular plate with aspect ratio, $\kappa = 1.633$, and consider the response approximation consisting of the four lowest modes defined by the mode numbers $(1,1)$, $(2,1)$, $(1,2)$ and $(3,1)$. The $(1,2)$ and $(3,1)$ modes are in 1:1 internal resonance and we assume that the excitation frequency, $\omega$, is close to the natural frequencies of $(1,2)$ and $(3,1)$ modes. We show that the response of $(1,1)$ and $(2,1)$ modes decays exponentially and the steady-state

response of the plate consists of only the (1,2) and (3,1) modes.

Defining $X_1 = W_{11}$, $X_2 = W_{21}$, $X_3 = W_{12}$, and $X_4 = W_{31}$, the four modal equations are of the form:

$$\ddot{X}_1 + \Omega_1^2 X_1 + c\dot{X}_1 + 4C_1 X_1^3 + 2C_6 X_1 X_3^2 + 2C_7 X_1 X_2^2 + 3C_5 X_1^2 X_4$$

$$+ C_{12} X_3^2 X_4 + C_{13} X_2^2 X_4 + 2C_8 X_1 X_4^2 = Q_1 \cos \omega t ,$$

$$\ddot{X}_2 + \Omega_2^2 X_2 + c\dot{X}_2 + 2C_7 X_1^2 X_2 + 2C_9 X_3^2 X_2 + 4C_2 X_2^3 + 2C_{13} X_1 X_2 X_4 \tag{A16}$$

$$+ 2C_{10} X_2 X_4^2 = Q_2 \cos \omega t ,$$

$$\ddot{X}_3 + \Omega_3^2 X_3 + c\dot{X}_3 + 2C_6 X_1^2 X_3 + 4C_3 X_3 + 2C_9 X_3 X_2^2 + 2C_{12} X_1 X_3 X_4$$

$$+ 2C_{11} X_3 X_4^2 = Q_3 \cos \omega t ,$$

$$\ddot{X}_4 + \Omega_4^2 X_4 + c\dot{X}_4 + C_5 X_1^3 + C_{12} X_1 X_3^2 + C_{13} X_1 X_2^2 + 2C_8 X_1^2 X_4$$

$$+ 2C_{11} X_3^2 X_4 + 2C_{10} X_2^2 X_4 + 4C_4 X_4^3 = Q_4 \cos \omega t ,$$

where $C_i$'s (i = 1,..., 13) are coefficients of nonlinear terms which can be easily obtained from $L_{mnrsijkl}$ in equations (12).

Now we rescale the variables and parameters with a small parameter $\mu$ as follows:

$$X_i = \mu^{\frac{1}{2}} \overline{X}_i , \quad c = \mu \overline{c} , \quad \text{and } Q_i = \mu^{3/2} \overline{Q}_i , \quad (i=1,...,4) , \tag{A17}$$

which represent small displacements, small damping and small external forces, respectively. We also introduce two detuning parameters $\sigma_1$ and $\sigma_2$ defined by

$$\omega^2 - \Omega_3^2 = \mu \sigma_1 \quad \text{and} \quad \Omega_4^2 - \Omega_3^2 = \mu \gamma , \tag{A18}$$

so that

$$\Omega_4^2 = \Omega_3^2 + \mu\gamma = \omega^2 - \mu(\sigma_1 - \gamma) \equiv \omega^2 - \mu\sigma_2 ,$$

where $\sigma_1$ and $\gamma$ are external and internal detuning parameter respectively, and $\sigma_2$ is the difference between $\sigma_1$ and $\gamma$. From equations (A16) - (A18) with

$$\vec{X}_i = p_i , \quad \text{and } \overline{X}_i = q_i , \quad (i=1,...,4) ,$$

it can be shown that the equations in (A16) transform to

$$\dot{q}_i = \frac{\partial H}{\partial p_i} , \quad \text{and } \dot{p}_i = -\frac{\partial H}{\partial q_i} - \mu\overline{C}p_i , \quad (i=1,2,3,4) \tag{A19}$$

where H is the Hamiltonian for the conservative system.

In terms of $p_i$ and $q_i$, the Hamiltonian is given as

$$H = H_0 + \epsilon H_1 , \tag{A20}$$

where

$$H_0 = \frac{1}{2}\left[\sum_{i=1}^{4} p_i^2 + \Omega_1^2 q_1^2 + \Omega_2^2 q_2^2 + \omega^2 q_3^2 + \omega^2 q_4^2\right] ,$$

and

$$H_1 = -\frac{1}{2}(\sigma_1 q_3^2 + \sigma_2 q_4^2)$$

$$- (q_1\overline{Q}_1 \cos \omega t + q_2\overline{Q}_2 \cos \omega t + q_3\overline{Q}_3 \cos \omega \omega t + q_4\overline{Q}_4 \cos \omega t)$$

$$+ \left[C_1 q_1^4 + C_2 q_2^4 + C_3 q_3^4 + C_4 q_4^4 + C_5 q_1^3 q_4\right.$$

$$+ C_6 q_1^2 q_3^2 + C_7 q_1^2 q_2^2 + C_8 q_1^2 q_4^2 + C_9 q_2^2 q_3^2$$

$$+ \left. C_{10} q_2^2 q_4^2 + C_{11} q_3^2 q_4^2 + C_{12} q_1 q_3^2 q_4 + C_{13} q_1 q_2^2 q_4\right] .$$

By the following canonical transformations,

$$q_m = \Omega_m^{-\frac{1}{2}} (\overline{q}_m \cos \Omega_m t + \overline{p}_m \sin \Omega_m t) ,$$

$$p_m = \Omega_m^{\frac{1}{2}}(-\overline{q}_m \sin \Omega_m t + \overline{p}_m \cos \Omega_m t) , m=1,2 ,$$

$$q_n = \omega^{-\frac{1}{2}}(\overline{q}_n \cos \omega t + \overline{p}_n \sin \omega t) , \qquad \text{(A21)}$$

and $p_n = \omega^{\frac{1}{2}}(-\overline{q}_n \sin \omega t + \overline{p}_n \cos \omega t)$, n=3,4,5,

the function H transforms to $K(\overline{q}_i, \overline{p}_i, t)$, and it can be shown that

$$K(\overline{q}_i , \overline{p}_i , t) = \mu H_1(\overline{q}_i , \overline{p}_i , t) = \mu K_0(\overline{q}_i , \overline{p}_i) + \mu K_1(\overline{q}_i , \overline{p}_i , t) \qquad \text{(A22)}$$

where $K_0$ consists of time-independent terms and $K_2$ consists of time-dependent fast oscillating terms. Therefore, by applying the method of averaging to equations (A19) it can be shown that the averaged equations are given by

$$\dot{\overline{q}}_m = \mu \frac{\partial K_o}{\partial \overline{P}_m} - \frac{1}{2}\mu\overline{c}\overline{q}_m \quad , \quad \dot{\overline{p}}_m = -\mu \frac{\partial K_0}{\partial \overline{q}_m} - \frac{1}{2}\mu\overline{c}\overline{q}_m , \quad m=1,2,3,4 . \qquad \text{(A23)}$$

Here it is assumed that the frequencies $\Omega_1, \Omega_2, \Omega_3$ and $\Omega_4$ donot satisfy any other frequency conditions other than that $\Omega_3 \approx \Omega_4$. By another canonical transformation

$$\overline{q}_m = (2\overline{I}_m)^{\frac{1}{2}} \sin \overline{\theta}_m \quad , \quad \overline{p}_m = (2\overline{I}_m)^{\frac{1}{2}} \cos \overline{\theta}_m \quad , \quad m=1,2,3,4 , \qquad \text{(A24)}$$

where $\overline{I}_m$ and $\overline{\theta}_m$ are the action and angle variables for the $m^{th}$ mode, $K_0$ is transformed to $K'(\overline{I}_m , \overline{\theta}_m)$, and $\overline{\theta}_1$ and $\overline{\theta}_2$ are found to be cyclic. Therefore, we have the equations for the action variables $\overline{I}_1$ and $\overline{I}_2$ as

$$\dot{\overline{I}}_m = -\mu\overline{c}\overline{I}_m , \quad m=1,2 . \qquad \text{(A25)}$$

This shows that $\overline{I}_1$ and $\overline{I}_2$, the actions for (1,1) and (2,1) modes, decay exponentially with time in the presence of damping. Thus, to investigate the steady-state response, we can always start with only the modes which are involved in internal and external resonances.
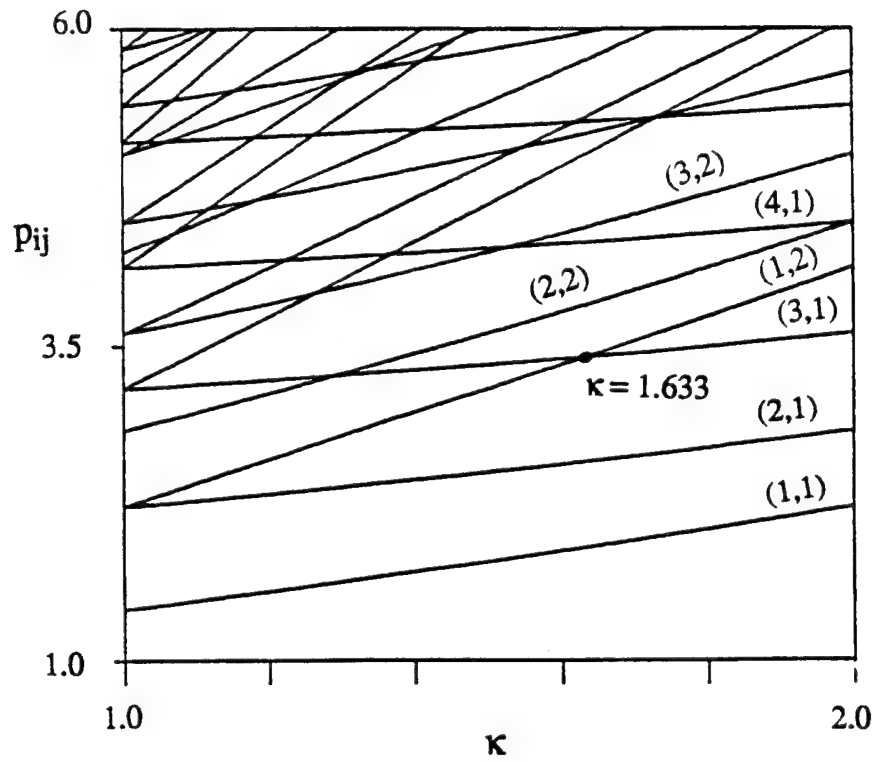
Fig. 1: Variation of linear natural frequencies with the aspect ratio $\kappa$.
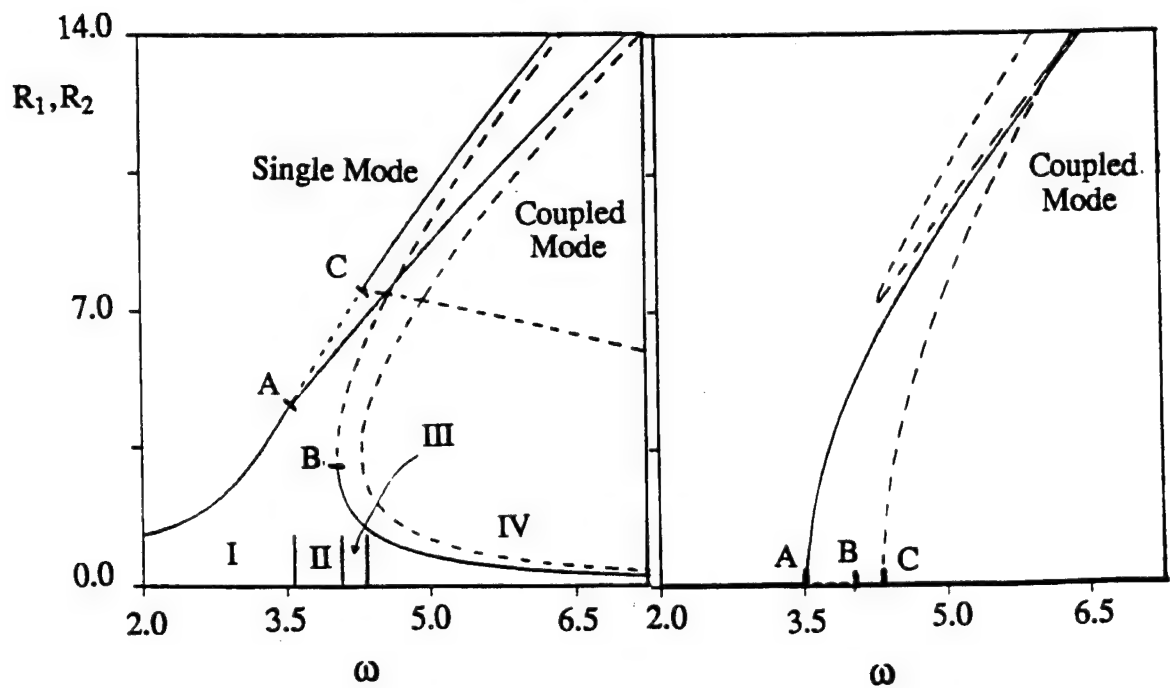


Fig. 2: Constant-amplitude response $R_1$, for the (1,2) plate mode, and $R_2$, for the (3,1) plate mode; $Q_1 = 10.0$, $Q_2 = 0.0$, $c = 0.0$.
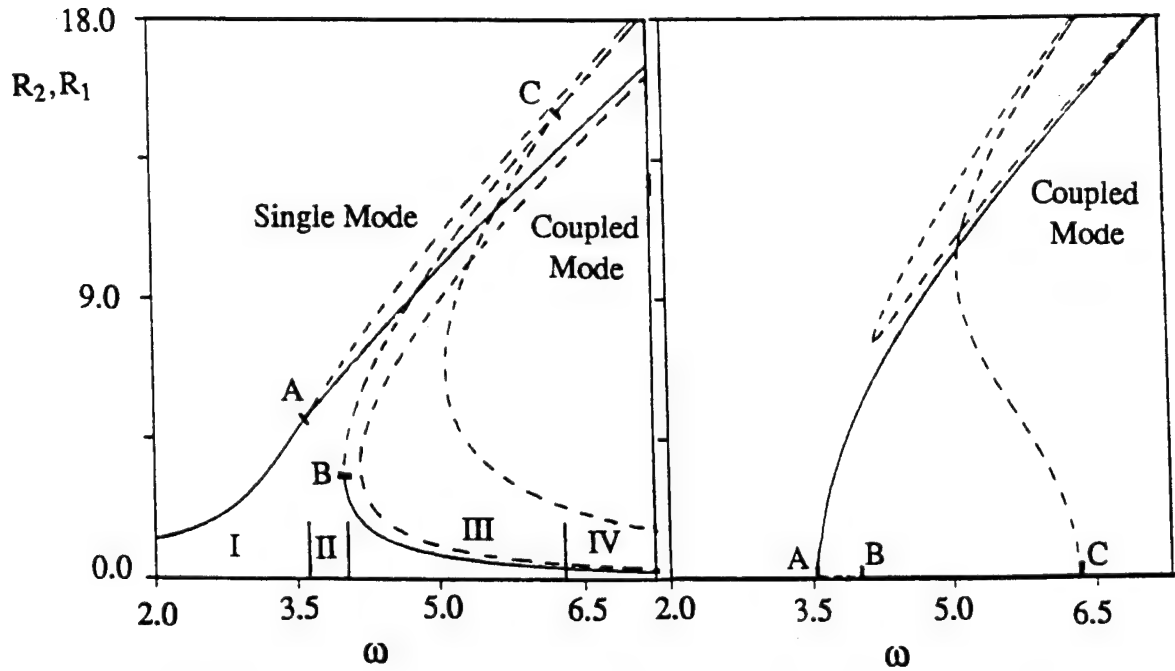
Fig. 3: Constant amplitude response $R_1$, for the (1,2) plate mode, and $R_2$, for the (3,1) plate mode; $Q_1 = 0.0$, $Q_2 = 10.0$, $c = 0.0$.
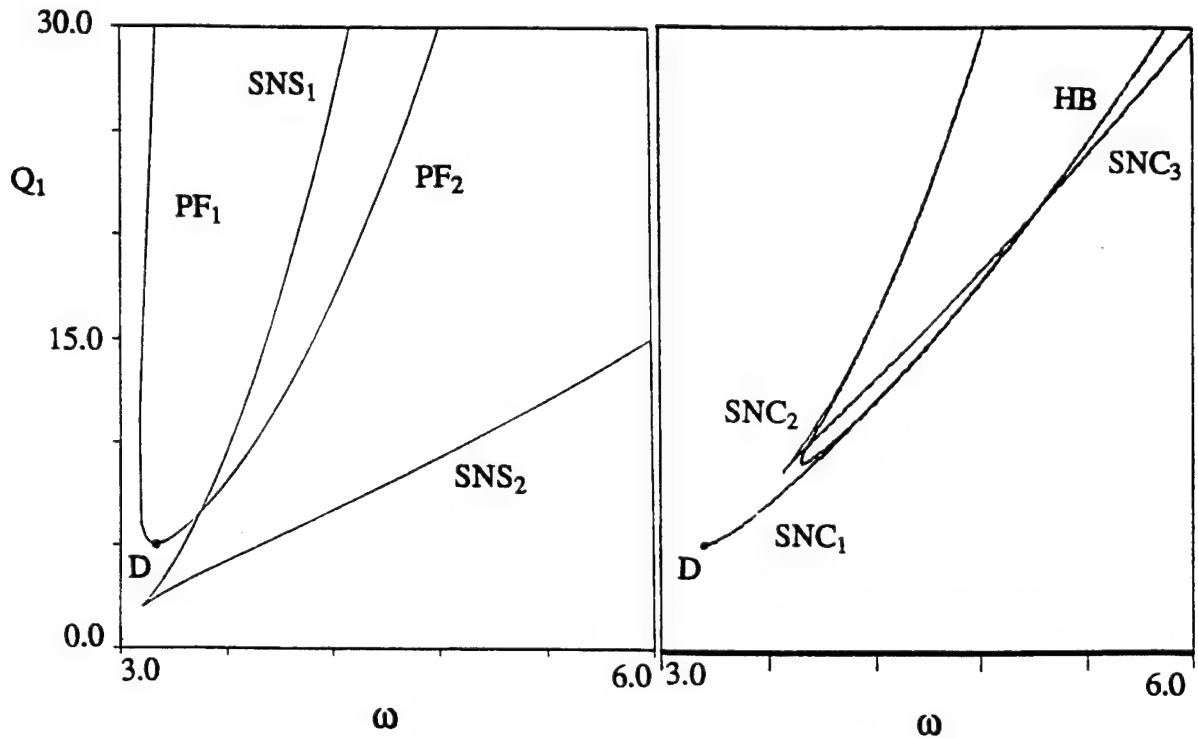


Fig. 4: Saddle-node and pitchfork bifurcation sets for single-mode solutions; $Q_2 = 0.0$, $c = 0.195$.

Fig. 5: Saddle-node and Hopf bifurcation sets for coupled-mode solutions; $Q_2 = 0.0$, $c = 0.195$.
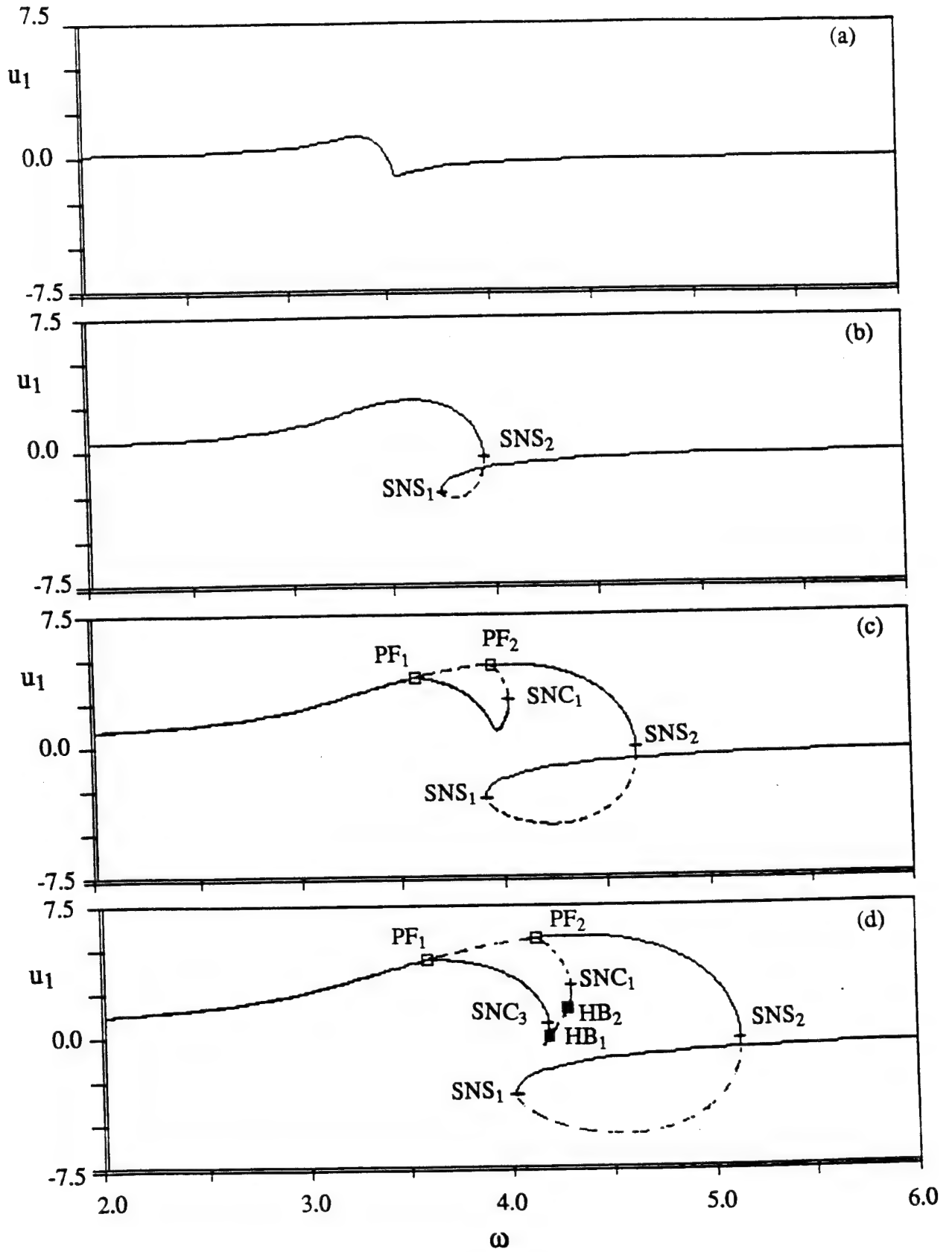
Fig. 6: Bifurcation response diagrams at various force levels; $c = 0.195$, $Q_2 = 0.0$. a) $Q_1 = 1.5$, b) $Q_1 = 4.0$, c) $Q_1 = 7.5$, d) $Q_1 = 10.0$.
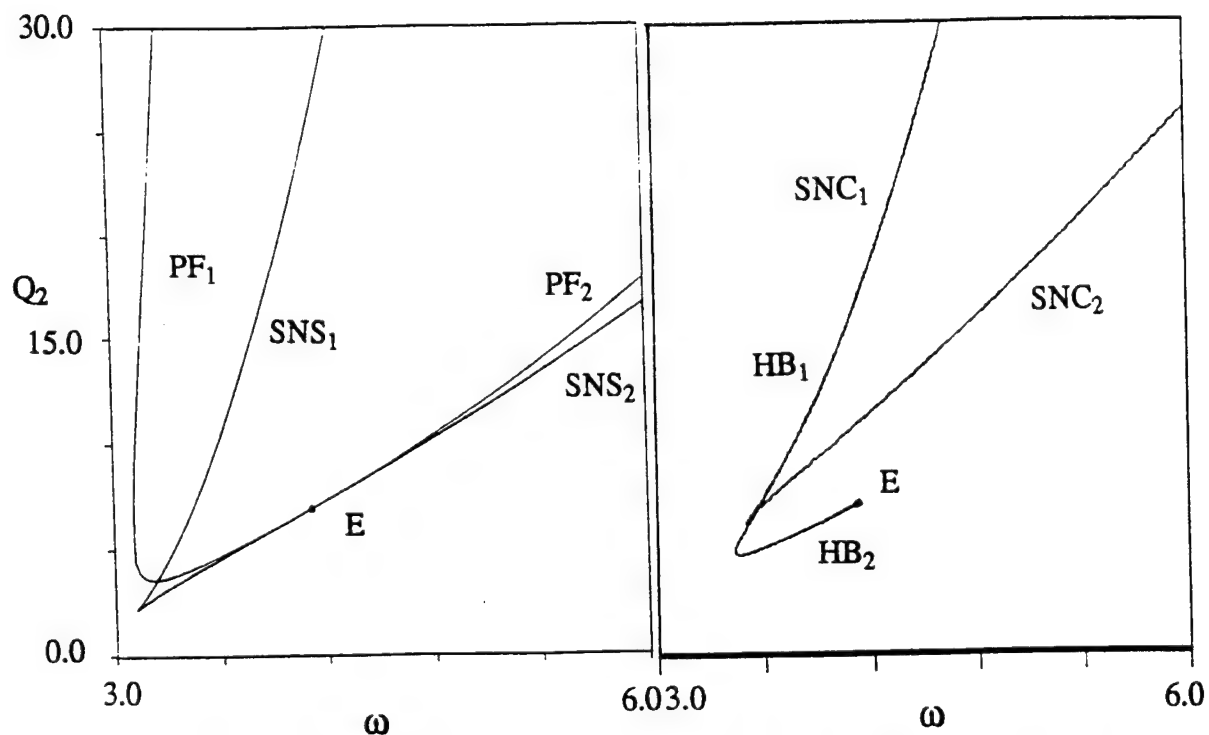
Fig. 7: Saddle-node and pitchfork bifurcation sets for single-mode solutions; $Q_1 = 0.0$, $c = 0.195$.

Fig. 8: Saddle-node and Hopf bifurcation sets for coupled-mode solutions; $Q_1 = 0.0$, $c = 0.195$.
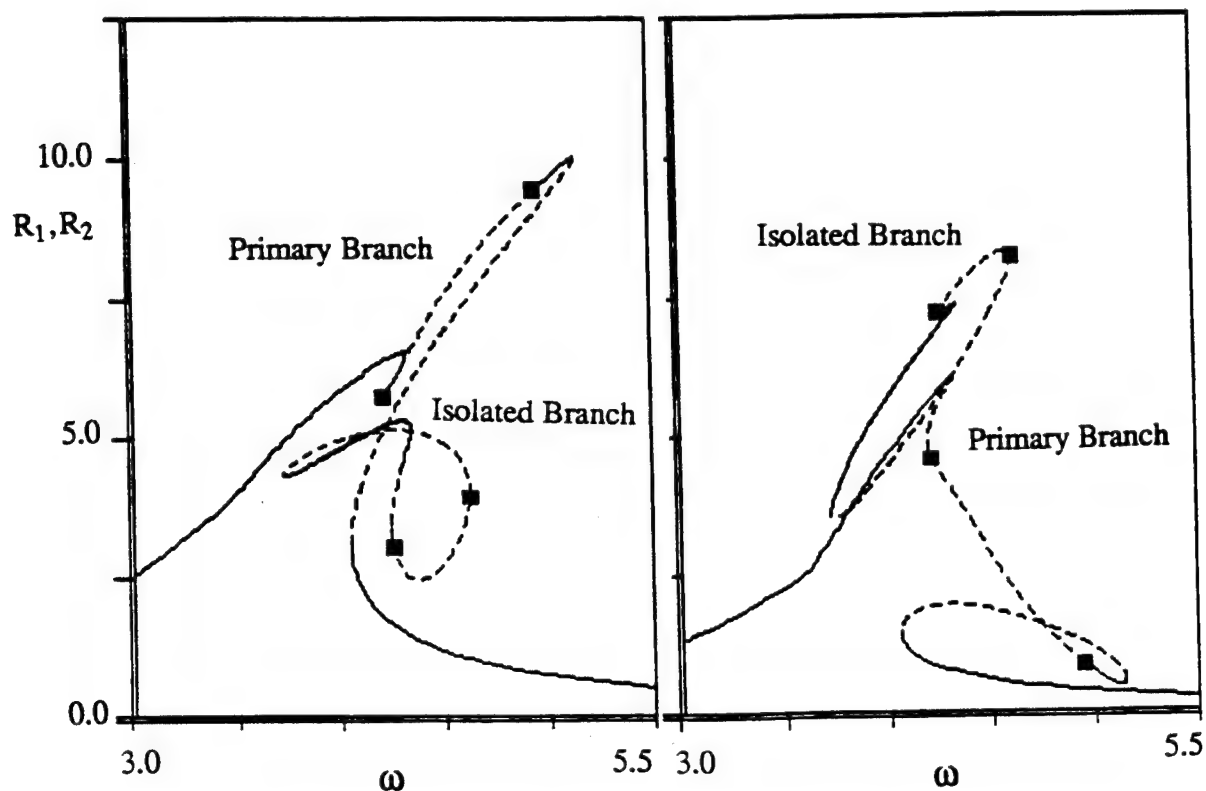


Fig. 9: Response amplitudes $R_1$ and $R_2$ as a function of the excitation frequency; $Q_1 = 10.0$, $Q_2 = 5.0$, $c = 0.195$.
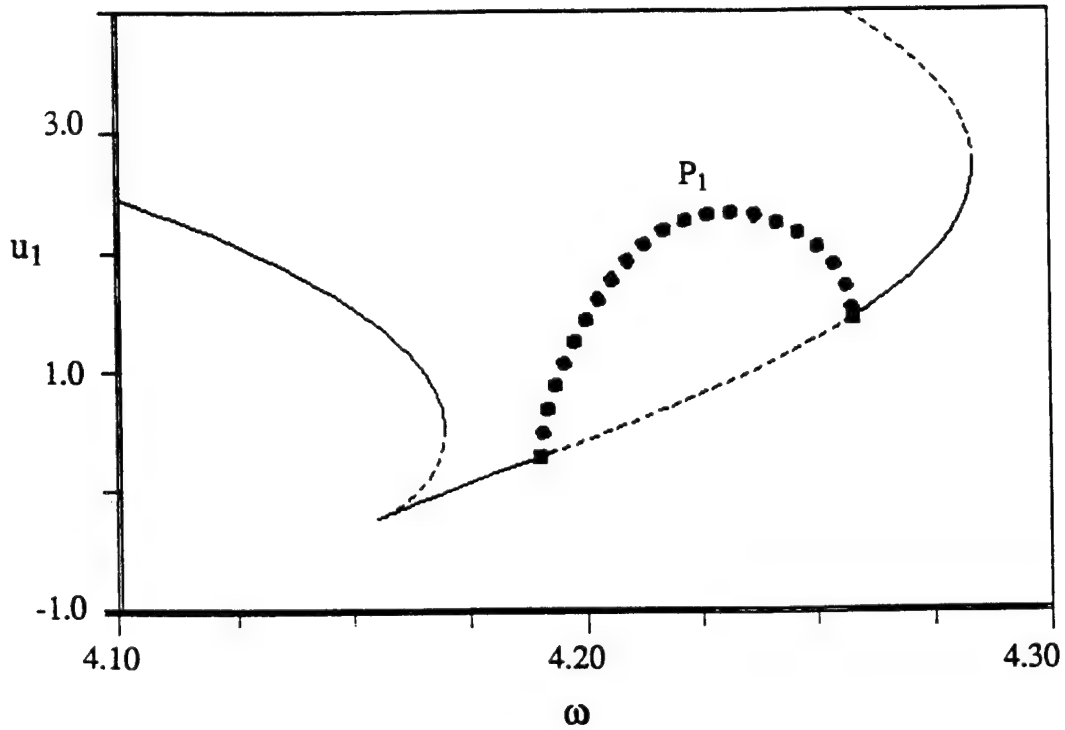
Fig. 10: Response amplitude for the limit cycle solution for $u_1$ as a function of the excitation frequency; $Q_1 = 10.0$, $Q_2 = 0.0$, $c = 0.20$.
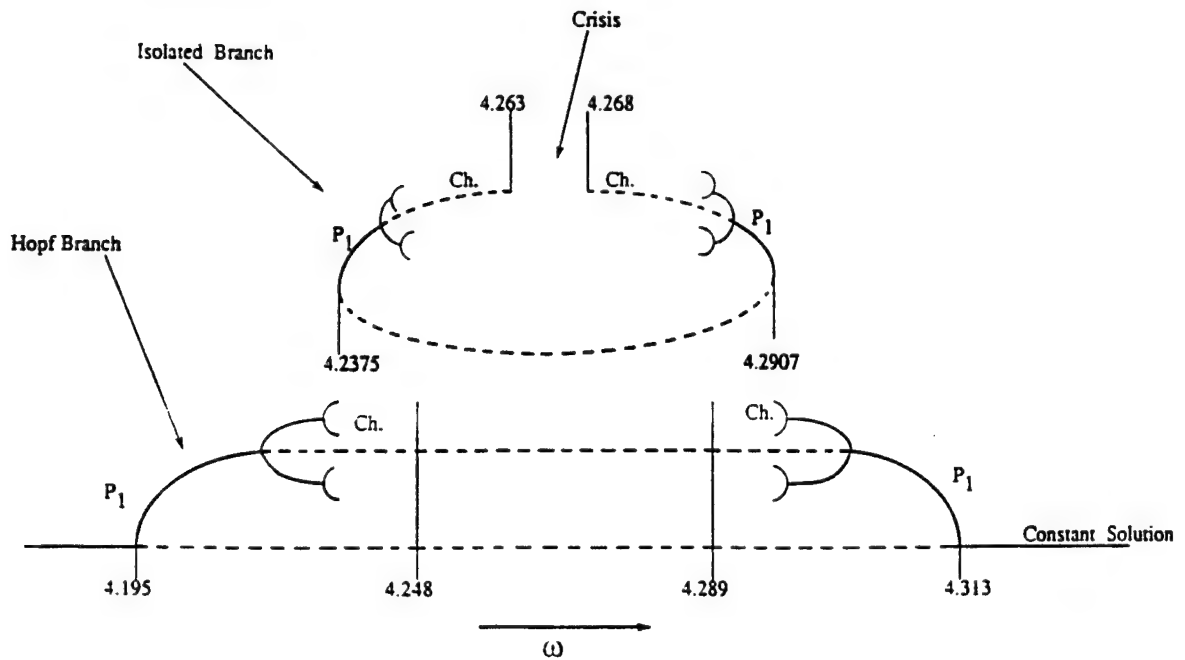


Fig. 11: Qualitative relationship between the Hopf and the isolated solution branches; $Q_1 = 10.0$, $Q_2 = 0.0$, $c = 0.19$.
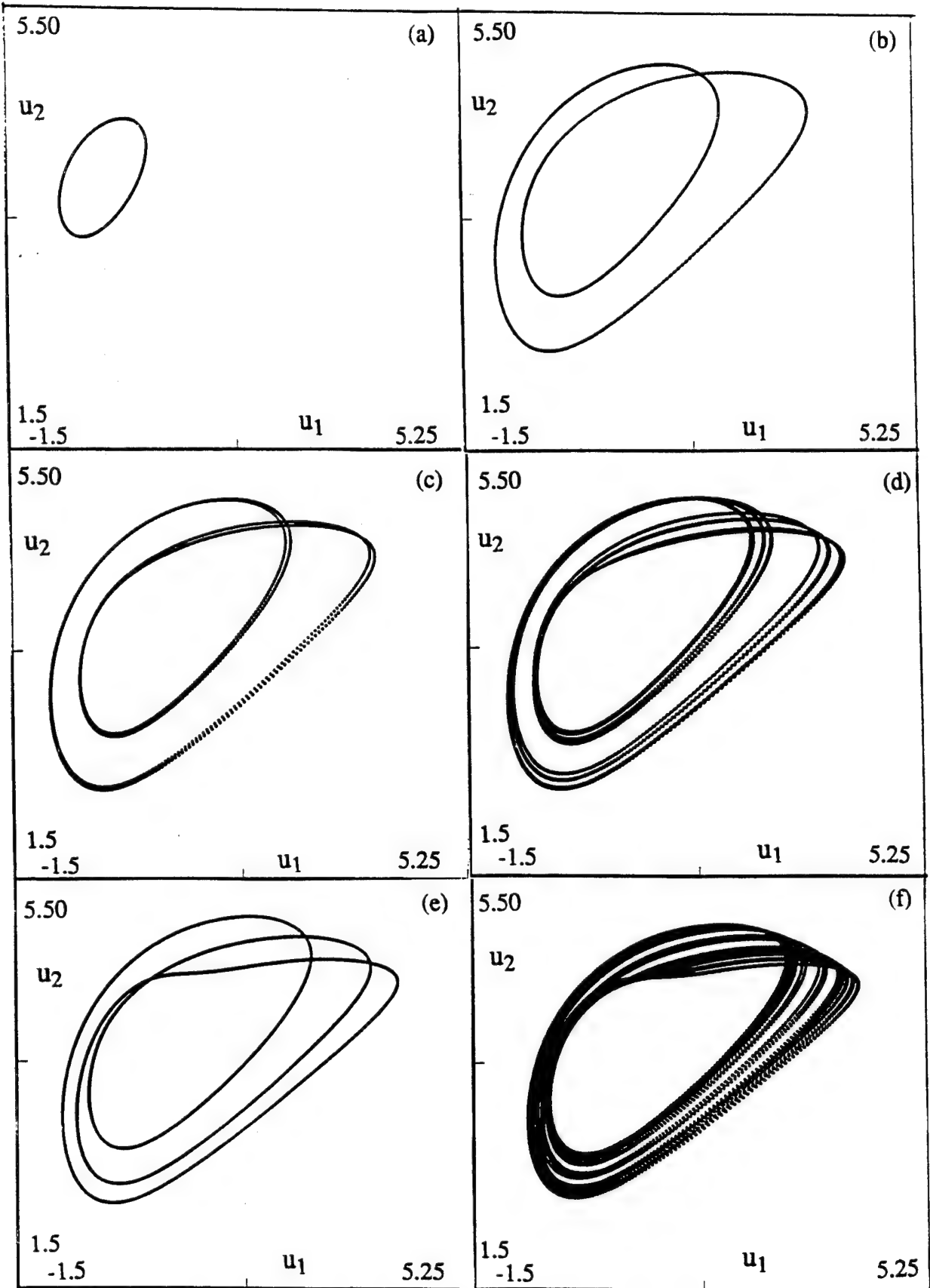
Fig. 12: Phase plots for the steady-state solutions in the Hopf bifurcating branch; $Q_1 = 10.0$, $Q_2 = 0.0$, $c = 0.19$. a) $\omega = 4.2$ ($P_1$), b) $\omega = 4.23$ ($P_2$), c) $\omega = 4.235$ ($P_4$), d) $\omega = 4.237$(Ch.), e) $\omega = 4.2425$ ($P_3$), f) $\omega = 4.248$ (Ch.).
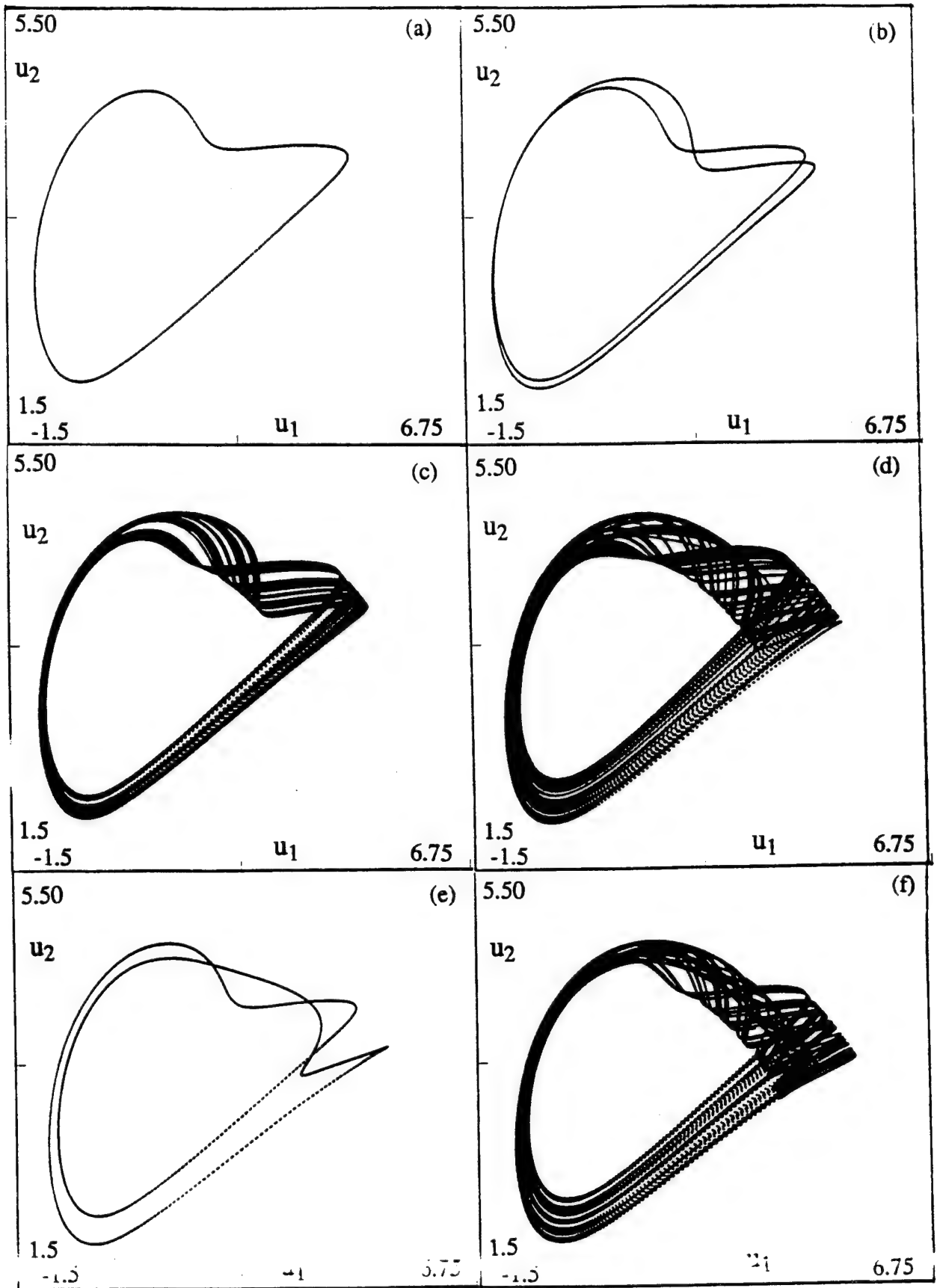
Fig. 13:   Phase plots for the steady-state solutions in the isolated branch; $Q_1 = 10.0$, $Q_2 = 0.0$, $c = 0.19$. a) $\omega = 4.238(P_1)$, b) $\omega = 4.241(P_2)$, c) $\omega = 4.243(Ch.)$, d) $\omega = 4.2485(Ch.)$, e) $\omega = 4.249(P_3)$, f) $\omega = 4.255(Ch.)$.
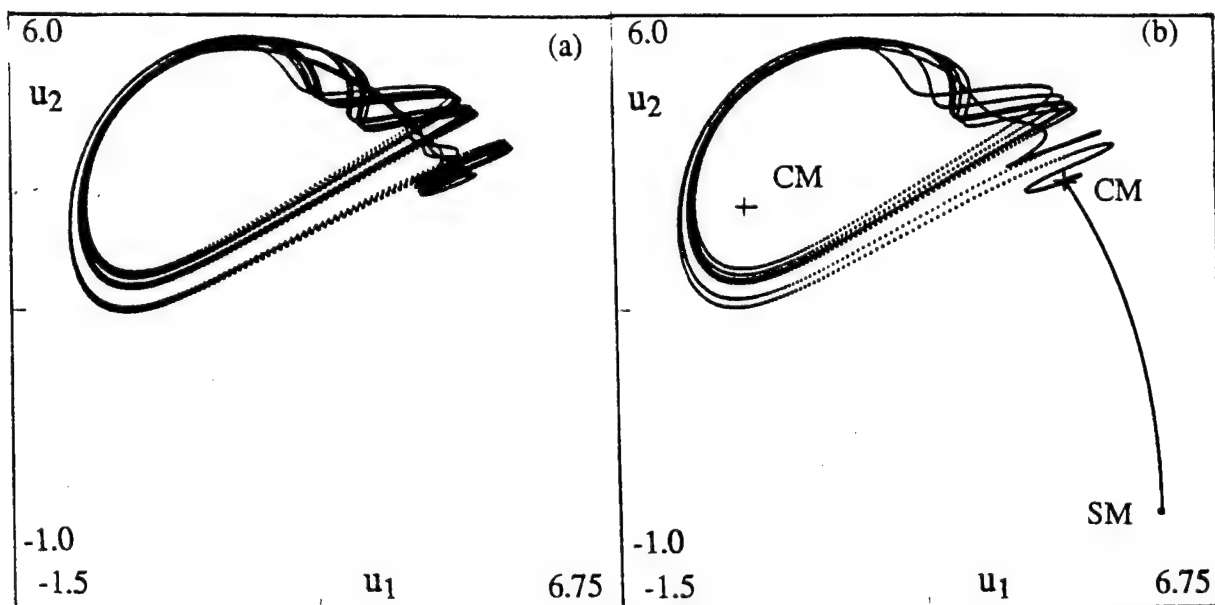
Fig. 14: 'Crisis' in the averaged equations; $Q_1 = 10.0$, $Q_2 = 0.0$, $c = 0.19$. a) chaotic attractor, $\omega = 4.262$, b) transient chaos, $\omega = 4.264$.
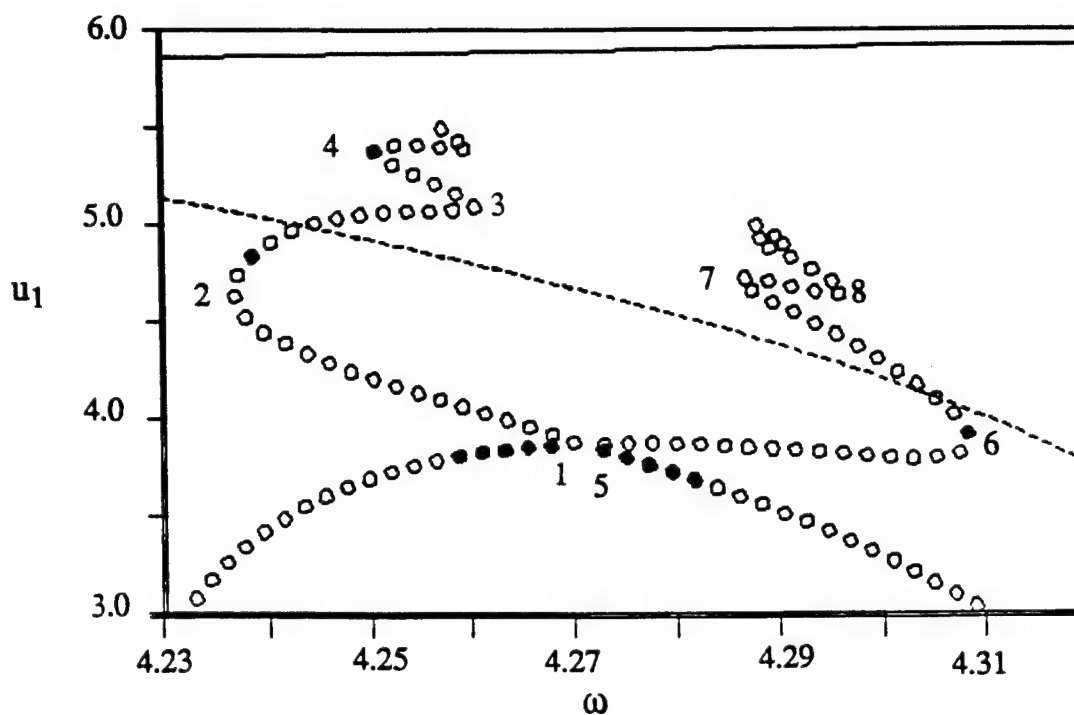


Fig. 15: Periodic solution branches continued from the two Hopf points on the coupled-mode branch; $Q_1 = 10.0$, $Q_2 = 0.0$, $c = 0.18755$.
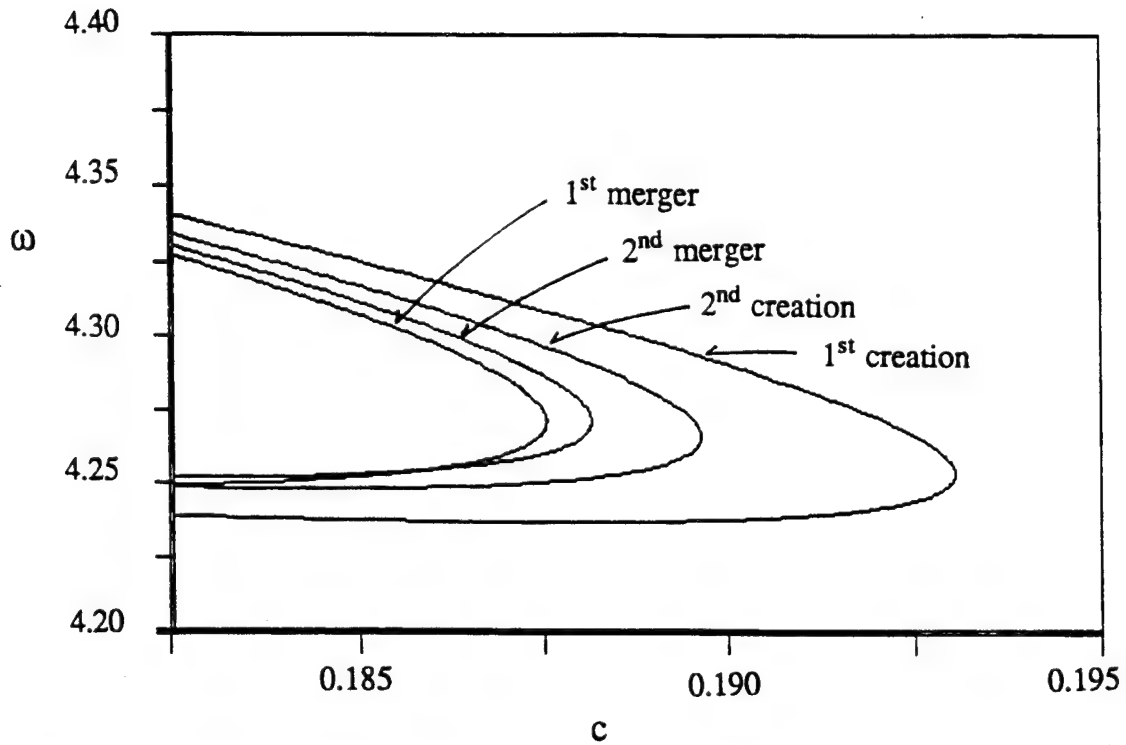
Fig. 16: Saddle-node bifurcation sets for the first and second isolated periodic solution branches in (c-$\omega$) plane; $Q_1 = 10.0$, $Q_2 = 0.0$.
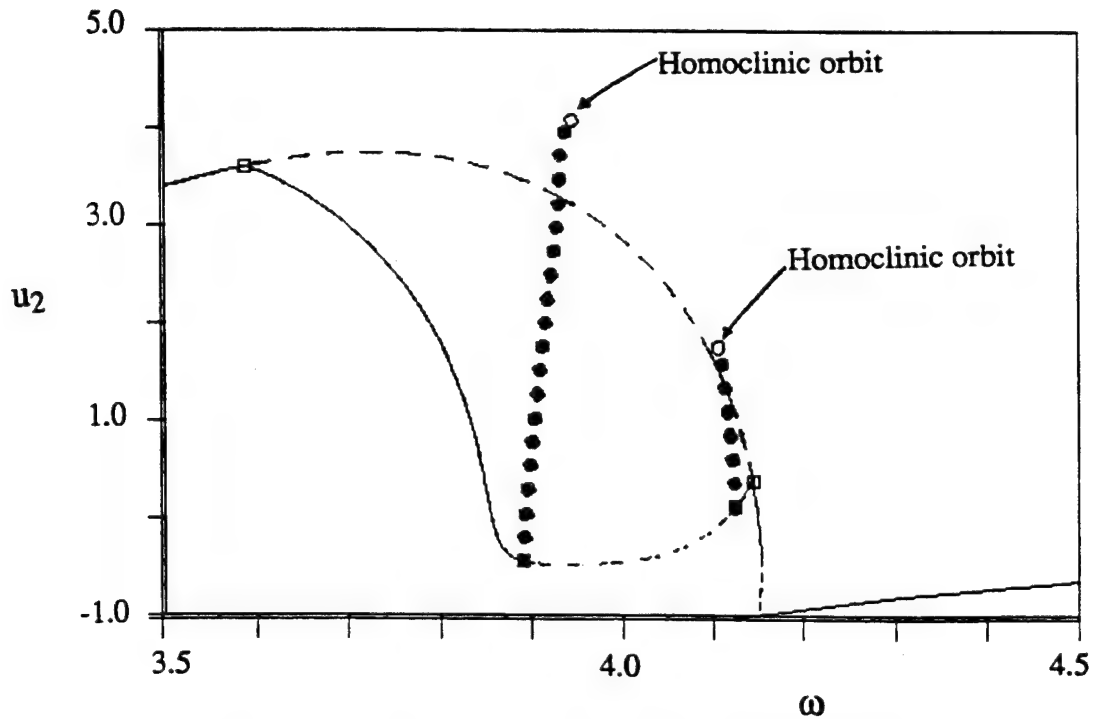


Fig. 17: Response amplitude $u_2$ as a function of the excitation frequency; $Q_1 = 0.0$, $Q_2 = 5.5$, c = 0.195.
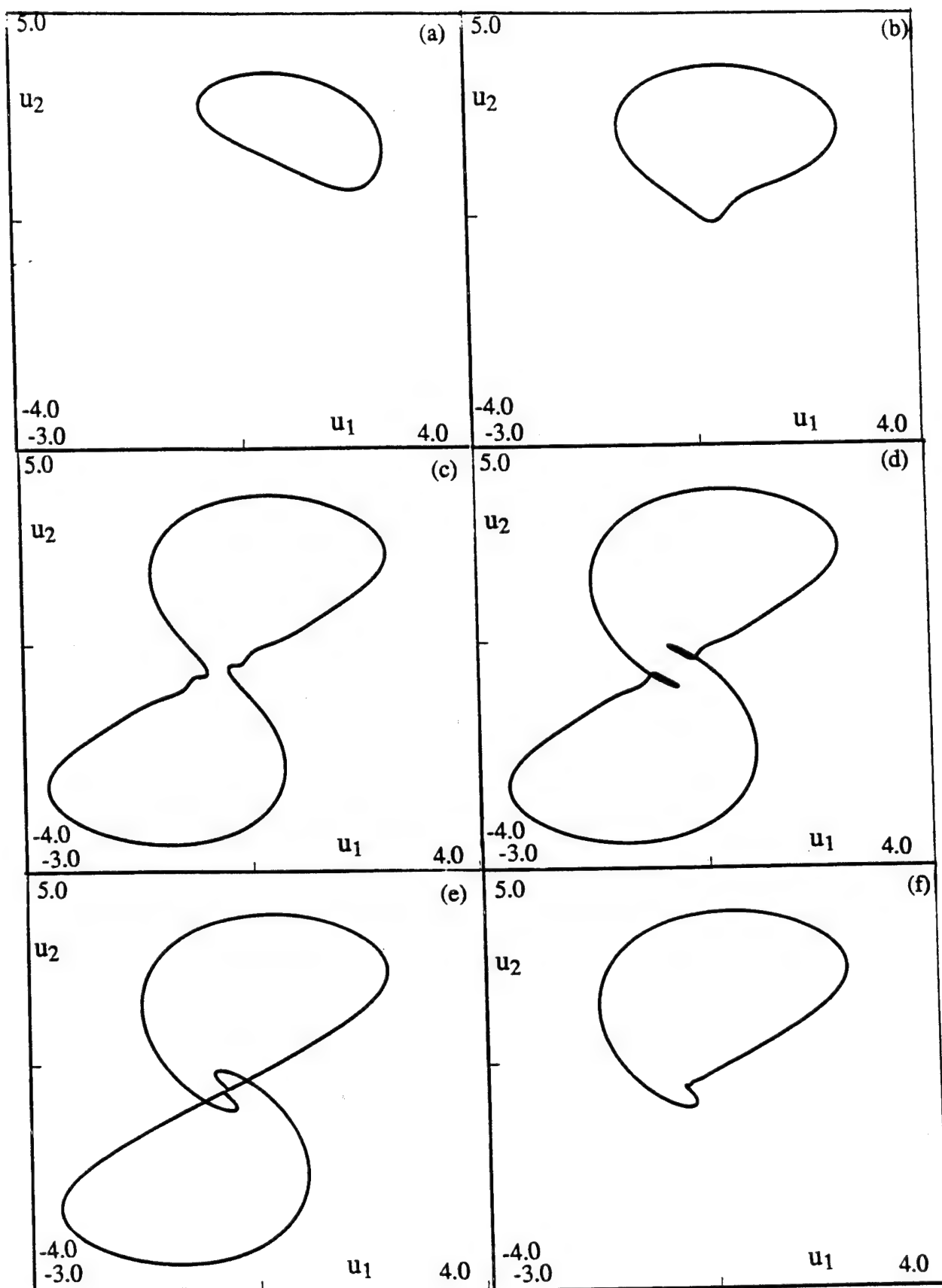
Fig. 18: Phase plots for the steady-state solutions; $Q_1 = 0.0$, $Q_2 = 5.5$, c = 0.195. a) $\omega = 3.93$, b) $\omega = 3.94$, c) $\omega = 3.95$, d) $\omega = 3.96$, e) $\omega = 3.9615$, f) $\omega = 3.962$.
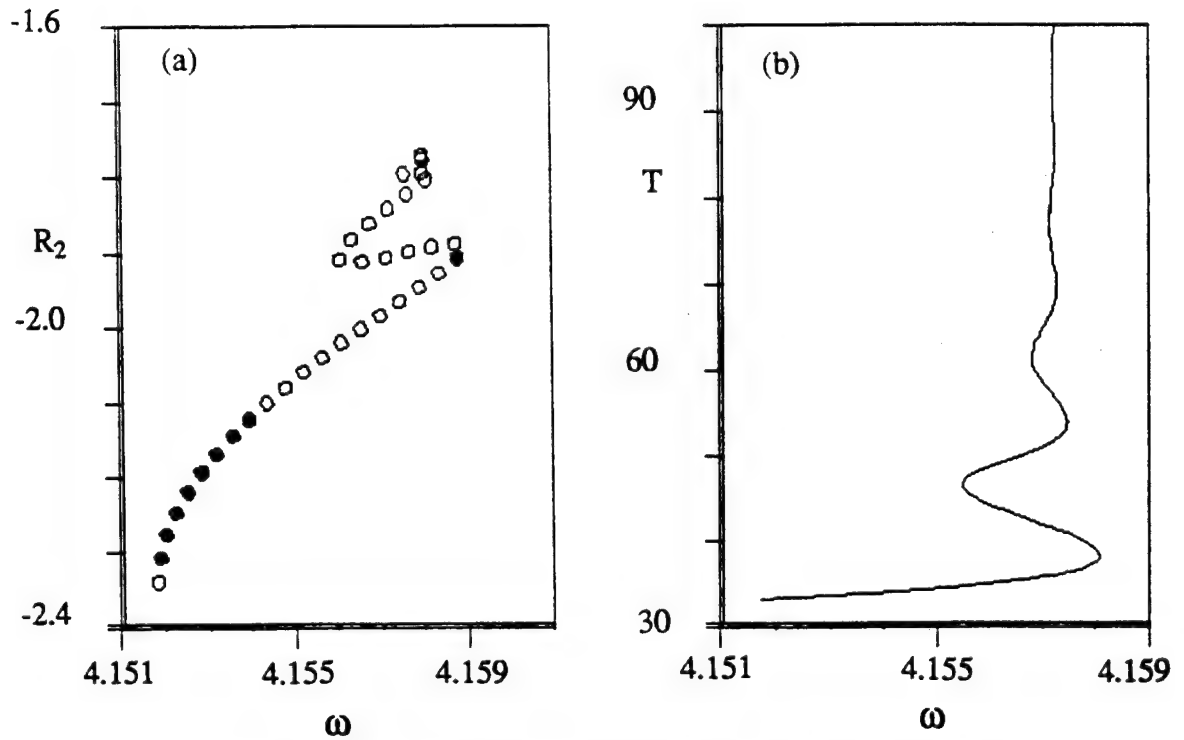
Fig. 19: The periodic solution branch continued from the left Hopf point; $Q_1 = 0.0$, $Q_2 = 10.0$, $c = 0.19$. a) amplitude of response, b) the variation of the period.
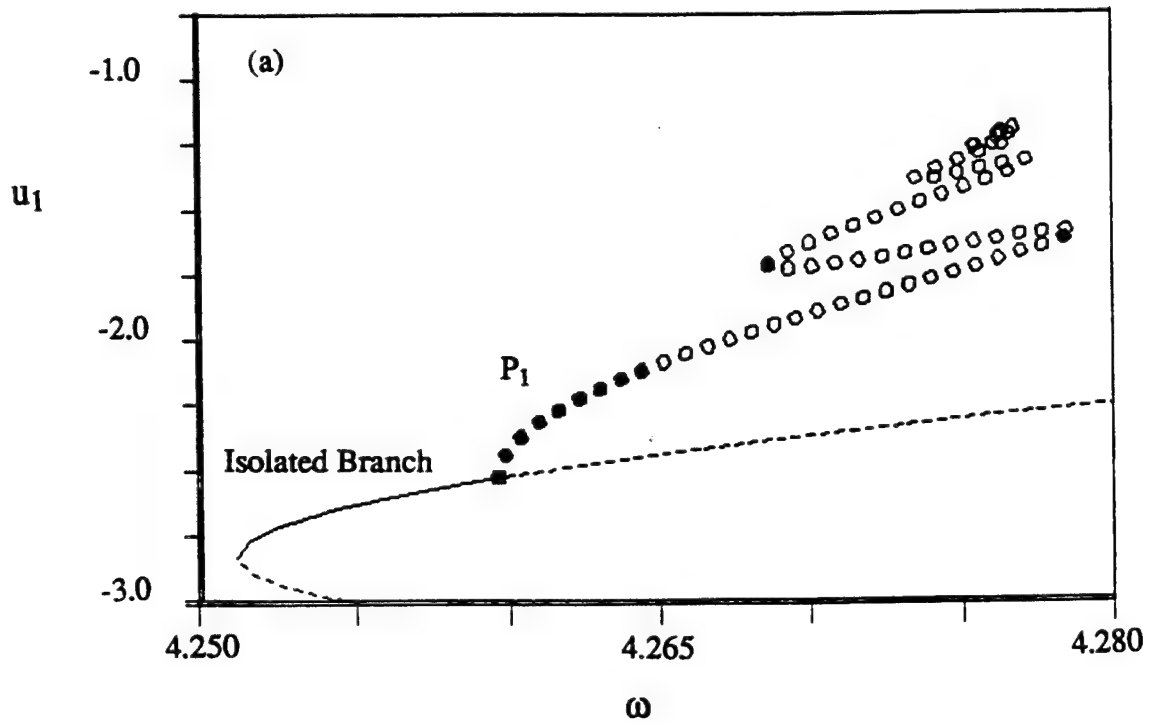


Fig. 20: The periodic solution branches; $Q_1 = 10.0$, $Q_2 = 5.0$, $c = 0.19$. a) isolated branch, b) primary branch.
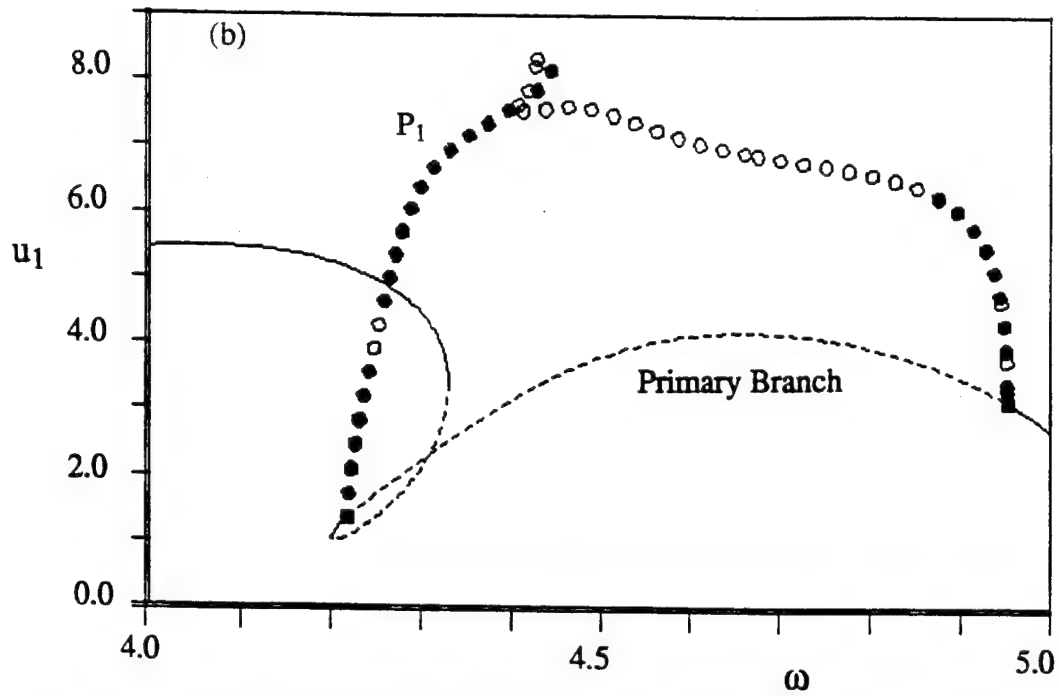
Fig. 20: The periodic solution branches; $Q_1 = 10.0$, $Q_2 = 5.0$, $c = 0.19$. a) isolated branch, b) primary branch.
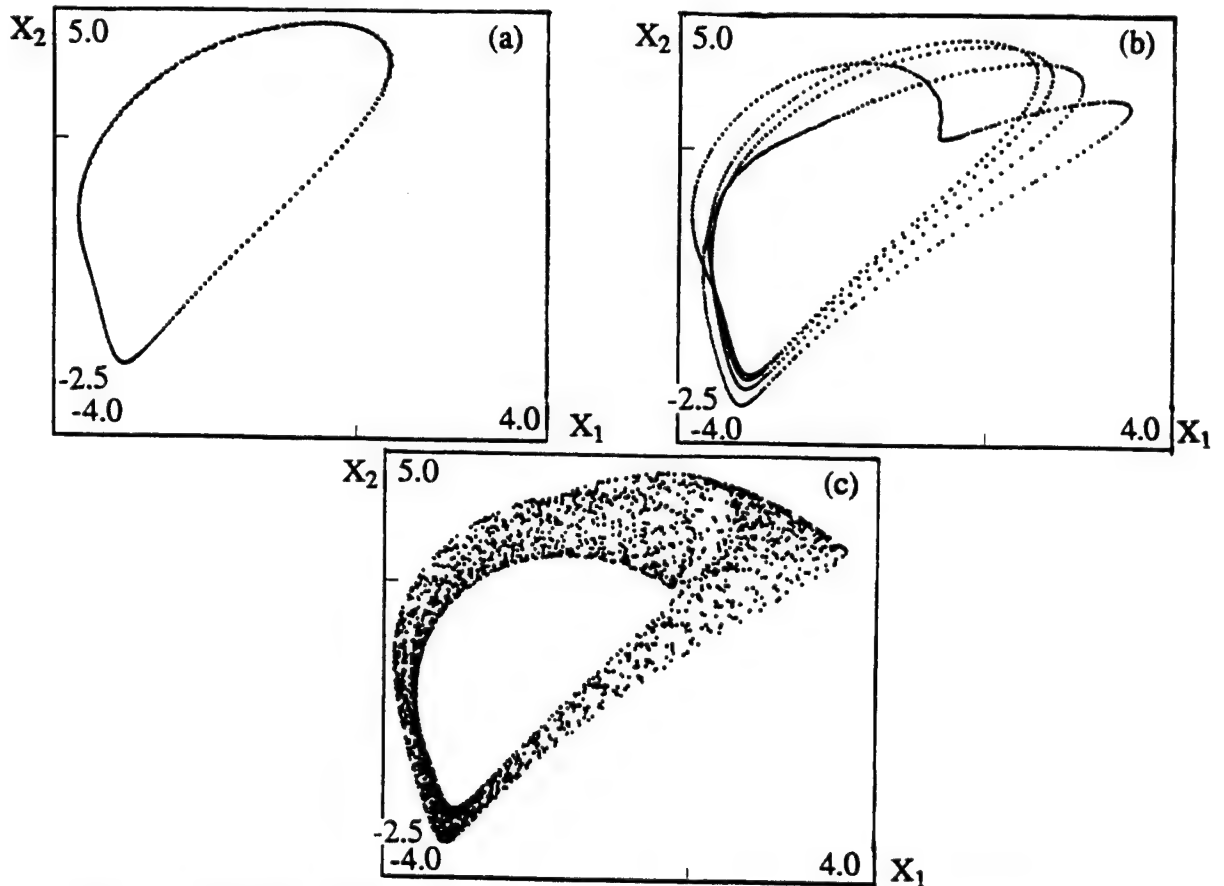


Fig. 21: Poincare' sections of the solutions of the two-mode approximation; $Q_1 = 10.0$, $Q_2 = 0.0$, $c = 0.18$. a) two-torus ($T_1$) solution, $\omega = 4.232$, b) $T_4$ solution, $\omega = 4.233$, c) chaotic solution, $\omega = 4.234$.

# APPENDIX 3

## Nonlinear response of a clamped plate to nonstationary excitation: experiments and theory

S. A. McCabe, S. I. Chang, P. Davies, A. K. Bajaj

# NONLINEAR RESPONSE OF A CLAMPED PLATE
## TO NONSTATIONARY EXCITATION:
### EXPERIMENTS AND THEORY

**Sarah A. McCabe, Seo I. Chang, Patricia Davies,
and Anil K. Bajaj**
School of Mechanical Engineering
Purdue University
West Lafayette, Indiana

## ABSTRACT

The paper contains a description of a series of experiments conducted on a thin rectangular plate. The initial objective of the experiments was to observe behavior predicted by theoretical studies and observed in simulations of the plate response. The theoretical work centered on predicting the behavior of plates having modes with coincident natural frequencies and driven with a constant sinusoidal excitation. Of particular interest was the modal coupling, due to nonlinearities, which give rise to the possibility of a coupled mode response when only a single mode is excited. Experimental constraints, and the sensitivity of the plate in configurations where more than one mode of response is possible, meant that the best experimental excitation of the plate would be a sine wave with a very slowly varying frequency. A PC based signal generator was developed to drive an array of loudspeakers so that particular modes of the plate could be strongly excited, and the frequency of excitation could be varied. To gain an understanding of the behavior of the plate when the excitation is nonstationary, the theoretical analysis of the plate behavior was extended to incorporate sinusoidal excitation where the frequency varied with time. The results of the analysis is a prediction of the response amplitude for slow and relatively fast swept sine wave excitations. In the paper, the qualitative features of the experimental response amplitudes are compared to those predicted by theory.

## INTRODUCTION

In this paper is a description of a series of experiments conducted on a thin rectangular plate. The overall objective of these experiments was to observe types of behavior predicted by theoretical and simulation studies (Chang, et al., 1993). These predictions were of the steady state response of the plate to a stationary sinusoidal excitation. The plate analyzed in the theory was a thin, steel, rectangular plate, simply supported at its boundaries and subject to in-plane tension loading. This plate is similar to that studied by Yasuda and Asano (1986).

For low excitation levels, the response of single modes of the plate, whose natural frequency is well separated from those of other modes, can be modeled by a second order differential equation with a cubic nonlinearity. The plate aspect ratio (length : width) was chosen so that the (3,1) and the (1,2) linear modes of the plate had coincident natural frequencies. Coupling between these modes, due to nonlinearities, gives rise to complex types of behavior. In particular configurations several possible solutions coexist; which response is observed is a function of initial conditions. Small perturbations introduced into the systems will also affect which solution is observed.

Due to equipment and experimental constraints, it is difficult to reproduce these steady state response predictions in configurations where more than one solution is possible. Small changes in the frequency or amplitude of the excitation can cause a large change in the response, because these changes may cause the plate to move from one possible solution to another. For these reasons, it was decided to excite the experimental plate with a sinusoidal excitation whose frequency varied very slowly. We felt that if the sweep rate was slow enough the response amplitude should approach that predicted by the stationary excitation theory.

Having built a flexible PC-based signal generator to generate arbitrarily slowly swept sine waves, it was now possible to observe the plate response at faster sweep rates. The results reported in this paper are primarily of the response of the plate to nonstationary excitation. The nonstationary response of nonlinear systems has been studied extensively by Evan-Iwanowski (1976). Here, the response of a single mode, well isolated from other modes, is studied as well as the response of two nearly coincident modes. In order to compare the experimental results with the theoretical behavior of the plate, the slowly varying amplitude and phase equations, that were used in the steady state response analysis, were modified to simulate the

slowly varying response to a nonstationary sinusoidal excitation. These simulations are presented together with the measured responses in later sections of this paper. A theoretical, as opposed to simulated, prediction of the nonstationary response is not presented here; a method for constructing the slowly varying response amplitude analytically is described by Raman, et al. (1993).

## THEORY

### Derivation of the Single Mode and Coupled Mode Models of the Plate

In this section we briefly describe the physical model and present a set of ordinary differential equations of motion obtained by Galerkin's procedure and a set of amplitude and phase equations of motion obtained by the method of averaging. The methods and procedures are described in detail by Chang, et al. (1993).

Consider a rectangular plate of thickness $h$ and edge lengths $a$ and $b$. Let $O_{xyz}$ be a Cartesian coordinate system with $O_{xy}$ in the mid plane of the plate and the origin at a corner. The plate is subjected to a uniform stretching force $N_0$. Under these conditions, the von Karman-type equations of motion for the plate are as follows:

$$\rho\, h\, w_{,tt} - N_0\, (w_{,xx} + w_{,yy}) + D\, (w_{,xxxx} + 2\, w_{,xxyy} + w_{,yyyy})$$

$$= F_{,yy}\, w_{,xx} - 2\, F_{,xy}\, w_{,xy} + F_{,xx}\, w_{,yy} - c\, w_{,t} + q \ , \tag{1}$$

$$F_{,xxxx} + 2\, F_{,xxyy} + F_{,yyyy} = E\, h\, (w_{,xy}^2 - w_{,xx}\, w_{,yy}) \ , \tag{2}$$

where $w(x,y,t)$, $F(x,y,t)$ and $q(x,y,t)$ are the transverse deflection, the stress function, and the external force normal to the plate, respectively. The parameters $\rho$, $E$, $D$, and $c$ are the density, the Young's modulus, the bending stiffness, and the damping coefficient, respectively. Furthermore, the subscript $x$, $y$, or $t$ denotes a partial differentiation with respect to that variable. The boundary conditions considered here are that all the edges are simply supported and immovable.

The interest in the present study is in motions when the plate is harmonically excited by the external force $q(x,y,t)$ with slowly varying excitation frequency. Large amplitude motions occur when the excitation frequency is near a linear natural frequency and the spatial motions of the plate are approximated by the linear vibratory modes. In this study, we assume the deflection to be a superposition of two distinct linear modes as follows:

$$w(x,y,t) =$$
$$X_1(t)\, \sin m\pi x\, \sin n\pi y + X_2(t)\, \sin r\pi x\, \sin s\pi y. \tag{3}$$

Thus, the motion consists of a linear combination of the two spatial modes of orders $(m,n)$ and $(r,s)$. The modal amplitudes $X_1$ and $X_2$ are functions of time and the nonlinear terms in the system determine their time evolution. Following the procedures described by Chang, et al. (1993), we obtain the following normalized discretized equations of motion:
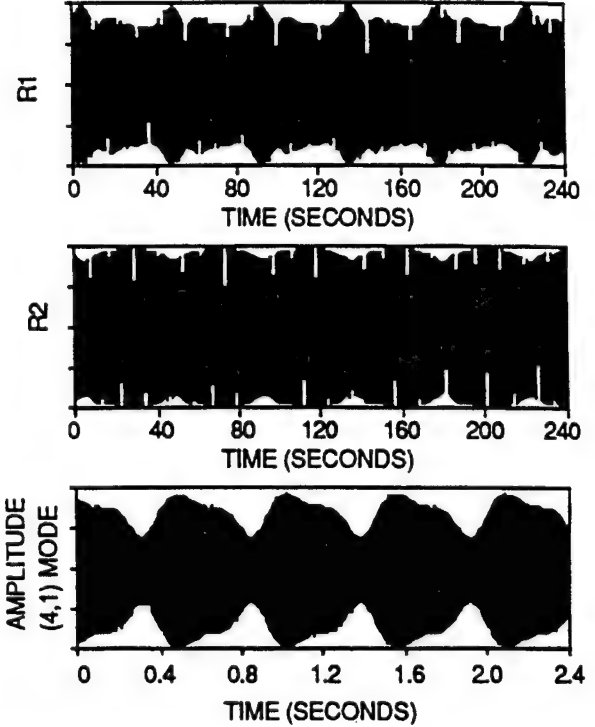


FIGURE 1: THE COUPLED MODE RESPONSE OF THE PLATE AS PREDICTED BY THEORY: (A) THE (1,2) MODAL RESPONSE, (B) THE (3,1) MODAL RESPONSE, AND AS MEASURED: (C) PREDOMINANTLY THE (4,1) MODAL RESPONSE.

$$\ddot{X}_1 + p_1^2\, X_1 = \varepsilon\, (A_1\, X_1^2 + A_2\, X_2^2)\, X_1 - c\, \dot{X}_1 + Q_1\, \sin \omega\, t \ ,$$

$$\ddot{X}_2 + p_2^2\, X_2 = \varepsilon\, (A_2 X_1^2 + A_3 X_2^2)\, X_2 - c\, \dot{X}_2 + Q_2\, \sin \omega\, t \ , \tag{4}$$

where $A_1$, $A_2$, and $A_3$ are the constant nonlinear coefficients which are determined for the specific mode combinations, and $p_1$ and $p_2$ are the corresponding natural frequencies of the two linear modes. The normalization introduces a time scaling factor of approximately 230. So simulations of the plate response will appear to be approximately 230 times slower than the response of the actual plate. The response of single isolated modes can be derived from these equations by setting $A_2$ to zero, which effectively decouples the equations.

For an aspect ratio of 1.633, the (3,1) and (1,2) modes of the simply supported plate have coincident natural frequencies. Due to non-uniformities in tension and non-ideal boundary conditions, the natural frequencies of the (3,1) and (1,2) modes of the experimental plate are not coincident. However the natural frequencies of the (4,1) and (3,2) modes are. In figures 1(a) and 1(b) are shown the simulated response to a sinusoidal excitation of the (1,2) and (3,1) modes of the plate, respectively. $\omega = 4.21911$
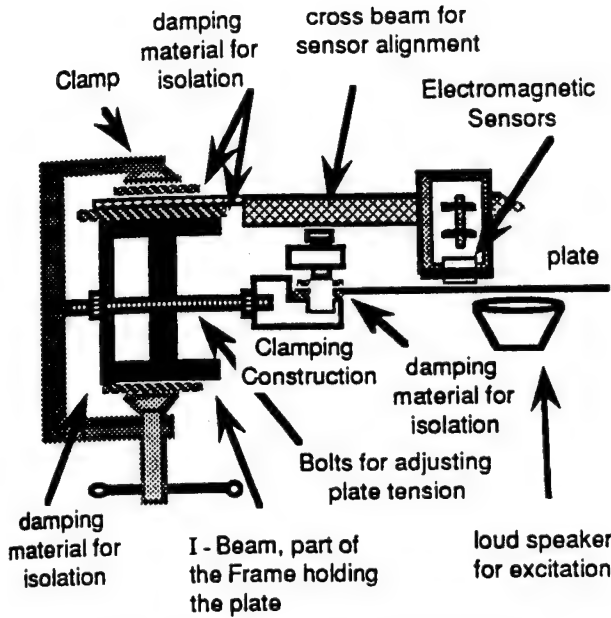
FIGURE 2. EXPERIMENTAL SETUP (SIDE VIEW).



FIGURE 3. EXPERIMENTAL SETUP (TOP VIEW)

rad/sec; $p_1 = p_2 = 3.4157$ rad/sec, $Q_1 = 10$, $Q_2 = 0$, $D = 0$, $\varepsilon = 0.0006$, $A_1 = -326.27$, $A_2 = -274.74$, and $A_3 = -268.43$, and $Q_1$ is the excitation amplitude for the (1,2) mode. In figure 1(c) is shown the response of the experimental plate at a location that primarily measures the response of the (3,2) mode. The excitation frequency was 173 Hz., and the natural frequencies of the (3,2) and (4,1) mode during this test were 171.4 Hz. and 174 Hz., respectively. The amplitude modulation indicates the presence of a coupled mode response.

To examine the behavior of the slowly varying amplitude and phase of the modal responses, let

$$X_1 = R_1 \cos (\omega t - \gamma_1), \qquad X_2 = R_2 \cos (\omega t - \gamma_2) \qquad (5)$$

Then, by using a variation of constants procedure and the method of averaging (Nayfeh and Mook, 1979; Hale, 1969; Guckenheimer and Holmes, 1983) and noting that the excitation frequency $\omega$ is near the two close natural frequencies, equations (4) result in the following averaged equations for the amplitudes $R_i$ and the phases $\gamma_i$:

$$\dot{R}_1 = -\frac{c}{2} R_1 + \frac{Q_1}{2 \omega} \sin \gamma_1 + \frac{\varepsilon A_2}{8 \omega} R_2^2 R_1 \sin 2 (\gamma_1 - \gamma_2),$$

$$\dot{\gamma}_1 = \frac{\omega^2 - p_1^2}{2 \omega} + \frac{Q_1}{2 \omega R_1} \cos \gamma_1 + \frac{3 \varepsilon A_1}{8 \omega} R_1^2$$
$$+ \frac{\varepsilon A_2}{8 \omega} R_2^2 \{2 + \cos 2 (\gamma_1 - \gamma_2)\},$$

$$\dot{R}_2 = -\frac{c}{2} R_2 + \frac{Q_2}{2 \omega} \sin \gamma_2 + \frac{\varepsilon A_2}{8 \omega} R_1^2 R_2 \sin 2 (\gamma_2 - \gamma_1),$$

$$\dot{\gamma}_2 = \frac{\omega^2 - p_2^2}{2 \omega} + \frac{Q_2}{2 \omega R_2} \cos \gamma_2 + \frac{3 \varepsilon A_3}{8 \omega} R_2^2$$
$$+ \frac{\varepsilon A_2}{8 \omega} R_1^2 \{2 + \cos 2 (\gamma_2 - \gamma_1)\}. \qquad (6)$$

The above amplitude equations were studied analytically and numerically by Chang, et al. (1993) for the case of stationary vibration. These equations can be used to simulate the response of the coincident modes when the excitation frequency changes as a function of time by adding a fifth equation to (6): $\dot{\omega} = \alpha$, where $\alpha$ is the sweep rate which is assumed to be very small. These equations were used to generate the theoretical responses shown later in the paper.

## PLATE RIG AND EXPERIMENTAL CONFIGURATION

### The Plate and Frame Construction

Schematics of the experimental setup are shown in figures 2 and 3. A representation of the experimental instrumentation is shown in figure 4. The plate is constructed of steel and has the following dimensions: thickness = 0.265 mm, length = 65.41 cm, and width = 40.16 cm. The actual aspect ratio is 1.629 which is close to the 1.633 used in the theoretical analysis described by Chang, et al. (1993).

There were two major difficulties in reproducing the theoretical results in the experimental setup. First was the problem of creating a simply supported edge. Since the plate is very thin, a clamped edge should be a good approximation to a simply supported edge. However, there are irregularities in the clamp and plate surfaces and non uniformities in the clamping. The second major obstacle was that of producing a uniform tension force throughout the plate. In order to achieve this, the clamping mechanism was attached to 14 bolts around the perimeter of
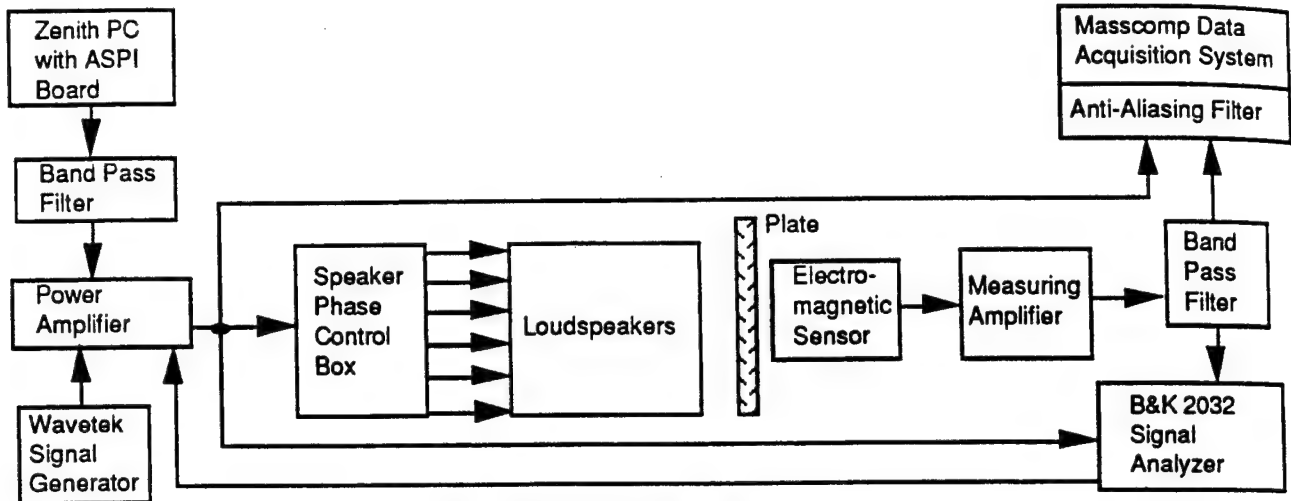
83

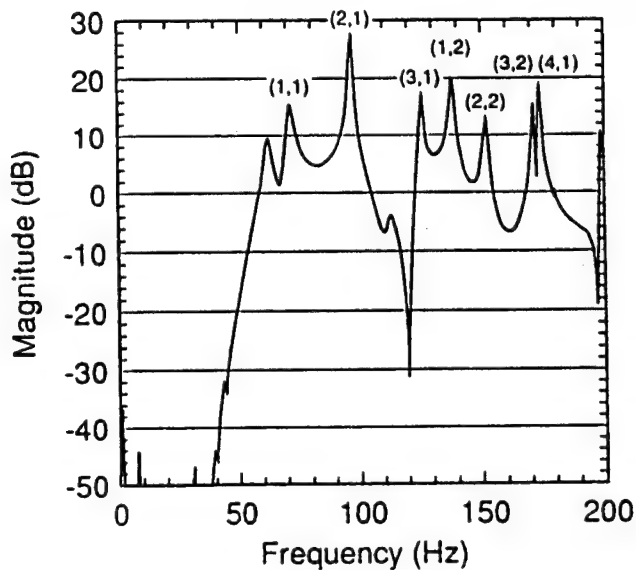FIGURE 4.    THE EXCITATION AND MEASUREMENT INSTRUMENTATION.



FIGURE 5. LINEAR TRANSFER FUNCTION OF
EXPERIMENTAL PLATE

**TABLE 1. EXPERIMENTAL LINEAR NATURAL FREQUENCIES**

| Mode | Linear Natural Frequency (Hz) |
|------|-------------------------------|
| (1,1) | 71.5 |
| (2,1) | 97.0 |
| (3,1) | 126.0 |
| (1,2) | 138.0 |
| (2,2) | 152.0 |
| (3,2) | 171.5 |
| (4,1) | 174.0 |

the plate.    Each of these bolts could be individually tightened.  The torque on each tightening nut was measured. The relation between this torque and the tension force in the bolt was presumed to be the same for each bolt.  In reality, this presumption is not completely accurate.  In addition, the tension in the plate would change over time due to environmental conditions.    These nonuniformities in tension and boundary conditions resulted in differences between the natural frequencies and mode shapes of the experimental plate and those predicted or assumed in the theory.

In order to compare the theoretical and experimental results, experimental modes, which had the same characteristics of the theoretical modes of interest, were studied.  To find the linear natural frequencies of the plate,

it was excited by a loudspeaker driven with low amplitude random noise.   The input to the loudspeaker and the response of the plate were recorded with the same B&K 2032 signal analyzer which generated the random noise signal.   This analyzer then calculated an estimate of the linear transfer function by taking 100 averages in the estimation process.  The resulting transfer function has a frequency resolution of 0.5 Hz (Randall, 1987).   The transfer function was computed at the start of each experiment in order to determine any changes in natural frequency which may have occurred due to environmental effects.   An example of such a linear transfer function is shown in figure 5.  The first six linear natural frequencies and associated mode shapes are listed in table 1.

In the experimental plate, the (1,2) mode occurred at nearly twice the natural frequency of the (1,1) mode, had a small damping factor and was well isolated from other modes.  The (2,2) mode in theory occurs at twice the natural frequency of the (1,1) and is well isolated from other modes. Therefore a study of the single mode response was obtained by examining the response of the (1,2) experimental mode and comparing this with the theoretical single mode response of the (2,2) mode.

Although the theory predicted that the (3,1) and (1,2) modes would have nearly coincident natural frequencies, in the actual plate these modes were well separated. However, the (3,2) and (4,1) modes of the experimental plate had nearly coincident natural frequencies and therefore, the responses of these modes are used to demonstrate qualitatively the experimental coupled mode behavior. This behavior is compared with the theoretical coupled mode response of the (3,1) and (1,2) modes.

An estimate of the damping factor for each of the modes of interest was obtained from the experimental transfer function by using the half power points method (Ewins, 1985). These values were used when computing the theoretical results.

## Excitation Mechanisms for the Plate

A variety of methods of exciting the plate were attempted. In the experiments performed by Yasuda and Asano (1986), electromagnetic exciters were used. We found that these did not provide high enough excitation levels to excite the nonlinear behavior of the plate we are studying. We also experimented with using a mechanical shaker to provide excitation. However, because the input impedance of the plate is a function of frequency, the force that a shaker imparts to a mechanical structure is not a constant proportion of the amplitude of the signal input to the shaker. As the frequency of the input signal approaches the resonant frequency of the mechanical system, the force imparted by the shaker reduces.

Another problem with these two types of excitation is that they are actually close to being point source excitations. In the theoretical analysis, only a single mode is excited; this point source excitation will excite all modes. Yasuda and Asano (1986) overcame this problem to some extent by using two electromagnetic exciters phased to strongly excite the mode that they wished to drive, and not excite the second mode. In order to reproduce the theoretical results, it is necessary that the excitation source match the shape of the mode of interest. We therefore decided to use an array of loudspeakers to acoustically excite the plate; this has the benefit of being a noncontacting, high amplitude (if wished), distributed source.

The loudspeakers used were chosen to meet the following specifications: have good performance at low frequencies, high response amplitude and low distortion. An array of 6 MTX Blue Thunder BTM 64 loudspeakers was positioned under the plate in a 3 by 2 grid (see figure 3). Each speaker could independently be set either in phase with the driving signal, out of phase, or off. In the off configuration the loudspeaker was replaced by a resistor chosen to match, to some degree, the input impedance of the loudspeaker. By adjusting the speaker phases one can tailor the acoustic wave output to match a particular mode shape. By using this array, each of the first 6 modes can be directly excited through the acoustic-mechanical coupling at the plate-air interface. The excitation level (sound field) was not directly measured, but the level was assumed to be directly proportional to the voltage input to the loudspeakers. This signal was monitored and recorded.

## Signal Generation

Four different types of experiments were run and the results are described below. First we desired to compare the theoretical results of a single mode response subjected to a stationary excitation with the actual response of the plate. In order to generate a plot of output amplitude as a function of input frequency, the plate was subjected to a constant amplitude sine wave with a slowly and linearly varying frequency. The rate of change of this frequency is so small as to approximate a series of stationary excitations in a frequency range. In this paper we refer to this type of excitation as "quasi-stationary".

In order to create such a signal, a program was written to run on an Atlantic Signal Processors Inc. Banshee Board which holds a TMS320C30 chip and was installed in a Zenith PC computer. This board generated a signal and output it through its D/A converter. This program enables the user to adjust the starting and ending frequency of the sweep as well as the sweep rate, each independently of the other. This allowed for the greatest flexibility when running an experiment. The output of the D/A converter was bandpass filtered (50-400 Hz., 48 dB./Octave) to remove the harmonics introduced by the sample and hold device in the converter and any DC offsets in the generated signal. The signal generation sampling frequency was 4000 Hz.

Two of the other experiments involved subjecting the plate to nonstationary excitations. These excitations were generated by using the same program described above. For the case of coupled mode response to stationary excitation, a constant frequency, constant amplitude sine wave was needed. This was produced by using a standard signal generator (Wavetek).

## Measurement of the Plate Response

Non-contacting vibration detectors (B&K model MM 0002), which measured the plate velocity through magnetic induction, were located above the plate. In the case of single mode response and the coupled mode amplitude modulated response, a single detector was placed at an anti-node of the mode shape in order to increase the signal to noise ratio to a maximum. In the case of the nearly coincident mode responses to nonstationary excitation, two detectors were used. An attempt was made to place one of the detectors on a nodal line of the (4,1) mode to measure only the response due to the (3,2) mode. Similarly, the other detector was placed on a nodal line of the (3,2) mode to measure only the response due to the (4,1) mode. However, due to the nonuniformities in the boundary conditions and tension, mode shapes of the experimental plate are not the same as the theoretical ones. Due to the modal coupling, it is difficult, if not impossible, to exactly find the nodal lines of these modes experimentally. As a result, the response measured by each detector is predominantly due to the mode that was intended to be measured, but each measurement includes some components from both the (3,2) and (4,1) modes.

Both the signal input to the loudspeakers and the signal received from the vibration detector were recorded on a MASSCOMP computer. The frequency of the sine wave of

the excitation signal was extracted from the former and the amplitude of the plate's vibration was computed from the latter.

## Calculation of the Slowly Varying Amplitude and Frequency

In order to calculate the slowly varying amplitude and frequency of a signal the signals were first bandpass filtered in a region around the frequency of excitation. This was to remove any higher or lower harmonic response, so that the response at frequencies close to the excitation frequency could be examined. The amplitude of this signal should then closely match the slowly varying amplitude predicted by the theory. The instantaneous amplitude and frequency were calculated by using Hilbert transform techniques (Oppenheim and Schafer, 1975). A digital filter was designed to emulate a Hilbert transformer, i.e., it turns cosine waves into sine waves of the same frequency and amplitude, and so $x(n\Delta)$, the sampled time history, becomes $\hat{x}(n\Delta)$. The amplitude is then calculated by using:

$$\sqrt{x(n\Delta)^2 + \hat{x}(n\Delta)^2},$$ and the frequency by using:

$\frac{d}{dt} \tan^{-1} \frac{\hat{x}(n\Delta)}{x(n\Delta)}$, where the $\frac{d}{dt}$ operation is implemented by using a digital filter that behaves as a differentiator.

When the "quasi-stationary" tests are run, the MASSCOMP is programmed to continually repeat this calculation on sequential 1024 point segments. The amplitude is generated from the response and the frequency is generated from the signal input into the loudspeaker array. The average amplitude of the response over a 1024 point segment is calculated and stored with the calculated average frequency. When this is completed, the next set of 1024 points are acquired and the calculations are repeated. Since the sweep is sufficiently slow (sweep rate is 0.01 Hz/sec), very little information is lost by sampling the response in this manner. When the faster sweeps are done, the entire response is measured and processed at one time, giving a *continuous* estimate of the instantaneous response amplitude and excitation frequency.

## RESULTS OF EXPERIMENTS

In all the experiments, described below, the plate was excited at a single frequency and allowed to reach its steady state before the frequency was varied. In tests where the frequency was swept up and then down, the excitation was kept stationary at the upper frequency for a period of time before starting the sweep down, to allow the plate to reach steady state again. The experimentally obtained results are compared with theoretical results obtained from numerical simulations of the averaged equations (6).

The nonuniformities in tension and boundary conditions mentioned above in made it impossible to obtain an exact comparison between theoretical and experimental amplitudes. Therefore, no numerical values are shown on any of the amplitude scales below. Multiple experimentally obtained plots shown together for the purposes of comparison are plotted on the same amplitude scale, as noted below.

## Experiment 1: Single Mode Response to "Quasi-Stationary" Excitation

In order to approximate the experimental system response to stationary excitation in a range of frequencies, the plate was subjected to a swept sine wave of constant amplitude and very slowly varying frequency. The sensor was located over an anti-node of the (1,2) mode shape and the loudspeakers configured to drive this mode. A plot of output amplitude versus input frequency, as the sine wave input frequency is varied in the range of the linear natural frequency, is shown in figure 6. The rate of change of the input frequency is 0.01 Hz per second. A theoretically predicted response to a stationary excitation, for a comparable range of frequencies in the region around the (2,2) mode of a simply supported plate, is shown in figure 7; computational limitations prevented the generation of the theoretical "quasi-stationary" response from equations (6) at this sweep rate. This mode has a natural frequency and damping ratio comparable to the experimental (1,2) mode and the input amplitude and sweep rate are set equal to those used in the experiment. The frequency axis of this plot has been scaled to correspond to the measured frequencies. The frequencies at which the output amplitude jumps from one solution branch, for both increasing and decreasing frequency, are well above the linear natural frequency of 145 Hz and similar behavior is observed in the simulated and the experimentally obtained data.

## Experiment 2: Single Mode Response to Nonstationary Excitation

In order to examine the single mode response of the plate to nonstationary excitation, the experimental setup was configured as follows. The sensor was positioned over an anti-node of the (1,2) mode shape, the loudspeakers configured to drive this mode, and the plate was subjected to a sine wave excitation. The amplitude of excitation remained constant and the frequency swept up through the linear natural frequency (138.0 Hz) at the rate of 8.4 Hz per second and then swept down at the same rate. The experimental result for low amplitude excitation is shown in figure 8 and the corresponding theoretical result of the response of the (2,2) mode is shown in figure 9. There is good agreement between the behavior of the experimental and simulated responses. The experimental system appears to have some nonlinear response characteristics; the maximum amplitude on the sweep up is higher than the maximum amplitude on the sweep down. This amplitude difference could be attributed to the fact that the simulation excitation amplitude and the experimental excitation amplitude were not exactly matched, and also due to the fact that the coefficients of the nonlinear terms in the equations are not correct for the experimental plate.

Under the same experimental conditions, figure 10 was generated from data recorded when the amplitude of excitation was increased by a factor of 60. The corresponding theoretically predicted response is shown in figure 11. The experimental results clearly show the expected jump phenomena and, once again, agree well with the expected response shown in the simulated response amplitude plot.
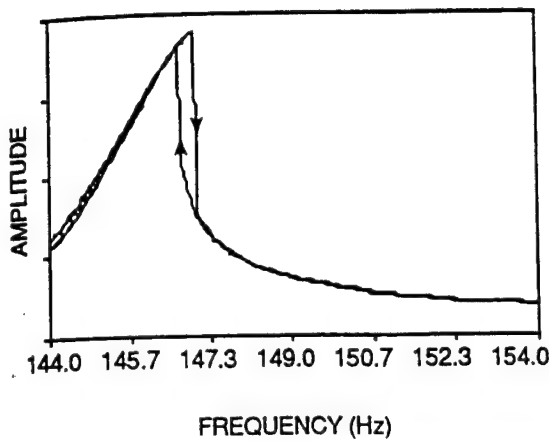
FIGURE 6. EXPERIMENTAL RESPONSE OF PLATE TO
"QUASI-STATIONARY" EXCITATION OF SINGLE MODE:
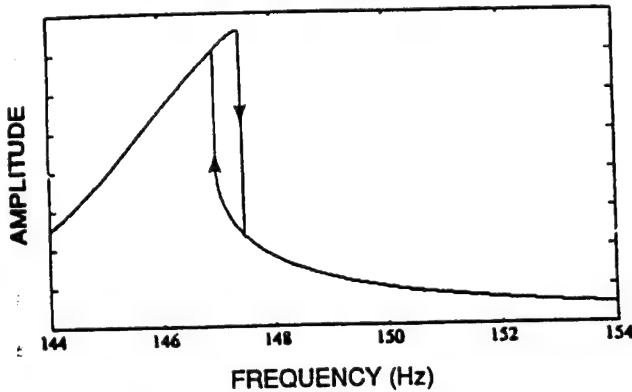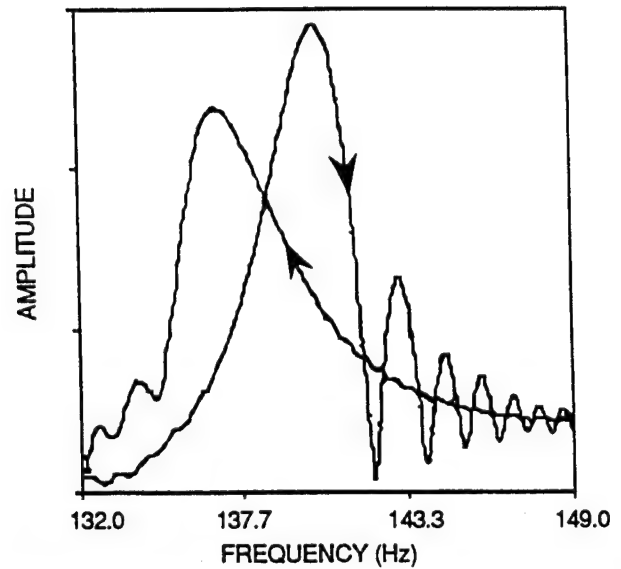→ = FREQUENCY SWEEP UP,
← = FREQUENCY SWEEP DOWN



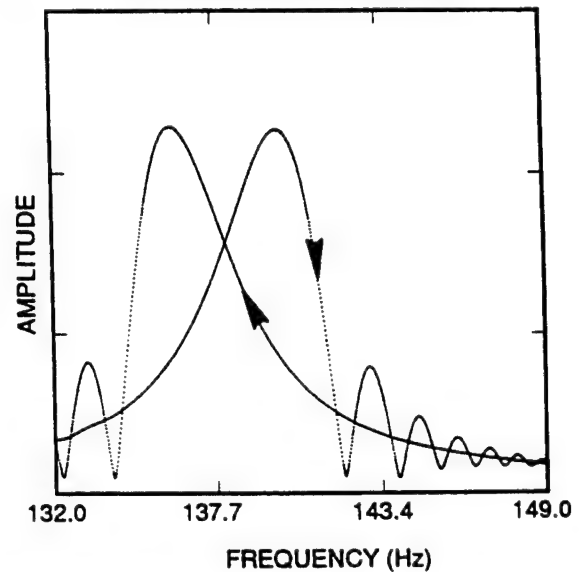FIGURE 7. THEORETICAL RESPONSE OF PLATE TO
STATIONARY EXCITATION OF SINGLE MODE

## Experiment 3: Response of Nearly Coincident Modes to "Quasi-Stationary" Excitation

In order to examine the response, to nonstationary excitation, of the modes of the plate with nearly coincident natural frequencies, two sensors were placed above the plate, one located at, or close to, a nodal line of the (4,1) mode and one near a nodal line of the (3,2) mode. The loudspeakers were configured to drive the (3,2) mode and the plate was subjected to a sine wave excitation. The amplitude of excitation remained constant and the frequency swept through the linear natural frequencies of the two modes (171.0 and 175.5 Hz) at the rate of 0.01 Hz per second. In figure 12 is the shown the measured response amplitudes at the two sensor locations. Again computational constraints meant that we could not simulate this response from the averaged equations. To examine the possible stationary solutions that exist in a frequency region where coupled modes can interact, the time derivatives in equation (6) were set to zero and the possible



FIGURE 8. EXPERIMENTAL RESPONSE OF PLATE TO
LOW AMPLITUDE NONSTATIONARY EXCITATION OF
SINGLE MODE: → = FREQUENCY SWEEP UP,
← = FREQUENCY SWEEP DOWN



FIGURE 9. THEORETICAL RESPONSE OF PLATE TO
LOW AMPLITUDE NONSTATIONARY EXCITATION OF
SINGLE MODE: → = FREQUENCY SWEEP UP,
← = FREQUENCY SWEEP DOWN

solutions for the steady state amplitudes of the two modes calculated. Here the two natural frequencies were detuned, as they are in the experimental plate. While we attempted to drive only the (3,2) mode of the plate, it is possible that the (4,1) mode of the plate is also excited at a very low level. The stationary response curves were therefore generated for an excitation amplitudes: $Q_1 = 10$ and
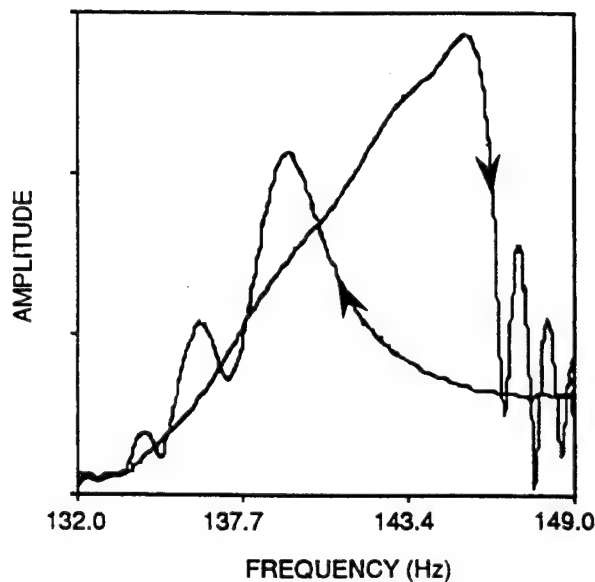
FIGURE 10. EXPERIMENTAL RESPONSE OF PLATE
TO HIGH AMPLITUDE NONSTATIONARY EXCITATION
OF SINGLE MODE: → = FREQUENCY SWEEP UP,
← = FREQUENCY SWEEP DOWN

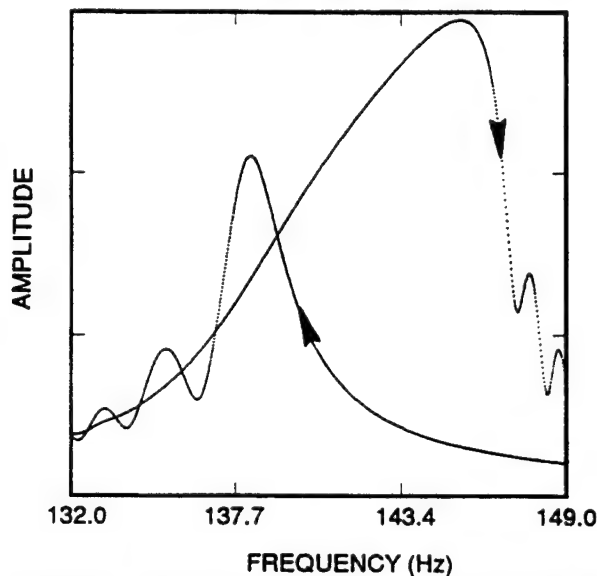

FIGURE 11. THEORETICAL RESPONSE OF PLATE TO
HIGH AMPLITUDE NONSTATIONARY EXCITATION OF
SINGLE MODE: → = FREQUENCY SWEEP UP,
← = FREQUENCY SWEEP DOWN

$Q_2 = 0.1$, $p_1 = 3.416$ rad/sec and $p_2 = 3.416$ rad/sec (normalized values) and a damping ratio of 0.002. These response curves are shown in figure 13.

The experimental and theoretical plots show agreement in the general trend of the responses. During the sweep up, at 169.5 Hz, the (3,2) mode response shows the same jump,
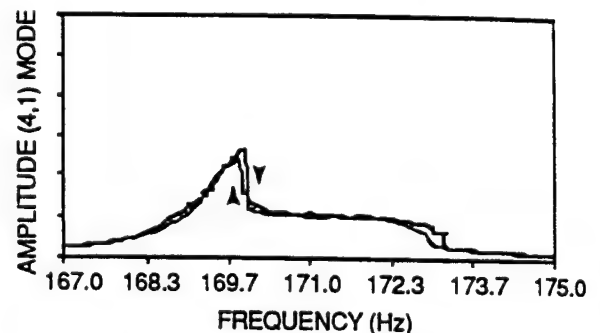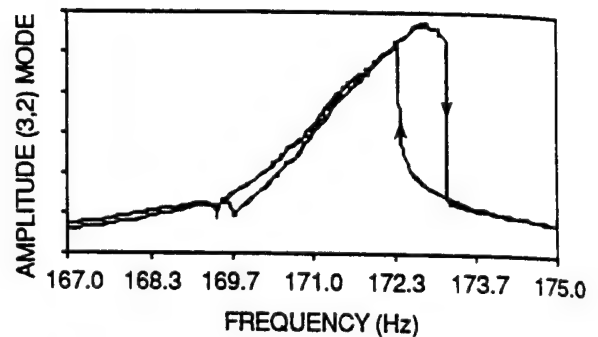




FIGURE 12. EXPERIMENTAL "QUASI-STATIONARY"
RESPONSE OF THE (3,2) AND (4,1) MODES DRIVEN
WITH THE LOUDSPEAKERS IN THE (3,2) MODE
CONFIGURATION: → = FREQUENCY SWEEP UP
← = FREQUENCY SWEEP DOWN

from one stable solution branch to another, as can be seen at 4.25 rad/sec in figure 13, (1,2) mode. At this same frequency the mode that was not being excited jumps from a higher branch to a lower in both the theoretical and the experimental results. At 173.0 Hz in the experimental excitation, the (3,2) mode undergoes a much larger jump that corresponds to the transition at 5.25 rad/sec in the theoretical plot. The low frequency jump occurs at a slightly different frequency during the downward sweep. This frequency shift could be an effect of the nonstationary input.

### Experiment 4: Response of Nearly Coincident Modes to Nonstationary Excitation

In order to observe the nearly coincident mode responses to nonstationary excitation the sensors and loudspeakers were configured as in Experiment 3. The plate was subjected to a similar excitation as above except the sine wave frequency sweep rate was 8.4 Hz. per second and the amplitude was turned down to a low level. The experimental results, for both the (3,2) mode and the (4,1) mode, are shown in figures 14. The amplitude scale is the same on both graphs shown. Similarly obtained experimental results, where the amplitude of excitation was increased by a factor of 60, are shown in figure 15.

In the first simulation conducted, the direct excitation of the second mode ($Q_2$) was set to zero, to correspond to driving the (3,2) mode only in the experiment. The
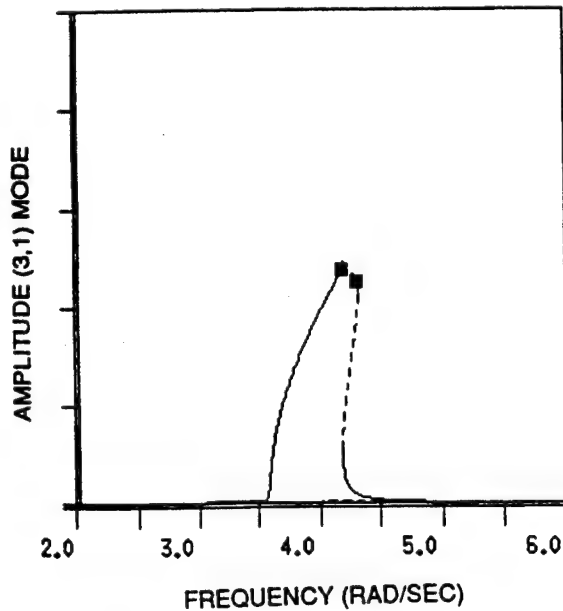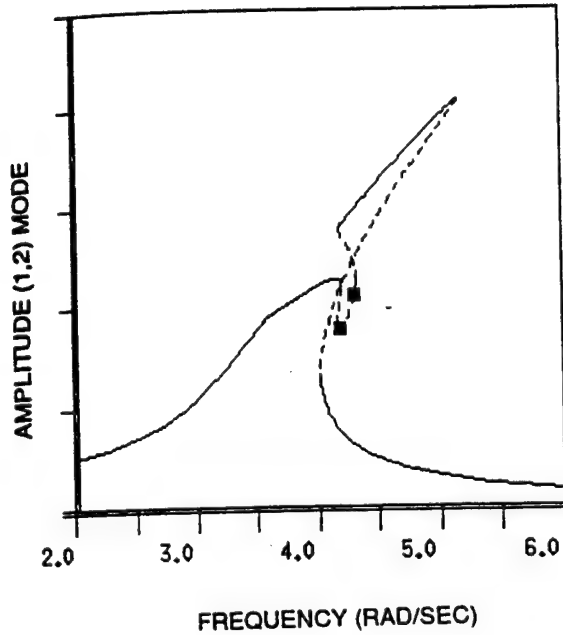
FIGURE 13. THEORETICAL STATIONARY RESPONSE OF
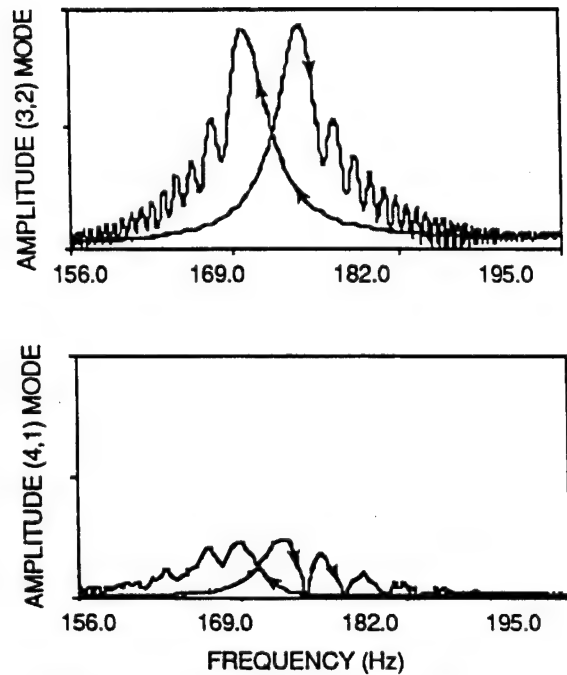THE COUPLED (1,2) AND (3,1) MODES



FIGURE 14. EXPERIMENTAL RESPONSE OF PLATE TO
LOW AMPLITUDE NONSTATIONARY EXCITATION OF
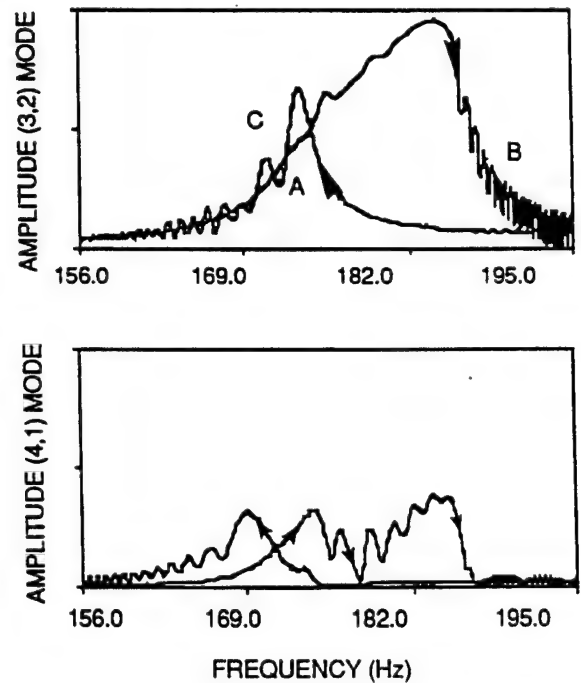NEARLY COINCIDENT MODES: → = FREQUENCY
SWEEP UP, ← = FREQUENCY SWEEP DOWN



FIGURE 15. EXPERIMENTAL RESPONSE OF PLATE TO
HIGH AMPLITUDE NONSTATIONARY EXCITATION OF
COUPLED MODE: → = FREQUENCY SWEEP UP,
← = FREQUENCY SWEEP DOWN

simulated response of the second mode was zero everywhere
and the driven mode followed the single mode response. In
order to investigate what would happen if the second mode
was excited at a low amplitude (compared to the first mode)
the simulation was repeated. The amplitude of the response
of the first mode, generated in several simulations where the
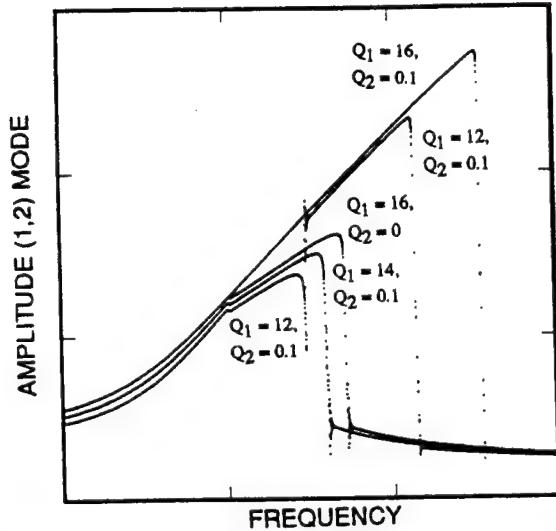
FIGURE 16. THEORETICAL RESPONSE OF (1,2) MODE OF PLATE TO NONSTATIONARY EXCITATION OF COUPLED MODE (DIFFERENT EXCITATION LEVELS)



FIGURE 17A. THEORETICAL COUPLED MODE RESPONSE OF (1,2) MODE TO HIGH AMPLITUDE NONSTATIONARY EXCITATION OF COUPLED MODES

values of $Q_1$ and $Q_2$ were varied, are shown in figure 16. It is interesting to note that the first mode response follows the coupled mode solution even at very low levels of second mode direct excitation. Coupled mode responses similar to these were observed in the experiment (figure 15). In figures 17a and 17b are shown the simulated amplitude of the response of the two modes to nonstationary excitation, sweeping up and down, respectively, through the frequency region around the two modes. In comparing figures 15 and 17a note the similarity in response: at points A , the change in the gradient of the up sweep amplitude; at points B, the high frequency behavior after the sweep up through the jump region; and at points C, the lower frequency behavior after the sweep down through the jump region. The parameter values used in the simulation were: $Q_1 = 10$ and $Q_2 = 0.1$, $p_1 = 4.3472$ rad/sec and $p_2 = 4.3205$ rad/sec (normalized values) and the damping ratio was set to 0.002.

## CONCLUSIONS

A series of experiments, run to examine the nonstationary response of a plate with coincident modes, are described in this paper. The amplitudes of the response of individual modes were measured. The results of the experiments were compared to the those generated from averaged equations derived from one and two mode approximations of the response of a plate, whose behavior is described by the von Karman plate equations. In the simulations the plate was assumed to be under uniform in-plane tension and the boundaries simply supported. With an aspect ratio of 1.633 this gave rise to the (1,2) and (3,1) modes having coincident natural frequencies. Due to nonuniformities in tension and boundary conditions, the experimental plate's (3,2) and (4,1) modes had nearly coincident natural frequencies. The simulations were of swept sine excitation of: (a) the (2,2) mode of the plate, which was well isolated from other modes, and (b) the coincident (1,2) and (3,1) modes. These were compared to
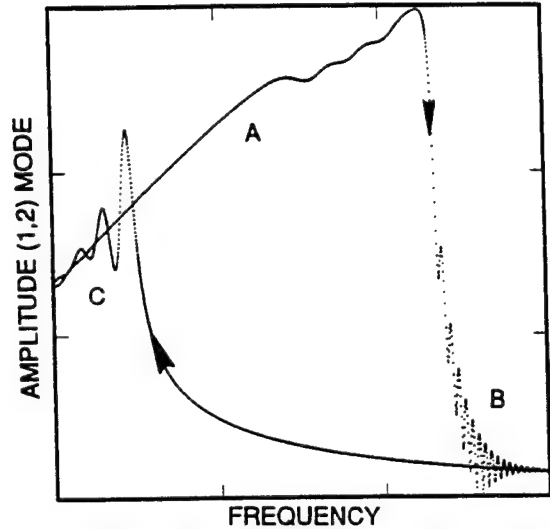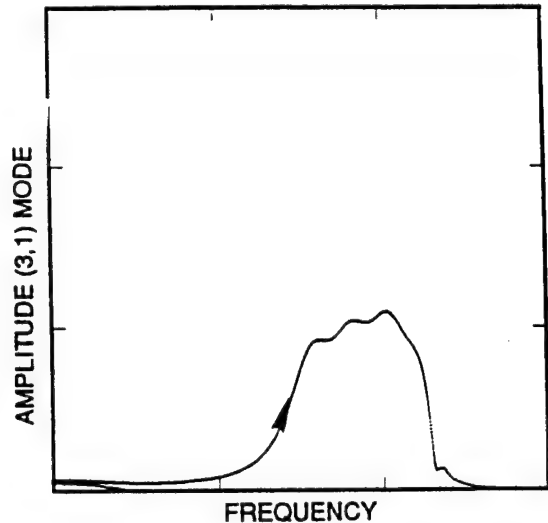


FIGURE 17B. THEORETICAL COUPLED MODE RESPONSE OF (3,1) MODE TO HIGH AMPLITUDE NONSTATIONARY EXCITATION OF COUPLED MODES

swept sine excitations of the experimental plate: (a) the (1,2) mode, which was well isolated from other modes, and (b) the nearly coincident (3,2) and (4,1) modes, respectively.

Practically, it is difficult to construct structures with the ideal boundary conditions assumed in the theoretical analysis. Non uniformities in tension, non-ideal boundary conditions and environmental changes all affect the behavior of the experimental structure. Despite these problems, many of the characteristic behavior patterns predicted by the *idealized* theory, were observed in the experiment. Of particular interest, was the case of sweeping through nearly coincident modes in an experimental configuration designed to excite only one of the modes.

Small levels of direct excitation of the second mode led to large differences in the nature of the response, producing coupled mode behavior. This was observed experimentally and also in the simulations.

Future work will consist of obtaining a theoretical model which more closely approximates the experimental situation. This will be achieved both by modifying the experimental setup to reduce the nonuniformities in plate tension and boundary conditions, as well as identify those nonuniformities which cannot be eliminated, and by adjusting the mathematical model to take into account those remaining nonuniformities.

## ACKNOWLEDGMENT

## REFERENCES

Chang, S. I., Bajaj, A. K., Krousgrill, C. M., 1993, "Nonlinear Vibrations and Chaos in Harmonically Excited Rectangular Plates with Internal Resonance," accepted for publication in *Nonlinear Dynamics*.

Evan-Iwanowski, R. M., 1976, *Resonance Oscillations in Mechanical Systems*, Elsevier, New York.

Ewins, D., 1985, *Modal Testing, Theory and Practice*, Bruel and Kjaer, Letchworth, England.

Guckenheimer, J. and Holmes, P. J., 1983, *Nonlinear Oscillations, Dynamical Systems and Bifurcations of Vector Fields*, Springer-Verlag, New York.

Hale, J. K., 1969, *Ordinary Differential Equations*, Wiley-Interscience, New York.

Nayfeh, A. H. and Mook, D. T., 1979, *Nonlinear Oscillations*, Wiley-Interscience, New York.

Oppenheim, A. V. and Schafer, R. W., 1975, *Digital Signal Processing*, Prentice-Hall International, London.

Raman, A., Bajaj, A. K. and Davies, P., 1993, "Analytical Prediction of Nonlinear System Response to Nonstationary Excitations", submitted to the Dynamics and Vibrations of Time-Varying Systems and Structures, at the 14th ASME Biennial Conference on Mechanical Vibration and Noise.

Randall, R. B., 1987, *Frequency Analysis*, Bruel and Kjaer, Denmark.

Yasuda, K. and Asano, T., 1986, "Nonlinear Forced Oscillations of a Rectangular Membrane With Degenerate Modes", *Bulletin of JSME 29*, pp. 3090-3095.

91

# APPENDIX 4

## Chaotic responses in two degree-of-freedom systems with 1:2 internal resonances

B. Banerjee, A. K. Bajaj

(accepted for publication).

# Chaotic Responses in Two Degree-of-Freedom Systems with 1:2 Internal Resonances

by

Bappaditya Banerjee
Anil K. Bajaj
School of Mechanical Engineering
Purdue University
West Lafayette, IN 47907-1288

Revised August 1994

1

**Abstract**

Dynamical systems with two degrees-of-freedom, with quadratic nonlinearities and harmonic external excitations are studied in this analysis. The 1:2 subharmonic internal resonance case is analyzed. Under resonant forcing conditions, the method of averaging is used to obtain a set of four first-order amplitude equations that govern the first-order approximation of the response. An analytical technique, based on Melnikov's method is used to predict the parameter range for which chaotic dynamics exists in the undamped averaged system. Numerical studies show that chaotic responses are quite common in these quadratic systems and chaotic responses occur even in presence of damping.

# 1 Introduction

Dynamical systems with two degrees-of-freedom often have quadratic terms in their equations of motion. These nonlinearities arise due to inertial effects of large motions, and due to the phenomena associated with centrifugal and coriolis forces [Sethna, 1965]. Interesting response of the systems is observed when the two modes of vibration of the system get coupled through the quadratic nonlinear terms. This situation arises when the linear natural frequencies of the system are in the ratios 1:2 or 2:1. This effect is called an internal resonance. In these systems with internal resonances, complicated motions are observed when the frequency of external excitation is close to one of the linear natural frequencies of the system.

In the present work , we study systems with subharmonic 1:2 internal resonance. The frequency of the first mode of vibration is taken close to 1, the normalized frequency of excitation, and that of the second mode, close to $\frac{1}{2}$. The method of averaging [Murdock, 1991; Wiggins, 1990] is used to reduce the nonautonomous system to an autonomous system. The autonomous system captures the essential dynamics of the original system for sufficiently small motions near resonance. Fixed points of the averaged system correspond to periodic solutions of the original system and periodic solutions of the averaged system imply periodically amplitude-modulated motions for the original system. Chaotic solutions of the averaged equations imply chaotic amplitude-modulated responses for the original system.

2

Extensive local analysis of the averaged equations for quadratic systems with internal resonances has been carried out by Sethna [1965] and Bajaj et al. [1993]. They found that even when only one oscillator is excited, the response can consist of nontrivial periodic motions for both the oscillators and this coupled-mode response can undergo Hopf bifurcations to amplitude-modulated motions. These motions can further undergo a torus doubling cascade to chaotic amplitude-modulated solutions. Tien et al. [1994] also studied these equations for 1:2 internal resonance in the context of a shallow arch.

For the undamped averaged system, we use an extension of Melnikov's method, developed for autonomous Hamiltonian systems by Holmes and Marsden [1982], and presented in considerable detail in Wiggins [1988], to analytically predict the parameter range for which chaos exists in the system. Numerical studies are then carried out to investigate the effects of damping and of increasing the amplitude of excitation to the system. An Autoparametric vibratory system [Bajaj et al. , 1993;Haxton and Barr, 1972] is finally discussed as an example of a system with quadratic nonlinearities. It is shown that through some scale changes, one can reduce the autoparametric system exactly to the form of quadratic systems being analyzed here.

## 2  Equations of Motion

Consider a holonomic dynamical system with two degrees-of-freedom in general normalized coordinates $\zeta_i$, i=1,2. The coordinates are chosen to be dimensionless and equal to zero when the system is in stable static equilibrium position. The system is assumed to have linear velocity proportional damping. The equations of motion can be then written as

$$
\begin{aligned}
\ddot{\zeta}_1 + C_1\dot{\zeta}_1 + \omega_1^2\zeta_1 + \bar{Q}_1(\zeta_1,\dot{\zeta}_1,\zeta_2,\dot{\zeta}_2) &= \bar{F}_1\cos t, \\
\ddot{\zeta}_2 + C_3\dot{\zeta}_2 + \omega_2^2\zeta_2 + \bar{Q}_2(\zeta_1,\dot{\zeta}_1,\zeta_2,\dot{\zeta}_2) &= \bar{F}_2\cos t,
\end{aligned}
\tag{1}
$$

where $C_i$ are the coefficients of damping; $\omega_i$ are the linear natural frequencies of the two oscillators; $\bar{F}_i\cos t$ are the external harmonic excitations with frequencies normalized to 1; $\bar{Q}_i$ are the quadratic nonlinear effects dependent on the generalized coordinates and velocities. Also, the dot over $\zeta_i$ denotes the derivative of $\zeta_i$ with respect to the time t.

3

We analyze the motions in the neighborhood of the static equilibrium position. To obtain interesting response at the first-order approximation we introduce an arbitrary small parameter $\epsilon$ with $0 < \epsilon \ll 1$ and choose the linear damping forces to be of the same order in $\epsilon$, as the nonlinear quadratic terms retained in the analysis, that is, $C_1 = \epsilon C_2$, $C_3 = \epsilon C_4$, $\bar{Q}_1 = \epsilon Q_1$, $\bar{Q}_2 = \epsilon Q_2$. Furthermore, we let $\bar{F}_1 = \epsilon F_1$ and $\bar{F}_2 = \epsilon F_2$. For 1:2 subharmonic resonance, we choose $\omega_1^2 = 1 + 2\epsilon\sigma_1$ and $\omega_2^2 = \frac{1}{4} + \epsilon\sigma_2$ , where $\sigma_1$ and $\sigma_2$ are the mistuning parameters. They characterize the differences between the excitation and the two natural frequencies $\omega_1$ and $\omega_2$. The equations of motion now become

$$\ddot{\zeta}_1 + \dot{\zeta}_1 = \epsilon[-Q_1 + F_1 \cos t - 2\sigma_1\zeta_1 - C_2\dot{\zeta}_1],$$
$$\ddot{\zeta}_2 + \frac{1}{4}\dot{\zeta}_2 = \epsilon[-Q_2 + F_2 \cos t - \sigma_2\zeta_2 - C_4\dot{\zeta}_2], \qquad (2)$$

where $Q_1$ and $Q_2$ can be written out as

$$Q_1(\zeta_1, \dot{\zeta}_1, \zeta_2, \dot{\zeta}_2) = a_{11}\zeta_1^2 + a_{13}\zeta_1\zeta_2 + a_{22}\dot{\zeta}_1^2 + a_{24}\dot{\zeta}_1\dot{\zeta}_2 + a_{33}\zeta_2^2 + a_{44}\dot{\zeta}_2^2,$$
$$Q_2(\zeta_1, \dot{\zeta}_1, \zeta_2, \dot{\zeta}_2) = b_{11}\zeta_1^2 + b_{13}\zeta_1\zeta_2 + b_{22}\dot{\zeta}_1^2 + b_{24}\dot{\zeta}_1\dot{\zeta}_2 + b_{33}\zeta_2^2 + b_{44}\dot{\zeta}_2^2. \quad (3)$$

If we let $\underline{z} = [\ z_1, z_2, z_3, z_4]^T = [\zeta_1, \dot{\zeta}_1, \zeta_2, \dot{\zeta}_2]^T$ , the equations of motion (2) can be written as

$$\dot{\underline{z}} = \underline{A}\,\underline{z} + \epsilon\underline{h}_1(\underline{z}, t), \qquad (4)$$

where

$$\underline{A} = \begin{bmatrix} 0 & 1 & 0 & 0 \\ -1 & 0 & 0 & 0 \\ 0 & 0 & 0 & 1 \\ 0 & 0 & -\frac{1}{4} & 0 \end{bmatrix}, \qquad (5)$$

and

$$\underline{h}_1 = \begin{bmatrix} 0 \\ -Q_1(z_1, z_2, z_3, z_4) + F_1 \cos t - 2\sigma_1 z_1 - C_2 z_2 \\ 0 \\ -Q_2(z_1, z_2, z_3, z_4) + F_2 \cos t - \sigma_2 z_2 - C_4 z_4 \end{bmatrix}. \qquad (6)$$

4

Let $\underline{\phi}$ be a fundamental matrix solution of (4), with $\epsilon = 0$. Then choosing $\underline{\phi}$ as a variation of parameter transformation, that is $\underline{z} = \underline{\phi}\underline{u}$, where $\underline{u} = [u_1, u_2, u_3, u_4]^T$, the equation (4) reduces to the standard form for averaging

$$\underline{\dot{u}} = \epsilon \underline{X}_1(\underline{u}, t). \tag{7}$$

Now, let $\underline{X}_1 = M_n[\underline{X}_1] + O_s[\underline{X}_1]$, where the two terms on the right hand side are the mean part of $\underline{X}_1$, $M_n[\underline{X}_1] = \lim_{T\to\infty} \frac{1}{T}\int_0^T \underline{X}_1(\underline{u}_1, \tau)d\tau$ and the oscillatory part of $\underline{X}_1$, $O_s[\underline{X}_1] = \underline{X}_1 - M_n[\underline{X}_1]$. Using the near identity transformation

$$\underline{u} = \underline{x} + \epsilon \underline{w}_1(\underline{x}, t) + O(\epsilon^2), \tag{8}$$

in equation (7), where $\underline{x} = [x_1, y_1, x_2, y_2]^T$, we obtain the first-order averaged equations

$$\underline{x}' = M_n[\underline{X}_1]. \tag{9}$$

The prime $(')$ here denotes the derivative with respect to the slow time $\tau = \epsilon t$. Using the scalings $x_1 = \alpha \bar{x}_1$, $y_1 = \alpha \bar{y}_1$, $x_2 = \beta \bar{x}_2$, $y_2 = \beta \bar{y}_2$, $F_1 = \alpha \bar{F}_1$, $C_2 = 2\bar{\xi}_1$, $C_4 = 2\bar{\xi}_2$ and

$$\alpha = \frac{1}{B} \ , \ \beta = \sqrt{\frac{2}{AB}}, \tag{10}$$

where

$$A = (a_{33} - a_{44}/4)/2 \ , \ B = (b_{13} + b_{24}/2)/2, \tag{11}$$

the equations (9) reduce to

$$
\begin{aligned}
x_1' &= -\bar{\xi}_1 x_1 + \sigma_1 y_1 + 2x_2 y_2, \\
y_1' &= \frac{\hat{F}}{2} - \sigma_1 x_1 + (y_2^2 - x_2^2) - \bar{\xi}_1 y_1, \\
x_2' &= -\bar{\xi}_2 x_2 + \frac{1}{2}(x_2 y_1 - x_1 y_2) + \sigma_2 y_2, \\
y_2' &= -\sigma_2 x_2 - \frac{1}{2}(x_1 x_2 + y_1 y_2) - \bar{\xi}_2 y_2,
\end{aligned}
\tag{12}
$$

where the variables $\{\bar{x}_1, \bar{y}_1, \bar{x}_2, \bar{y}_2, \bar{F}_1\}$ have been replaced by $\{x_1, y_1, x_2, y_2, \hat{F}\}$. Using the following transformation to polar coordinates

$$x_1 = a_1 \cos\beta_1 \ , \ y_1 = -a_1 \sin\beta_1 \ , \ x_2 = a_2 \cos\beta_2 \ , \ y_2 = -a_2 \sin\beta_2, \tag{13}$$

5

the equations (12) become

$$\dot{a}_1 = -\bar{\xi}_1 a_1 - \frac{\hat{F}}{2}\sin\beta_1 + a_2^2\sin(\beta_1 - 2\beta_2),$$

$$a_1\dot{\beta}_1 = \sigma_1 a_1 - \frac{\hat{F}}{2}\cos\beta_1 + a_2^2\cos(\beta_1 - 2\beta_2),$$

$$\dot{a}_2 = -\bar{\xi}_2 a_2 - \frac{a_1 a_2}{2}\sin(\beta_1 - 2\beta_2),$$

$$a_2\dot{\beta}_2 = \sigma_2 a_2 + \frac{a_1 a_2}{2}\cos(\beta_1 - 2\beta_2). \tag{14}$$

Equations (12) and (14) are the desired averaged equations for the general system with 1:2 subharmonic resonance and are valid for any two degree-of-freedom system with quadratic nonlinearities. They have been extensively studied for their equilibrium solutions and bifurcations therefrom, as indicated in the introduction. In the following section, we review these results for completeness.

# 3 Local Analysis

From equations (14) the steady state constant solutions for which $a_2 = 0$, that is, the single-mode solutions, can be obtained as

$$a_1 = \frac{\hat{F}}{2\sqrt{\bar{\xi}_1^2 + \sigma_1^2}} \;,\; \tan\beta_1 = -\frac{\bar{\xi}_1}{\sigma_1}. \tag{15}$$

The steady state constant solutions for which $a_1 \neq 0$ and $a_2 \neq 0$, are the coupled-mode solutions. They are given by

$$a_1 = 2\sqrt{\bar{\xi}_2^2 + \sigma_2^2} \tag{16}$$

and $a_2$ is obtained as a root of the following quadratic in $a_2^2$

$$a_2^4 + 4(\bar{\xi}_1\bar{\xi}_2 - \sigma_1\sigma_2)a_2^2 + 4(\bar{\xi}_1^2 + \sigma_1^2)(\bar{\xi}_2^2 + \sigma_2^2) - \frac{\hat{F}^2}{4} = 0, \tag{17}$$

which has real solutions only for $\hat{F}^2 \geq 16(\bar{\xi}_1\sigma_2 + \bar{\xi}_2\sigma_1)^2$ . The eigenvalues for the Jacobian of the averaged system in equation (12) for the single-mode

solution $(a_1 \neq 0, a_2 = 0)$ are determined by

$$(\lambda^2 + 2\bar{\xi}_1\lambda + \sigma_1^2 + \bar{\xi}_1^2)(\lambda^2 + 2\bar{\xi}_2\lambda + \sigma_2^2 + \bar{\xi}_2^2 - \frac{a_1^2}{4}) = 0, \qquad (18)$$

where $\lambda$ is an eigenvalue. It is seen that no $\lambda$ can become imaginary for the damped system $(\bar{\xi}_1 \neq 0, \bar{\xi}_2 \neq 0)$, and therefore, no Hopf bifurcations can arise from the single-mode steady state solutions.

The eigenvalues of the Jacobian for the coupled-mode solutions $(a_1 \neq 0, a_2 \neq 0)$ satisfy the following equation

$$J_4\lambda^4 + J_3\lambda^3 + J_2\lambda^2 + J_1\lambda + J_0 = 0, \qquad (19)$$

where

$$
\begin{aligned}
J_0 &= 2a_2^2(\bar{\xi}_1\bar{\xi}_2 - \sigma_1\sigma_2 + \frac{a_2^2}{2}), \\
J_1 &= (2\bar{\xi}_2\bar{\xi}_1^2 + 2\bar{\xi}_2\sigma_1^2 + 2(\bar{\xi}_1 + \bar{\xi}_2)a_2^2), \\
J_2 &= (\bar{\xi}_1^2 + 4\bar{\xi}_1\bar{\xi}_2 + \sigma_1^2 + 2a_2^2), \\
J_3 &= 2(\bar{\xi}_1 + \bar{\xi}_2), \\
J_4 &= 1, \qquad\qquad\qquad\qquad\qquad\qquad (20)
\end{aligned}
$$

and $a_1$ and $a_2$ are obtained from equations (16) and (17). Using the Routh-Hurwitz criterion [Sethna, 1965; Sethna and Bajaj, 1978] , it can be shown that for the case when $\sigma_1\sigma_2 - \bar{\xi}_1\bar{\xi}_2 < 0$, the coupled mode solution has a complex conjugate pure imaginary pair of eigenvalues for parameter combinations determined by

$$J_1(J_2J_3 - J_1J_4) - J_0J_3^2 = 0. \qquad (21)$$

This condition corresponds to the loss of stability by a Hopf bifurcation, which may then lead to a period doubling transition of the limit cycles, and finally to chaos in the averaged equations.

The Hopf bifurcation set in equation (21) is given by

$$\bar{\xi}_1\bar{\xi}_2(\bar{\xi}_1^2 + \sigma_1^2)(\bar{\xi}_1^2 + 4\bar{\xi}_1\bar{\xi}_2 + 4\bar{\xi}_2^2 + \sigma_1^2) + (\bar{\xi}_1 + \bar{\xi}_2)^2 a_2^2[\bar{\xi}_1^2 + \sigma_1^2 + 2\sigma_1\sigma_2 + 2\bar{\xi}_1\bar{\xi}_2] = 0. \qquad (22)$$

7

It is shown in Bajaj et al. [1993], that for $\bar{\xi}_1 = \bar{\xi}_2 > 0.214$, no Hopf bifurcations arise. Furthermore, for $\bar{\xi}_1, \bar{\xi}_2 > 0$, the equation (22) is satisfied only for $\sigma_1 \sigma_2 < 0$. Using AUTO, a numerical simulation package [Doedel, 1986] the response curves in figure (1) were obtained. Here, the single-mode and the coupled-mode solutions are shown with respect to the mistuning $\sigma_1$, for $\sigma_2 = 0.66$. The dark squares in the figure indicate Hopf bifurcation points. The coupled-mode solutions are known to bifurcate to limit cycle motions. Over the region $-0.2925 < \sigma_1 < -0.1489$ (for $\sigma_2 = 0.66$, $\bar{\xi}_1 = 0.10$, $\bar{\xi}_2 = 0.10$), that is, between the two Hopf points, the limit cycle solutions are known to undergo period doubling bifurcation to chaos [Bajaj et al., 1993].

The main objective of the next section is to analytically find the existence of chaotic motions for the averaged system using some global perturbation techniques.

# 4    Melnikov's Method

Melnikov's method is a global perturbation technique that allows one to analytically obtain the parameter range for which chaotic dynamics exists for a class of systems. The underlying theme of Melnikov's idea is to consider an unperturbed Hamiltonian system, having a hyperbolic fixed point connected to itself by a homoclinic orbit. On perturbing this system with time periodic perturbations (not necessarily Hamiltonian), the hyperbolic fixed point becomes a hyperbolic periodic orbit, whose stable and unstable manifolds may intersect transversely, giving rise to Smale horseshoes and hence complex invariant sets. The distance between the stable and the unstable manifolds can be calculated using the Melnikov function or Melnikov Integral. The parameter values for which the Melnikov function has simple zeroes, as a function of initial time, gives the desired parameter regions.

The analysis here uses a generalized version of the Melnikov's method, which is applicable to autonomous multi degree-of-freedom systems [Holmes and Marsden, 1982; Wiggins, 1988]. It was applied by Feng and Sethna [1990] to the averaged equations for parametrically excited coupled oscillators with 1:1 internal resonance, and by Tien et al. [1994] to the averaged equations governing the dynamics of a shallow arch with 1:2 internal resonance in the interacting modes. The development here closely follows the work of Tien et al. [1994].

8

There are several distinct steps in this analysis. First, the averaged system is transformed into a Hamiltonian form using canonical transformations. Then, the hyperbolic fixed points and the homoclinic and heteroclinic orbits of the unperturbed system $(\delta = 0)$ are found. Explicit expressions for these orbits are written as a function of time. Using a theorem in [Wiggins, 1988] the Melnikov function can be then evaluated. This analysis holds only for the undamped case of the averaged equations (14), which, as shown below, form a Hamiltonian system.

## 4.1  Canonical Transformations

The undamped averaged equations (14) are first transformed from the polar variables to Action - Angle form using the transformations $a_1 = \sqrt{2I_1}$ and $a_2 = \sqrt{2I_2}$. Subsequent canonical transformations $P_1 = I_1/2$, $Q_1 = \beta_1 - 2\beta_2$, $P_2 = I_1 + 2I_2$, and $Q_2 = \beta_2$, and the substitutions $\mu = \sigma_1 - 2\sigma_2$ and $\hat{F} = \delta\bar{F}_0$, result in the Hamiltonian system

$$
\begin{aligned}
P_1' &= \sqrt{P_1(P_2 - 2P_1)}\sin Q_1 - \delta\frac{\bar{F}_0\sqrt{P_1}}{2}\sin(Q_1 + 2Q_2), \\
Q_1' &= \mu + \frac{1}{\sqrt{P_1}}\left(\frac{P_2}{2} - 3P_1\right)\cos Q_1 - \delta\frac{\bar{F}_0}{4\sqrt{P_1}}\cos(Q_1 + 2Q_2), \\
P_2' &= -\delta\bar{F}_0\sqrt{P_1}\sin(Q_1 + 2Q_2), \\
Q_2' &= \sigma_2 + \sqrt{P_1}\cos Q_1,
\end{aligned}
\tag{23}
$$

where $\delta$ is an arbitrary small parameter, $0 < \delta \ll 1$, reflecting on the smallness of the external excitation. The Hamiltonian for the above system is given by $H = H_0 + \delta H_1$ , where

$$
H_0 = \mu P_1 + 2\sqrt{P_1}\left(\frac{P_2}{2} - P_1\right)\cos Q_1 + P_2\sigma_2
\tag{24}
$$

is the unperturbed Hamiltonian and

$$
H_1 = -\frac{\bar{F}_0\sqrt{P_1}}{2}\cos(Q_1 + 2Q_2)
\tag{25}
$$

is the perturbation due to the external excitation. We first consider the geometry of the unperturbed system $(\delta = 0)$.

9

## 4.2 Fixed Points and Their Stability

The unperturbed Hamiltonian system is given by

$$
\begin{aligned}
P_1' &= 2\sqrt{P_1}(P_{20}-P_1)\sin Q_1, \\
Q_1' &= \mu + \frac{1}{\sqrt{P_1}}(P_{20}-3P_1)\cos Q_1, \\
P_2' &= 0, \\
Q_2' &= \sigma_2 + \sqrt{P_1}\cos Q_1.
\end{aligned}
\tag{26}
$$

Here, the dynamics in the $(P_1,Q_1)$ plane is decoupled from that in the $(P_2,Q_2)$ plane and $P_2$ is a cyclic variable. Since $P_2' = 0$, we have set $P_2 = 2P_{20}$ in equations (26). Also note that $P_2$ is a combination of the actions $I_1$ and $I_2$ of the averaged equations and thus $0 \le P_1 \le 2P_{20}$. Further, $Q_1$ is periodic and can be restricted to $0 \le Q_1 \le 2\pi$. The Jacobian for the unperturbed system in the $(P_1,Q_1)$ plane is

$$
Jac(P_1,Q_1) = \begin{bmatrix}
\frac{1}{\sqrt{P_1}}(P_{20}-3P_1)\sin Q_1 & 2\sqrt{P_1}(P_{20}-P_1)\cos Q_1 \\
\frac{-2}{P_1\sqrt{P_1}}(P_{20}+3P_1)\cos Q_1 & \frac{1}{\sqrt{P_1}}(3P_1-P_{20})\sin Q_1
\end{bmatrix}
\tag{27}
$$

and $S_s = Trace(Jac) = 0$,
$P_s = Det(Jac) = -9P_1 + 6P_{20} - \frac{P_{20}^2}{P_1} + (6P_1 - 4P_{20} + \frac{2P_{20}^2}{P_1})\cos^2 Q_1$.

The sign of $P_s$ determines the stability of the fixed points. They are saddles when $P_s < 0$ and centres when $P_s > 0$. It is seen from equations (26) that in the $(P_1,Q_1)$ plane, the equilibrium points are as follows :

$(P_{20},Q_1^*)$ and $(P_{20},2\pi - Q_1^*)$ are saddle points and $(P_1^{*+},0)$, $(P_1^{*+},2\pi)$ (note that this is actually the same as $(P_1^{*+},0)$), and $(P_1^{*-},\pi)$ are centres, where,

$$
Q_1^* = \cos^{-1}\left(\frac{\mu}{2\sqrt{P_{20}}}\right), \; and \; P_1 = P_{20}, for\, P_{20} \neq 0, Q_1^* \neq 0,\pi,
\tag{28}
$$

$$
P_1^{*+} = \frac{1}{18}\left[6P_{20} + \mu^2 + \mu\sqrt{12P_{20}+\mu^2}\right], \; and \; Q_1 = 0, for\, P_1^{*+} \neq 0, P_{20},
\tag{29}
$$

$$
P_1^{*-} = \frac{1}{18}\left[6P_{20} + \mu^2 - \mu\sqrt{12P_{20}+\mu^2}\right], \; and \; Q_1 = \pi, for\, P_1^{*-} \neq 0, P_{20}.
\tag{30}
$$

## 4.3 Heteroclinic Orbits

The orbits in the $(P_1, Q_1)$ plane (including heteroclinic orbits) are the level curves of the unperturbed Hamiltonian $H_0$ restricted to the plane. Thus, the orbits through the saddle points are defined by

$$H_0(P_{20}, Q_1^*) = H_0(P_1, Q_1). \tag{31}$$

(Note that $P_2 = 2P_{20}$). Solving equation (31) for $P_1$, we get

$$
\begin{array}{lll}
Orbit\,A_1: & P_1 & = \quad \frac{\mu^2}{4\cos^2 Q_1} \\
Orbit\,A_2: & P_1 & = \quad P_{20}.
\end{array}
\tag{32}
$$

We get the same orbits from $H_0(P_{20}, 2\pi - Q_1^*)$. To get the explicit form for $Q_1$ as a function of time $\tau$, we substitute the expressions from equation (32) for $P_1$ into the equation (26) for $Q_1{}'$ and integrate. Thus for orbit $A_1$, we get

$$Q_1' = (2P_{20} - \mu^2 + 2P_{20}\cos 2Q_1)/(2\mu). \tag{33}$$

On integrating, we obtain

$$Q_1^+(\tau) = \tan^{-1}\left[\frac{\sqrt{4P_{20} - \mu^2}}{\mu}\tanh\left(\frac{\sqrt{4P_{20} - \mu^2}}{2}\tau\right)\right], \tag{34}$$

where $0 < \mu < 2\sqrt{P_{20}}$ and the initial condition is $Q_1(\tau = 0) = 0$ , and

$$Q_1^-(\tau) = \tan^{-1}\left[\frac{\sqrt{4P_{20} - \mu^2}}{\mu}\tanh\left(\frac{\sqrt{4P_{20} - \mu^2}}{2}\tau\right)\right] + \pi, \tag{35}$$

where $-2\sqrt{P_{20}} < \mu < 0$ with initial condition $Q_1(\tau = 0) = \pi$.

The explicit expression of $P_1$, along the orbit $A_1$, is then given by

$$P_1(\tau) = \frac{\mu^2}{4} + \frac{4P_{20} - \mu^2}{4}\tanh^2\left(\frac{\sqrt{4P_{20} - \mu^2}}{2}\tau\right). \tag{36}$$

(Note from equation (32), the expression for orbit $A_2$, $P_1(\tau) = P_{20}$, a constant). And finally, to calculate $Q_2$ as a function of time $\tau$, we substitute the expressions for $Q_1^+(\tau)$ and $P_1(\tau)$ from equation (34) and equation (36) into the expression for $Q_2'$ to get

$$Q_2' = \sigma_2 + \frac{\mu}{2} = \frac{\sigma_1}{2} \tag{37}$$

11

since $\mu = \sigma_1 - 2\sigma_2$. On integrating, we obtain

$$Q_2(\tau) = \frac{\sigma_1 \tau}{2} + Q_{20} \tag{38}$$

where $Q_{20}$ is a constant obtained from initial conditions.

The structure of the geometry in the $(P_1, Q_1)$ space is seen in figure (2), where the phase portraits have been plotted for $\mu < 0$ ($\sigma_1 = 1, \sigma_2 = 0.66$) in figure (2a); $\mu = 0$ ($\sigma_1 = 1.32, \sigma_2 = 0.66$) in figure (2b) and $\mu > 0$ ($\sigma_1 = 1.5, \sigma_2 = 0.66$) in figure (2c).

## 4.4   Melnikov Function

Identifying the averaged equations (23) as System-III, following Wiggins notation [Wiggins, 1988], we obtain

$$\begin{aligned}
\dot{\underline{x}} &= J D_x H_0(\underline{x}, I) + \delta g^x(\underline{x}, I, \gamma, \mu, \delta), \\
\dot{I} &= \delta g^I(\underline{x}, I, y, \mu, \delta), \\
\dot{\gamma} &= D_I H_0(\underline{x}, I) + \delta g^\gamma(\underline{x}, I, \gamma, \mu, \delta),
\end{aligned} \tag{39}$$

where

$$(\underline{x}, I, \gamma) \in R^2 \times R \times S, 0 < \delta \ll 1, \mu \in R, \underline{x} = [P_1, Q_1]^T, I = P_2, \gamma = Q_2, \tag{40}$$

and J is the $2 \times 2$ symplectic matrix. The perturbation terms to the vector field determined by the Hamiltonian $H_0$, that is, $g^x, g^I$ and $g^\gamma$, are themselves derivable from the Hamiltonian $H_1$. An explicit solution of the unperturbed system $(P, Q)$ is then given by

$$q_0^I(\tau) = \{(\underline{x}^I(\tau))^T, I, \int^\tau D_I H(\underline{x}^I(s))ds + \gamma_0\} = \{P_1(\tau), Q_1(\tau), P_2(\tau), Q_2(\tau)\}. \tag{41}$$

Note that, here and in the following analysis, $P_1(\tau), Q_1(\tau), P_2(\tau), Q_2(\tau)$ are the explicit solutions of the unperturbed system ($\delta = 0$) derived in the previous subsection.

The Melnikov function for system-III, $M^I$, can be written as

$$M^I = \int_{-\infty}^{\infty} (<D_x H, g^x> + <D_I H, g^I>)d\tau - <D_I H, \int_{-\infty}^{\infty} g^I d\tau> \tag{42}$$

12

where $<,>$ denotes the inner product.

Using equations (39) we obtain

$$
\begin{aligned}
M^I &= \int_{-\infty}^{\infty} \frac{\bar{F}_0\sqrt{P_1}}{2}\left(\mu + \frac{1}{\sqrt{P_1}}(P_{20} - 3P_1)\cos Q_1\right)\sin(Q_1 + 2Q_2)d\tau \\
&\quad - \int_{-\infty}^{\infty} \frac{\bar{F}_0}{2}(P_{20} - P_1)\sin Q_1\cos(Q_1 + 2Q_2)d\tau \\
&\quad - \int_{-\infty}^{\infty} \bar{F}_0\sqrt{P_1}(\sigma_2 + \sqrt{P_1}\cos Q_1)\sin(Q_1 + 2Q_2)d\tau \\
&\quad + \bar{F}_0(\sigma_2 + \sqrt{P_1}\cos Q_1)\int_{-\infty}^{\infty}\sqrt{P_1}\sin(Q_1 + 2Q_2)d\tau,
\end{aligned}
\tag{43}
$$

which further reduces to

$$
\begin{aligned}
M^I &= \bar{F}_0\left[\frac{\mu}{2} + \sqrt{P_1}\cos Q_1\right]\int_{-\infty}^{\infty}\sqrt{P_1}\sin(Q_1 + 2Q_2)d\tau \\
&\quad + \frac{\bar{F}_0}{2}\int_{-\infty}^{\infty}(P_{20} - P_1)\sin 2Q_2\,d\tau \\
&\quad - 2\bar{F}_0\int_{-\infty}^{\infty}P_1\cos Q_1\sin(Q_1 + 2Q_2)d\tau.
\end{aligned}
\tag{44}
$$

Evaluating $M^I$ for orbit $A_1$, from equation (32), and letting $Q_2(\tau) = Q_{20} + \bar{Q}_2(\tau)$, where $\bar{Q}_2(\tau) = \frac{\sigma_1\tau}{2}$, we obtain

$$
M^I{}_1 = \frac{\bar{F}_0\sin 2Q_{20}}{2}\int_{-\infty}^{\infty}(P_{20} - P_1)\cos 2\bar{Q}_2\,d\tau.
\tag{45}
$$

Substituting for $P_1$ from equation (36) and evaluating the integral in equation (45), we obtain

$$
M^I{}_1 = \frac{\sigma_1\pi\bar{F}_0}{2}\sin(2Q_{20})\operatorname{cosech}\frac{\sigma_1\pi}{\sqrt{4P_{20} - \mu^2}}
\tag{46}
$$

for $\sigma_1 > 0$ and $4P_{20} - \mu^2 > 0$.

If $M^I{}_1$ has a simple zero with respect to $Q_{20}$, which is the case when the coefficient of $\sin(2Q_{20})$ is not zero, the heteroclinic orbit $A_1$ breaks with transversal intersections. The physical implication of the condition $P_{20} > \frac{\mu^2}{4}$ is that the energy in the system, $P_2$, needs to have a certain minimum value ($P_{20}$) before chaotic dynamics can occur. And then, for any $\bar{F}_0 > 0$, we

13

have the existence of Smale horseshoes and hence chaotic dynamics for the undamped, quadratic systems with 1:2 subharmonic internal resonances.

For orbit $A_2$, for which $P_1(t) = P_{20}$, the Melnikov function (44) reduces to

$$M^I{}_2 = \bar{F}_0 \left( \frac{\mu\sqrt{P_{20}}}{2} + P_{20}\cos Q_1 \right) \int_{-\infty}^{\infty} \sin(Q_1 + 2Q_2)d\tau$$
$$- 2\bar{F}_0 P_{20} \int_{-\infty}^{\infty} \cos Q_1 \sin(Q_1 + 2Q_2)d\tau. \tag{47}$$

From equation (33) for $Q_1'$ we observe that $Q_1(\tau)$ will be an odd function. Similarly, we will get $Q_2(\tau)$ as another odd function. Using this information in equation for $M^I{}_2$, we observe that the integrands for both the integrals are odd functions, and therefore, $M^I{}_2 = 0$. Thus, at the first order in $\delta$, the orbit $A_2$ does not break under perturbations.

## 4.5 Numerical Simulations

In figure (3) we show results of numerical simulations displaying the effects of perturbing the system. The solid lines are the orbits for the unperturbed system. The dots represent the Poincare section, at $Q_2 = 0$, for the solution of the perturbed system. The figure (3a) is for $\mu < 0$ ($\sigma_1 = 1, \sigma_2 = 0.66$) and the figure (3b) is for $\mu > 0$ ($\sigma_1 = 1.5, \sigma_2 = 0.66$). It should be noted that only some initial conditions, taken sufficiently close to the heteroclinic orbit of the unperturbed system, lead to chaotic motions. The orbits for the unperturbed system, away from the heteroclinic orbits do not result in chaotic motions, as is expected from the KAM theory [Wiggins, 1988]. For $\mu > 0$, from figure (3b), we again observe the breakup of heteroclinic orbits for initial conditions close to the heteroclinic orbits of the unperturbed system.

Even though the analysis presented here is valid only for an undamped system, numerical investigations show the persistence of chaos even for small damping. The numerical simulations for the damped case were performed by using a modified version of equations (23) that included damping terms. For $\mu < 0$, $\delta = 0.01$ and $\bar{\xi}_1 = \bar{\xi}_2 = 0.0001$, in figure (4) we see the breaking up of heteroclinic orbits resulting in chaotic dynamics.

On increasing the damping further, we find that the orbits breakup and chaos persists for awhile before the motion slowly starts diffusing towards the zero solution. Thus, there is only a transient chaotic motion. In this

14

case, for $\mu < 0$, $\delta = 0.01$, $\bar{\xi}_1 = \bar{\xi}_2 = 0.001$ (figure 5) both the orbits, that is, the ones close to the heteroclinic orbit of the unperturbed system and the smaller orbits far away from the saddle-type fixed points, diffuse towards the zero solution. The motion is still irregular and complicated and thus the chaotic effects persist even for increased damping. On increasing the damping further, the heteroclinic orbits break up and diffuse towards the zero solution much more rapidly.

The effect of increasing the perturbation strength can be seen by comparing figure (3) to figure (6), which is for $\delta = 0.1$. Note that since $\hat{F} = \delta\bar{F}$, an increase in $\delta$ corresponds to an increase in the amplitude of the external excitation $\hat{F}$. On increasing the perturbation to the system it is observed that the chaotic motions now occupy a much larger region of the phase space.

## 5  Example

A simple example of the type of systems under consideration is an Autoparametric vibratory system shown in figure (7). The Autoparametric system consists of a linear spring-mass-dashpot system to which a damped pendulum is attached. Quadratic nonlinearities arise because of inertial effects of large amplitude motions of the pendulum. The equations of motion for this system are

$$
\begin{aligned}
(M+m)\ddot{x} + C_1\dot{x} + k_1 x - ml(\ddot{\theta}\sin\theta + \dot{\theta}^2\cos\theta) &= P_0\cos\omega t, \\
ml^2\ddot{\theta} + C_2\dot{\theta} + (mgl - ml\ddot{x})\sin\theta &= 0,
\end{aligned}
\tag{48}
$$

where

M is the mass of the block; $C_1$ and $C_2$ are the coefficients of viscous damping; $k_1$ is the spring constant; m is the mass of the pendulum bob; l is the length of the pendulum; x is the vertical displacement of the block; $\theta$ is the angular displacement of the pendulum; $P_0$ is the amplitude of the external forcing; and $\omega$ is the frequency of the forcing.

Using the following transformations:

$\tau = \omega t$, dimensionless time ; $\eta = \frac{x}{l}$ ; $r = \frac{m}{M}$, mass ratio ; $F = \frac{P_0}{K_1 l}$ ; $P = \frac{\omega}{\Omega_1}$, excitation frequency ratio ; $\Omega_1 = \sqrt{\frac{k_1}{M}}$, natural frequency of the block ; $q = \frac{\omega_2}{\omega_1}$, frequency ratio of the combined system ; $\omega_1 = \sqrt{\frac{k_1}{M+m}}$, frequency of the locked pendulum ; $\omega_2 = \sqrt{\frac{g}{l}}$, natural frequency of the pendulum ;

15

$\xi_1 = \frac{C_1}{2M\Omega_1}$, damping ratio of the block ; $\xi_2 = \frac{C_2}{2ml^2\omega_2}$, damping ratio of the pendulum ;

and the scalings:

$\eta = \epsilon\hat{\eta}, \theta = \epsilon\hat{\theta}, \xi_1 = \epsilon\hat{\xi_1}, \xi_2 = \epsilon\hat{\xi_2}, F = \epsilon^2\hat{F}$, where $0 < \epsilon \ll 1$,

and expanding the equations (48) in a Taylor's series, we obtain the following

$$\begin{aligned}
\hat{\eta}'' + \Omega_{n1}^2\hat{\eta} &= \epsilon(\hat{F}\Omega_{n1}^2\cos\tau - 2\bar{\xi}_1\Omega_{n1}^2\hat{\eta}' + 8\bar{\theta}^2 - 8\Omega_{n2}^2\bar{\theta}^2) + O(\epsilon^2), \\
\bar{\theta}'' + \Omega_{n2}^2\bar{\theta} &= \epsilon(-4\bar{\xi}_2\Omega_{n2}\bar{\theta}' - \Omega_{n1}^2\bar{\theta}\hat{\eta}) + O(\epsilon^2),
\end{aligned} \tag{49}$$

where $\bar{\theta} = \frac{1}{2}\sqrt{\frac{R}{2(1+R)}}\hat{\theta}, \bar{\xi}_1 = P\hat{\xi}_1, \bar{\xi}_2 = \frac{1}{2}\hat{\xi}_2, \Omega_{n1} = \frac{1}{P\sqrt{1+R}}$, and $\Omega_{n2} = \frac{q}{P\sqrt{1+R}}$.

Let $\Omega_{n1}$ be near 1 and $\Omega_{n2}$ be near $\frac{1}{2}$, in order to study the response for the case of interest of 1:2 subharmonic internal resonance. Defining the state vector as

$$\underline{z} = [\hat{\eta}, \hat{\eta}', \bar{\theta}, \bar{\theta}']^T = [z_1, z_2, z_3, z_4]^T, \tag{50}$$

we write the equations (49) in the form

$$\underline{z}' = \underline{A}\,\underline{z} + \epsilon\underline{h}_1(\underline{z}, \tau), \tag{51}$$

where

$$\underline{h}_1(z_1, z_2, z_3, z_4, \tau) = \left\{ \begin{array}{c} 0 \\ \hat{F}\cos\tau - 2\bar{\xi}_1 z_2 + 8z_4^2 - 2z_3^2 \\ 0 \\ -2\bar{\xi}_2 z_4 - z_1 z_3 \end{array} \right\}. \tag{52}$$

Comparing equation (4) to equation (51) and identifying the coefficients of the nonlinear quadratic terms, we get $a_{33} = 2, a_{44} = -8, b_{13} = 1, b_{24} = 0$. Therefore, from equations (11) we have $A = 2, B = \frac{1}{2}$ and so from equations (10) we get $\alpha = 2$ and $\beta = \sqrt{2}$.

Using these scalings, the autoparametric system reduces exactly to the form in equation (2) for the general system. The coordinate $\zeta_1$ now corresponds to the motion of the block with the pendulum locked in the vertical position and the coordinate $\zeta_2$ corresponds to the motion of the pendulum. Thus, $a_1$ is the amplitude of the locked-pendulum and $a_2$ is the amplitude of the pendulum oscillation.

16

We now describe the various physical motions that the autoparametric pendulum system exhibits for the different values of system parameters. Note that these descriptions are valid for every two degree-of freedom system within the class of systems being investigated.

From the transformation to Action - Angle form (described in Section 4.1) and the subsequent canonical transformation, we see that $a_1^2 = 4P_1$ and $a_2^2 + \frac{a_1^2}{2} = P_2$. Thus, $a_1 = 2\sqrt{P_1}$ and $a_1$ behaves exactly like $P_1$. For the unperturbed system ($\delta = 0$), figure (2), most motions in the $(P_1, Q_1)$ plane are periodic and the period depends on initial conditions. Since $P_2 = P_{20}$ is a constant, both $a_1$ and $a_2$ vary periodically, with $a_1$ attaining its maximum where $a_2$ is at a minimum and vice-versa. For initial conditions on the orbits near the heteroclinic orbit, the period is very long. For example, for $\mu < 0$ (figure (2a)), the variation of $a_1$ and $a_2$ for initial conditions near the line $P_2 = P_{20}$, is shown in figure (8a). Note that $a_1$ essentially remains constant over a long time, rapidly reaches a minimum, and then quickly regains the maximum amplitude of motion. In this figure (8a), the solid line ('-') refers to $a_1$ and the dashed line ('- -') refers to the modal amplitude $a_2$.

The modal response of on periodic orbit, away from the heteroclinic orbit is seen in figure (8b), where as before, $a_1$ is shown by a solid line ('-') and $a_2$ is shown by a dashed line ('- -'). As expected, the time-period of this motion is less than that of a periodic orbit close to the heteroclinic orbit.

Now consider the effects of various perturbations. For $\delta = 0.01$, and zero damping, corresponding to the Poincare section of the chaotic motion shown in figure (3a), the modal responses in time are shown in figures (9a) and (9b). A careful examination of the figures shows that the motion is indeed non-periodic and the amplitudes do not repeat. (Note however, the time responses by themselves are not a sufficient indicator of chaos). These motions persist for sufficiently small damping. For larger daming however, the complicated motion is only a transient and it slowly diffuses towards the zero solution. This is clear from the slow decay in the amplitudes of the modal responses shown in figures (10a) and 10(b). Finally, when the external excitation is quite strong (say for $\delta = 0.10$, figure (6)), as seen in figure (11a) and 11(b), the modal amplitudes $a_1$ and $a_2$ are much more irregular.

17

# 6  Summary and Conclusions

Two degree-of-freedom nonlinear dynamical systems with quadratic nonlinearities and resonant harmonic excitations are considered. For the case of 1:2 subharmonic internal resonance, the weakly nonlinear response of the system is determined by the averaged equations. In the case of zero damping, the averaged system is derivable from a Hamiltonian and is integrable in the limiting case when the external forcing amplitude goes to zero. For the unperturbed Hamiltonian system, saddle-type equilibrium points and the associated heteroclinic orbits are identified. Then, using Melnikov's method for multi degree-of-freedom conservative systems, it is shown that any small external excitation breaks the heteroclinic orbits and leads to transverse intersections of the stable and unstable manifolds, leading to Smale horseshoes and hence complex invariant sets in the dynamics of the averaged system. These results are verified by numerical simulations of the averaged equations, and it is shown that the chaotic responses persist even in the presence of sufficiently small damping (as compared to the amplitude of the external forcing), although the analytical results are not valid for the damped case.

# 7  Acknowledgements

# 8  References

Bajaj, A.K., Chang, S.I. and Johnson, J., 1993 "Amplitude modulated dynamics of a resonantly excited autoparametric two degree-of- freedom system", Nonlinear Dynamics, to appear.

Banerjee, B., Bajaj, A.K. and Davies, P., 1993, "Second order averaging study of an autoparametric system", Proceedings of the Fourteenth Biennial ASME Conference on Mechanical Vibration and Noise, Albuquerque, NM.

Doedel, E., 1986, "AUTO: Software for continuation and bifurcation

problems in ordinary differential equations", Report, Department of Applied Mathematics, California Institute of Technology, Pasadena, CA.

Feng, Z.C. and Sethna, P.R., 1990, "Global bifurcation and chaos in parametrically forced systems with one-one resonance", Dynamics and Stability of Systems, Vol. 5, no. 4, pp. 201-225.

Guckenheimer, J., Kim, S., Myers, M. R., Wicklin, F. J., Worfolk, P. A., 1992, "dstool : A Dynamical System Toolkit with an Interactive Graphical Interface", Users Manual, Centre for Applied Mathematics, Cornell University, Ithaca, NY.

Haxton, R.S. and Barr, A.D.S., 1972, "The autoparametric vibration absorber", ASME Journal of Engineering for Industry, Vol. 94, pp. 119-125.

Holmes, P. and Marsden, J., 1982, "Horseshoes in perturbations of Hamiltonian systems with two degrees of freedom", Communications in Mathematical Physics, Vol. 82, pp. 523-544.

Murdock, J.A., 1991, "Perturbations: Theory and Methods", John Wiley and Sons, NY.

Sethna, P.R., 1965, "Vibrations of dynamical systems with quadratic nonlinearities", ASME Journal of Applied Mechanics, Vol. 32, pp. 576-582.

Sethna, P.R. and Bajaj, A.K., 1978, "Bifurcations in dynamical systems with internal resonances", ASME Journal of Applied Mechanics, Vol. 45, pp. 895-902.

Tien, W.M., Namachchivaya, N.S. and Bajaj, A.K., 1994 , "Nonlinear dynamics of a shallow arch under periodic excitation, Part I-1:2 internal resonance", International Journal of Nonlinear Mechanics, Vol. 29, pp. 349-366.

Wiggins, S., 1988, "Global Bifurcations and Chaos", Springer-Verlag, NY.

Wiggins, S., 1990, "Introduction to Applied Nonlinear Dynamical Systems and Chaos", Springer-Verlag, NY.

Figure 1. Steady state response $a_1$ and $a_2$ as a function of mistuning $\sigma_1$. $\bar{\xi}_1 = \bar{\xi}_2 = 0.10, \sigma_2 = 0.66, \bar{F} = 1.0$ . '-' Stable solution. '- -' Unstable solution.
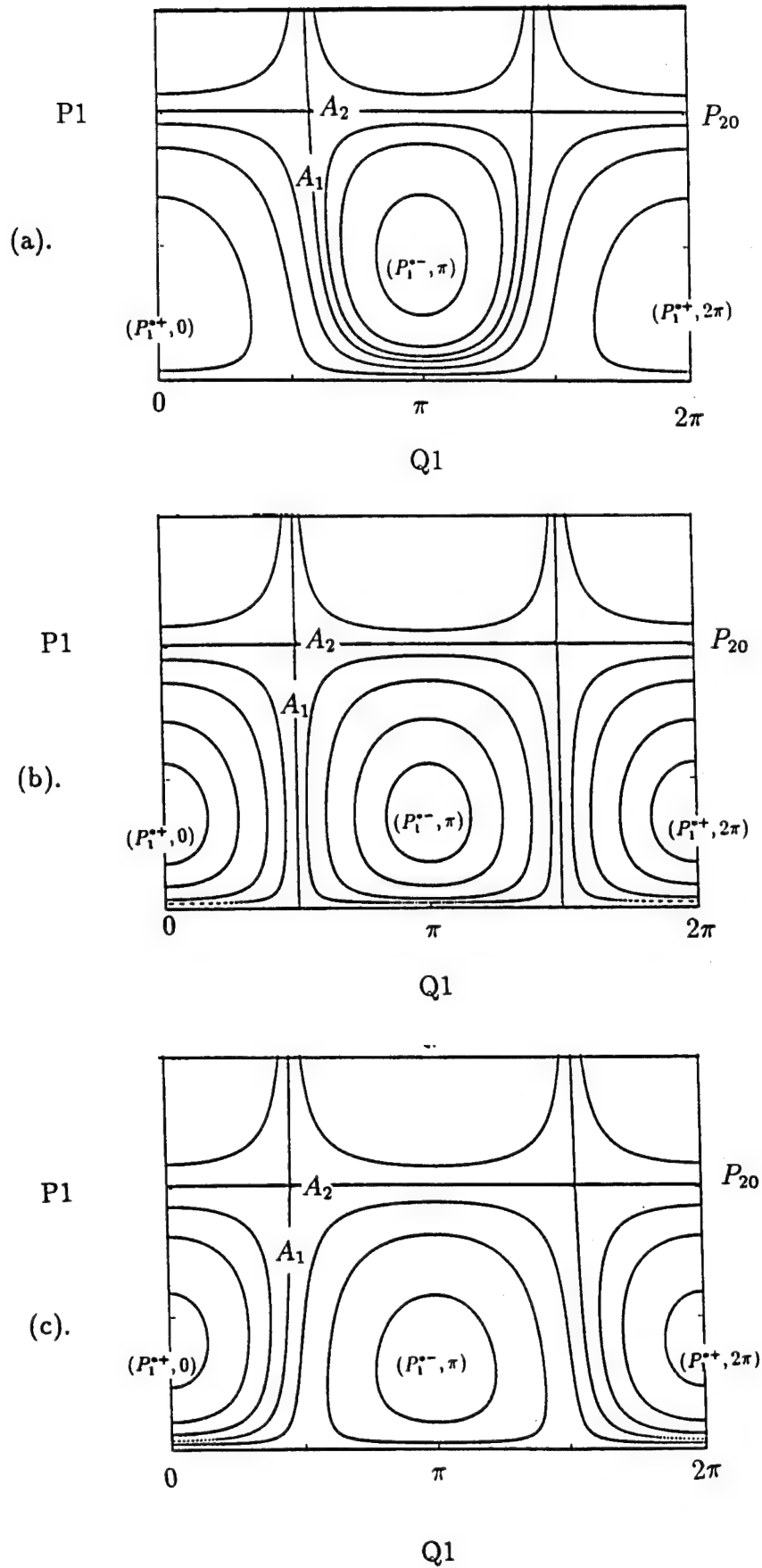
Figure 2. Phase portraits of the unperturbed Hamiltonian system in $(P_1, Q_1)$ plane. $\delta = 0.0$ , $\sigma_2 = 0.66$ , $\bar{F} = 1.0$ . (a). $\mu < 0$ ($\sigma_1 = 1.00$), (b). $\mu = 0$ ($\sigma_1 = 1.32$), (c). $\mu > 0$ ($\sigma_1 = 1.50$)
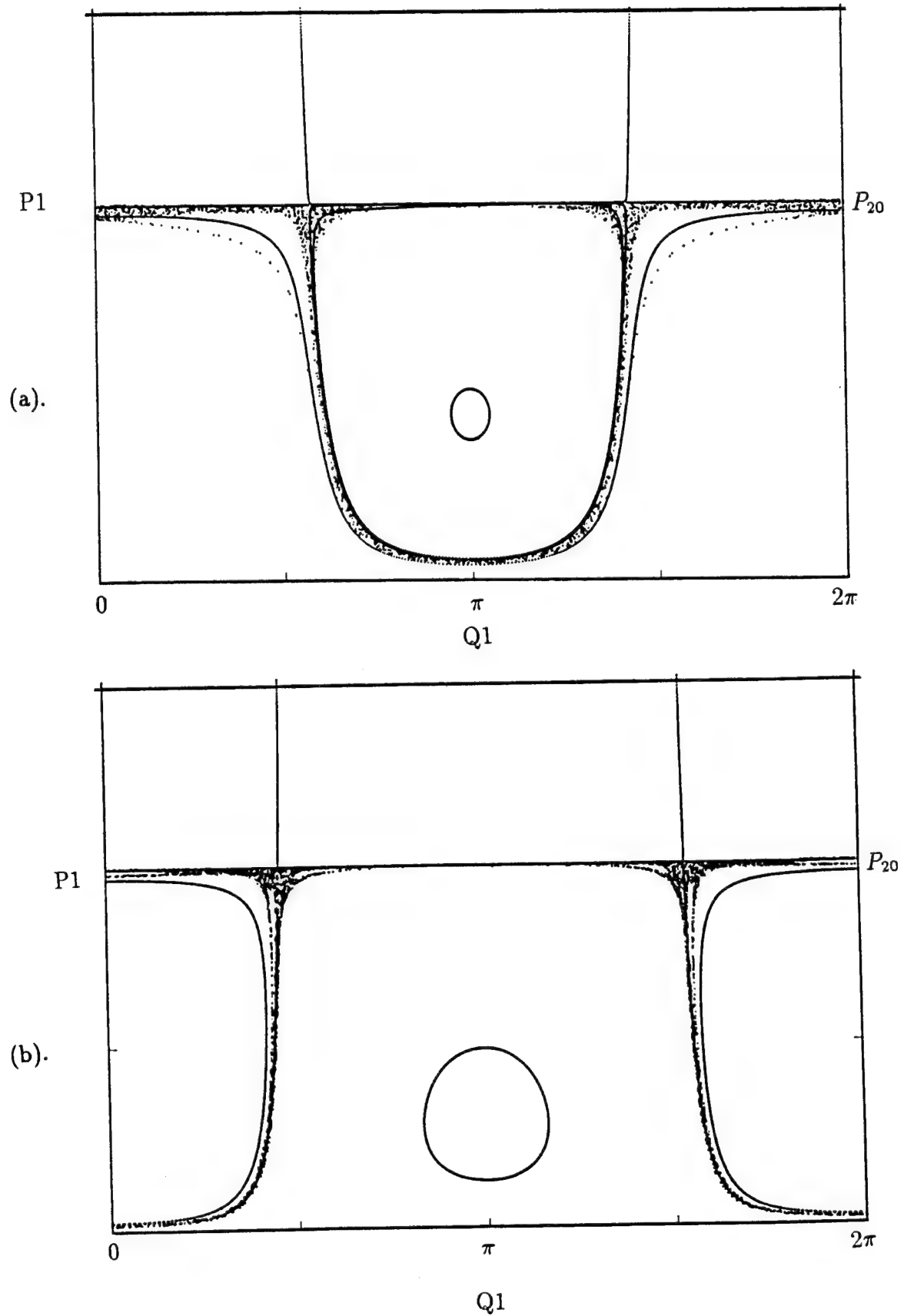
Figure 3. Effect of perturbation. $\delta = 0.01$ . Poincare sections in $(P_1, Q_1)$ plane. $\sigma_2 = 0.66$ , $\bar{F} = 1.0$ . (a). $\mu < 0$ ($\sigma_1 = 1.00$), (b). $\mu > 0$ ($\sigma_1 = 1.50$)
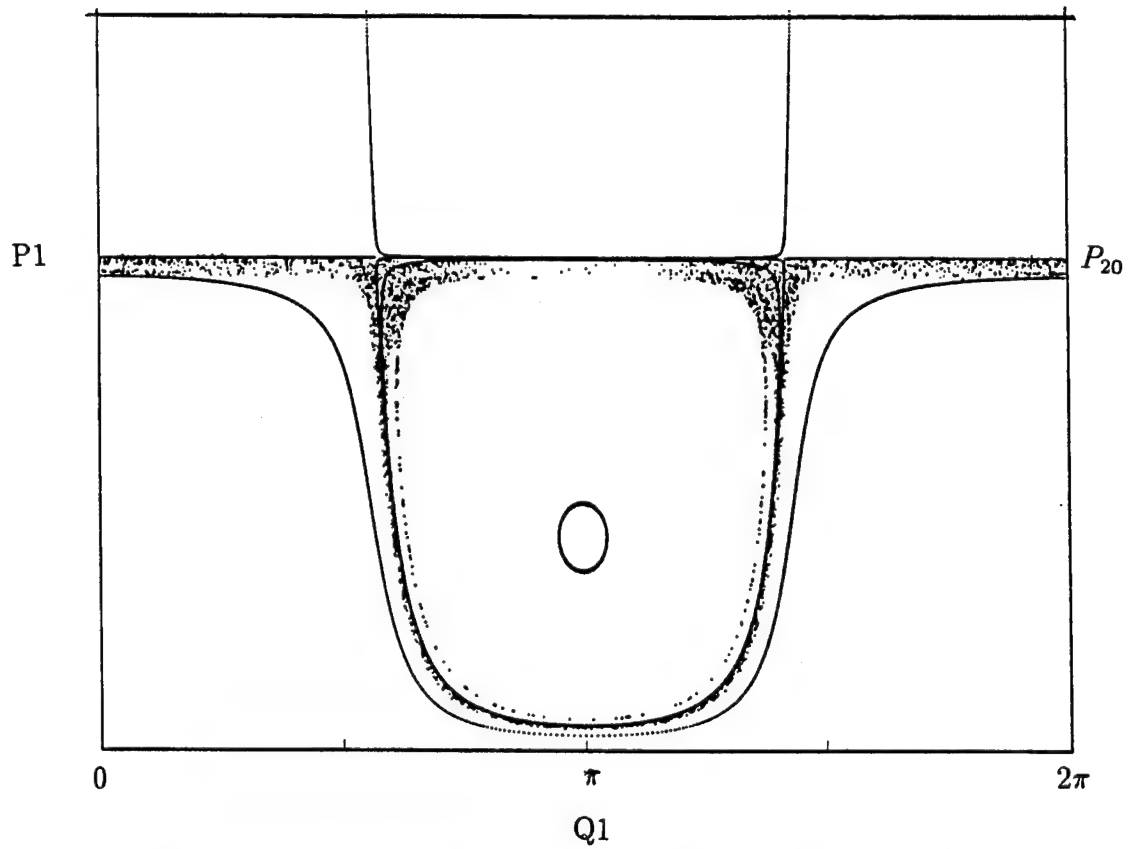
Figure 4. Effects of damping. $\bar{\xi}_1 = 0.0001, \bar{\xi}_2 = 0.0001$. Poincare sections in $(P_1, Q_1)$ plane. $\mu < 0$ ($\sigma_1 = 1.00, \sigma_2 = 0.66$), $\bar{F} = 1.0, \delta = 0.01$
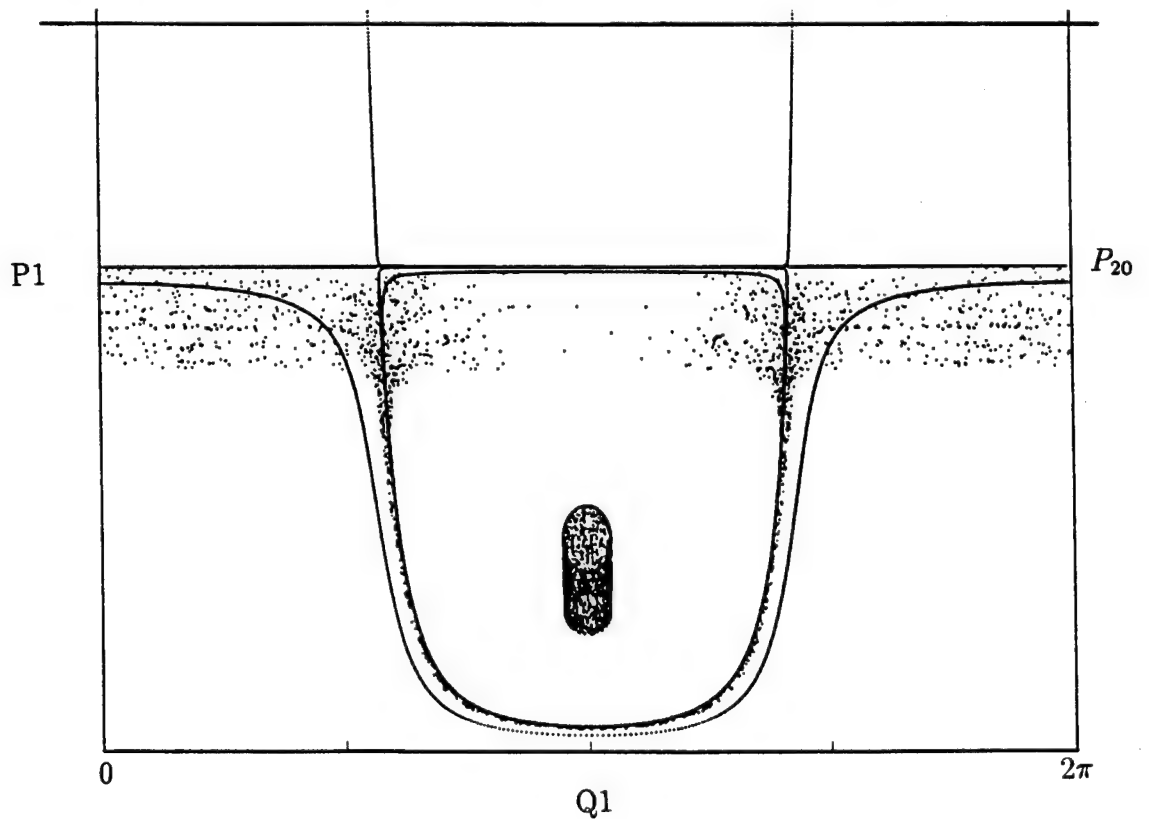
Figure 5. Effects of increasing damping. $\bar{\xi}_1 = 0.001, \bar{\xi}_2 = 0.001$. Poincare sections in $(P_1, Q_1)$ plane. $\mu < 0$ ($\sigma_1 = 1.00, \sigma_2 = 0.66$), $\bar{F} = 1.0, \delta = 0.01$
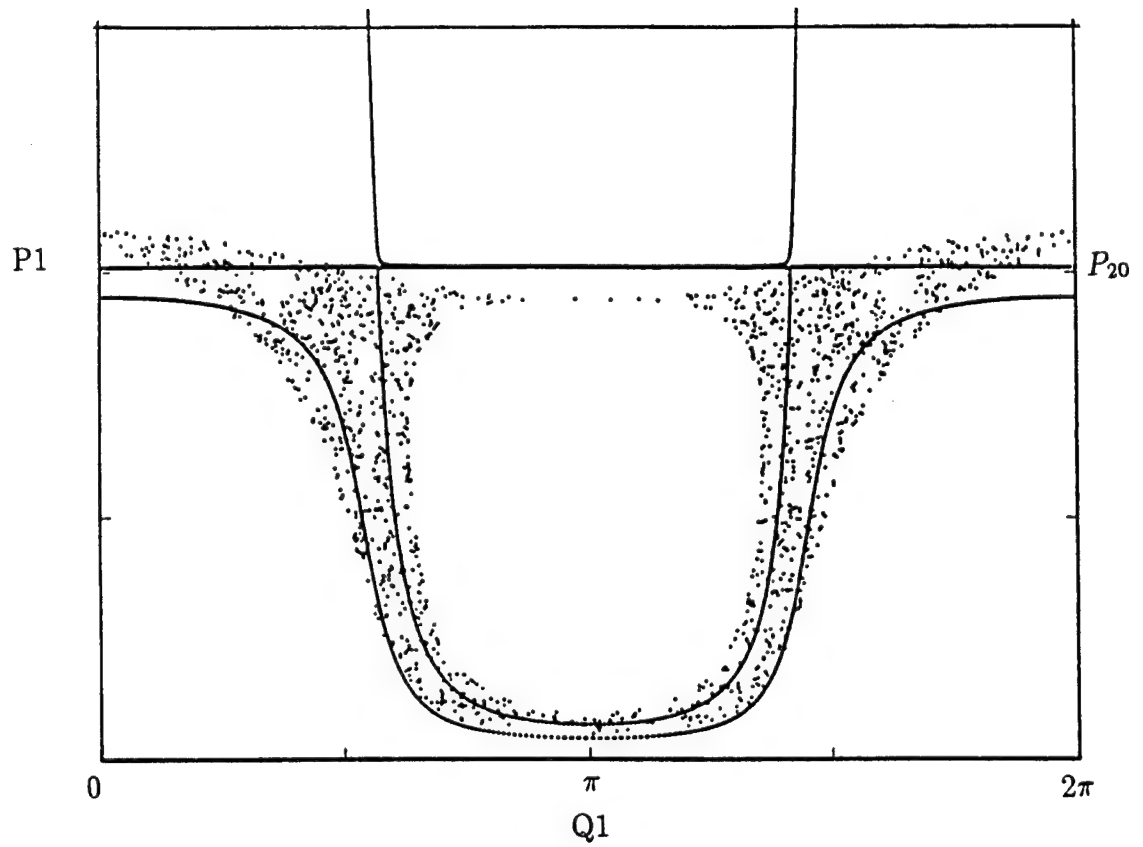
Figure 6. Effects of increasing perturbation. $\delta = 0.1$ . Poincare section in $(P_1, Q_1)$ plane. $\mu < 0$ ($\sigma_1 = 1.00, \sigma_2 = 0.66$), $\bar{F} = 1.0$

Figure 7. Autoparametric vibratory system

Figure 8. Response history of the unperturbed, undamped autoparametric system. $\delta = 0.0$ , $\sigma_1 = 1.00$ , $\sigma_2 = 0.66$ ($\mu < 0$) , $\bar{F} = 1.0$ . (a). Initial conditions close to heteroclinic orbit , (b). Initial conditions away from heteroclinic orbit.

Figure 9. Response history of the perturbed, undamped autoparametric system. $\delta = 0.01$ , $\sigma_1 = 1.00$ , $\sigma_2 = 0.66$ ($\mu < 0$) , $\bar{F} = 1.0$ . (a). The modal

amplitude $a_1$, (b). The modal amplitude $a_2$.

Figure 10. Response history of the perturbed, strongly damped autoparametric system. $\delta = 0.01$ , $\sigma_1 = 1.00$ , $\sigma_2 = 0.66$ ($\mu < 0$) , $\bar{F} = 1.0$ , $\bar{\xi}_1 = \bar{\xi}_2 = 0.10$. (a). The modal amplitude $a_1$, (b). The modal amplitude $a_2$.
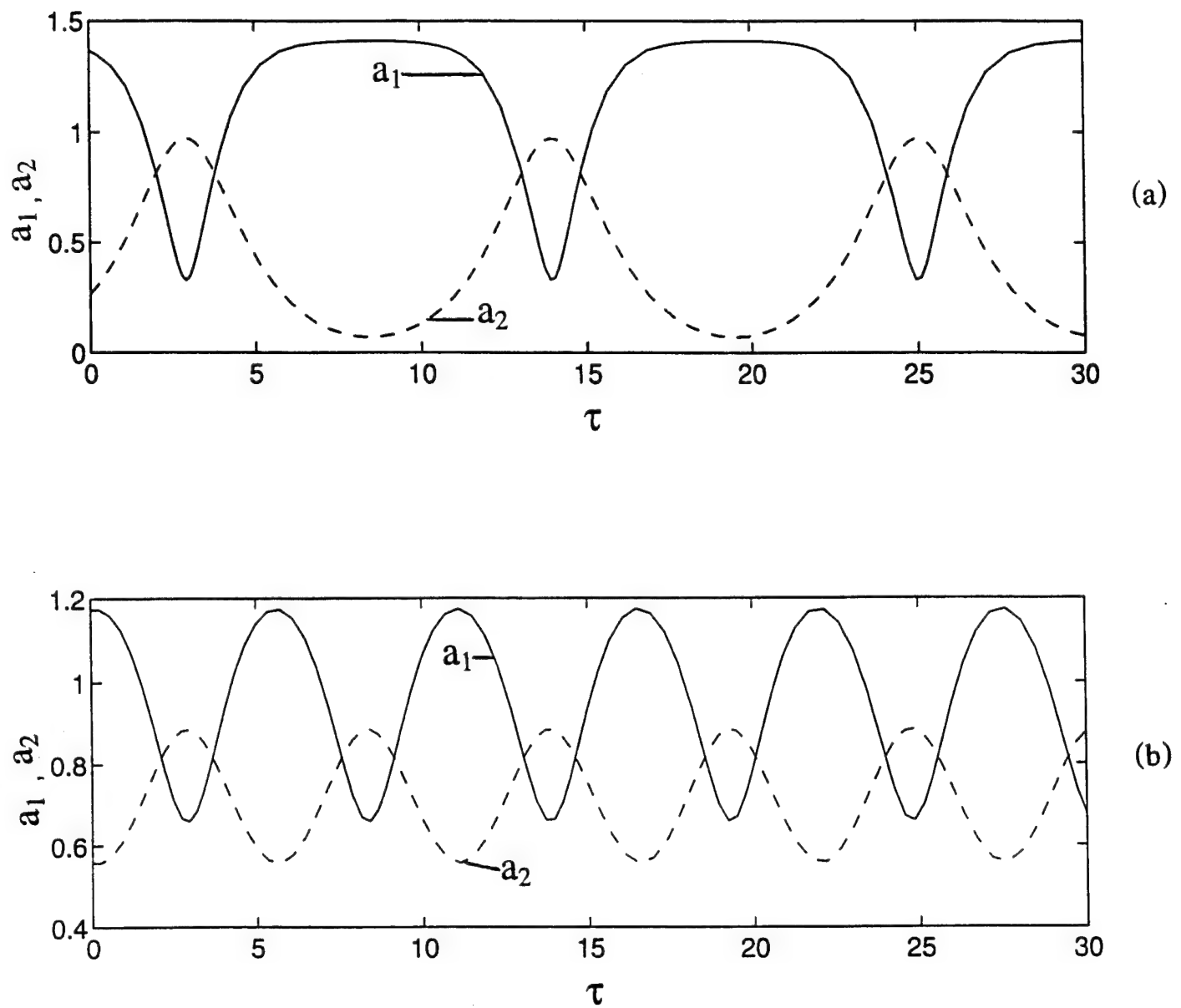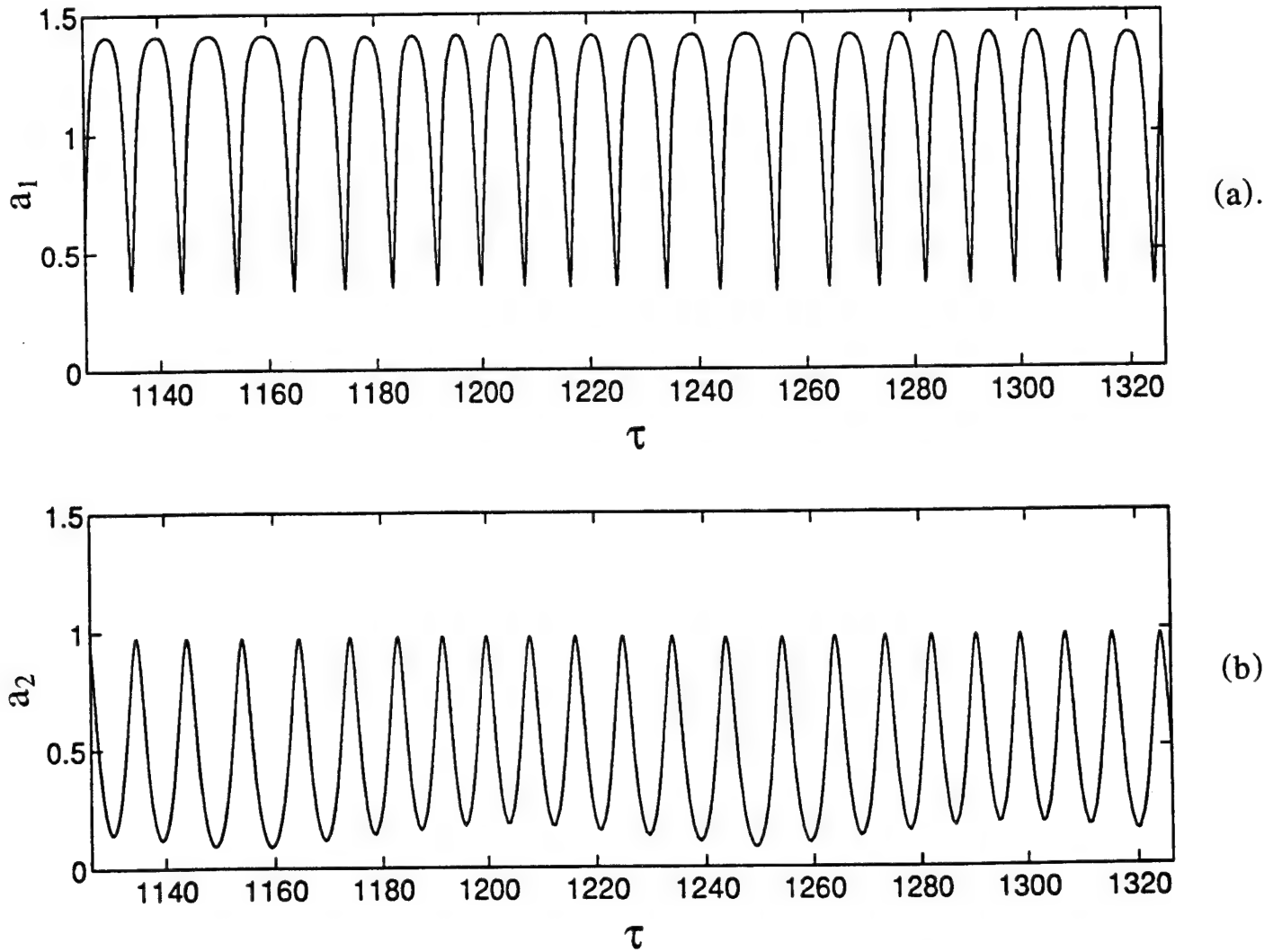
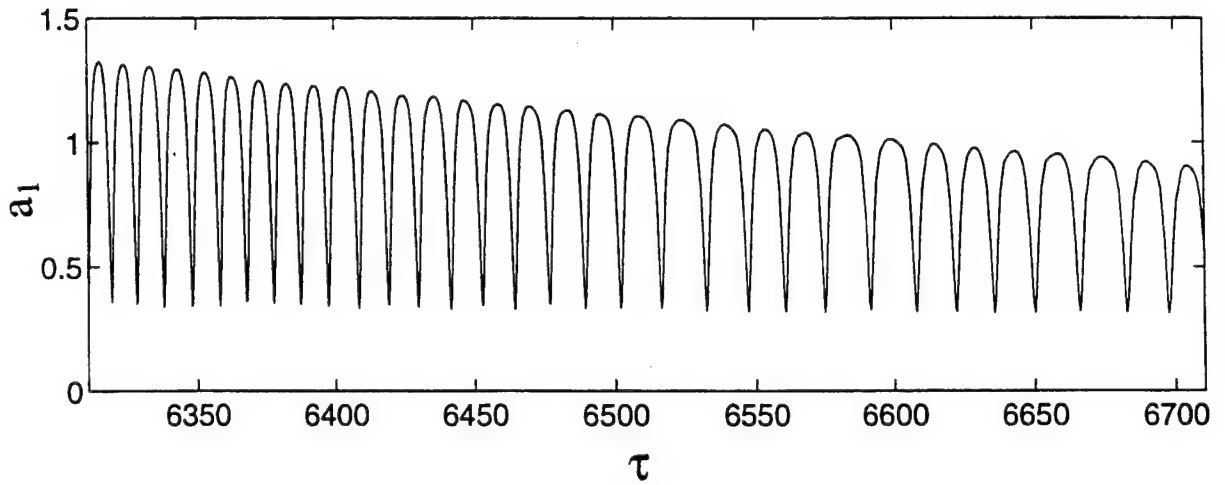Figure 11. Response history of the strongly perturbed, undamped autoparametric system. $\delta = 0.10$ , $\sigma_1 = 1.00$ , $\sigma_2 = 0.66$ ($\mu < 0$) , $\bar{F} = 1.0$ . (a). The modal amplitude $a_1$, (b). The modal amplitude $a_2$.

Figure 1. Steady state response $a_1$ and $a_2$ as a function of mistuning $\sigma_1$. $\bar{\xi}_1 = \bar{\xi}_2 = 0.10, \sigma_2 = 0.66, \bar{F} = 1.0$ . '—' Stable solution. '- -' Unstable solution.

Figure 2. Phase portraits of the unperturbed Hamiltonian system in $(P_1, Q_1)$ plane. $\delta = 0.0$, $\sigma_2 = 0.66$, $\bar{F} = 1.0$. (a) $\mu < 0$ ($\sigma_1 = 1.00$), (b) $\mu = 0$ ($\sigma_1 = 1.32$), (c) $\mu > 0$ ($\sigma_1 = 1.50$)

Figure 3. Effect of perturbation. $\delta = 0.01$ . Poincare sections in $(P_1, Q_1)$ plane. $\sigma_2 = 0.66$ , $\bar{F} = 1.0$ . (a) $\mu < 0$ ($\sigma_1 = 1.00$), (b) $\mu > 0$ ($\sigma_1 = 1.50$)

Figure 4. Effects of damping. $\bar{\xi}_1 = 0.0001, \bar{\xi}_2 = 0.0001$. Poincare sections in $(P_1, Q_1)$ plane. $\mu < 0$ $(\sigma_1 = 1.00, \sigma_2 = 0.66), \bar{F} = 1.0, \delta = 0.01$



Figure 5. Effects of increasing damping. $\bar{\xi}_1 = 0.001, \bar{\xi}_2 = 0.001$. Poincare sections in $(P_1, Q_1)$ plane. $\mu < 0$ $(\sigma_1 = 1.00, \sigma_2 = 0.66), \bar{F} = 1.0, \delta = 0.01$

Figure 6. Effects of increasing perturbation. $\delta = 0.1$ . Poincare section in $(P_1, Q_1)$ plane. $\mu < 0$ $(\sigma_1 = 1.00, \sigma_2 = 0.66)$, $\bar{F} = 1.0$
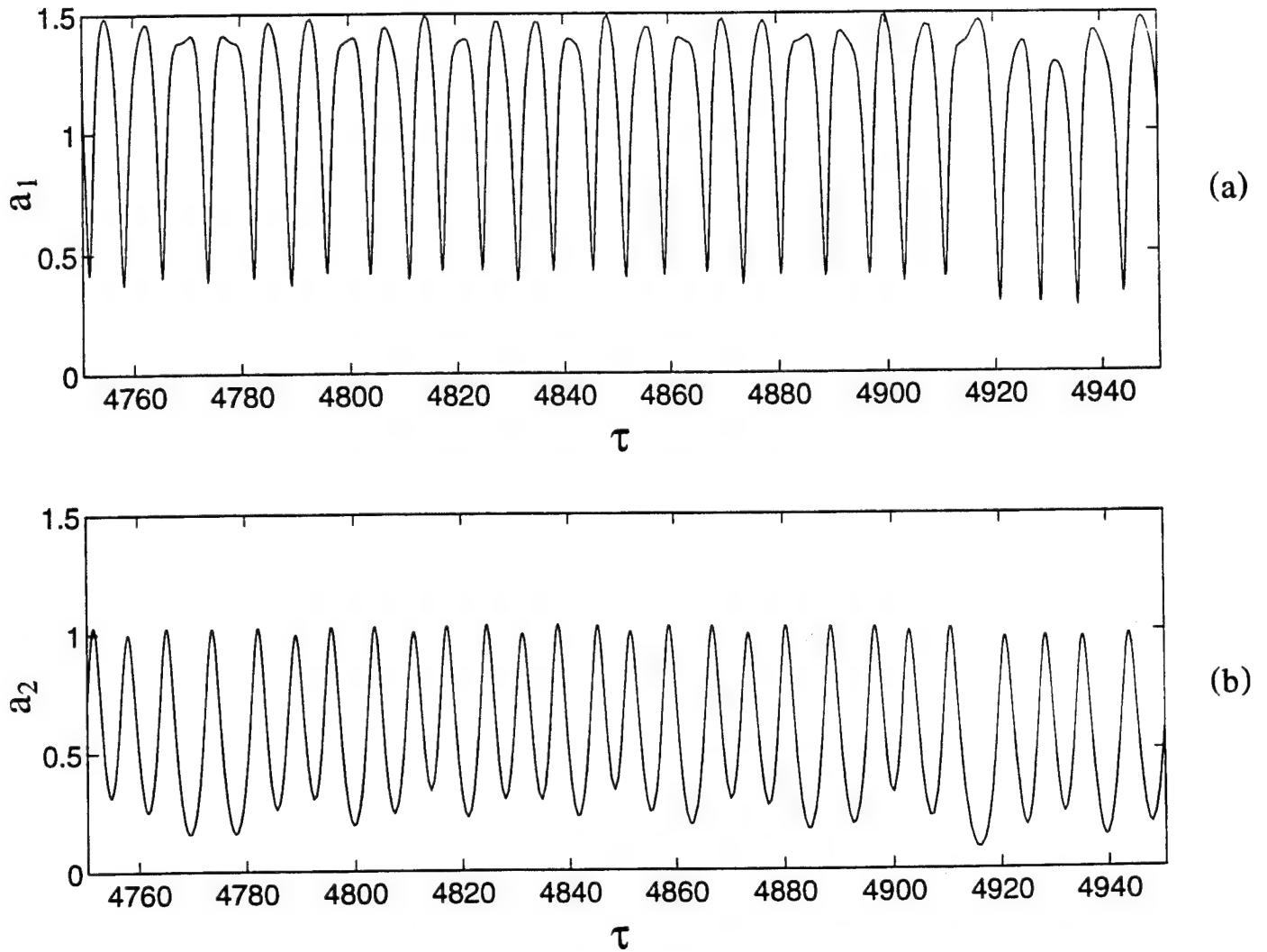


Figure 7. Autoparametric vibratory system

Figure 8. Response history of the unperturbed, undamped autoparametric system. $\delta = 0.0$, $\sigma_1 = 1.00$, $\sigma_2 = 0.66$ ($\mu < 0$), $\bar{F} = 1.0$. (a) Initial conditions close to heteroclinic orbit, (b) Initial conditions away from heteroclinic orbit.

Figure 9. Response history of the perturbed, undamped autoparametric system. $\delta = 0.01$, $\sigma_1 = 1.00$, $\sigma_2 = 0.66$ ($\mu < 0$), $\bar{F} = 1.0$. (a) The modal amplitude $a_1$, (b) The modal amplitude $a_2$.

Figure 10. Response history of the perturbed, strongly damped autoparametric system. $\delta = 0.01$, $\sigma_1 = 1.00$, $\sigma_2 = 0.66$ ($\mu < 0$), $\bar{F} = 1.0$, $\bar{\xi}_1 = \bar{\xi}_2 = 0.10$. (a) The modal amplitude $a_1$, (b) The modal amplitude $a_2$.

Figure 11. Response history of the strongly perturbed, undamped autoparametric system. $\delta = 0.10$ , $\sigma_1 = 1.00$ , $\sigma_2 = 0.66$ ($\mu < 0$) , $\tilde{F} = 1.0$ . (a) The modal amplitude $a_1$, (b) The modal amplitude $a_2$.

# APPENDIX 5

## Analytical prediction of nonlinear system response to non-stationary excitations

A. Raman, P. Davies, A. K. Bajaj

# ANALYTICAL PREDICTION OF NONLINEAR SYSTEM RESPONSE TO NON-STATIONARY EXCITATIONS

Arvind Raman, Patricia Davies, and Anil K. Bajaj
School of Mechanical Engineering
Purdue University
West Lafayette, Indiana

## ABSTRACT

The study of the non-stationary response of systems has many applications in problems related to transition through resonance in rotating machinery, aerospace structures and other physical systems.

In this paper, we present methods to analytically predict the response of some weakly nonlinear systems to slowly varying parameter changes. We consider systems which can be averaged and represented as two first order equations. The evolution of the solutions of such systems through critical (jump or bifurcation) points is studied using the method of matched asymptotic expansions. As an example, the method is used to predict the response of the forced Duffing's oscillator during passage through resonance.

Starting with a general system of two, first-order equations, we set up a slowly varying equilibrium or 'outer' solution as an asymptotic expansion about the stationary solution. This solution is seen to be invalid in a small neighborhood of the critical points - the 'inner' region. In this inner layer, the system of equations is transformed into the Jordan canonical form, which is easier to study. Using approximations from the center manifold theory, the problem is reduced to one first-order equation. By making appropriate scale changes, an 'inner' solution is developed. This solution is asymptotically matched with the outer expansion to yield a unified solution valid for all time.

## 1. INTRODUCTION

Non-stationary excitations in nonlinear systems occur in a wide variety of engineering problems. The variation of rotational speed during start up and shut down of turbomachinery, for example, causes the structure to be excited by a frequency which varies with time. Passage through resonance in rotating machinery and gyroscopic systems, vibrations in some aerospace structures, flow-induced vibrations due to deceleration during re-entry of space vehicles - are some relevant examples where a better understanding of the response of nonlinear systems to non-stationary excitation is important.

Analytical studies of the vibrations of weakly nonlinear systems have traditionally been carried out by the methods of averaging, multiple time scale analysis etc. These methods can be extended to the non-stationary case if the excitation is assumed to be slowly varying in time. An overview of asymptotic methods used in the theory of such non-stationary systems can be found in Mitropolskii (1965), Bogoliubov and Mitropolskii (1961), and Evan-Iwanowski (1976).

Lately, there has been considerable interest in looking at nonlinear non-stationary systems from the point of view of bifurcation theory. According to this view, a nonlinear dynamic system dependent on some *bifurcation parameter*, admits steady state solutions at given values of the parameter. As the parameter is varied infinitesimally slowly, i.e. in a quasi-static manner, the steady solutions follow *solution branches*. For certain values of the parameter, there is a sudden qualitative change in the nature of the solutions. Solution branches may exchange stability, give rise to more branches, undergo turning points etc. These points are the *critical or bifurcation points* of the system. The non-stationary case, then, is the problem of analyzing the system as the bifurcation parameter varies in time.

We are, in particular, interested in analytical methods for predicting the response of nonlinear systems as some system parameter varies slowly with time across bifurcation/critical points. A variety of physical phenomena: jumps, sudden transitions, oscillations etc., can occur during this transition.

The result of varying a system parameter across different kinds of bifurcation points is qualitatively different. This is discussed by Erneux *et al* (1991). Very often, it is observed that the bifurcation does not occur at the bifurcation point, but is delayed.
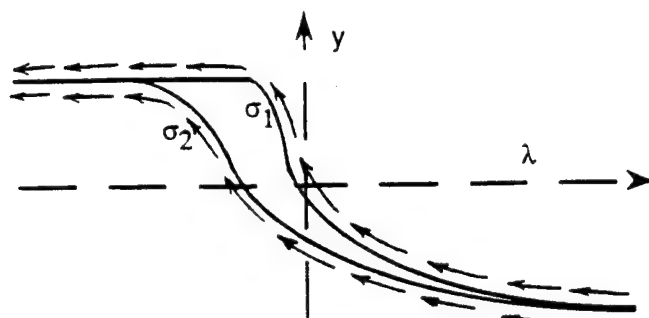
FIGURE 1A. NUMERICAL SIMULATION OF EQUATION (1.1) FOR SWEEP RATES $\sigma_1$, $\sigma_2$. $|\sigma_2|>|\sigma_1|$.
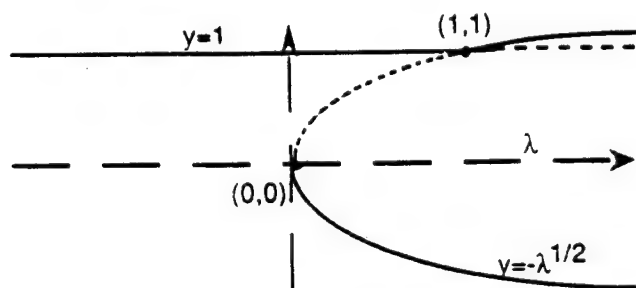


FIGURE 1B. STATIONARY SOLUTION, $y_r$.



FIGURE 1C. ASYMPTOTIC EXPANSION, EQUATION (1.4).

Descriptions of delayed bifurcations and associated memory effects have been given by Mandel and Erneux (1979), and Diener and Diener (1991). A number of references related to the analysis of such effects in chemical reactions, lasers and optically bistable devices, nerve conduction, developmental biology etc., are listed by Erneux et al (1991).

To better understand the analytical methods used in this paper, consider the following first order equation governing the variable $y$, in time $t$:

$$\frac{dy}{dt} = (y-1)(\lambda - y^2) \ , \qquad (1.1)$$

where $\lambda$ is a slowly varying system parameter which can be written as $\lambda(\varepsilon t)$ for sufficiently small $\varepsilon$. The bifurcation points of this system occur at $\lambda=0$- an example of a *jump phenomenon*, and at $\lambda=1$- an example of *transcritical or straight-straight bifurcation* (explained in detail in section 2). Let us look at the case where $\lambda$ decreases across the jump bifurcation point at $\lambda=0$ in a linear sweep.

Defining a slow time scale, $T=\varepsilon t$, equation (1.1) becomes:

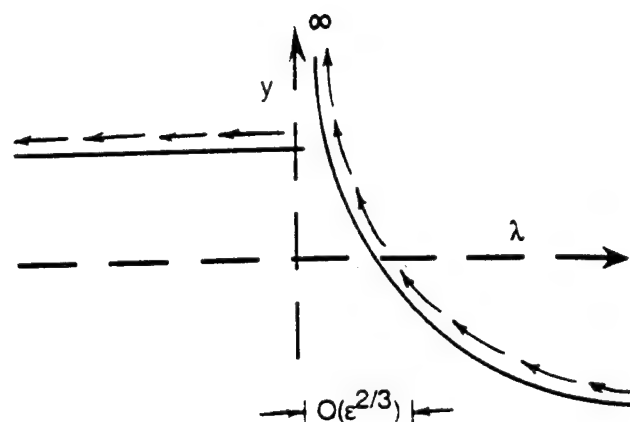$$\varepsilon\frac{dy}{dT} = (y-1)(\lambda(T)-y^2), \qquad (1.2)$$

with $\lambda=\sigma T$. $\sigma$ is the negative linear sweep rate and for convenience, $T=0$ when $\lambda=0$. The numerically integrated solution of equation (1.1), for $\sigma=\sigma_1,\sigma_2$ where $|\sigma_2|>|\sigma_1|$ is schematically shown in Fig. 1a.

The corresponding stationary solution of equation (1.2), denoted as $y_r$, is derived by substituting $\varepsilon=0$ in equation (1.2):

$$(y_r-1)(\lambda - y_r^2) = 0. \qquad (1.3)$$

This solution is shown in Fig. 1b. In general, the solution of equation (1.3) is not a solution for the non-stationary case. However, let us assume a solution of equation (1.2) in the form of an asymptotic expansion about the stationary solution:

$$y = y_r + \varepsilon y_1 + \varepsilon^2 y_2...., \qquad (1.4)$$

and calculate the coefficients $y_1$, $y_2$ etc. by substituting equation (1.4) into equation (1.2) and equating the coefficients of like powers of $\varepsilon$. Based on equation (1.4), the solution is shown in Fig. 1c. It is seen that the expansion (1.4) becomes divergent and goes to infinity in the vicinity, $T=O(\varepsilon^{2/3})$, of the jump bifurcation point. The problem, then, is to construct a uniformly convergent solution that provides a transition from $y_r=-\sqrt{\lambda}$, say, to $y_r=1$, across, and in the neighborhood of $\lambda=0$.

This result is not surprising, because it is well established that regular perturbation methods fail in a small *inner region* around the bifurcation point. It is, thus, necessary to develop a transition equation in the inner region on the basis of appropriate scalings. These inner solutions, then, need to be asymptotically matched (Bender and Orszag, 1978, Kevorkian and Cole, 1981) to (1.4) in the *outer region*. Lebovitz and Schaar (1975a, 1975b) and Haberman (1979) detail methods to develop transition solutions across different types of bifurcation points. The cases they study are concerned with a *single* first or second order equation.

Many systems, like the Duffing's equation with damping or the nonlinear Mathieu's equation, can be averaged and represented as systems of *two* first order equations. In the present work, we analyze singular perturbation methods for such systems across bifurcation points. As an illustration, the theory developed for transition across jumps, is applied to the Duffings oscillator. Recent work by Neal and Nayfeh (1990) addresses this problem by numerically integrating the equations derived by multiple time scale analysis. Collinge and Ockendon (1979) have related the responses obtained, to the timescales involved in the various regions, for a quadratic variation in the frequency.

We set up perturbation expansions about the reduced (or stationary) path which are seen to be divergent in a small inner region around the critical or bifurcation point. In the vicinity of these critical points, it is possible to construct an invariant *center manifold*, on which the motion of the system is restricted. The equations are accordingly transformed to study the motion along the center manifold. Methods described by Haberman (1979) are used to develop inner transition solutions on the center manifold. These solutions are then transformed back and asymptotically matched with the outer perturbative expansions.

Finally, the averaged equations for the Duffing's oscillator are analyzed. Amplitude and phase responses are determined analytically and compared with numerical simulations.

## 2. EQUILIBRIA AND CRITICALITY IN SYSTEMS OF TWO FIRST ORDER EQUATIONS

Consider the following system of equations describing the behavior of two variables $a$ and $\psi$, which are dependent on the slowly varying parameter, $\lambda$ :

$$\frac{da}{dt} = F_1(a, \psi, \lambda) \qquad (2.1a)$$

$$\frac{d\psi}{dt} = F_2(a, \psi, \lambda). \qquad (2.1b)$$

$\lambda$, varies slowly with time and can be written as $\lambda(\varepsilon t)$, where $\varepsilon$ is sufficiently small. Introducing a slower time scale, $T = \varepsilon t$, we can rewrite equations (2.1) as:

$$\varepsilon \frac{da}{dT} = F_1(a, \psi, \lambda(T)) \qquad (2.2a)$$

$$\varepsilon \frac{d\psi}{dT} = F_2(a, \psi, \lambda(T)). \qquad (2.2b)$$

We begin by looking at the *reduced solution*, or the solution of the corresponding stationary problem. This can be done by setting $\varepsilon = 0$ in equations (2.2a) and (2.2b). The reduced solutions $a_r$, $\psi_r$ are then deduced by simultaneously solving:

$$F_1(a_r, \psi_r, \lambda) = 0 \qquad (2.3a)$$

$$F_2(a_r, \psi_r, \lambda) = 0. \qquad (2.3b)$$

These represent the response of the system when $\lambda$ is constant in time. The linear stability of these solutions is studied through the linearization of (2.1) about $a = a_r$ and $\psi = \psi_r$. The eigenvalues of the Jacobian $J$, given by

$$J = \begin{pmatrix} \dfrac{\partial F_1}{\partial a} & \dfrac{\partial F_1}{\partial \psi} \\ \dfrac{\partial F_2}{\partial a} & \dfrac{\partial F_2}{\partial \psi} \end{pmatrix}_{a = a_r, \psi = \psi_r} \qquad (2.4)$$

are used to determine the stability of the stationary response.

When $\lambda$ varies slowly with time, $a_r$ and $\psi_r$ are no longer equilibrium solutions of (2.1). However, we may expect equilibrium solutions to be very near the reduced solutions. These new equilibrium solutions are called *slowly varying equilibrium (sve) solutions*, which we construct from perturbation expansions about the corresponding reduced solution:

$$a_{sve} = a_r(\lambda) + \varepsilon a_1 + \varepsilon^2 a_2 \ldots \qquad (2.5a)$$

$$\psi_{sve} = \psi_r(\lambda) + \varepsilon \psi_1 + \varepsilon^2 \psi_2 \ldots \qquad (2.5b)$$

To determine the unknown coefficients, $a_1$, $a_2$,..... and $\psi_1$, $\psi_2$...., we first express $F_1(a, \psi, \lambda(T))$ and $F_2(a, \psi, \lambda(T))$ as Taylor series expansions about $a_r$ and $\psi_r$. Thus,

$$F_1(a, \psi, \lambda(T)) = \sum_{j=0}^{\infty} \sum_{k=0}^{\infty} A_{jk}(a - a_r)^j (\psi - \psi_r)^k$$

$$= \varepsilon \frac{da}{dT} \qquad (2.6a)$$

$$F_2(a, \psi, \lambda(T)) = \sum_{j=0}^{\infty} \sum_{k=0}^{\infty} B_{jk}(a - a_r)^j (\psi - \psi_r)^k$$

$$= \varepsilon \frac{d\psi}{dT} \qquad (2.6b)$$

where,

$$A_{jk} = \frac{1}{j!k!} \frac{\partial^{j+k} F_1}{\partial a^j \partial \psi^k} \bigg|_{a = a_r, \psi = \psi_r} \qquad (2.7a)$$

and,

$$B_{jk} = \frac{1}{j!k!} \frac{\partial^{j+k} F_2}{\partial a^j \partial \psi^k} \bigg|_{a = a_r, \psi = \psi_r}. \qquad (2.7b)$$

Substituting equation (2.5) into equation (2.6), equating coefficients of like powers of $\varepsilon$, and simultaneously solving the resulting equations gives:

$$a_1 = (B_{01} a_r' - A_{01} \psi_r')/(B_{01} A_{10} - A_{01} B_{10}) \qquad (2.8a)$$

$$\psi_1 = (A_{10} \psi_r' - B_{10} a_r')/(B_{01} A_{10} - A_{01} B_{10}), \qquad (2.8b)$$

and so on, where the primed quantities are derivatives with respect to slow time, $T$. From equations (2.8) and (2.5), it can be seen that the first order coefficients, $a_1$ and $\psi_1$, of the slowly varying equilibrium solutions become of $O(\varepsilon^{-1})$ in a region where,

$$Det(J) = B_{01} A_{10} - A_{01} B_{10} = O(\varepsilon). \qquad (2.9)$$

Thus the expansion (2.5) is non-convergent when $Det(J) = 0$. The corresponding point in phase space where $Det(J) = 0$, is called the *critical point*, and the critical values are denoted as $a_c$, $\psi_c$ and $\lambda_c$. For convenience, we also choose $T = 0$ when $\lambda = \lambda_c$. We now consider the Taylor series expansions of $F_1(a, \psi, \lambda)$ and $F_2(a, \psi, \lambda)$ around the critical point:

$$\frac{d\bar{a}}{dt} = \bar{F}_1(\bar{\lambda}, \bar{a}, \bar{\psi}) = \sum_{m=0}^{\infty} \sum_{n=0}^{\infty} \sum_{p=0}^{\infty} \alpha_{mnp} \bar{\lambda}^m \bar{a}^n \bar{\psi}^p \qquad (2.10a)$$

$$\frac{d\bar{\psi}}{dt} = \bar{F}_2(\bar{\lambda}, \bar{a}, \bar{\psi}) = \sum_{m=0}^{\infty} \sum_{n=0}^{\infty} \sum_{p=0}^{\infty} \beta_{mnp} \bar{\lambda}^m \bar{a}^n \bar{\psi}^p, \qquad (2.10b)$$

where,

$$\bar{a} = a - a_c, \quad \bar{\psi} = \psi - \psi_c \text{ and } \bar{\lambda} = \lambda - \lambda_c, \qquad (2.11)$$

and,

$$\alpha_{mnp} = \frac{1}{m!n!p!} \frac{\partial^{m+n+p} F_1(\bar{\lambda}, \bar{a}, \bar{\psi})}{\partial \bar{\psi}^p \partial \bar{a}^n \partial \bar{\lambda}^m}\bigg|_{\bar{\lambda} = \bar{a} = \bar{\psi} = 0} \qquad (2.12a)$$

$$\beta_{mnp} = \frac{1}{m!n!p!} \frac{\partial^{m+n+p} F_2(\bar{\lambda}, \bar{a}, \bar{\psi})}{\partial \bar{\psi}^p \partial \bar{a}^n \partial \bar{\lambda}^m}\bigg|_{\bar{\lambda} = \bar{a} = \bar{\psi} = 0}. \qquad (2.12b)$$

Further, let us also look at the eigenvalues of the Jacobian matrix,

$$J = \begin{pmatrix} A_{10} & A_{01} \\ B_{10} & B_{01} \end{pmatrix} = \begin{pmatrix} \alpha_{010} & \alpha_{001} \\ \beta_{010} & \beta_{001} \end{pmatrix}, \qquad (2.13)$$

at the critical point. Taking into account that the determinant of the Jacobian is zero at the critical point, it can be easily seen that the eigenvalues $\pi_{1,2}$ are given by:

$$\pi_{1,2} = 0, A_{10} + B_{01}. \qquad (2.14)$$

While on a stable branch of a stationary solution, the eigenvalues of the Jacobian (2.13) are negative. As we approach the critical point, though, as can be seen from equation (2.14), one eigenvalue reduces to zero, while the other stays negative. For the linear problem, the plane formed by the eigenvector corresponding to the zero eigenvalue and the $\bar{\lambda}$ axis is called the *center eigenspace*. The plane formed by the eigenvector corresponding to the negative eigenvalue and the $\bar{\lambda}$ axis is the *stable eigenspace*. Because of the negative eigenvalue, motion on the stable eigenspace converges exponentially fast to the center eigenspace. If we, then, construct an orthogonal coordinate frame oriented along the eigenvectors and the $\bar{\lambda}$ axis, *only one first order equation along the center eigenspace is needed to describe the motion*. We thus, proceed to define the matrix of (normalized) vectors as:

$$R = \begin{pmatrix} u_1 & u_2 \end{pmatrix} = \begin{pmatrix} r_{11} & r_{12} \\ r_{21} & r_{22} \end{pmatrix}, \qquad (2.15)$$

where $u_1$ and $u_2$ are the normalized eigenvectors corresponding to the eigenvalues $\pi_1 = 0$ and $\pi_2 = A_{10} + B_{01}$. The original coordinate plane is transformed by:

$$\pi_2 = A_{10} + B_{01}. \qquad (2.16)$$

Introducing this transformation in (2.10) and rearranging, we get:

$$(R) \begin{Bmatrix} \dfrac{du}{dt} \\ \dfrac{dv}{dt} \end{Bmatrix} = \begin{Bmatrix} \alpha_{000} \\ \beta_{000} \end{Bmatrix} + (J)(R) \begin{Bmatrix} u \\ v \end{Bmatrix} + nonlinear\ terms. \qquad (2.17)$$

Realizing that $(R)^{-1}(J)(R)$ gives the singular values of the Jacobian,

$$(R)^{-1}(J)(R) = \begin{pmatrix} 0 & 0 \\ 0 & -\pi_2 \end{pmatrix}, \qquad (2.18)$$

we will get the following form of expressions for $\dfrac{du}{dt}$ and $\dfrac{dv}{dt}$ :

$$\frac{du}{dt} = \gamma_{000} + \gamma_{100} \bar{\lambda} + \gamma_{200} \bar{\lambda}^2 + \gamma_{020} u^2 + \gamma_{002} v^2 +$$
$$\gamma_{011} u v + \gamma_{110} \bar{\lambda} u + \gamma_{101} \bar{\lambda} v .... \qquad (2.19a)$$

$$\frac{dv}{dt} = \delta_{000} - \pi_2 v + \delta_{100} \bar{\lambda} + \delta_{200} \bar{\lambda}^2 + \delta_{020} u^2 + \delta_{002} v^2 +$$
$$\delta_{011} u v + \delta_{110} \bar{\lambda} u + \delta_{101} \bar{\lambda} v .... \qquad (2.19b)$$

In the vicinity of the critical point, when $\bar{\lambda}$ and $u$ are small, we can assume, from the center manifold theory that
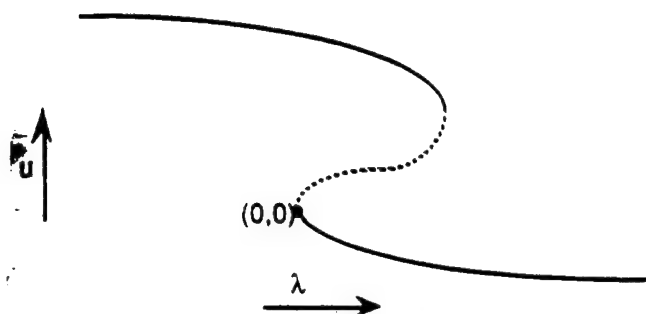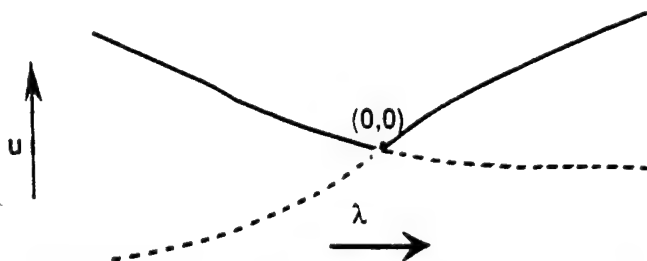
FIGURE 2A. JUMP PHENOMENON.



FIGURE 2B. STRAIGHT-STRAIGHT OR TRANSCRITICAL BIFURCATION.

$v = v(u, \bar{\lambda})$, and is generally parabolic in nature (Wiggins, 1990):

$$v = \eta_{020} u^2 + \eta_{110} \bar{\lambda} u + \eta_{200} \bar{\lambda}^2 + \eta_{030} u^3 +$$
$$\eta_{120} \bar{\lambda} u^2 + \eta_{210} \bar{\lambda}^2 u + \eta_{300} \bar{\lambda}^3 \dots \qquad (2.20)$$

To determine the values of the unknown coefficients up to quadratic order , we substitute equation (2.20) in equations (2.19) and equate the coefficients of $u^2$, $\bar{\lambda}u$ and $\bar{\lambda}^2$:

$$\eta_{020} = -\frac{\delta_{020}}{\delta_{001}}, \qquad (2.21a)$$

$$\eta_{110} = -\frac{2\delta_{020}\gamma_{100}}{\delta_{001}^2} - \frac{\delta_{110}}{\delta_{001}}, \qquad (2.21b)$$

and,

$$\eta_{200} = -\left(\frac{2\delta_{020}\gamma_{100}^2}{\delta_{001}^3}\right) - \left(\frac{\delta_{110}\gamma_{100}}{\delta_{001}^2}\right) - \frac{\delta_{200}}{\delta_{001}}. \qquad (2.21c)$$

Similarly, the coefficients for the cubic terms may be calculated. The results from (2.20) and (2.21) when substituted into (2.19a) show that up to the quadratic order, $\frac{du}{dt}$ is given by:
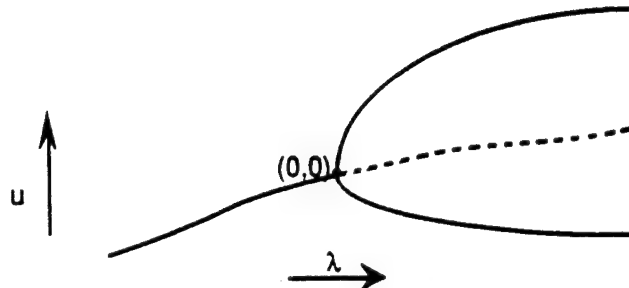


FIGURE 2C. PARABOLIC OR PITCHFORK BIFURCATION.

$$\frac{du}{dt} = \gamma_{000} + \gamma_{100}\bar{\lambda} + \gamma_{200}\bar{\lambda}^2 + \gamma_{020}u^2 + \gamma_{110}\bar{\lambda}u. \quad (2.22a)$$

And up to the cubic order by:

$$\frac{du}{dt} = \gamma_{000} + \gamma_{100}\bar{\lambda} + \gamma_{200}\bar{\lambda}^2 + \gamma_{020}u^2 + \gamma_{110}\bar{\lambda}u +$$
$$\Gamma_{030}u^3 + \Gamma_{120}\bar{\lambda}u^2 + \Gamma_{210}\bar{\lambda}^2u + \Gamma_{300}\bar{\lambda}^3, \qquad (2.22b)$$

where, the $\Gamma$ terms include contributions from different $\gamma$ terms.

We can express equation (2.22) as: $\frac{du}{dt} = G(u, \bar{\lambda})$. $G(u, \bar{\lambda})$ determines the behavior of the system near the critical point. The stationary solution of equation (2.22), denoted by $u_r$, is then given by $G(u_r, \bar{\lambda}) = 0$. Sketching such a solution for different values of the coefficients would show three qualitatively distinct cases. These are shown in Figures 2a, 2b and 2c. In each figure, the critical point is represented as (0,0). Further, the unstable reduced solutions are shown in dashed lines.

In Fig. 2a is shown the case of a first order *jump phenomenon*. At the critical point here the slope of the reduced (equilibrium) solution reaches infinity. We consider a simple case where, for $\bar{\lambda} > 0$, a parabolic equilibrium exists. Then,

$$G(u, \bar{\lambda}) = \gamma_{100}\bar{\lambda} + \gamma_{020}u^2 + \gamma_{200}\bar{\lambda}^2, \qquad (2.23)$$

where $\gamma_{020} < 0$ and $\gamma_{100} > 0$.

The case of the *straight-straight* or *transcritical bifurcation*, is shown in Fig. 2b. Two equilibrium solutions cross and exchange stabilities at $\bar{\lambda} = 0$. In the neighborhood of the critical point, therefore,

$$G(u, \bar{\lambda}) = \gamma_{020}u^2 + \gamma_{110}\bar{\lambda}u + \gamma_{200}\bar{\lambda}^2. \qquad (2.24)$$

Here $\gamma_{110}^2 - 4\gamma_{200}\gamma_{020} > 0$ for two real solutions to exist before and after the critical point. Also, $\gamma_{020} < 0$, so that the upper branch is always stable, say.

The third case that arises is shown in Fig. 1c. This is called *parabolic bifurcation* (Haberman, 1979). In the neighborhood of $\bar{\lambda} = 0$:

$$G(u,\bar{\lambda}) = \gamma_{110}\bar{\lambda} u + \gamma_{200}\bar{\lambda}^2 + \Gamma_{030}u^3 + \Gamma_{120}\bar{\lambda} u^2 +$$
$$\Gamma_{210}\bar{\lambda}^2 u + \Gamma_{300}\bar{\lambda}^3 \qquad (2.25)$$

with $\gamma_{020} = 0$, $\gamma_{110} > 0$ (so that a parabolic equilibrium exists above the critical point) and $\Gamma_{030} > 0$.

As seen earlier, the slowly varying equilibrium solution gets disordered in the neighborhood of the critical point. By using the transformations given in equation (2.16) and $G(u,\bar{\lambda})$, we are now in a position to look at how to develop solutions in the inner region around the critical point. Once these *inner solutions* are found, they need to be transformed back into the original coordinate frame and asymptotically matched with the outer slowly varying equilibrium solutions.

# 3. INNER SOLUTIONS FOR JUMP PHENOMENA

For determining the inner solution in this case, we need to introduce a scale change near the critical point. Haberman (1979) has tabulated that for a first order jump phenomenon, the slowly varying equilibrium breaks down when $T = O(\varepsilon^{2/3})$. It may be recalled that $T = 0$ at the critical point. This prompts the scale change

$$\varnothing = T = \varepsilon^{2/3}z, \qquad (3.1)$$

where $z$ is the new scaled time. Assuming that $\lambda$ varies with slow time across the critical point, we can express it as a series expansion about $\lambda_c$, the critical parameter value.

$$\bar{\lambda} = \lambda_c'T + \lambda_c''\frac{T^2}{2!} + \dots \qquad (3.2)$$

where the primes indicate derivatives with slow time, evaluated at the critical point. Also the method of matched asymptotic expansions (Haberman, 1979) and (3.1) imply that the inner equations follow the scaling:

$$u = \varepsilon^{1/3}w(z). \qquad (3.3)$$

On making these scale changes, (2.22b) becomes

$$\frac{dw}{dz} = \gamma_{100}\lambda_c'z + \gamma_{020}w^2 +$$
$$\varepsilon^{1/3}\left(\gamma_{110}\lambda_c'wz + \Gamma_{030}w^3\right) + O(\varepsilon^{2/3}) \qquad (3.4)$$

We then assume an inner expansion of the form

$$w = w_0 + \varepsilon^{1/3}w_1 + \dots, \qquad (3.5)$$

and equate powers of $\varepsilon$ to yield to the leading order:

$$\frac{dw_0}{dz} = \gamma_{100}\lambda_c'z + \gamma_{020}w_0^2 + O(\varepsilon^{1/3}). \qquad (3.6)$$

The higher order terms are governed by:

$$\frac{dw_1}{dz} = 2\gamma_{020}w_0w_1 + \gamma_{110}\lambda_c'w_0z + \Gamma_{030}w_0^3. \qquad (3.7)$$

(3.6) is an exactly solvable Riccati equation (Ince, 1956). The solution to this equation must match the slowly varying equilibrium solution as $z \to -\infty$. Here we consider the case where $\lambda$ decreases across the jump (Fig. 2a). To ensure matching, then,

$$\frac{dw}{dz} = \frac{du}{dt} \to \frac{du_{sve}}{dt} \text{ as } z \to -\infty. \qquad (3.8)$$

$u_{sve}$ is the slowly varying equilibrium solution corresponding to equation (2.23) and can be determined by using the transformation (2.16) on equation (2.5) in the original phase plane. Since $u_{sve}$ depends on slow time, $T$, $\frac{du_{sve}}{dt} = 0$. Thus, from (3.6) and (3.8) we see that for matching,

$$w \to \left(\frac{-\gamma_{100}\lambda_c'z}{\gamma_{020}}\right)^{1/2} \text{ as } z \to -\infty. \qquad (3.9)$$

Equation (3.6) can be transformed by defining:

$$w_0 = \left(\frac{\gamma_{100}\lambda_c'}{\gamma_{020}^2}\right)^{1/3}\frac{1}{\phi}\frac{d\phi}{dx}, \qquad (3.10)$$

with the scaling $x = -\left(\gamma_{100}\gamma_{020}\lambda_c'\right)^{1/3}z$. The Riccati equation (3.9), then, becomes Airy's differential equation $d^2\phi/dx^2 = x\phi$, whose solution is given by

$$c_1Ai(x) + c_2Bi(x). \qquad (3.11)$$

The general solution of (3.6) is therefore

$$w_0 = \left(\frac{\gamma_{100}\lambda_c'}{\gamma_{020}^2}\right)^{1/3} \frac{c_1 Ai'(x) + c_2 Bi'(x)}{c_1 Ai(x) + c_2 Bi(x)}, \qquad (3.12)$$

where $Ai'(x)$ is the derivative with $x$, of $Ai(x)$ etc. From the asymptotic behavior of the Airy's function, as described in Abramowitz and Stegun (1971), the matching condition (3.9) can be met only if $c_2 = 0$. Therefore, the poles of equation (3.12) occur at the zeros of $Ai(x)$. Abramowitz and Stegun (1971) show that the first zero of $Ai(x)$ occurs at $x = -2.33810....$ . Since $z$ depends on $x$, the value of $z$ at which the first pole of (3.12) occurs (denoted by $z = z_0$) is given by:

$$z_0 = \frac{-2.33810....}{\left(\gamma_{100}\gamma_{020}\lambda_c'\right)^{1/3}}. \qquad (3.13)$$

For the case when $\lambda$ decreases across the critical point, $\lambda_c'$ is negative. From (2.23) and (3.13), then, we see that $z = z_0$ is positive. This means that the inner transition solution becomes non-uniform later in time after the critical point. This accounts for the previously observed phenomenon of *delayed jump* (Mandel and Erneux, 1979, Diener and Diener, 1991) in first order systems.

The transition equation (3.12) must connect the slowly varying equilibrium solution $u_{sve}$ to the fully nonlinear outer solution of (2.1). To achieve this, the variational equation corresponding to (2.1) about the slowly varying equilibrium may be derived. This, then needs to be matched to the transition solution (3.12). This is demonstrated for the case of the Duffing's oscillator in section 5.

# 4. INNER SOLUTIONS FOR BIFURCATION PHENOMENA

The two cases of straight-straight and parabolic bifurcation are considered.

## 4.1. Straight-Straight Bifurcation

This will be denoted as $s \rightarrow s$ type bifurcation (Haberman, 1979). In the neighborhood of the critical point, $G(u,\bar{\lambda})$ is given by:

$$G(u,\bar{\lambda}) = \gamma_{020}u^2 + \gamma_{110}\bar{\lambda}u + \gamma_{200}\bar{\lambda}^2 = \gamma_{020}(u - \mu_1\bar{\lambda})(u - \mu_2\bar{\lambda}), \qquad (4.1)$$

where $\gamma_{020} < 0$, and, $\mu_2 > \mu_1$.

The asymptotic expansion of the slowly varying equilibrium for the straight-straight bifurcation case is non-convergent at the critical point. This prompts the scale change

$$T = \varepsilon^{1/2}z, \qquad (4.2)$$

where $z$ is the inner transition timescale. The dependent inner variable is then defined by:

$$u = \varepsilon^{1/2}w(z), \qquad (4.3)$$

and the transition layer equation becomes:

$$\frac{dw}{dz} = \gamma_{020}(w - \mu_1\lambda_c'z)(w - \mu_2\lambda_c'z). \qquad (4.4)$$

Lebovitz and Schaar (1975a), have shown that (4.4) provides a transition between the two straight line equilibrium solutions only if $\mu_1 < 0$. For this case, as $z \rightarrow \infty$, $w \rightarrow \mu_2\lambda_c'z$. Otherwise, if $\mu_1 > 0$, $w$ reaches $-\infty$ in a finite time, $w \rightarrow -\left[\gamma_{020}(z - z_0)\right]^{-1}$ as $z \rightarrow z_0$. If $\mu_1 = 0$, then the solution becomes non-uniform only if initially $w < 0$. This case is discussed in detail by Haberman (1979).

## 4.2. Parabolic Bifurcation

This is denoted by $s \rightarrow p$ and $p \rightarrow s$ bifurcation, referring to the cases where the bifurcation parameter is increased or decreased, respectively, across the bifurcation point (Fig. 2c). The governing equation about the critical point, as mentioned earlier, is:

$$G(u,\bar{\lambda}) = \gamma_{110}\bar{\lambda}u + \gamma_{200}\bar{\lambda}^2 + \Gamma_{030}u^3 + \Gamma_{120}\bar{\lambda}u^2 + \\ \Gamma_{210}\bar{\lambda}^2u + \Gamma_{300}\bar{\lambda}^3, \qquad (4.5)$$

with $\gamma_{020} = 0$, $\gamma_{110} > 0$ and $\Gamma_{030} > 0$.

### 4.2.1. Parabolic to straight transition. $(p \rightarrow s)$

It is found appropriate to choose the scaling $T = \varepsilon^{1/2}z$. The inner variable is given by:

$$u = \varepsilon^{1/4}w(z). \qquad (4.6)$$

Since such a bifurcation would involve the parameter $\lambda$ decreasing with time, the matching condition requires that as $z \rightarrow -\infty$, the transition equation approach the parabolic equilibrium:

$$w \rightarrow \left(\frac{-\gamma_{110}\lambda_c'z}{\Gamma_{030}}\right)^{1/2} \text{ as } z \rightarrow -\infty. \qquad (4.7)$$

Applying the scaling (4.6) to equation (4.5) gives the inner equation:

$$\frac{dw}{dz} = \gamma_{110}\lambda_c' zw + \Gamma_{030}w^3 +$$

$$\varepsilon^{1/4}(\gamma_{200}\lambda_c'^2 z^2 + \Gamma_{210}\lambda_c' zw + \Gamma_{040}w^4) + O(\varepsilon^{1/2}) \quad (4.8)$$

The dependent variable is expressed as a perturbation expansion again,

$$w = w_0 + \varepsilon^{1/4}w_1 + \varepsilon^{1/2}w_2 + \dots \quad (4.9)$$

Then, substituting equation (4.9) in (4.8) and comparing powers of $\varepsilon$, we get the leading order transition layer equation:

$$\frac{dw_0}{dz} = \gamma_{110}\lambda_c' zw_0 + \Gamma_{030}w_0^3. \quad (4.10)$$

This is an exactly solvable Bernoulli's equation, and can be transformed (Ince, 1956) by $\vartheta = w_0^{-2}$, which results in the following explicit expression:

$$w_0 = \left( -2\Gamma_{030}e^{-\gamma_{110}\lambda_c' z^2}\int_{-\infty}^{z} e^{\gamma_{110}\lambda_c' \bar{z}^2}d\bar{z} \right)^{-1/2}. \quad (4.11)$$

Haberman (1979) has shown that equation (4.11) matches the outer expansions on both sides of the critical point.

### 4.2.2. Straight to parabolic transition. $(s \rightarrow p)$

Near the critical point, in this case, the disordering of the slowly varying equilibrium occurs when:

$$T = \varepsilon^{1/2}z. \quad (4.12)$$

The matching condition would then imply that as $z \rightarrow -\infty$, the solution should approach the straight equilibrium, $u \approx -\gamma_{200}\bar{\lambda}/\gamma_{110}$. The scaling of the dependent variable is:

$$u = \varepsilon^{1/2}w(z). \quad (4.13)$$

And the matching condition is:

$$w \rightarrow \left( \frac{-\gamma_{200}z\lambda_c'}{\gamma_{110}} \right) \text{ as } z \rightarrow -\infty. \quad (4.14)$$

With these scale changes, the inner equation assumes the form:

$$\frac{dw}{dz} = z(\gamma_{110}\bar{\lambda}_c' w + \gamma_{200}\bar{\lambda}_c'^2 z) + \varepsilon^{1/2}(\Gamma_{030}w^3 +$$

$$\Gamma_{120}\bar{\lambda}_c'^2 zw^2 + \Gamma_{210}\bar{\lambda}_c'^2 z^2 w + \Gamma_{300}\bar{\lambda}_c'^3 z^3) + \dots \quad (4.15)$$

Assuming,

$$w = w_0 + \varepsilon^{1/2}w_1 + \dots, \quad (4.16)$$

and comparing powers of $\varepsilon$, the leading order transition equation is:

$$\frac{dw_0}{dz} = z(\gamma_{110}\bar{\lambda}_c' w_0 + \gamma_{200}\bar{\lambda}_c'^2 z). \quad (4.17)$$

This equation is linear and needs to solved with the matching condition (4.14). The exact solution of (4.17) is:

$$w_0 = \gamma_{200}\lambda_c' e^{\gamma_{110}\lambda_c' z^2/2}\int_{-\infty}^{z} s^2 e^{-\gamma_{110}\lambda_c' s^2/2}ds. \quad (4.18)$$

Asymptotically as $z \rightarrow +\infty$,

$$w_0 \rightarrow \frac{\gamma_{200}}{\gamma_{110}}\sqrt{\frac{2\pi}{\gamma_{110}\lambda_c}}e^{\gamma_{110}\lambda_c' z^2/2}. \quad (4.19)$$

This is exponentially increasing. For higher order terms it has been shown (Haberman, 1979), that as $z \rightarrow +\infty$,

$$w_1 \rightarrow \frac{\Gamma_{030}}{2\gamma_{110}\lambda_c'}\left( \frac{\gamma_{200}\lambda_c'}{\gamma_{110}} \right)^3 \left( \frac{2\pi}{\gamma_{110}\lambda_c'} \right)^{3/2}\frac{e^{3\gamma_{110}\lambda_c' z^2/2}}{z}. \quad (4.20)$$

From equations (4.19) and (4.20) it can be seen that *the inner expansion (4.16) becomes disordered as $z \rightarrow +\infty$*. This requires the creation of a *second* transition layer. To determine the new scaling a nonlinear transformation is introduced:

$$\varepsilon^{1/2}\frac{e^{\gamma_{110}\lambda_c' z^2/2}}{z} = \Phi, \quad (4.21)$$

where $\Phi$ is an independent variable. Thus, as $\Phi \rightarrow 0$, $z \rightarrow +\infty$. To leading order, then, as described by Haberman (1979),

$$w = \varepsilon^{-1/4}z^{1/2}f(\Phi), \quad (4.22)$$

where,

$$f(\Phi) \approx \frac{\gamma_{200}}{\gamma_{110}}\left( \frac{2\pi}{\gamma_{110}\lambda_c'} \right)^{1/2}\Phi^{1/2}. \quad (4.23)$$

Using equations (4.23), (4.22) and (4.15) it can be shown that the leading order equation is:

$$2\Phi \frac{df}{d\Phi} = f + \frac{\Gamma_{030}}{\gamma_{110}\lambda_c} f^3. \tag{4.24}$$

Letting $s = \ln \Phi$, equation (4.24) reduces to

$$2\frac{df}{ds} = f + \frac{\Gamma_{030}}{\gamma_{110}\lambda_c} f^3. \tag{4.25}$$

The matching condition from equations (4.19) and (4.25) is

$$f \to \frac{\gamma_{200}}{\gamma_{110}} \left( \frac{2\pi}{\gamma_{110}\lambda_c} \right)^{1/2} e^{s/2} \text{ as } s \to -\infty. \tag{4.26}$$

As $s \to \infty$, $\Phi \to \infty$ and hence $z \to +\infty$, from equation (4.25):

$$f \to (sgn\,\gamma_{200}) \left( \frac{-\gamma_{110}\lambda_c'}{\Gamma_{030}} \right)^{1/2}. \tag{4.27}$$

or, from equation (4.22), as $z \to +\infty$, the solution in this region is approaching

$$w \to \varepsilon^{-1/4}(sgn\,\gamma_{200}) \left( \frac{-\gamma_{110}\lambda_c' z}{\Gamma_{030}} \right). \tag{4.28}$$

This shows that the second transition layer matches the slowly varying straight line equilibrium as $z \to +\infty$.

In summary,

(1) The only case where two transition layers are necessary, is the $p \to s$ parabolic bifurcation case. One layer is characterized by $z = O(1)$, and the other by $s = O(1)$.

(2) For the other bifurcation cases, ie., $s \to s$ and $s \to p$, only one transition layer is needed, and the slowly varying equilibria are approached by the transition solutions.

(3) For the case of the jump phenomenon, nonlinear oscillations around the new equilibrium positions occur.

(4) In all cases, after the solutions are matched in the vicinity of the critical point, they need to be transformed back to the original $a - \psi$ plane by using the rotation matrix $R$, given in equation (2.15).

## 5. EXAMPLE OF THE JUMP PHENOMENON: THE DUFFING'S OSCILLATOR

In this section, we will apply the theory developed in sections 2 and 3, to the case of transition through resonance in the Duffing's oscillator, with a linearly varying frequency. Consider the following dimensionless equation:
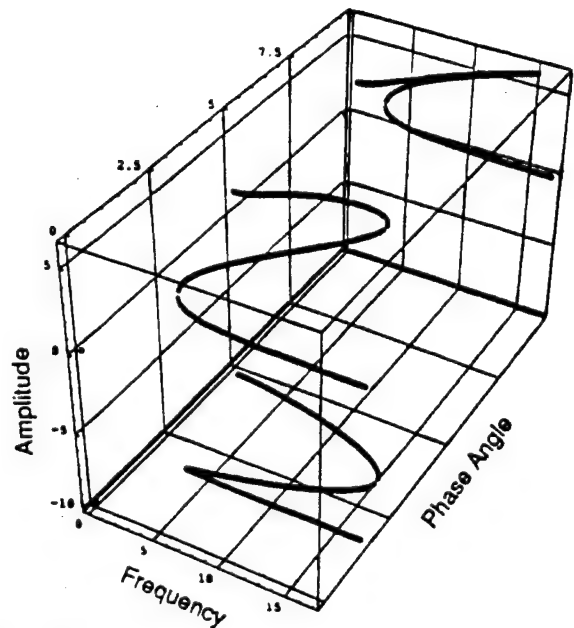


FIGURE 3. STATIONARY SOLUTION FOR THE DUFFING'S EQUATION (5.1). $E_1 = 10.0$, $\zeta = 0.1$.

$$\frac{d^2\chi}{dt^2} + 2\zeta \frac{d\chi}{dt} + \chi + \chi^3 = E_1 \sin \theta, \tag{5.1}$$

where $\chi$ is the dependent variable- the displacement of the oscillator. $\zeta$ and $E_1$ are the damping and the amplitude of forcing, respectively. Both are assumed to be of $O(\varepsilon)$. The instantaneous frequency of excitation is $\lambda = \lambda(\varepsilon t) = \frac{d\theta}{dt}$, where $\varepsilon$ is chosen to be sufficiently small. We assume a solution of the form:

$$\chi = a\cos(\theta + \psi), \tag{5.2}$$

where $a$ and $\psi$ are the slowly varying amplitude and phase of response. Carrying out first order averaging of this system as described by Mitropolskii (1965), results in the following equations for amplitude and phase, respectively:

$$\frac{da}{dt} = -\zeta a - \frac{E_1}{1 + \lambda(T)} \cos \psi, \tag{5.3a}$$

$$\frac{d\psi}{dt} = 1 - \lambda(T) + \frac{3a^2}{8} + \frac{E_1}{a(1 + \lambda(T))} \sin \psi. \tag{5.3b}$$

Or, setting $T = \varepsilon t$,

$$\varepsilon \frac{da}{dT} = -\zeta a - \frac{E_1}{1 + \lambda(T)} \cos \psi, \tag{5.4a}$$
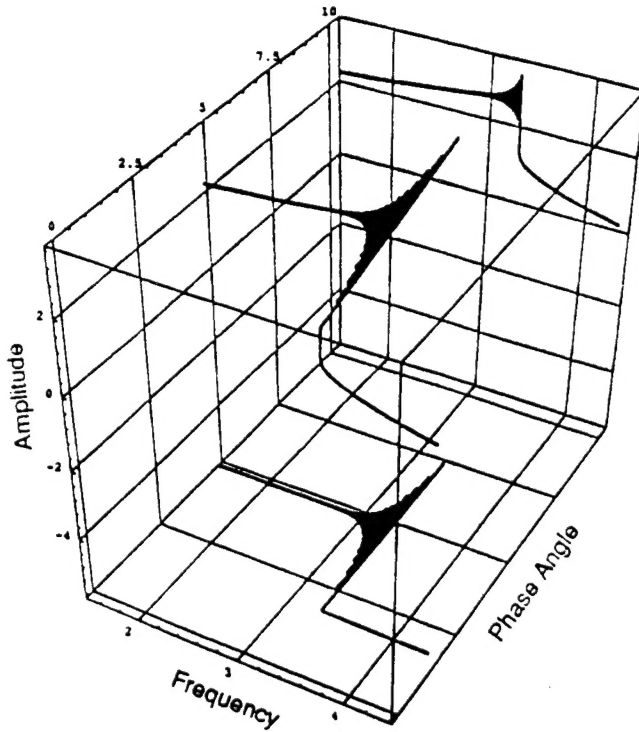
FIGURE 4A. ANALYTICAL 3D RESPONSE. $\lambda_c' = -0.1$, $\varepsilon = 0.1$.

$$\varepsilon \frac{d\psi}{dT} = 1 - \lambda(T) + \frac{3a^2}{8} + \frac{E_1}{a(1+\lambda(T))} \sin\psi . \quad (5.4b)$$

These equations are now of the same form as equations (2.2). Setting $\varepsilon = 0$, we get the reduced or the stationary response curve defined by the equations:

$$-\zeta a_r - \frac{E_1}{1+\lambda(T)} \cos\psi_r = 0, \quad (5.5a)$$

$$1 - \lambda(T) + \frac{3a_r^2}{8} + \frac{E_1}{a_r(1+\lambda(T))} \sin\psi_r = 0. \quad (5.5b)$$

This curve is shown in Fig. 3. The values of the constants are chosen throughout as $E_1 = 10.0$, and $\zeta = 0.1$. The projection of this curve on the $a - \lambda$ plane and on the $\psi - \lambda$ plane, show the familiar stationary response curves for amplitude and phase, respectively.

Setting up the slowly varying equilibrium solution as indicated in (2.8), we see that the expansion (2.5) becomes non-uniform when the determinant of the Jacobian,

$$J = \begin{pmatrix} -\zeta & \dfrac{E_1 \sin\psi_r}{1+\lambda(T)} \\ \dfrac{3a_r}{4} - \dfrac{E_1 \sin\psi_r}{a_r^2(1+\lambda(T))} & -\zeta \end{pmatrix}, \quad (5.6)$$
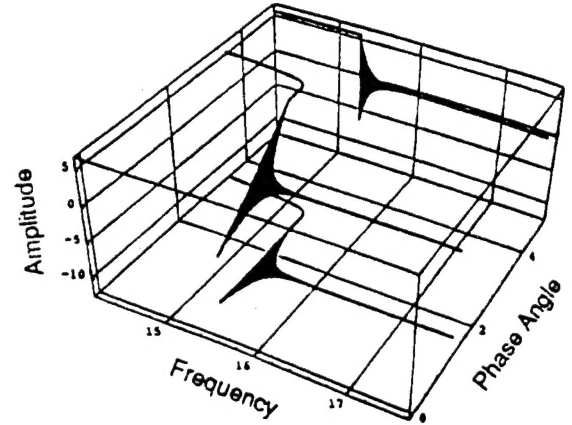


FIGURE 4B. ANALYTICAL 3D RESPONSE. $\lambda_c' = 0.1$, $\varepsilon = 0.1$.

becomes zero. Solving equations (5.5) and the condition (5.6) simultaneously gives the critical values, $a_c$, $\psi_c$ and $\lambda_c$. The transformation matrix is, then:

$$R = \begin{pmatrix} \dfrac{E_1 \sin\psi_c}{\sqrt{\zeta^2(1+\lambda_c)^2 + E_1^2 \sin^2\psi_c}} & \dfrac{a_c \tan\psi_c}{\sqrt{1+a_c^2 \tan^2\psi_c}} \\ \dfrac{d(1+\lambda_c)}{\sqrt{\zeta^2(1+\lambda_c)^2 + E_1^2 \sin^2\psi_c}} & \dfrac{1}{\sqrt{1+a_c^2 \tan^2\psi_c}} \end{pmatrix} .(5.7)$$

By applying this transformation, and calculating the important coefficients $\gamma_{100}$, $\gamma_{020}$ and $\gamma_{200}$, we can get the actual numerical form of equation (2.23) for this case. Following this, the inner solutions are set up as described by equation (3.12). To match this to the fully nonlinear outer problem, we construct the variational equation of (5.3) about the slowly varying equilibrium path, by perturbing the slowly varying amplitude and phase by $\hat{a}$ and $\hat{\psi}$, respectively:

$$a = a_{sve} + \hat{a}, \text{ and } \psi = \psi_{sve} + \hat{\psi} . \quad (5.8)$$

The variational equations are:

$$\frac{d\hat{a}}{dt} = -\zeta\hat{a} + \frac{E_1 \sin\psi_{sve}}{(1+\lambda(T))} \hat{\psi} , \quad (5.9a)$$

$$\frac{d\hat{\psi}}{dt} = \left(\frac{3a_{sve}}{4}\right)\hat{a} + \frac{E_1 \cos\psi_{sve}}{a_{sve}(1+\lambda(T))}\left(1 - \frac{\hat{a}}{a_{sve}}\right)\hat{\psi} . \quad (5.9b)$$

To solve this analytically, we consider the following perturbation expansion:

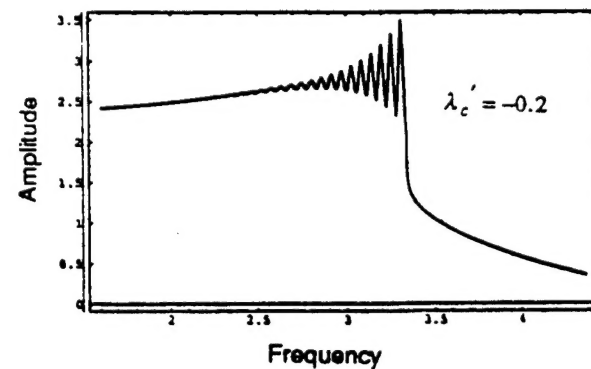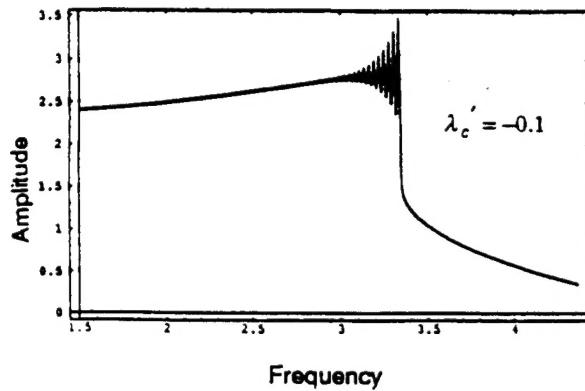$$\hat{a} = \hat{a}_1 + \varepsilon\hat{a}_2 + ..... \quad (5.10a)$$

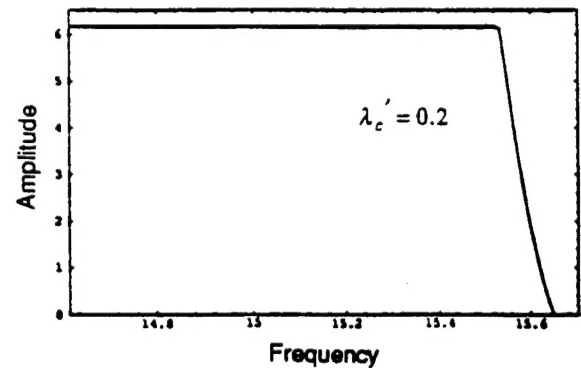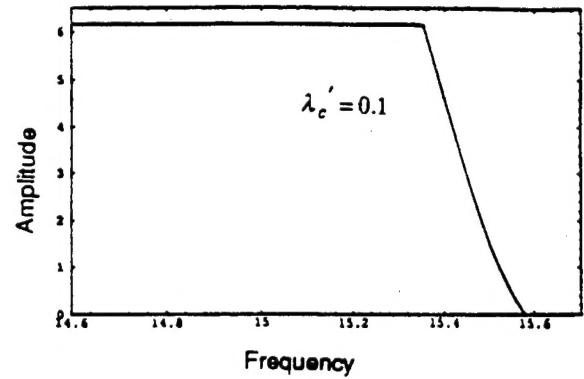FIGURE 5A. AMPLITUDE RESPONSE. $\lambda_c' = -0.1, -0.2$, $\varepsilon = 0.1$.



FIGURE 5B. AMPLITUDE RESPONSE. $\lambda_c = 0.1, 0.2$, $\varepsilon = 0.1$.

$$\hat{\psi} = \hat{\psi}_1 + \varepsilon\hat{\psi}_2 + .... \tag{5.10b}$$

Substituting equation (5.10) in (5.9) and comparing the coefficients of $\varepsilon$, the leading order equations are:

$$\frac{d\hat{a}_1}{dt} = -\zeta\hat{a}_1 + \frac{E_1 \sin \psi_r}{1+\lambda_0}\hat{\psi}_1, \tag{5.11a}$$

$$\frac{d\psi_1}{dt} = \frac{3a_r\hat{a}_1}{4} + \frac{E_1 \cos \psi_r}{a_r(1+\lambda_0)}\hat{\psi}_1. \tag{5.11b}$$

For matching this to the inner solution, the rates of change of the variables in the equations (3.12) and (5.11) need to be equated. By using this matching point as initial conditions for (5.11), the outer solution can be completed. *This matching point, then represents the point at which the jump can be said to occur.* By calculating this we can get an approximation of the delay that occurs during the jump. Equation (5.11) can also be used to predict the maximum overshoot that occurs for a given matching point.

As a result of this type of analysis, *it is possible to get an analytical estimate of the maximum amplitude reached while linearly sweeping through the resonance points of a Duffing's oscillator.*

## 6. SUMMARY AND CONCLUSION

In this work, we considered the response of some nonlinear systems to non-stationary excitations. In particular, systems reducible to a system of two, first-order equations are studied. The method of matched asymptotic expansions is used to analytically predict the behavior of such systems near critical/bifurcation points. As an illustration, the method is applied to analyze the response of the Duffing's oscillator during a linear sweep through resonance.

It is seen that regular asymptotic expansions become divergent in an inner region around the critical points. Further, it is shown that using postulates from the center manifold theory, it is possible to reduce the dimensionality of the system near the critical points. Methods for deriving transition equations, in the inner region, for different kinds
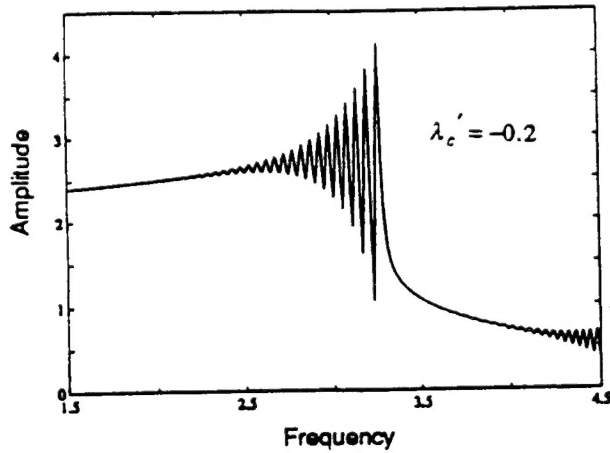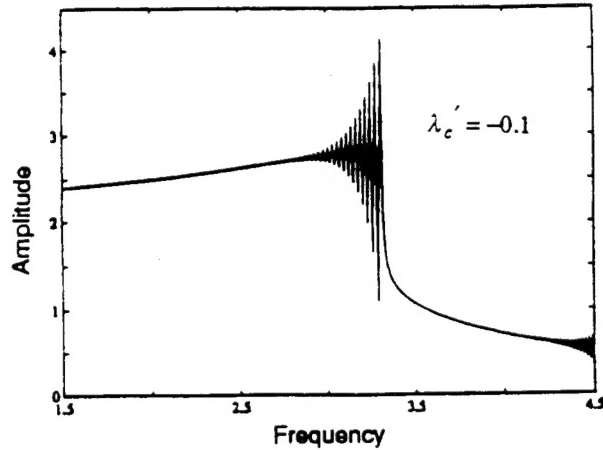
393

FIGURE 6A. NUMERICAL SIMULATION OF
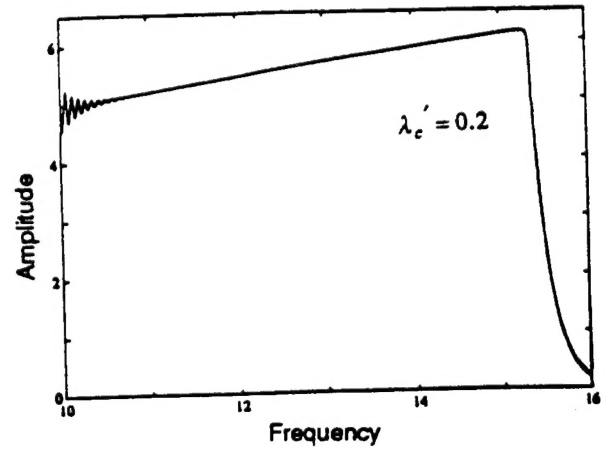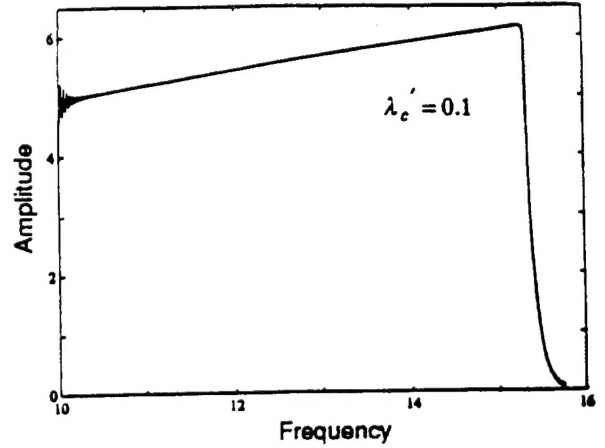EQUATIONS (5.3). $\lambda_c' = -0.1, -0.2$.



FIGURE 6B. NUMERICAL SIMULATION OF
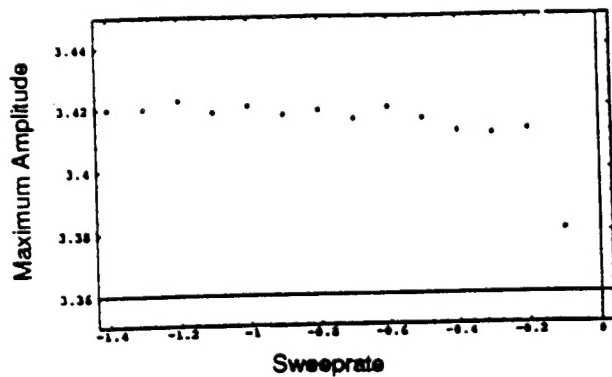EQUATIONS (5.3). $\lambda_c' = 0.1, 0.2$.



FIGURE 7. MAXIMUM AMPLITUDE REACHED FOR
NEGATIVE SWEEP.

of bifurcations are analyzed. For the case of the Duffing's oscillator, the method developed for transition across jump phenomena, is applied to the system of averaged equations. The generated responses are seen to be in good correspondence with the numerically simulated results. It is also shown that the method can be used to analytically determine the maximum amplitude, during passage through resonance in the Duffing's oscillator.

## ACKNOWLEDGMENT

## REFERENCES

Abramowitz, M., and Stegun, I.A., 1971, *Handbook of Mathematical Functions*, Dover, 9th edition.

Bender, C.M., and Orszag, S.A., 1978, *Advanced Mathematical Methods for Scientists and Engineers*, McGraw Hill.

Bogoliubov, N.N., and Mitropolskii, V.A., 1961, *Asymptotic Methods in the Theory of Nonlinear Oscillations*, Hindustan Publishing, Delhi.

Collinge, I.R., and Ockendon, J.R., 1979, "Transition Through Resonance of a Duffings Oscillator," *SIAM Journal on Applied Mathematics*, Vol. 17(2), pp. 350-357.

Diener, F., and Diener, M., 1991, "Maximal Delay," *Dynamic Bifurcations, Lecture Notes in Mathematics*, Vol 1493, Springer-Verlag, Berlin.

Erneux, T., Reiss, E.L., Holden, L.J., and Giorgiou, M., 1991, "Slow Passage Through Bifurcations and Limit Points," *Dynamic Bifurcations, Lecture Notes in Mathematics*, Vol. 1493, Springer-Verlag, Berlin.

Evan-Iwanowski, R.M., 1976, *Resonance Oscillations in Mechanical Systems*, Elsevier Scientific, New York.

Haberman, R., 1979, "Slowly Varying Jump and Transition Phenomena Associated with Algebraic Bifurcation Problems," *SIAM Journal on Applied Mathematics*, Vol. 37(1), pp. 69-106.

Ince, E.L., 1956, *Ordinary Differential Equations*, Dover, New York.

Kevorkian, J., and Cole, J.D., 1981, *Perturbation Methods in Applied Mathematics*, Springer-Verlag, New York.

Lebovitz, N.R., and Schaar, R.J., 1975a, "Exchange of Stabilities in Autonomous Systems," *Studies in Applied Mathematics*, Vol. 54(3), pp. 229-260.

Lebovitz, N.R., and Schaar, R.J., 1975b, "Exchange of Stabilities in Autonomous Systems-II. Vertical Bifurcation," *Studies in Applied Mathematics*, Vol. 56, pp. 1-50.

Mandel, E., and Erneux, T., 1979, "The Slow Passage Through a Steady Bifurctation: Delay and Memory Effects," *Journal of Statistical Physics*, Vol.48(5/6),pp. 1059-1070.

Mitropolskii, V.A., 1965, *Problems of the Asymptotic Theory of Nonstationary Vibrations*, Israel Program for Scientific Translations Ltd.

Neal, H.L., and Nayfeh, A.A., 1990, "Response of a Single-Degree-of-Freedom System to a Nonstationary Principal Parametric Excitation," *International Journal of Non-Linear Mechanics*, Vol. 25(2/3) pp. 275-284.

Wiggins, S., 1990, *Introduction to Applied Nonlinear Dynamical Systems and Chaos*, Springer-Verlag, New York.